



UNIVERSITÀ
DEGLI STUDI
FIRENZE

DOTTORATO DI RICERCA IN
AREA DEL FARMACO E TRATTAMENTI INNOVATIVI

CICLO XXXIII

COORDINATORE Prof.ssa Carla Ghelardini

**New therapeutic strategies for the treatment of
inflammatory diseases**

Settore Scientifico Disciplinare CHIM/08

Dottorando

Dott. Niccolò Cantini

(firma)

Tutore

Prof.ssa Maria Paola Giovannoni

(firma)

Coordinatore

Prof.ssa Carla Ghelardini

(firma)

Anni 2017/2020

Table of general contents

Introduction	4
Inflammation mechanism	4
Anti-inflammatory therapies	6
Projects	
A. Design, synthesis and pharmacological evaluation of new human neutrophil elastase (HNE) inhibitors with heterocyclic scaffold	8
B. Study of antiinflammatory activity of FPR1/2 agonists	152
References	170

Introduction

Inflammation is a process that triggers the immune system upon harmful stimuli, such as pathogens, toxic compounds, or irradiation, resulting in the activation of the healing process, and it can be classified as either acute or chronic. Therefore, the inflammation can be considered a defense mechanism fundamental for health [Chen, L. et al. 2017]. During an acute inflammatory response, either cellular or molecular events generally reduce the effect of the injury or of the infection; this process contributes to restore tissue homeostasis and resolve acute inflammation itself. Nevertheless, when not adequately controlled, acute inflammation can turn to chronic, thereby leading to the onset of several diseases. The tissue inflammation is characterized by sweating, heat, pain and loss of tissue functionality, which is due to the local immune, vascular and inflammatory system response to infection or damage. The innate immune system plays a major role in the process, and also promotes the involvement of the acquired immunity. Macrophages as well as dendritic cells are essential for the innate response, but also epithelial or endothelial cells and fibroblast can contribute as well. Significant microcirculatory factors that arise from the inflammatory response include vascular permeability alteration, recall and accumulation of leukocytes and liberation of inflammatory mediators [Ferrero-Miliani, L. et al., 2007].

Inflammation mechanism

Inflammation involves the activation of several pathways that regulate the levels of mediators within the tissues and the recruitment of inflammatory cells from the blood. The activation of a specific pathway rather than another depends on the nature of the initial stimulus and its location, but they all share the common initial mechanism of activation of the tissue-resident macrophages, followed by the activation of the appropriate inflammatory pathway and the release of the inflammatory markers, which finally initiate the recruitment of the inflammatory cells.

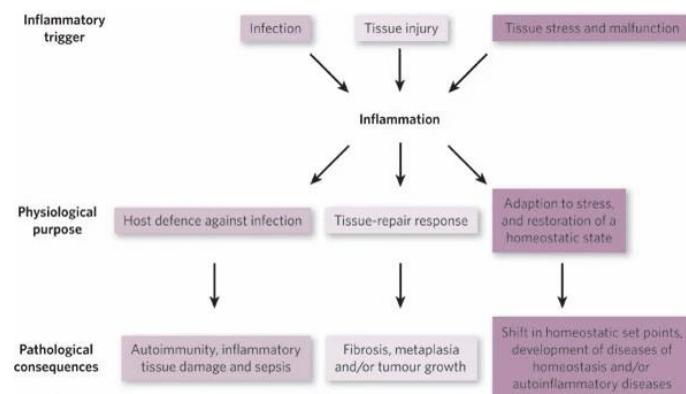


Figure 1. Physiopathological outcomes of inflammation.

The primary and more direct effect of these mediators is a local inflammatory exudate. The plasma proteins as well as leukocytes (mostly neutrophils) normally confined into the blood vessels are now able to move into the extravascular tissues around the infection (or injury) site.

Once arrived to the affected tissue, neutrophils are triggered either by direct exposure to pathogens or by the effect of cytokines secreted by local cells. Neutrophils then attempt to eliminate the invading pathogen by secreting the components of their granules, consisting of proteases and other cellular components such as reactive oxygen (ROS) and reactive nitrogen species, proteinase 3, cathepsin G, and elastase. These very potent effectors inadequately discriminate between the pathogen and the host itself, thereby resulting in some inevitable collateral damage [Nathan, C., 2002].

An acute successful inflammatory response materializes in the removal of the infectious agents shortly followed by a healing phase, which is mainly mediated by tissue-resident and recruited macrophages. The resolution of inflammation was originally considered as a passive process, but recently it was demonstrated that resolution of inflammation is an active response carried out by specific pro-resolving mediators (SPMs), such as protectins, maresins, resolvins, and lipoxins macrophages [Serhan, C. N. et al., 2011]. SPMs perform a dual role by combining pro-resolving and anti-inflammatory activities, both mediated by interactions with specific receptors. N-formyl peptide receptor 2 (FPR2) has been reported to be a target for SPMs, and its activation by these pro-resolving mediators can contribute to the resolution of inflammation [Crocetti L. et al., 2020]. If the acute inflammatory response fails to resolve the primary stimulus, the neutrophil infiltrate is replaced by macrophages and by T cells; if also this second response is not able to afford a resolution, a state of chronic inflammation occurs, leading to a granuloma formation [Chen, L. et al., 2017].

The receptors capable of activating the inflammatory response are known as pattern recognition receptors (PRRs), and can be triggered by different types of sources, such as pathogen-associated molecular patterns (PAMPs) or danger-associated molecular patterns (DAMPs). These recognition receptors include toll-like receptors (TLRs), C-type lectin receptors (CLRs), and NOD-like receptors (NLRs) [Takeuchi, O. et al., 2010]. The signal paths triggered by TLRs, and NLRs lead to the activation of some main transcription factors such as NF- κ B (Nuclear Factor κ -light chain-enhancer of activated B cells), AP-1 (Activated Protein-1) and IRF3, 7 and 5 (Interferon Regulatory Factors). The NF- κ B family consists of 5 transcription factors, namely p50, p52, RelA (p65), RelB and c-Rel, all playing a key role in inflammation, immune response, survival, and even cell apoptosis processes [Moynagh, P. N., 2005].

Among the principal kinases involved in PRR cascade are found IRAK (Interleukin-1 Receptor-Associated Kinase), TRAF (TNF Receptor-Associated Factor), MAPK (Mitogen-Activated Protein Kinase) and IKK (I κ B Kinase).

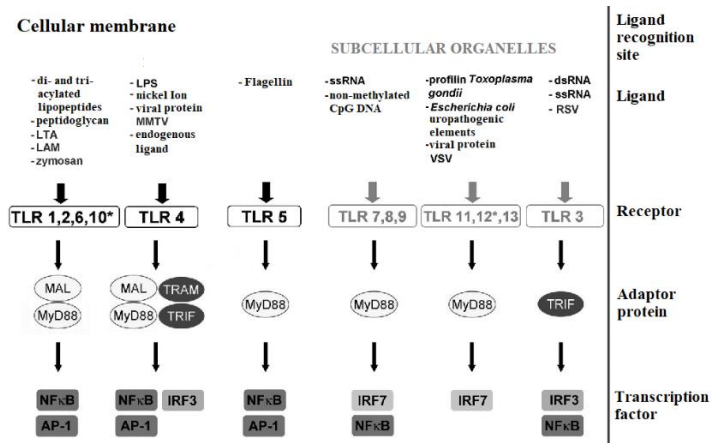


Figure 2. Classification and properties of mammalian TLRs.

Regarding the MAPKs, they are a family of serine or threonine proteases, which include the extracellular-signal-regulated kinases ERK1/2, p38 MAP kinase, and C-Jun N-terminal kinase (JNK). Each pathway involves three components: a MAPK, a MAPK kinase (MAPKK), and a MAPKK kinase (MAPKKK). ERKs are generally triggered by mitogens and cell differentiation signals, whereas inflammatory stimuli and stress activate JNKs and p38 [Sabio, G. et al., 2014].

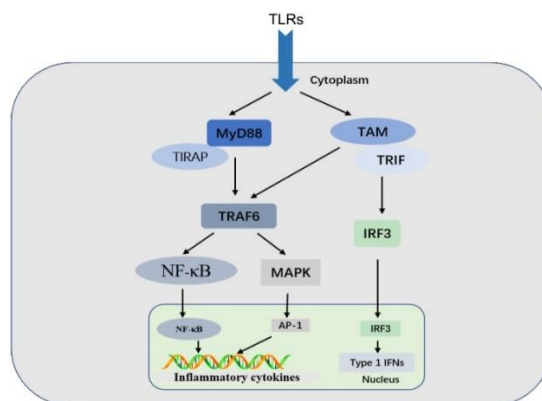


Figure 3. Intracellular cascade MyD88- dependent pathway activated by TLRs.

Anti-inflammatory therapies

Several drugs classes can control the inflammation processes, each having as benefits and disadvantages. The first class of drugs worthy of mention are non-steroidal anti-inflammatory drugs (NSAIDs) and of course among them the COX1/2 inhibitor Aspirin is the most well-known and widely used drug in the world. However, the use of NSAIDs, also COX2 selective inhibitors, is always accompanied by side effects, such as gastrointestinal problems and adverse cardiovascular events [Dinarello, C. A., 2010].

The second most widely used class of anti-inflammatory drugs, with different therapeutic applications then NSAIDs, are the glucocorticoids which show severe side effects, especially for prolonged therapies, including increased blood glucose concentration, type 2 diabetes mellitus, reduced

calcium fixation and subsequent osteoporosis, impotence, decreased libido, hypoandrogenism, depression, loss of skin and muscle mass and hypertension [Dinarello, C. A., 2010].

Another class that contains a wide selection of drugs is the so-called "biologicals". They include agents that reduce the activity of specific cytokines or their receptors, compounds able to block lymphocyte passage in tissues or to prevent the action of monocytes and lymphocytes or finally, compounds that inhibit B lymphocytes. The therapy with cytokine inhibitors is widely applied in autoimmune diseases, such as rheumatoid arthritis, inflammatory bowel disease, psoriasis, and multiple sclerosis, but these drugs show severe side effect, in particular the lowering of immune defenses and also a carcinogenic effect [Dinarello, C. A. 2009].

Other targets for novel drug discovery are inhibitors of protease, which have an important part either in initiating the inflammatory process as well as maintaining it [Pott, G. B. et al., 2009].

A series of small molecules noted as DMARDs (disease-modifying antirheumatic drugs), not chemically related but exhibiting a common effect on rheumatoid arthritis, have been identified. Despite their name, they are also very effective in other inflammatory diseases, such as Chron's disease. This class includes methotrexate (a folate reductase inhibitor), chloroquine and hydroxychloroquine (antimalarial agents), rituximab (a monoclonal antibody), etc.



UNIVERSITÀ
DEGLI STUDI
FIRENZE

***A. Design, synthesis and pharmacological
evaluation of new human neutrophil elastase
(HNE) inhibitors with heterocyclic scaffold***

Supervisor: Prof.ssa Maria Paola Giovannoni

Table of Contents

1. Introduction	10
1.1. Neutrophil serine protease	10
1.2. Human neutrophil elastase (HNE)	12
1.3. Physiological role of HNE	14
1.4. HNE endogenous inhibitors	16
1.5. Pathologies related to HNE	19
1.6. HNE inhibitors	29
Section I	40
2. Background and aims of the work	40
3. Chemistry	42
4. Schemes	45
5. Results and discussion	49
5.1. Biological evaluation and structure-activity relationships (SARs) analysis	49
5.2. Molecular Modeling	56
5.3. ADMET assessment	61
6. Conclusions	64
Section II	65
7. Background and aims of the work	65
8. Chemistry	68
9. Schemes	73
10. Results and discussion	77
10.1. Biological evaluation and structure-activity relationship (SAR) analysis	77
10.2. Gas chromatography-mass spectrometry (GC-MS)	81
10.3. X-ray crystallography	84
10.4. Molecular Modeling	87
11. Conclusions	88
12. Experimental section	89
12.1. Methods	142

1. Introduction

1.1. Neutrophil serine protease

Proteases are proteolytic enzymes, which are able to transform the proteins in smaller fragments by hydrolyzing the peptide bonds. Performing such an important reaction, they are involved in many physiological processes and they are considered essential signaling molecules [Page, M. J. et al., 2007].

In 1993, Rawlings & Barrett classified the proteases in four types depending on the aminoacids of the catalytic site: serine, cysteine, aspartic, and metallo proteases [Rawlings, N. D. et al., 1993]. In serine proteases the serine hydroxyl is responsible for the nucleophilic attack at the peptide bond, while for cysteine proteases is the thiol group of the catalytic site. In both aspartic and metallo-peptidases, the nucleophile is a water molecule, activated by two aspartates in the aspartic proteases, or by one or two metal ions (mainly zinc but also cobalt, manganese, nickel, copper, and iron) in metallo-peptidases.

In 1995, a fifth catalytic type was discovered when, solving the structure of the proteasome, three of the fourteen different subunits possessed an N-terminal threonine acting as nucleophile [Seemüller, E. et al., 1995]. Lately, in 2004, the sixth catalytic type was identified. Certain fungal endopeptidases, now known as eqolysins, were discovered to be glutamate peptidases [Fujinaga, M. et al., 2004]. Finally, among the proteolytic enzyme, in 2011 were listed the asparagine peptide lyase as seventh catalytic type. However, these enzymes are not peptidases because the cleavage of the peptide bonds does not involve hydrolysis, but an elimination reaction through the asparagine in the active site [Rawlings, N. D. et al., 2011].




<chem>NC(CO)C(=O)O</chem> Serine	<chem>NC(CS)C(=O)O</chem> Cysteine	<chem>NC(CC(=O)O)C(=O)O</chem> Aspartate	 Metalloprotease	<chem>NC(C(O)C)C(=O)O</chem> Threonine	<chem>NC(CC(=O)O)C(=O)O</chem> Glutamate	<chem>NC(C(=O)N)C(=O)O</chem> Asparagine
Elastase Kallikrein Plasmin Prostate-specific antigen Protein C Thrombin Trypsin	Cathepsin B Cathepsin C Cathepsin L	Cathepsin D Cathepsin E Pepsin Renin	MMP-1 MMP-2 MMP-9	Proteasome	 Not found in mammals so far	 Not found in mammals so far

Figure 1. Classification of the known proteases.

Over one third of all proteolytic enzymes are serine proteases and they are classified into 13 clans or super families depending on the catalytic mechanism, and 40 families on the basis of common ancestry [Di Cera, E., 2009]. The clan, the family and the holotype are classified using an identifier. Two letters identify a clan: the first one indicates the catalytic type, such as 'A' for aspartic peptidase, 'C' for cysteine peptidase, 'G' for glutamic peptidase, 'I' for inhibitors that are proteins, 'M' for metallopeptidase, 'P' for peptidases of mixed catalytic type, 'S' for serine peptidase, 'T' for threonine peptidase, 'N' for asparagine lyase, and 'U' for peptidases of unknown catalytic type. The second letter is assigned sequentially as each clan is identified [Rawlings, N. D. et al., 2018].

Their family name “serine” comes from the fundamental amino acid serine present inside the active site, which attacks the carbonyl moiety of the substrate’s peptide bond, forming an acyl-enzyme intermediate [Hedstrom, L., 2002]. The four main clans of serine proteases include the superfamily A or PA (e.g., chymotrypsin), the subtilisin (SB), SC (e.g., carboxypeptidase C), and SF (e.g., bacterial leader peptidase I) [Rawlings, N. D. et al., 2014]. Significant differences exist in the distribution of each clan across species. For example, proteases of superfamily A are highly expressed in eukaryotes and less in prokaryotes and plant genomes, while clans SB and SC are most expressed in other organisms. The main three subfamilies of PA serine proteases can be distinguished based on their substrate specificity: the trypsin-like serine proteases, including some granzymes and tryptase, cleave protein substrates at positively charged lysine and arginine residues. Chymotrypsin-like family members cleave substrates after large hydrophobic amino acids such as alanine and leucine. Finally, elastase-like serine proteases cleave substrates by small hydrophobic residues such as valine.

Human neutrophil elastase (HNE) and proteinase 3 (PR3) belong to this last family. Cathepsin G (CG) possesses both chymotrypsin-like and trypsin-like substrate specificity, demonstrating that a serine protease can belong to more than one family [Heutinck, K. M. et al., 2010]. In 2012, Perera N. C. et al. identified an additional serine protease of the family of NE and PR3, named neutrophil serine protease 4 (NSP4) [Perera, N. C. et al., 2012].

HNE, PR3, CG and NSP4 are called neutrophil serine proteases (NSP) since they are synthesized and stored inside neutrophils, which are a type of white blood cell that, among other functions, are addressed to the protection from infections. Neutrophils make up approximately 40 - 60 percent of the white blood cells in our body, and are the first line of defense against invading microorganisms. Neutrophils are able to phagocytose and degrade pathogens with a combination of reactive oxygen species (ROS), proteases and antimicrobial peptides [Reeves, E. P. et al., 2002]. Neutrophils are polymorphonuclear cells (PMN), being their nucleus divided in 3-5 lobes, and contain four types of granules: azurophilic granules (primary), specific granules (secondary), gelatinase granules (tertiary), and secretory granules [Manley, H. R. et al., 2018].

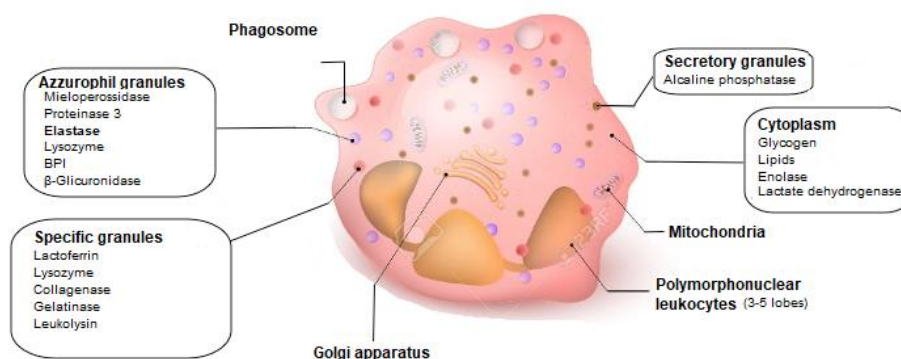


Figure 2. Polymorphonuclear neutrophil composition (PMNs).

These four classes of granules are produced sequentially during different stages of neutrophil differentiation in the bone marrow, and are classified according to their protein content and their ability to be released after neutrophil activation. In particular, azurophil granules are mainly involved in intracellular degradation of the pathogen inside the phagolysosome, due to their high content of myeloperoxidase (MPO), defensins and serine proteases, such as the above mentioned HNE, CG and PR3 [Pham, C. T. N., 2006]. In addition, human neutrophils also express azurocidin (AZU), an inactive serine protease homolog with chemotactic and antimicrobial activities [Almeida, R. P. et al., 1996].

It has been shown that the release of serine proteases from neutrophils modulates the inflammation response, modifying or activating chemokines, cytokines and growth factors, and cleaving specific cell surface receptors. Serine proteases can also induce caspase-independent cell apoptosis and initiate adaptive immune responses through the activation of lymphocytes [Pham, C. T. N., 2008].

NSP are synthesized as inactive zymogens that require two N-terminal proteolytic modifications to become active. After the signal peptide removal, the pro-enzyme is further processed by the lysosomal cysteine protease dipeptidyl peptidase I (DPPI, also known as cathepsin C or CatC) and transferred to the granules where they are stored as active enzymes [Adkison, A. M. et al., 2002]. In addition, neutrophil serine proteases also undergo C-terminal processing. Although this proteolytic modification is not required for enzymatic activity, the removal of this C-terminal sequence reveals a docking site that allows HNE to interact with AP3 (Adaptor Protein 3, responsible for protein trafficking to lysosomes and other related organelles). The retention of this C-terminus apparently results in mistrafficking of HNE and its relocation to the surface membrane [Benson, K. F. et al., 2003].

1.2. Human neutrophil elastase (HNE)

HNE is a globular glycoprotein of about 30 kDa belonging to the chymotrypsin family. It consists of a single polypeptide chain of 218 amino acids and two asparagine-linked carbohydrate side chains at Asn95 and Asn144. It is stabilized by four disulfide bridges and exhibits basic properties due to the presence of 19 arginine residues, resulting in an isoelectric point around 10-11. The active HNE structure is composed of an N-terminal activation domain and three flexible loops [Tsai, Y. F. et al., 2015].

The primary structure shows homology with PR3 (57%) and CG (37%), in agreement with their evolution from a common gene. The gene expressing HNE is called ELA2, it consists of five exons and four introns and it is located in the terminal region of the short arm of chromosome 19. The region of ELA2 also contains the genes for the homologous proteases PR3 and azurocidin [Zimmer, M. et al., 1992]. Mutations in ELA2 can be a risk factor for severe congenital and cyclic neutropenia, a rare disease characterized by oscillations in the production of neutrophils and other blood cells. In addition to neutrophils, HNE is also present in other cells, like mast cells, monocytes, eosinophils,

keratinocytes, and fibroblasts [Tsuji, N. et al., 2001]. HNE in neutrophils exceeds 5 mM concentration, and the total amount in a single cell has been estimated to be up to 3 picograms, all sequestered by compartmentalization in azurophil granules [Liou, T. G. et al., 1995]. Azurophil granules rapidly release into the extracellular space the active form of HNE, which in part remains associated with the outer plasma membrane of the neutrophil [Owen, C. A. et al., 1995]. The X-ray three-dimensional structure of HNE in complex with the turkey ovomucoid third domain (OMTKY-III), or with the two synthetic inhibitors MeO-Suc-Ala-Ala-Pro-Val chloromethyl ketone or MeO-Suc-Ala-Ala-Pro-Ala chloromethyl ketone, shows the two six-stranded β -barrel domains typical of chymotrypsin-like serine proteases. Only an intermediate segment and the carboxy-terminal segment is organized in an α -helix. The active-site residues are located in a crevice between the two β -sheet, and they contain the so-called catalytic triad constituted by Ser195, Asp102 and His57 [Korkmaz, B. et al., 2008].

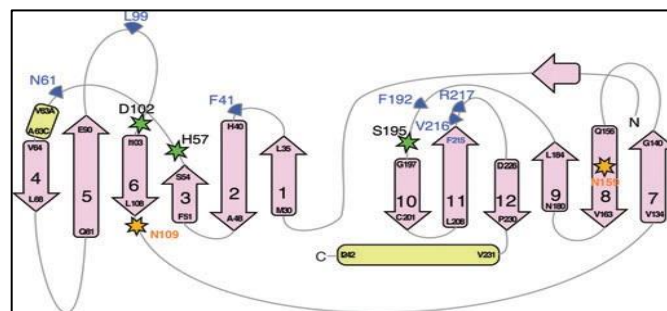


Figure 3. Secondary structure of human neutrophil elastase (HNE).

The powerful nucleophile Ser195 hydroxyl group is responsible for the attack at the amidic bond of the substrate and for its hydrolysis. Going more into detail, the hydrolysis of the peptide bond occurs via two tetrahedral intermediates. The OH group of Ser195, activated by His57 attacks the carbonyl group of the substrate leading to the first tetrahedral intermediate [Hajjar, E. et al., 2010]. This intermediate is then stabilized by the backbone N-atoms of Gly193 and Ser195, which together generate a positively charged pocket within the active site known as the “oxyanion hole”. Hydrogen bond interactions in the “oxyanion hole” contribute to ground and transition state stabilization (1.5 - 3.0 kcal/mol) [Bobofchak, K. M. et al., 2005]. His57 transfers a proton to the amine of the tetrahedral intermediate, causing the break of the bond and resulting in the formation of a covalent acyl-enzyme complex. Finally, a molecule of water attacks the acyl-enzyme complex to generate a new tetrahedral intermediate, stabilized by the “oxyanion hole” as well, which then collapses regenerating the enzyme HNE [Walker, B. et al., 2010].

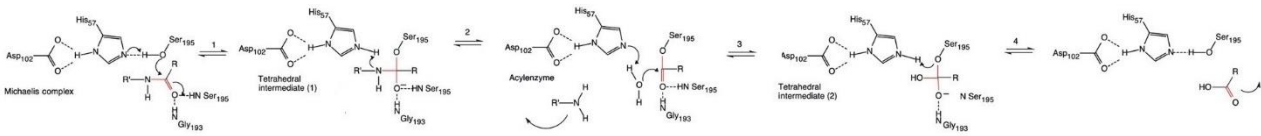


Figure 4. Cleavage mechanism of HNE.

1.3. Physiological role of HNE

HNE is involved in many different functions; being an important component of the neutrophil extracellular traps (NETs), it takes part in antimicrobial defence. It is also an important regulator in the local inflammatory response modulating activation and degradation of chemokines; even if this effect is not entirely clear, it is known that it helps the regulation of cell recruitment, the activation of lymphocytes and the induction of apoptosis. Finally, HNE contribute to the maintenance tissues homeostasis, repairing damaged tissues as well as degrading structural proteins.

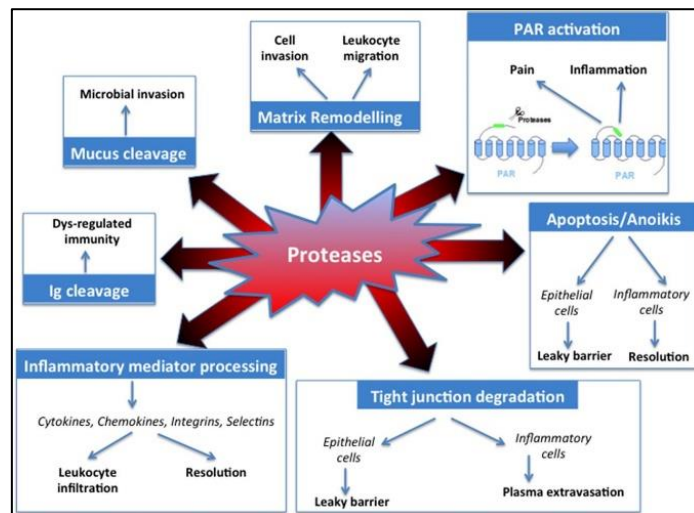


Figure 5. Physiological processes involving HNE.

- ***Anti-inflammatory activity:***

Chemokine and cytokine bioavailability regulation has been correlated with serine protease activity. Moreover, growing evidences suggest that neutrophil serine proteases can modify the activity of several chemokines, thus providing an alternative mechanism to convert cytokine precursors into their active form. Since the importance of chemokines and cytokines in the inflammatory response is well known, it is clear that also proteases, such as HNE, are strongly implicated in the regulation of this process.

It has been shown that mature IL-18 released by neutrophils can be hydrolyzed by HNE, leading to a decrease of biological activity [Robertson, S. E. et al., 2006]. Despite the most part of the precursor of tumor necrosis factor alpha (TNF- α) is activated by the TNF- α converting enzyme (TACE), as well as the pro-IL-1 β is converted to its active form by caspase 1, recent studies indicate that TNF- α and IL-1 β may be alternatively processed also by serine proteases. Other studies report further and

sometime controversial information. Scuderi and co-workers indicated that HNE can degrade TNF- α , resulting in its loss of its activity [Scuderi, P. et al., 1990], others suggest that CG and HNE at the appropriate concentrations can process the membrane-bound TNF- α into a soluble and biologically active form [Mezyk-Kopec, R. et al., 2005].

Finally, HNE has been shown to degrade and inactivate IL-6 at sites of inflammation [Bank, U. et al., 2000], and also to be able to process and modulate some receptors, such as protease-activated receptors (PARs) and Toll-like receptors (TLRs). The first mentioned group of receptors are ubiquitously expressed in various tissues and cells, and are able to activate a signaling cascade via phospholipase C [Vergnolle, N., 2009]; Toll-like receptors (TLRs) are transmembrane glycoproteins that remarkably contribute to host defense against microbial infections and innate immune response [Akira, S. et al., 2006].

- Anti-bacterial activity:

HNE plays a key role in the defense against invading microorganism. Its antibacterial function can be a direct intracellular killing of bacterial cells, as demonstrated for Klebsiella pneumonia, Escherichia coli [Belaouaj, A. A. et al., 2000], [Belaouaj, A. A. et al., 1998] and for the Gram-positive Streptococcus pneumonia, for which a concerted action of HNE, CG, and PR3 within the phagocytic vacuole was reported [Standish, A. J. et al., 2009]. Nevertheless, the direct antimicrobial activity is demonstrated only for few bacterial species, and it is generally combined with the myeloperoxidase and the reactive oxygen species generated by the NADPH oxidase complex [Segal, A. W., 2005].

In addition to intracellular killing, a second mechanism of extracellular killing is used by neutrophils, and this occurs through neutrophil extracellular traps (NETs), which are structures able to bind or trap bacteria. Upon NET induction, HNE translocates to the nucleus and cleaves histones to facilitate the DNA decondensation, central to this process [Papayannopoulos, V. et al., 2010]. The release mechanism of NETs outside the cell is called NETosis, a form of neutrophil specific cell death, which is stimulated by cytokines, such as TNF- α or IL-8 [Keshari, D. R. et al., 2012], or antibodies [Kessenbrock, K. et al., 2009].

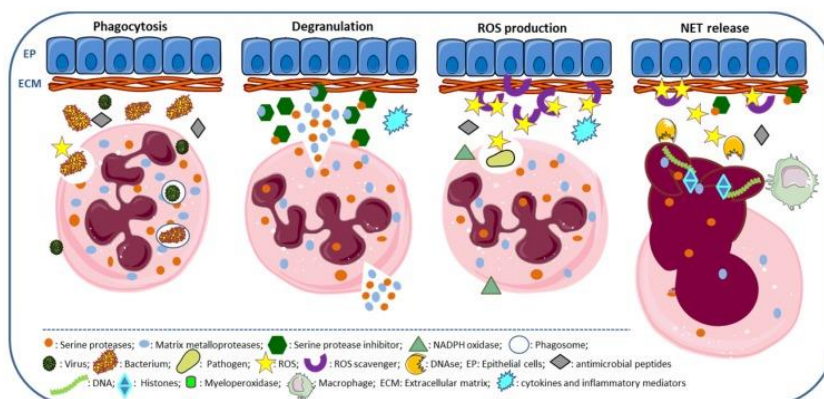


Figure 6. Antimicrobial mechanism of neutrophils.

NETs consist of chromatin fibers with diameters of 15-17 nm containing DNA and the histones H1, H2A, H2B, H3, and H4. Moreover, the DNA fibers are decorated with several proteins like neutrophil elastase (HNE), myeloperoxidase (MPO), cathepsin G (CG), proteinase 3 (PR3), high mobility group protein B1 (HMGB1), and LL37 [Brinkmann, V. et al., 2004]. NETs are currently believed to have three functions: first, they catch the extracellular NSPs and other antimicrobial agents released from neutrophils to prevent host damage at distal sites; second, the capture of the bacteria to prevent its spreading, and third to kill all the invading microorganism via the antimicrobial agents inside NETs themselves [Papayannopoulos, V. et al. 2010]. The ability of trapping invading microorganism is due to the formation of electrostatic interaction of the NSP bonded to the traps and the envelope of the bacteria. The spectrum of activity of this neutrophil defensive mechanism is very broad and it can work either on gram negative or positive bacteria [Yang, H. et al., 2016].

- Tissue homeostasis:

HNE contributes to the maintenance of tissue homeostasis repairing damaged tissues as well as degrading structural proteins. The term elastase is not quite correct, since HNE does not only degrade elastin, a protein responsible for the elasticity of lung tissue, rather, HNE degrades a variety of extracellular matrix and plasma proteins, including collagen (types I-IV), fibronectin, laminin, and proteoglycans [Chua, F. et al., 2006].

Other HNE substrates are coagulation factors (fibrinogen and factors V, VII, XII, and XIII), plasminogen, immunoglobulin G (IgG), IgA and IgM, thrombomodulin, platelet, complement factors C3 and C5, complement receptors [Taylor, C. et al., 1997; Anderssen, T. et al., 1993; Turkington, P. T., 1991]. HNE can also degrade other proteases present inside neutrophil granules, as well as some protease inhibitors, leading to their activation or inactivation [Senior, R. M. et al., 1983].

1.4.HNE endogenous inhibitors

Since HNE has a potent proteolytic activity and it is released in millimolar concentration in the external environment, its action must be adequately regulated by endogenous inhibitors in order to prevent accessory damages. So far, 37 HNE different inhibitors have been identified in the human body all belonging to the family of SERPINS, divided into 9 subgroups (clade A to I) based on their phylogenetic relationship [Lawrence, D. A. et al., 1994]. SERPINS include: α 1-antitripsin (α 1-AT, ATT or α 1-proteinase inhibitor) [Miravittles M., 2012], monocyte/neutrophil elastase inhibitor (MNEI, also called serpinB1) [Cooley, J. et al., 2001], secretory leukocytes proteinase inhibitor (SLPI) [Sallenave, J. M., 2000], elafin [Alam, S. R. et al., 2012] and α -1-macroglobulin, which is a general plasma inhibitor of serine, cysteine and metalloproteases [Groutas, W. C. et al., 1997]. These endogenous inhibitors can be classified as systemic (α 1-AT) or alarm proteinase (SLPI and elafin) [Roghani, A. et al., 2006]. SERPINS are particularly abundant in the liver, but are ubiquitously expressed in the body.

α1-antitrypsin (ATT): α1-AT is a blood plasma glycoprotein and its main function is to regulate the activity of HNE in the low respiratory tract, with a smaller role in defending against damage by other serine proteases, such as cathepsin G and proteinase 3. The AAT protein is encoded by the protease inhibitor (Pi) locus on chromosome 14q and contains 394 amino acids. The part interacting with the protease is constituted by 3 β-sheet and a central reactive loop; the methionine at position 358 in the loop is the amino acid responsible for its activity [Wood, A. M. et al., 2007].

α1-antitrypsin deficiency (AATD) was first described in 1963 by Laurell and Eriksson [Laurell, C. B. et al., 1963] and is one of the main factors of the onset of pathologies such as COPD (chronic obstructive pulmonary disease), cirrhosis and hepatocellular carcinoma [Sorrorche, P. B. et al., 2015].

SerpinB1: SerpinB1 is one of the most efficient inhibitors of HNE, belongs to the clade B serpins, and it is able to inhibit the serine proteases HNE, PR3, and CG. SerpinB1 is mainly expressed in macrophages and neutrophils, and it accumulates in high concentration in the cytoplasm and granules of neutrophils [Benarafa, C. et al., 2007].

SerpinB1 lacks a signal peptide and it is not released in the extracellular environment via the classic secretory pathway, but it was speculated its extracellular presence was the result of cell necrosis [Yasumatsu, R. et al., 2006]. SerpinB1 is a multifunctional cytoplasmic protein since it acts as a protease inhibitor in its native form, but the cleavage of SerpinB1 by its corresponding proteases can lead to the loss of antiprotease properties and to the acquisition of other functions, such as DNase activity. In fact, a SerpinB1 derivative equipped with nuclease activity, called L-DNase II, was isolated from porcine spleen [Torrighia, A. et al., 1998].

Moreover, studies showed that SerpinB1 plays a pro-survival role in neutrophils, as demonstrated by the recently reported regulation of the spontaneous death of aging neutrophils, via counterbalancing the activity of PR3 during leakage of the protease from azurophilic granules [Loison, F. et al., 2014]. An intrinsic defect in survival, observed in neutrophils derived from SerpinB1 knock-out mice, may also be caused by a higher propensity of these cells to die by NETosis, indicating that SerpinB1 may also act as negative regulator of NETosis [Majewski, P. et al., 2016].

Secretory Leukocyte Protease Inhibitor (SLPI): Secretory leukocyte protease inhibitor is a single polypeptide cationic protein of 107 amino acids, also known as antileukoprotease (ALP), bronchial secretory inhibitor (BI), human seminal inhibitor I (HUSI-I), cervix uterine secretion inhibitor (CUSI), mucous proteinase inhibitor (MPI), or secretory leukoprotease inhibitor (SLI). Its more documented role is the inhibition of serine proteases, including human HNE and CG but not PR3 [Doumas, S. et al., 2005].

The inhibitor is composed of two four-disulfide core domains, also called “whey acidic protein” (WAP) domains. The N-terminal WAP I and C-terminal WAP II domains share 35% homology, but their biological function is distinct [Vogelmeier, C. et al., 1996]. The WAP II domain is primarily responsible for the antiprotease activity of the SLPI, while the biological function of the N-terminal WAP I domain

it is not completely understood, although the antimicrobial potential of SLPI is thought to mainly reside in this domain.

In contrast to SerpinB1, SLPI is predominantly secreted at mucosal surfaces as a product of epithelial cells. The inhibitor is also expressed in leukocytes, including neutrophils, macrophages, and dendritic cells [Majchrzak-Gorecka, M. et al., 2016]. Even if SLPI was shown to inhibit a broad spectrum of proteases, one of its main target is HNE, and the complex that SLPI form with HNE is the strongest among all the complexes of the same inhibitor with any other proteases [Moreau, T. et al., 2008]. Notably, although SLPI is thought to be the principal inhibitor of HNE in the neutrophil cytosol, it is primarily stored in secondary granules in neutrophils [Jacobsen, L. C. et al., 2008]. This contrast might be a result of different activation, since SLPI, similarly to HNE, is likely to migrate between different cell compartments in response to neutrophil stimulation.

Secretory leukocyte protease inhibitors may also be useful to protect the cells from the harmful effects of NETosis in synergy with serpinB1, inhibiting the NETs formation [Zabieglo, K. et al., 2015].

Elafin: It is known as peptidase inhibitor 3 or SKALP (skin derived anti-leukoproteinase). Elafin is a 6 kDa soluble protein, which contains 57 amino acids, and it is composed of an N-terminal whey acidic protein (WAP)-domain exerting its antiproteolytic properties [Shaw, L. et al., 2011].

It is generated from pre-elafin, also known as trappin-2, a longer peptide containing 117 amino acids (10 kDa), which undergoes proteolytic cleavage releasing elafin [Butler, M. W. et al., 2006]. Both proteins, elafin and trappin-2, are inhibitors of neutrophil serine proteases [Zani, M. L. et al., 2004]. Besides the presence in the human skin, elafin can be found in a variety of organs and tissues, including the oral mucosa, esophagus, vagina [Pfundt, R. et al., 1996], uterus, ovary tubes [Ghosh, M. et al., 2010], lung [Sallenave, J. M. et al., 1991] and in epithelial cells, including keratinocytes as well as in neutrophils and macrophages. Furthermore, it was detected in ovarian carcinoma [Claus, A. et al., 2010]. Other than protease inhibitor function, Elafin presents immunomodulatory activity, either reducing or stimulate immunological reactions, and antimicrobial properties [Guyot, N. et al., 2010]. Elafin is currently in clinical development for the use in post-operative inflammatory diseases [Kaschwich, M. et al., 2016].

α_2 -macroglobulin (α_2M): it is a 725 kDa homotetrameric plasmatic proteinase inhibitor and the four identical subunits contain 1451 amino acid [Andersen, G. R. et al., 1995]. The broad specificity of the α_2 -macroglobulins is due to its inhibitory mechanism, different from the other active site directed proteinases inhibitors. In fact, it seems that the large size of human α_2M was responsible for the trapping of the proteases, which, in turn, afford a conformational change of α_2M [Barrett, A. B. et al., 1973]. This modification is the result of the break of a single peptide bond in the central region of one subunit constituting the protein, and the specific bond cleaved depends on the protease entrapped. Only endopeptidases can cause the conformational change fundamental for the inhibitory activity and, by analogy with the “waiting trap”, the proteinase-susceptible region has been called the “bait region” [Salvesen, G. S. et al., 1980]. Because of physical constraints, entrapped proteinase

molecules, are unable to hydrolyze big substrates but retain the ability to hydrolyze small ones. Due to α_2 -macroglobulin dimension, the diffusion through the vascular endothelium is not possible, and, for this reason, its antiprotease activity occurs only in the blood circulation [Sottrup-Jensen, L. 1989].

1.5. Pathologies related to HNE

Several inflammatory pathologies, especially of the respiratory system, are related to the potent proteolytic activity of HNE, and, in many cases, the onset of these disorders depends on an imbalance between HNE and its antiproteases. The massive migration and infiltration of neutrophils and the subsequent release of high concentration of proteolytic enzymes, including serine proteases, not adequately controlled, are the responsible for the degradation of the matrix component such as elastin and elastic component of the lung connective tissue [Gadek, J. E. et al., 1990]. The main pathologies are cystic fibrosis (CF), chronic obstructive pulmonary disease (COPD), acute respiratory distress syndrome (ARDS) and acute lung injury (ALI), pulmonary arterial hypertension (PAH) and idiopathic pulmonary fibrosis (IPF). Furthermore, HNE is involved in different type of cancer, such as lung and breast cancer, but also in atherosclerosis, rheumatoid arthritis and psoriasis [Crocetti, L. et al., 2019].

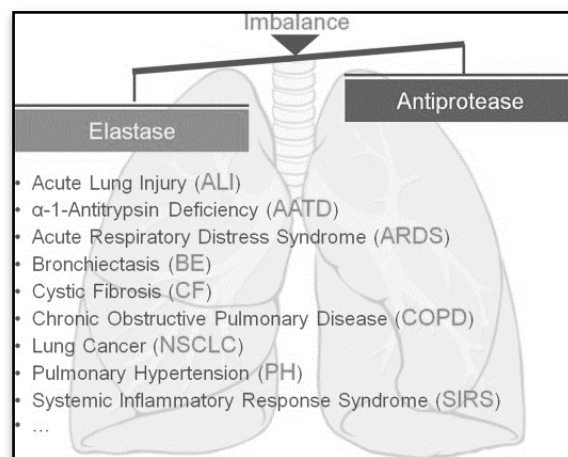


Figure 7. Representation of the imbalance between HNE and antiproteases.

Cystic fibrosis: It is the most common lethal genetic disease in white populations. Cystic fibrosis is caused by a mutation of the gene encoding cystic fibrosis transmembrane conductance regulator (CFTR) protein, which is expressed in many epithelial and blood cells [Vankeerberghen, A. et al., 2002].

Although CFTR functions mainly as a chloride channel, it has many other regulatory roles, including inhibition of sodium transport through the epithelial sodium channel, regulation of the outwardly rectifying chloride channel, regulation of ATP channels, regulation of intracellular vesicle transport, acidification of intracellular organelles, and inhibition of endogenous calcium-activated chloride channels [Mehta, A., 2005]. CFTR is also involved in bicarbonate-chloride exchange and a deficiency

in bicarbonate secretion leads to a decrease of solubility and aggregation of luminal mucins [Quinton, P. M., 2008].

More than 1500 CFTR mutations have been identified, but the functional importance of only a small number is known. There are several hypotheses regarding how CFTR dysfunction leads to the phenotypic disease known as cystic fibrosis, and one of the most accredited is the low-volume hypothesis. This hypothesis suggests that the absence of the CFTR gene results in a reduction in the total volume of NaCl in cystic fibrosis patients at the level of airway fluids, reducing the osmotic force essential for the transport of water to the lumen. As a result, the airway surface becomes dehydrated and mucociliary clearance slowed [Clunes, M. T., 2007]. The subsequent decrease in periciliary water volume results in a reduction in the lubricating layer between epithelium and mucus, with compression of cilia by mucus, causing inhibition of normal ciliary and cough clearance of mucus. According to this hypothesis, mucus on the epithelium forms plaques with hypoxic niches that can harbor bacteria, particularly, *Pseudomonas aeruginosa* [Matsui, H. et al., 2006].

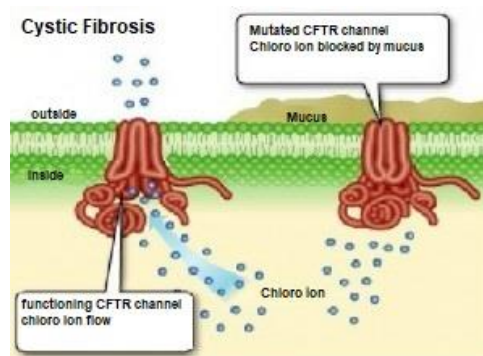


Figure 8. Chloro efflux in normal and mutated CFTR canal.

One of the most serious aspects of the lung disease associated with cystic fibrosis is the sustained, intense inflammation caused by neutrophils and present from very early in life [Kelly, E. et al., 2008]. Normally, neutrophils account for ~ 1% of the inflammatory cell population in epithelial lining fluid, while in lungs affected of CF, neutrophils represent 70% of the inflammatory cells [Birrer, P. et al., 1994]. These neutrophils are ineffective in the clearance of bacteria but play a significant role in the pathogenesis of the lung derangement associated with CF. The lung derangement is in large part mediated by neutrophil proteases and oxidants that overwhelm the normal antiprotease defense of the respiratory epithelial surface [Suter, S., 1989].

Neutrophil elastase (HNE) is the major protease released by neutrophils, and, although it is not the only protease causing the damage, it is clearly its important role in the pathology. HNE directly injures epithelial cells and interferes with the defense mechanisms of the lung by reducing ciliary beat frequency; it deranges mucus glycoprotein secretion, cleaves complement components, and immunoglobulins, and interferes with the ability of neutrophils to kill *Pseudomonas*. Furthermore, HNE plays a major role in the inactivation of elafin [Guyot, N. et al., 2008]. HNE upregulates a host of pro-inflammatory cytokines in lung epithelium acting through toll-like receptors [Greene, C. M. et

al., 2005] and the EGF receptor [Fischer, B. M. et al., 2002]. In addition, it now seems probable that HNE plays a pivotal role in the upregulation of other proteases, including metalloproteinases (MMPs) and cysteinyl cathepsins [Geraghty, P. et al., 2007].

Chronic obstructive pulmonary disease (COPD): pathology distinguished by a persistent airflow obstruction with progressive decline of lungs functions. Its pulmonary component is characterized by airflow limitation that is not fully reversible and usually progressive, associated with an abnormal inflammatory response of the lung to noxious particles or gases [Decramer, M. et al., 2012].

The development of the disease is influenced by environmental determinants, most commonly cigarette smoking, air pollution and occupational exposure. Additionally, genetic risk and possible protective factors play a role in the development of COPD, but, currently, the only known inherited risk factor is α 1-antitrypsin deficiency (AAT) [Matsson, H. et al., 2016]. This pathology is characterized by obstructed airways, followed by loss of alveolar attachments, mucosal inflammation, and mucous obstruction of lumen. The inflammation causes structural damage, narrowing the airways and degrading the lung parenchyma, thus emphysema [Demedts, I. K. et al., 2006]. Other factors involved in the pathogenesis of COPD are an imbalance between proteases and antiproteases, and imbalance between oxidants and antioxidants.

COPD broadly encompasses two pathologic entities, emphysema and chronic bronchitis. Emphysema is defined by alveolar wall destruction and irreversible enlargement of the air spaces distal to the terminal bronchioles and without evidence of fibrosis [Pandey, K. C. et al., 2017].

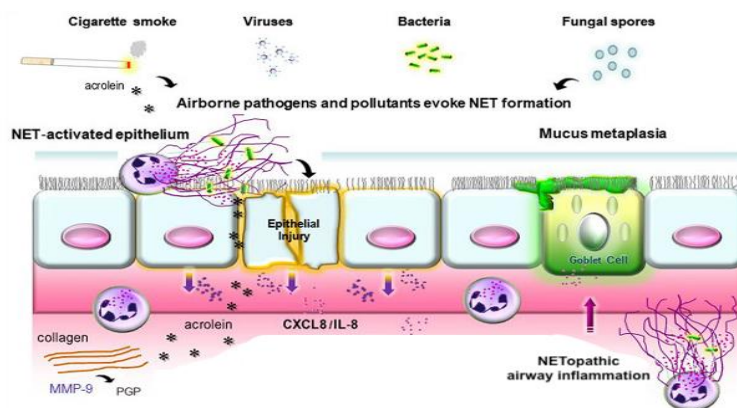


Figure 9. HNE involvement in chronic obstructive pulmonary disease (COPD).

The protease-antiprotease imbalance arises from the activity of inflammatory cells, especially neutrophils recruitment, hence, various proteases including HNE, are released in the site of inflammation. HNE contributes to the pathogenesis of emphysema by the cleavage of extracellular matrix and lung destruction [Abboud, R. T., 2008]. During the cleavage of extracellular matrix, chemotactic fragments are produced, which results in continued accumulation of inflammatory cells and tissue destruction [Weathington, N. M. et al., 2006]. Therefore, inflammation and proteases action are likely to be mutually reinforcing.

Furthermore, HNE induces small airway and alveolar epithelial cell apoptosis using intrinsic pathway; these reactions slow down a serine/threonine protein kinase phosphorylation and activate proteinase activated receptor-1 (PAR1), and finally proceed for apoptosis pathway by caspase3 [Lee, K. M. et al., 2015].

Acute lung injury (ALI) and acute respiratory distress syndrome (ARDS): ALI is a common condition characterized by acute and severe hypoxia that is not due to left atrial hypertension. The term ALI encompasses a continuum of clinical and radiographic changes that affect the lungs, while ARDS represents the more severe end of ALI.

This pathology is defined by a ratio of arterial oxygen fraction of 200 mmHg or less and it shows a high mortality rate because of its resistance to most therapies [Ragaller, M. et al., 2010]. Patients with ALI and ARDS progress through a similar pathophysiological process, irrespective of whether the damage is a direct effect on the alveolar epithelial cells by an external stimulus, or an indirect process resulting from a more distant systemic inflammatory process mediated by cytokines. The inflammatory response consists of vascular endothelial and alveolar epithelial cell damage, production of inflammatory mediators, and accumulation of inflammatory cells, mainly neutrophils, in the lung [Thille, A. W. et al., 2013].

The structural damage is translated clinically into a syndrome of acute respiratory failure that debuts with dyspnea, progressive arterial hypoxemia secondary to severely impaired gas exchange, pulmonary edema, intrapulmonary hemorrhage, and marked increase in ventilatory work [Matthay, M. A. et al., 2012].

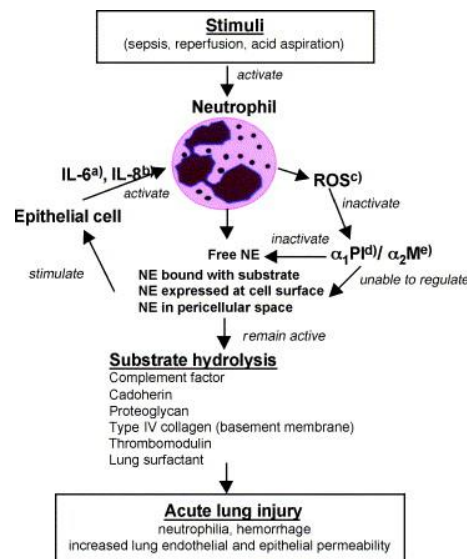


Figure 10. HNE involvement in ALI and ARDS.

According to the Berlin Definition consensus ALI and ARDS are defined as the acute inflammatory response present in patients within 1 week of an insult, with bilateral pulmonary infiltrates, non-cardiogenic pulmonary edema, and arterial hypoxemia, using the arterial oxygen to inhaled oxygen

ratio as mild ($\text{PaO}_2/\text{FiO}_2=200$ to 300), moderate ($\text{PaO}_2/\text{FiO}_2=100$ to 200), and severe ($\text{PaO}_2/\text{FiO}_2$) [Force, A. D. T. et al., 2012].

In ARDS, an initial insult triggers massive liberation of inflammatory mediators, including alarmins, complement activation products, cytokines, chemokines, proteases, and oxidants. Recent studies suggest that neutrophil elastase plays an important role in the pathophysiology of acute lung injury, since HNE can increase the solute permeability of endothelial and epithelial cells and of the basement membrane barrier, important in the development of interstitial alveolar edema [Kawabata, K. et al., 2002].

Neutrophil elastase may also play a critical role in lung inflammation, either by influencing neutrophil chemotaxis and cell adhesion or by inducing the release of inflammatory mediators, such as IL-8, granulocyte-macrophage colony-stimulating factor, and complement factors. Furthermore, exists a possibility that human neutrophil elastase may also contribute to a decrease in respiratory function, not only by inducing alveolar edema but also by damaging alveolar surfactant [Liau, D. F. et al., 1996].

Pulmonary arterial hypertension (PAH): pathology characterized by progressive cardiopulmonary disease in which extensive closure or collapse of the lumen are prevalent in the small to mid-sized pulmonary arterioles, narrowing the blood vessels [Rabinovitch, M. et al., 2014]. Alterations in structure and function of the endothelium occur in conjunction with excessive vascular proliferation, fibrosis and reduced apoptosis of neointimal, medial and adventitial layers, culminating in an occlusive arteriopathy associated with high resistance to blood flow and right heart failure, leading finally to death [Stacher, E. et al., 2012].

It is evident both in experimental and clinical studies that neutrophil elastase can influence pathogenesis of PAH [Kim, Y. M. et al., 2011]. Perivascular inflammation has been observed in all subsets of PAH and correlates with clinical markers of disease progression such as an increase in pulmonary vascular resistance and a decrease in the 6-min walk test [Soon, E. et al., 2010]. The consequences of perivascular inflammation include cytokine production by vascular and inflammatory cells, and degradation of the extracellular matrix (ECM) by proteases [Humbert, M. et al., 2004]. Both the increased cytokine production and the peptides that are released as a result of ECM degradation, cause activation and recruitment of circulating immune cells.

Inhibition of neutrophil elastase activity arrests the progression and induces the regression of the experimentally induced PAH [Cowan, K. N. et al., 2000], while the release of HNE can stimulate adverse remodeling by degrading virtually all the components of the ECM including collagen, fibronectin, and laminin [Lee, K. M. et al., 1998]. As a consequence, the degraded ECM releases bioactive peptides and growth factors such as epidermal growth factor (EGF) and fibroblast growth factor (FGF), which have both mitogenic and motogenic effects on smooth muscles cells and fibroblasts [Chen, P. Y. et al., 2016]. In addition to the impact of HNE on smooth muscles cells

migration and proliferation, this enzyme contributes to PAH pathogenesis by proteolytic modification of cytokines [Taylor, T. et al., 2018].

Idiopathic pulmonary fibrosis (IPF): This pathology is a chronic, progressive, fibrotic disease of unknown etiology characterized by the radiographic and histopathologic pattern of usual interstitial pneumonia [Desai, O. et al., 2018]. Although the origin of IPF is not known, several risk factors have been identified, including cigarette smoking, antidepressant use, gastroesophageal reflux, occupational dust exposure, and genetic predisposition [Enomoto, T. et al., 2003].

The pathogenic cascade of lung fibrosis is thought to be initiated by perpetuated microinjuries to the alveolar epithelium that engenders a dysregulated wound healing response [Fernandez, I. E. et al., 2012]. Through poorly understood processes involving the recruitment and activation of myofibroblasts, the normal lung tissue is obliterated by the accumulation of extracellular matrix (ECM) components [Wynn, T. A. et al., 2011]. Neutrophils might also contribute to fibrosis via their regulation of ECM turnover. Human neutrophil elastase, the main proteolytic product of alveolar neutrophils, is increased in bronchoalveolar lavage (BAL) fluid of IPF patients [Obayashi, Y. et al., 1997]. HNE generates DAMPs (Damage-associated molecular patterns) by degrading various ECM components, such as collagens I, II, III, IV, fibronectin, laminin, and elastin as already explained above, and ex vivo work demonstrates that HNE can induce fibroblast proliferation and myofibroblast differentiation [Gregory, A. D. et al., 2015].

Cancer: HNE seems to be involved in the development and progression of some tumors, which is consistent with the observation that many types of cancer originate in areas of the body where chronic inflammatory states occur, and where neutrophils and their proteases contribute to the progression of the tumor itself [Lerman, I. et al., 2017]. The pro-tumorigenic role of HNE has been established in lung, breast, and colon cancers, among others.

Global deletion of HNE in genetic mouse models of breast and lung cancer notably reduces the number and size of the tumors [Houghton, A. M. et al., 2010; Gong, L. et al., 2013]. HNE may contribute to tumor growth by directly increasing proliferation, migration, and invasion of cancer cells or by inducing angiogenesis within the microenvironment; it may also contribute to tumorigenesis by inactivating tumor suppressors, thereby disinhibiting growth [Pivetta, E. et al., 2014]. Moreover, HNE is one of the main mediators of neutrophil extracellular trap (NET) formation, which in turn play an important role in cancer pathology, promoting primary tumor growth and development of a metastatic niche [Demers, M. et al., 2016].

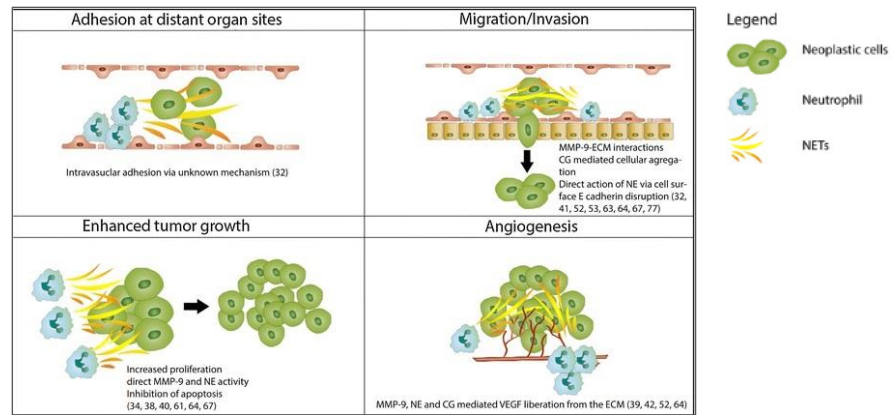


Figure 11. HNE involvement in cancer migration and development.

Several mechanisms have been proposed to account for the pro-tumorigenic activity of human neutrophil elastase: 1) HNE can directly stimulate proliferative pathways by extracellular transactivation of membrane receptors such as epidermal growth factor receptor (EGFR) and toll-like receptor 4 (TLR4), inducing mitogen activated protein kinase (MAPK) signaling and downstream effects. 2) Human neutrophil elastase may trans-activate EGFR through cleavage and release of a variety of membrane bound ligands, including TGF α , EGF-like ligands, and PDGF. In both breast and prostate cancer cells, HNE acts through MAPK to induce ERK phosphorylation and transcription of ERK-dependent genes like FOS [Lerman, I. et al., 2018]. 3) Human neutrophil elastase can additionally activate the phosphoinositide 3-kinase (PIK)-Akt proliferative pathway through internalization and degradation of insulin receptor substrate 1 (IRS-1) in lung cancer cells [Xu, Y. et al., 2012].

Recent studies have identified possible methods of endosomal internalization of HNE; specifically, clathrin and neuropilin-1 appear to mediate the process [Gregory, A. D. et al., 2012; Kerros, C. et al., 2017]. Intriguingly, MDA-MB-231 breast cancer cells express HNE endogenously, and shRNA mediated down-regulation results in decreased activity [Hunt, K. K. et al., 2013]. Furthermore, the loss of tumor suppressor function is a critical step in initiation of many cancers, and neutrophil elastase may contribute to this suppressing EMILIN1 [Maiorani, O. et al., 2017] and thrombospondin-1 (Tsp-1) [El Rayes, T. et al., 2015].

Rheumatoid arthritis: Rheumatoid arthritis (RA) is a systemic inflammatory autoimmune disorder in which genetic and environmental risk factors contribute to its development. Joint inflammation and damage in RA are mediated by the influx of innate and adaptive immune cells into the synovial joint space. An inflamed rheumatoid joint is typically swollen, containing excess synovial fluid and an inflamed and hyperplastic synovial lining. An invasive tissue or pannus is formed, comprising activated synovial fibroblasts, lymphocytes, macrophages and neutrophils, which secrete in turn proinflammatory mediators such as cytokines, chemokines and prostaglandins [Sabe, F. et al., 2010].

At the pannus-cartilage interface, the osteoclasts become inappropriately active and resorb bone, while the fibroblast-like synoviocytes mobilize various matrix metalloproteinases to the plasma membrane, where they dissolve and invade collagen rich cartilage [Miller, M. C. et al., 2009]. In addition, neutrophils at the pannus-cartilage junction contribute to matrix degradation through the secretion of MMP-8, MMP-9, HNE, cathepsin G and proteinase 3 [Murphy, G. et al., 2008].

In particular, the role of HNE in arthritis seems to be not directly correlated to ECM degrading mechanism, but it enhances the inflammation activating proteolysis of chemokines, such as CXCL8 or CXCL2, or cytokines, such as pro-TNF α , pro-IL1 β or IL 6. Additionally, it can modulate integrin clustering and activate TLR-4 and PARs. Finally, HNE is involved in arthritis pathology because of its ability to induce MMP activation, which are the main responsible for matrix degradation in RA [Milner, J. M. et al., 2012].

Type 1 diabetes (T1D): autoimmune disease that afflicts millions of people worldwide. It occurs as the consequence of destruction of insulin-producing pancreatic β -cells triggered by genetic and environmental factors. The initiation and progression of the disease involves a complicated interaction between β -cells and immune cells of both innate and adaptive systems. Immune cells, such as T cells, macrophages and dendritic cells, have been well documented to play crucial roles in type 1 diabetes pathogenesis.

Several studies have shown that in diabetes patients, neutrophil count is increased and they were observed to infiltrate the pancreas. Additionally, they are recruited to the pancreatic islets and are responsible for the initiation of autoimmune diabetes in non-obese diabetic mice. Furthermore, human neutrophil elastase was proven to increase in type 1 diabetes patients and to be associated with the pathogenesis of β -cell autoimmunity as well as diabetic complications. Finally, therapies with anti-neutrophil agents were shown to dampen and reduce the development of the pathology [Huang, J. et al., 2016].

High concentrations of plasma HNE can also be considered as a marker of the development of complications, such as diabetic angiopathy and coronary artery disease, because it might contribute to the progression of vascular disease [Piwowar, A. et al., 2000]. It has been demonstrated that serum HNE could act as a susceptible biomarker for the prediction and early diagnosis of type 1 diabetes. Furthermore, NETs formation was found to be elevated and closely associated with increased circulating neutrophil elastase levels, suggesting that it might play a key role in the initiation of β -cell autoimmunity [Wang, Y. et al., 2014]. Still more studies must be done to better understand the role of neutrophil, and thus HNE, in diabetes.

Atherosclerosis: Atherosclerosis is a chronic inflammatory disease of arterial blood vessels. Extracellular proteolysis is central to atherosclerotic plaque growth and the onset of complications, such as aneurysm development and plaque rupture, leading to myocardial infarction [Garcia-Touchard, A. et al., 2005]. Endothelial function is compromised by neutrophil-mediated injury, the

loss of the permeability barrier leads to edema and hemorrhage, while loss of antithrombotic activity is conducive to platelet adhesion and fibrin deposition.

Activated endothelial cells release signaling cytokines and present adhesion molecules that induce functional changes in neutrophils. Platelet activating factor and interleukin-8 (IL-8) are expressed by endothelial cells, allowing paracrine activation of neutrophil degranulation. HNE directly stimulates IL-8 production and increases endothelial cell production in response to other stimuli such as LPS [Henriksen, P. A. et al., 2004]. Cleavage of cellular matrix bonds and intercellular cadherins by HNE results in apoptosis of anchorage dependent cells [Mtairag, E. M. et al., 2002]. Once released within the ECM, HNE action on elastin, collagen, fibronectin and proteoglycans, leads to the exposure of the recognitions sites that bind cellular integrin and tyrosine receptors, allowing orchestration of the cell response to tissue injury. Recognition of elastin-derived products by the elastin receptor produces a range of pro-atherogenic effects, including monocyte and vascular smooth muscle cell chemotaxis [Robert, L. et al., 1998]. Excessive elastin and collagen breakdown weakens the arterial wall, leaving it susceptible to arterial pressure induced expansion and aneurysm development [Houard, X. et al., 2006].

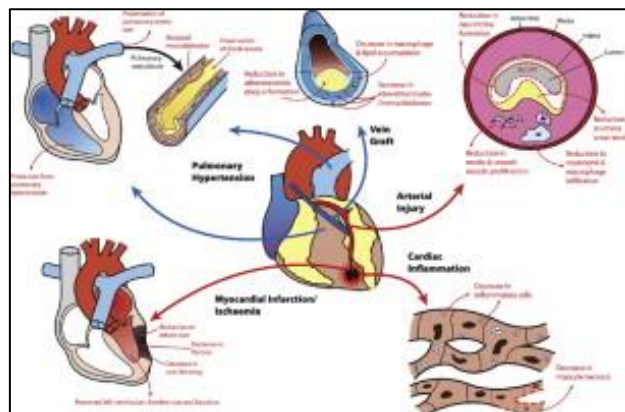


Figure 12. HNE involvement in atherosclerosis.

HNE has a central role alongside MMPs and cysteine proteases in atherosclerotic aneurysm development; in fact, blood clots are usually present over the surface of larger aneurysms, providing an active interface for neutrophil recruitment and activation. The thrombus from abdominal aortic aneurysms is rich in HNE, particularly within the luminal compartment [Gacko, M. et al., 1998], and this contributes to aneurysm growth by preventing in-growth of smooth muscle cells and recolonization by circulating progenitors [Fontaine, V. et al., 2004].

Blood clots are continuously turning over, and together with neutrophil recruitment provide a supply of HNE, plasmin and activated MMPs.

Psoriasis: pathology morphologically characterized by epidermal hyperproliferation and neutrophil infiltration in the epidermis. HNE is present in psoriatic lesions and induces keratinocyte hyperproliferation via the epidermal growth factor receptor-signaling pathway. The low concentration

of specific elastase inhibitors in psoriatic skin increases the excessive hydrolytic activity of HNE released from migrating cells [Glinski, W. et al., 1990].

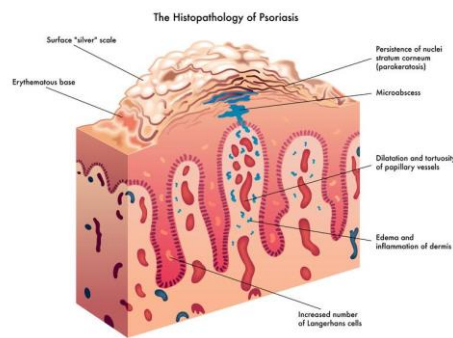


Figure 13. HNE involvement in psoriasis.

Furthermore, the neutrophil granule-derived serine proteinases, such as HNE, proteinase 3, and cathepsin G, can activate IL-36 and lead to the escalation of local psoriatic tissue inflammation. In addition, HNE proteolytically activates the epidermal growth factor receptor (EGFR) signaling pathway resulting in excessive keratinocyte proliferation [Meyer-Hoffert, U. et al., 2004].

Chronic kidney disease (CKD): it is a long-term condition, characterized by the loss of renal function over time and leading, as last stage, to kidney failure and to end-stage renal disease (ESRD). The chronic inflammation in patients with ESRD under hemodialysis, has been associated with an imbalanced neutrophils activation, which thus release ROS species and granules content, such as HNE and active inflammatory cells through stimulation of cytokines [Bronze-da-Rocha, E. et al., 2018].

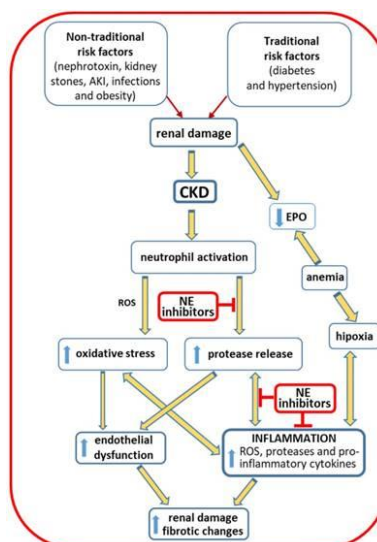


Figure 14. HNE involvement in chronic kidney disease (CKD).

Finally, is worth mentioning other important HNE-driven inflammatory diseases, such as inflammatory bowel disease, Crohn's disease [Langhorst, J. et al., 2008], severe pneumonia

[Matsuse, H. et al., 2007], and graft-versus-host disease [Arafat, S. N. et al., 2017] all related to an excessive HNE activity.

1.6. HNE inhibitors

In the last three decades, many pharmaceutical companies and academia have discovered a variety of innovative elastase inhibitors [Crocetti, L. et al., 2019]. Low molecular weight synthetic HNE inhibitors may offer several advantages over peptide inhibitors, including enhanced enzyme selectivity, oral bioavailability, lower susceptibility to proteolytic inactivation, and decreased risk of an immunogenic response. Moreover, a 'small molecule' is more easily modifiable in order to allow physical and pharmacokinetic properties optimization for the production of viable clinical candidates. In the literature are also reported many HNE inhibitors from natural sources [Siedle, B. et al., 2007], [Martins, F. T. et al., 2009; Kim, J. Y. et al., 2018; Uddin, Z. et al., 2017], but none of these compounds have become drug candidate since they generally have low potency, selectivity and poor metabolic stability. An important exception to this trend is represented by Lyngbyastatin 7 isolated from cyanobacteria of marine environment by Salvador et. al in 2013 [Salvador, L. A. et al., 2013] and later obtained for total synthesis via 31 steps by Luo and co-workers [Luo, D. et al., 2016]. This compound displays a 19-membered cyclic hexadepsipeptide core and has a potent HNE inhibitor activity ($IC_{50} = 23 \text{ nM}$), with a good selectivity for HNE against a panel of 68 proteases.

1st generation of HNE inhibitors: peptides analogues of endogenous inhibitors originally isolated from human plasma; currently, these inhibitors are obtained through DNA recombinant techniques to better accommodate potential safety and cost issues. The most important inhibitors of this class are α 1-antitrypsin (**Prolastin**, **Zemaira**, **Aralast**) used for the α 1-antitrypsin deficiency [Van der Linden, M. et al., 2016], elafin [Wang, T. et al., 2017], and SLPI [Majchrzak-Gorecka, M. et al., 2016], all belonging to the Serpin's family. Among them, **Prolastin**[®] represent the only drug that have reached the market.

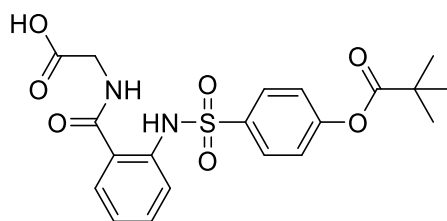
These proteases act as pseudo-irreversible inhibitors, but they lack of stability, especially under pathophysiological oxidative stress conditions. **Tiprelestat** (elafin) entered the clinic phase for subcutaneous use in pulmonary arterial hypertension (PAH) [Bronze da Rocha, E. et al., 2018]. The intrinsic physicochemical properties of these inhibitors allow only an intravenous administration or inhalative route, and thus they are not suitable for chronic diseases like COPD. Consequently, their current clinical development is focused on more acute settings with intravenous or the recently proposed inhaled applications.

The other generations include non peptidic inhibitors, which can be natural or synthetic and interact with the target through reversible or irreversible covalent bond.

2nd generation: In contrast with the 1st generation, this class includes low molecular weight molecules. It is possible to define four inhibitor types belonging to this class depending on their mechanism of inhibition: acylating-enzyme inhibitors, mechanism-based inhibitors, transition-state analogs and non-covalent inhibitors.

For acylating agents and acyl-enzyme inhibitors, the protease inhibition starts from the nucleophilic attack of HNE serine OH residue and with the formation of a tetrahedral intermediate which is stabilized by hydrogen bonds with the backbone NH groups of the so-called oxyanion hole [Powers, J. C. et al., 2002]. When this tetrahedral intermediate is stable enough, it prevents the hydrolytic process and reversibly inhibits the enzyme-transition state. On the contrary, in the presence of acylating inhibitors, the tetrahedral transition state analog collapses with the displacement of a leaving group, to afford a very stable acyl-enzyme complex frequently leading to an irreversibly inactivated enzyme. The main concern related to acyl-enzyme inhibitors is their susceptibility to hydrolysis, which affects the time needed to reverse their inhibitory activity; this phenomenon depends upon the acylating power of the inhibitor itself, and it is evaluated by its acylating-deacylating rates, thus k_{on} and k_{off} respectively [Ohbayashi, H., 2005].

Sivelestat (Elaspol[®]100) (1) (Fig. 15) is the most representative compound of the 2nd generation with an IC_{50} of 44 nM and it was approved for intravenous use in Japan and South Korea for the treatment of ALI and ARDS [Nakayama, Y. et al., 2002].



1. Sivelestat IC_{50} = 44 nM

Figure 15. Sivelestat (ONO-5046).

In 2007, Schepetkin et al. reported N-benzoylpyrazoles from a high-throughput chemolibrary screening (**2**) (**Fig. 16**) as potent and specific HNE inhibitors. Kinetic evaluation demonstrated that N-benzoylpyrazoles are pseudo-irreversible inhibitors of HNE and molecular modeling studies revealed that active compounds fit well into the catalytic site, whereas inactive derivatives contain substituents or take on conformations that hindered binding or accessibility to the catalytic site [Schepetkin, I. A. et al., 2007]. Moreover, computational SAR analysis based on atom pair descriptors in combination with 2-dimensional molecular descriptors was performed on a series of 53 N-benzoylpyrazoles; the results showed that the main factors influencing elastase inhibitory activity are the presence of methyl groups in the pyrazole scaffold and in the ortho-substituents at the benzoyl group [Khlebnikov, A. I. et al., 2008].

In the pioneering studies conducted on HNE inhibitors, Teshima et al reported in 1982 the 4H-3,1-benzoxazin-4-ones (**3**) (**Fig. 16**) as serine protease inhibitors, although not specific for HNE [Teshima, T. et al., 1982].

Gütschow's group reported a further modification of the benzoxazinone scaffold where the fused benzene ring was replaced by a thiophene in order to improve intrinsic stability due to the enhanced electron density at the thiophene carbon atoms leading to the thieno-1,3-oxazin-4-ones (**4**) (**Fig. 16**) [Gütschow, M. et al., 1998; Gütschow, M. et al 1999].

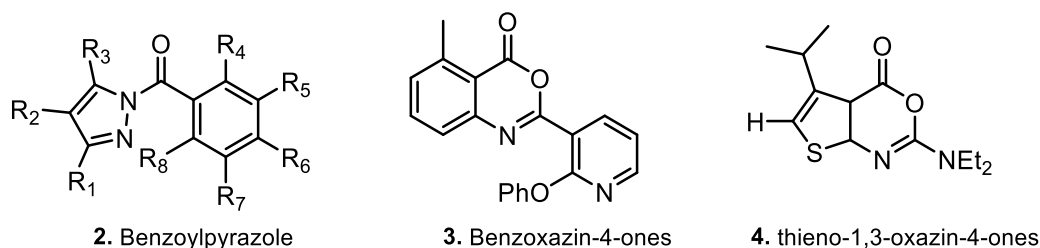


Figure 16. Structures of compounds synthesized by Schepetkin et al. (A), Teshima et al. (B) and Gütschow et al. (C).

Later, Santagati et al. extended the studies on 2-sec-amino-substituted thieno-oxazinones to 2-phenylamino substituted compounds [Santagati, N. A. et al., 2007]. In addition, β -lactam based HNE inhibitors (**5**, **6**) (**Fig. 17**) were developed and the first was **Merck & Co.** back in 1986 [Doherty, J. B. et al., 1986], but since then many different scaffolds based on β -lactam inhibitors were synthesized [Lucas, S. D. et al., 2011].

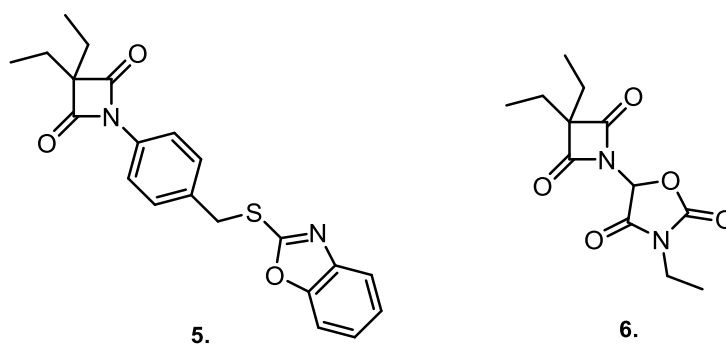


Figure 17. Examples of 4-oxo- β -lactam.

As regard the transition-state analogue inhibitors, also belonging to the 2nd generation, they form a stable tetrahedral intermediate through a ketone carbonyl group. The location of the tetrahedral hemiacetal oxygen in the oxyanion hole and the formation of hydrogen bonds to the backbone NH groups of Ser195 and Gly193 of the enzyme enforce the stabilization of the tetrahedral intermediate, which potently prevents reverse hydrolytic processing of HNE. Abeles of Brandeis University and Trainor of ICI (**AstraZeneca** nowadays) were the pioneers in the study of peptidyl trifluoromethyl ketones (TFMKs) and among them the potent HNE inhibitor **ZD0892 (ICI200,880)** (**7**) (**Fig. 18**) was proved to reduce tobacco smoke-induced emphysema and pulmonary cell recruitment in a guinea pig model [Wright, J. L. et al., 2002].

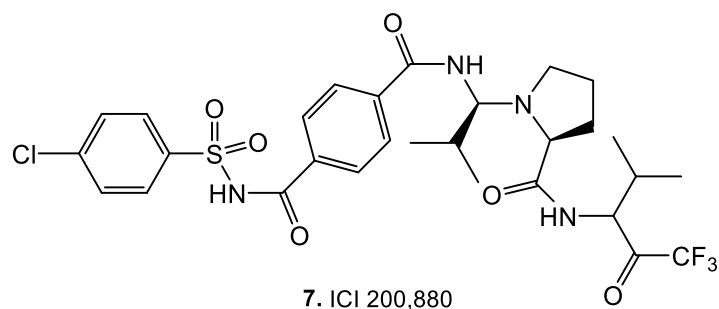


Figure 18. Structure of ICI 200,880 (TFMK).

During a screening program carried out by **Ono Pharmaceutical Co., LTD** to find orally active HNE inhibitors, a peptidyl α -keto-1,3,4-oxadiazole was identified as a hit. Its next modifications, in particular, the insertion of the 5-amino-2-phenylpyrimidin-6-one moiety led to **ONO-6818 (Freselestat) (8) (Fig. 19)**, a promising therapeutic agent for the treatment of HNE related chronic inflammatory diseases, such as COPD, ALI, and ARDS.

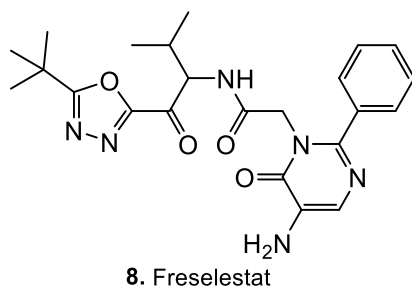


Figure 19. Structure of Freselestat (ONO-6818).

ONO-6818 proved to be a potent HNE inhibitor with $K_i = 12.16$ nM and exhibited a highly potent oral activity ($ED_{50} = 1.4$ mg/kg) which lasted for more than 8 hours [Ohmoto, K. et al., 2000]. **ONO-6818** reached Phase II clinical trials in 2002, but the development was discontinued since COPD patients showed an abnormal elevation in liver functions [Ohbayashi, H et al., 2005].

The last type of compounds belonging to this generation are mechanism-based inhibitors. These molecules, upon binding to the active site of the enzyme, are processed by the catalytic machinery of the enzyme, so leading to highly reactive electrophilic species which will further react with a nucleophilic residue at the active site, resulting in irreversible inactivation of the enzyme itself. In a simplified approach, the reversible enzyme–inhibitor complex (that can be an acyl-enzyme complex) can either regenerate the free enzyme and product, or it can react with a second residue of the enzyme providing a covalent irreversible complex [Wei, L. et al., 2004]. As example of molecules acting as mechanism-based inhibitors, we can mention potent HNE inhibitors with peptidomimetic scaffold 1,2,5-thiadiazolidin-3-one 1,1-dioxide developed by Groutas et al. [Groutas, W. C. et al., 2004].

The next three generations include compounds with an innovative binding mode, and defined as non-reactive, reversible inhibitors.

The study of Hansen G. et al. on three-dimensional structure of a potent dihydropyrimidone inhibitor (DHPI) showed that it is possible to block the enzyme, without reacting with the catalytic site. In fact, the inhibitor binds the active site in a unique orientation, which change the conformation of the protease itself. The overall structure remains intact but the trifluoromethyl-phenyl moiety of DHPI occupies the hydrophobic S1 pocket, forming a closer interaction with respect to the previous generations of inhibitors. This deep insertion into the S1 pocket leads to a conformational change of the catalytic site, widening the otherwise closed S2 pocket.

In the previous generations, the orientation of the Leu99B side chain toward the S2 pocket leads to a shallow S2 binding site with no significant cavity. This conformation could be regarded as a “closed conformation” with respect to the S2 binding site. In contrast, the binding of the P2 moiety of DHPI is totally unique, as its p-cyanophenyl moiety inserts deeply into the large and deep S2 cavity that is created by a conformational rearrangement of the Asp95-Leu99B loop and the Leu99B side chain, and this can be referred to as “open conformation” (**Fig. 20**) [Hansen, G. et al., 2011].

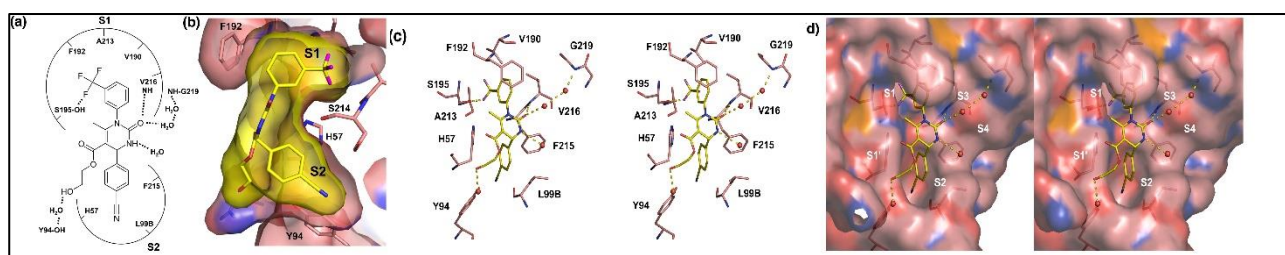


Figure 20. (a) Scheme showing the chemical structure of DHPI with specificity binding pockets of HNE. (b) Connolly like surface of DHPI binding to the S1 and S2 subsites of HNE. (c) Stereo representation of DHPI and interacting amino acids. (d) Stereo surface representation in the same orientation as in (c) with enzyme subsites S1'–S4 indicated.

3rd generation: To this generation belong compounds able to induce the “open conformation”, but not to interact with the S2 pocket. The main representative inhibitor of this class is **Alvelestat** (**AZD9818**, $IC_{50} = 12$ nM, $K_i = 9.4$ nM), compound with a 2-pyridone scaffold, investigated by **AstraZeneca** in 2007, and developed as oral formulation for the treatment of COPD and α -1-AT deficiency and currently in Phase II clinical trials [Stevens, T. et al., 2011] (**Fig. 21**).

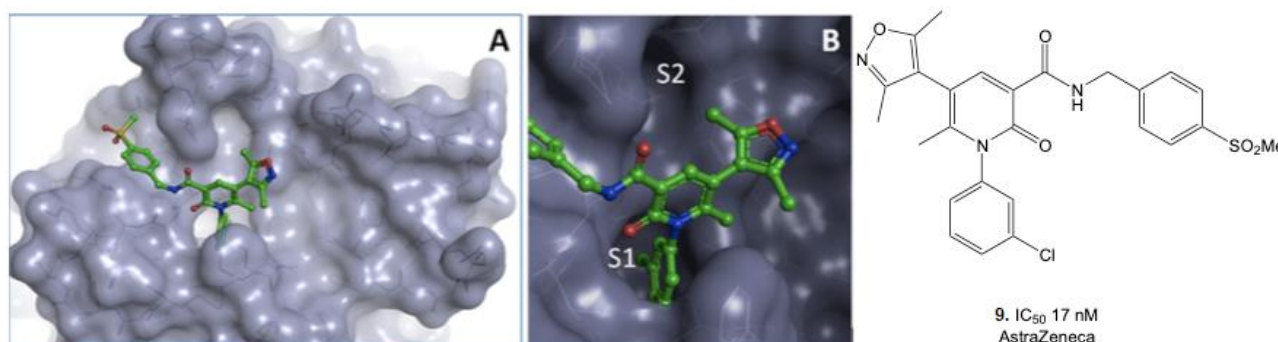


Figure 21. Crystalline complex of HNE with 3rd generation's inhibitor.

4th generation and 5th generation: These modern inhibitors have displayed an outstanding selectivity versus similar serine proteases and a very high target specificity with no significant interactions with other biological relevant targets, in contrast to compounds belonging to 2nd generation. Both these two classes are able to induce the “open conformation” and interact with the widened S2 pocket (**Fig. 22**).

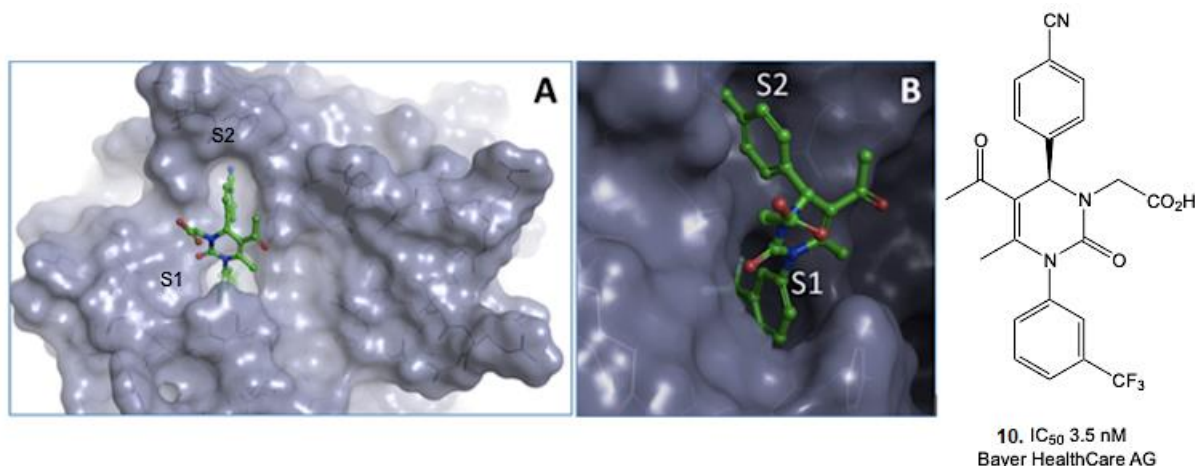


Figure 22. Cristal complex of HNE with 4th generation's inhibitor.

The difference between 4th and 5th generation lies in an additional substituent resulting in an unprecedented improvement in potency. Although this substituent does not directly interact with the target, it is able to raise the rotational barrier at the crucial pyrimidinone-cyanophenyl axis and thereby ‘freezes’ the structure in an ideal bioactive conformation. Inhibitors of the 5th generation follow the “pre-adaptive pharmacophore model” [Cairns, J. et al., 1988] (**Fig.23**).

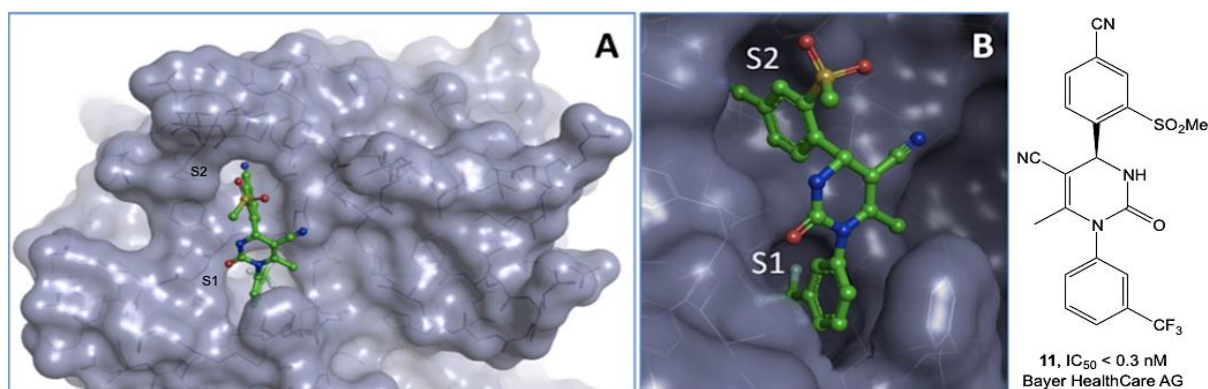


Figure 23. Crystal complex of HNE with 5th generation's inhibitor.

Many pharmaceutical companies have shown a big interest in the study of new 4th and 5th generation of inhibitors.

Bayer Healthcare AG developed **BAY-678 (13)** (**Fig. 24**), belonging to the 4th generation, having a pyrimidinone scaffold and active per os. This compound showed a significant efficacy in preclinical studies on ALI and emphysema and positive effect on blood circulation in rat and mice PAH model [Klein, M. el al., 2008]. It reached the phase I clinical trial but the test was discontinued. Other

compounds belonging to the 4th generation are the triazolopyridines synthesized by **Chiesi Farmaceutici S.p.A.** (**15**), the cyclopenta[d]pyrimidinone (**14**) from **Boehringer Ingelheim**, and finally compound (**12**) developed by **AstraZeneca** [Von Nussbaum, F. et al., 2015a] (**Fig. 24**).

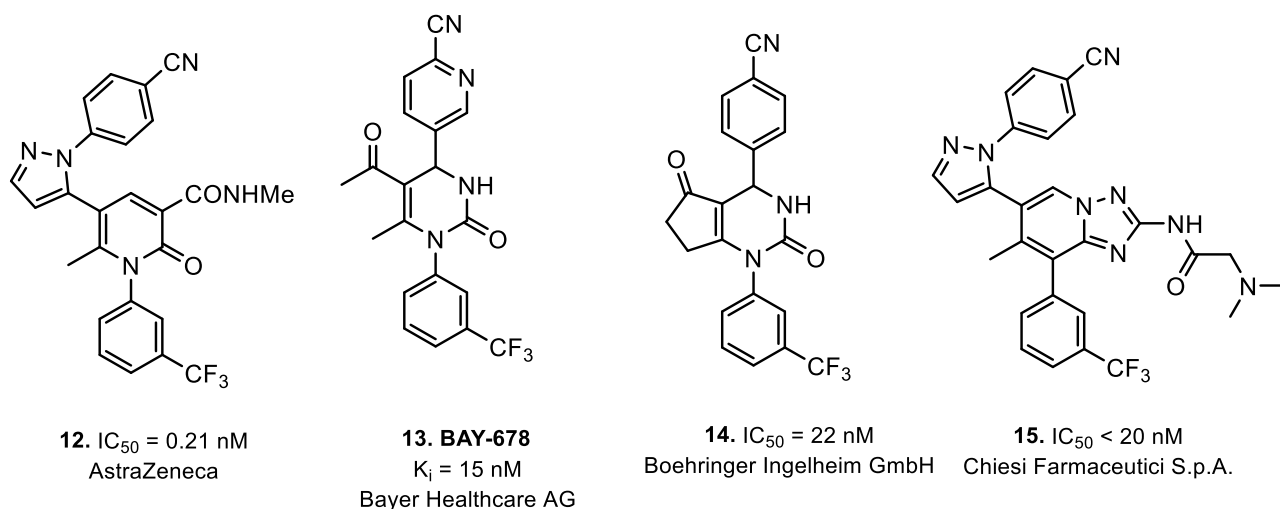


Figure 24. Example of 4th generation's inhibitor.

Chiesi Farmaceutici S.p.A is studying **CHF6333**, a promising inhibitor belonging to the last generation, and whose structure is still undisclosed. Currently it is in phase I clinical trial for the treatment of HNE-driven lung diseases; it is the first HNE inhibitor administered as dry powder nebulizer. In vitro, **CHF6333** is a highly potent HNE inhibitor ($IC_{50} = 0.2$ nM) with good selectivity against other proteases. In addition, **CHF6333** significantly reduces lung neutrophils recruitment induced by cigarette smoke exposure in mice, and reduces both lung tissue infection and inflammation when administered intratracheally to *P. aeruginosa*-infected rats for 7 days [Miglietta, D. et al., 2016].

Other **Chiesi Farmaceutici S.p.A.** compounds are 2,3,5,8-tetrahydro-[1,2,4]triazolo-[4,3-a]pyrimidine and [1,2,4]triazolo[1,5-a]pyridine derivatives, active in the nanomolar range and by inhalatory administration [Alcaraz, L. et al., 2018; Capaldi, C. et al., 2015]. The most interesting is compound **16** (**Fig. 25**). In addition, **Chiesi Farmaceutici S.p.A.** synthesized monocyclic compounds with imidazolone and pyrazolone scaffold [Capaldi, C. et al., 2018], [Armani, E. et al., 2016], which are able to interact with the catalytic site positioning perpendicularly to it, and compound **17** is an example (**Fig. 25**).

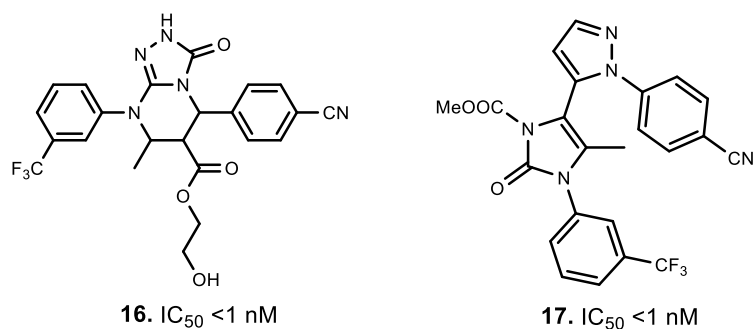


Figure 25. Examples of new 5th generation's inhibitor developed by Chiesi Farmaceutici S.p.A.

Boehringer Ingelheim GmbH patented a series of HNE inhibitors with monocyclic and bicyclic structure for the prevention and treatment of pulmonary disease, skin and eyes inflammation, autoimmune and allergic disorders, transplant rejection and cancer [Oost, T. et al., 2016a]. An example is the oxo-1,4-dihydropyridine **18** [Oost, T. et al., 2016b], which present a chiral center in the 1-(4-cyanophenyl) ethyl fragment at position N-1. The eutomer R showed 4 fold higher potency than the distomer S, highlighting the importance of the chiral center for the activity. Another example is the 2-oxo-1,2,3,4-tetrahydropyrimidine **19** (**Fig. 26**).

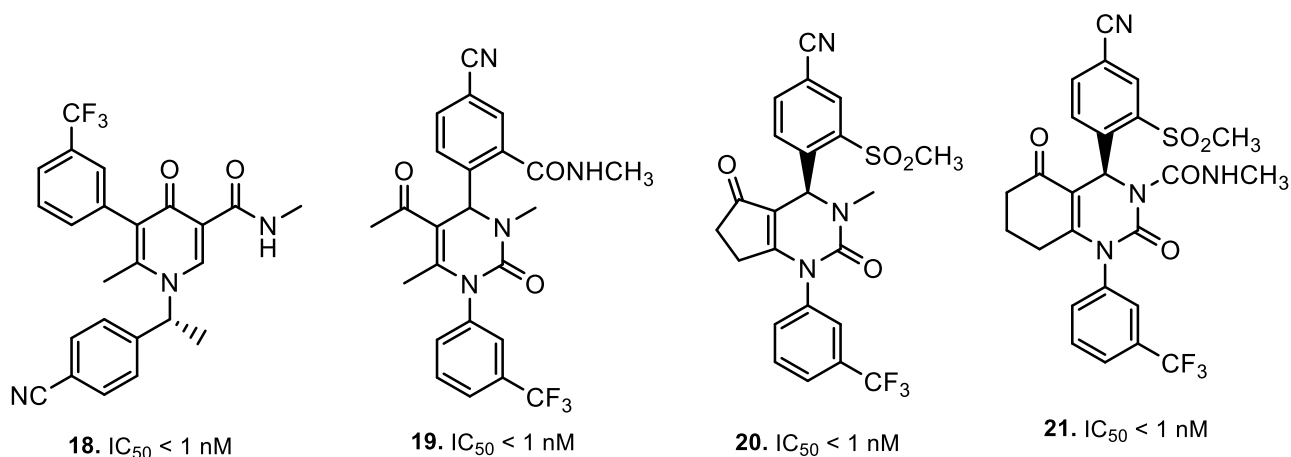


Figure 26. Examples of 5th generation's inhibitor developed by Boehringer Ingelheim GmbH.

Both these products are characterized by good pharmacokinetic properties, good metabolic stability, good permeability and, furthermore, are water soluble, thus are suitable for oral administration [Peters, S. et al., 2018].

Boehringer Ingelheim GmbH also developed a series of very potent 3,4,6,7-tetrahydrocyclopentapyrimidin-2,5-dione and 4,6,7,8-tetrahydrochinazolin-2,5-dione derivatives and compounds **20** and **21** (**Fig. 26**) [Peters, S. et al., 2016] are the most interesting, showing $IC_{50} < 1$ nM, a metabolic stability over 130 minutes, good permeability and low clearance [Gnamm, C. et al., 2017].

However, the most promising compound of this Company is **BAY 85-8501 (22)** (**Fig. 27**), which is currently in phase II clinical trials for bronchiectasis [Von Nussbaum, F. et al., 2015b]. **BAY 85-8501**

and its derivatives have a good in vivo stability, even under strong oxidative stress conditions, and good half-life; furthermore, they can be given by oral route.

Additionally, Bayer has developed bi-heterocycles derivatives (6:6 or 5:6) [Von Nussbaum, F. et al., 2015c] and among them the pyrimidopyridazine **BAY-8040 (23)** (**Fig. 27**) ($IC_{50} = 28$ nM) gave the best results in vivo studies.

It showed from days 14 to 28 significantly decreased right ventricular systolic pressure and right ventricular hypertrophy relative to placebo, with a significant beneficial effect on right ventricular dysfunction and preservation of systemic arterial pressure. Furthermore, **BAY-8040** improved the cardiac output and arterial oxygenation in rats with MCT-induced PAH. Thus, it was able, not only to suppress the inflammation at the basis of the pathology but also reverse tissue remodeling in the PAH setting [Von Nussbaum, F. et al., 2016].

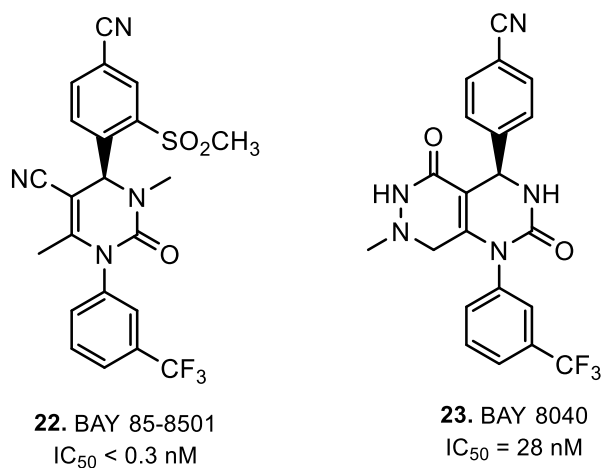


Figure 27. HNE inhibitor BAY 85-8501 (5th generation) and BAY 8040 (4th generation) developed by Bayer HealthCare AG.

Miscellaneous: **KRP-109 (24)** (**Fig. 28**) is claimed to be a selective, water-soluble competitive HNE inhibitor developed by **Kyorin Pharmaceutical Co., Ltd.** (Tokyo, Japan) [Yamada, K. et al., 2011]. A distinct feature of **KRP-109** is its ability to gather in high concentrations in lung tissue, thereby inhibiting the activity of HNE released by infiltrating neutrophils under inflammatory conditions. Moreover, **KRP-109** reduced lung inflammation in a murine model of severe pneumococcal pneumonia and it was able to decrease the degradation of mucin in CF sputum in vitro [Chillappagari, S. et al., 2016]. Worthy of mention is a new class of HNE inhibitors with a diazaborine nucleus (**25**) (**Fig. 28**).

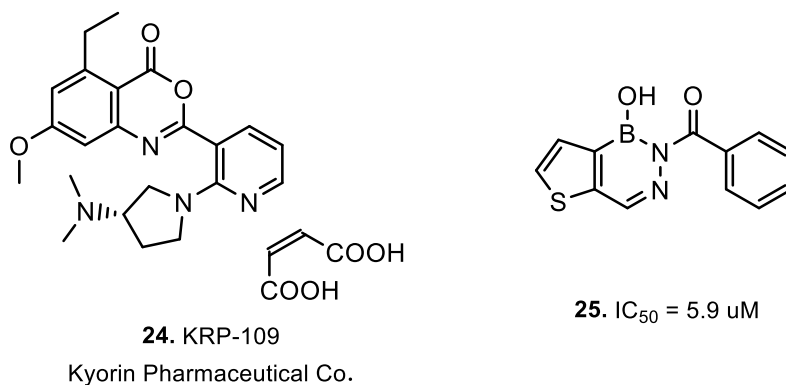


Figure 28. Other examples of HNE inhibitor.

Although endowed with moderate activity in the micromolar range, these compounds exhibit good selectivity toward elastase, and no inhibition was observed against a panel of five closely related serine proteases. Moreover, they are very stable in phosphate buffer at pH 7.4 and in human plasma. Computational studies performed on this system suggest that the mechanism of action involves the formation of a reversible covalent bond between the diazaborine boron center and the catalytic serine oxygen [António, J. P. M. et al., 2018].

Finally, **ER-143** is a coumarin-oxo- β -lactam derivative studied for the treatment of skin pathologies, such as psoriasis. This inhibitor, if associated with a starch-based nanoparticulate system (StNC), exhibited interesting characteristics and in vivo studies showed that the topical application of **StNC-ER143** strongly inhibited the acute inflammatory response as evident by the decrease of edema (about 92% inhibition), erythema and neutrophil infiltration [Martó, J. et al., 2016].

California Institute of Biomedical Research developed compounds constituted by two fragments of Sivelestat or Alvelestat (**26**) (**Fig. 29**) connected through a long linker. They are potentially useful for the treatment of COPD, CF and bowel chronic inflammation disease [Chatterjee, A. K. et al., 2017].

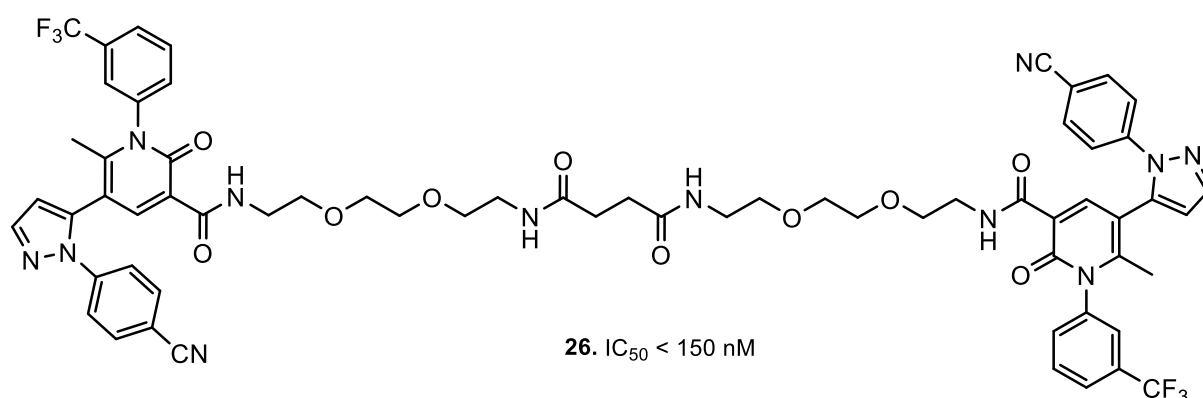
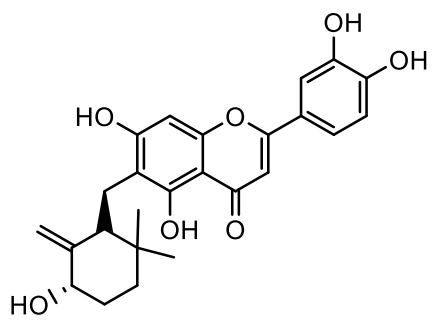
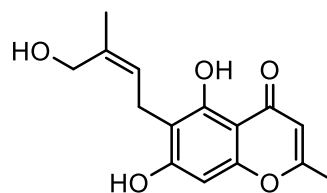


Figure 29. Other examples of HNE inhibitor.

Finally, taking into account their anti-inflammatory properties some natural compounds, such as flavonoids (**27**), lignans and coumarins (**28**) (**Fig. 30**), have been recently tested as HNE inhibitor or associated with other HNE inhibitors as transporters [Saleem, M. et al., 2018].



27. $IC_{50} = 0.49 \mu M$



28. $IC_{50} = 3.20 \mu g/mL$

Figure 30. Other examples of HNE inhibitor.

Section I

2. Background and aims of the work

Our research group has been working for several years in the field of human neutrophil elastase inhibitors, and over this period a wide variety of nitrogen bi-heterocycle scaffolds have been designed and synthesized, such as indazoles [Crocetti, L. et al., 2011; Crocetti, L. et al., 2013], indoles [Crocetti, L. et al., 2016], cinnolines [Giovannoni, M. P. et al., 2016] and 7-azaindoles [Crocetti, L. et al., 2018; Giovannoni, M. P. et al., 2019]; moreover, we also investigated nitrogen mono-heterocyclic scaffolds such as isoxazolones [Vergelli, C. et al., 2017; Giovannoni, M. P. et al., 2018; Giovannoni, M. P. et al., 2020] and thiazolones [Crocetti, L. et al., 2017] obtaining interesting results. Among all the studied scaffolds, 7-azaindoles and indazoles emerged as the best nuclei, affording compounds with potent HNE inhibitory activity in the nanomolar range; compound **A** (for 7-azaindole series) and compound **B** (for indazole series) are two representative terms (**Fig. 31**). All these compounds act as competitive pseudo-irreversible inhibitors and the nucleophilic attack of Ser-OH takes place at the N-CO function at position 1 of the five-membered nucleus. This has been highlighted by molecular modelling studies as well as by the loss of inhibitory activity of those compounds lacking the N-CO function at position 1. [Crocetti, L. et al., 2018]

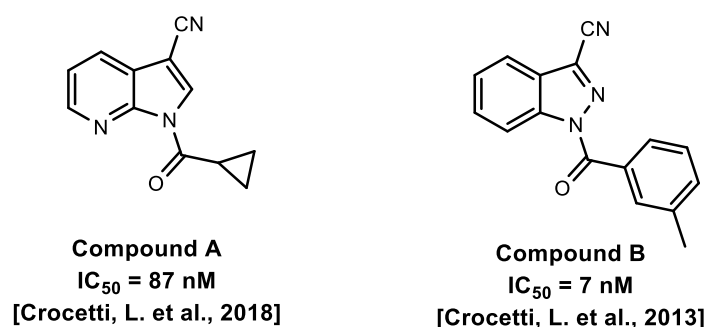


Figure 31. Representative compounds previously published by us.

Taking into account the above-mentioned findings, during this first part of my PhD experience, new HNE inhibitors have been designed as further modification of both indazoles and 7-azaindoles, with the goal to investigate the impact that either the shift of the nitrogen in the pyridine ring as well as the total number of nitrogens in the molecules can have on the biological activity.

Hence, we have been explored the following nuclei:

1. 4-, 5- and 6-azaindoles as the result of the 7-azaindole pyridine nitrogen shift (**Fig. 32A**).
2. 5H-pyrrolo[2,3-b]pyrazines by inserting a nitrogen atom at position 4 of the 7-azaindole nucleus, (**Fig. 32A**).
3. 5- and 7-azaindazoles (1H-pyrazolo[3,4-b]pyridine and 1H-pyrazolo[4,3-c]pyridine) as aza-analogues of the potent indazoles (**Fig. 32B**).

In all new compounds, we inserted those fragments and substituents that led to the optimal biological results based on our previous studies and on data reported in the literature and in particular keeping the *m*-toluyl and cyclopropyl groups bound to the N-CO function at position 1.

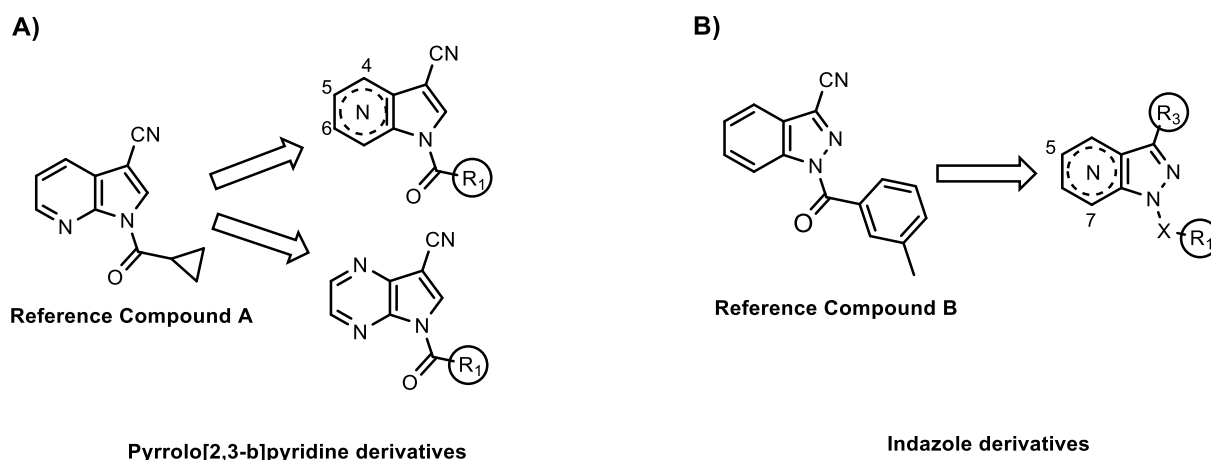


Figure 32. 7-Azaindole and indazole derivative modifications.

Finally, we synthesized some pyrazolopyrimidine (**Fig. 33A**) and pyrazole (**Fig. 33B**) derivatives which, differently from all our previous compounds, showed the amide group in a side chain.

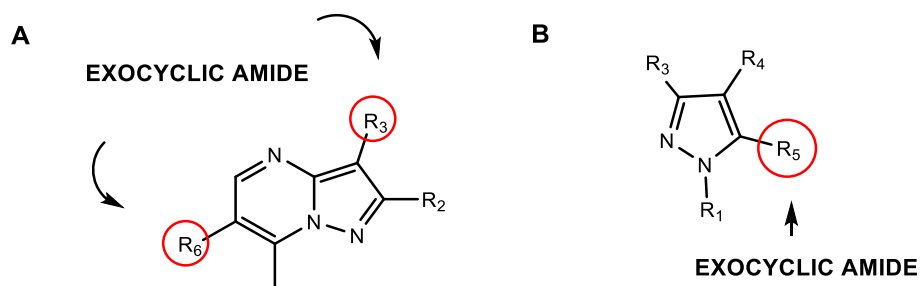


Figure 33

Stability, molecular modeling, and *in silico* pharmacokinetic (ADMET) studies have been performed on selected compounds in order to identify potential candidates for future *in vivo* studies.

3. Chemistry

In the Schemes 1-6 are reported the synthetic pathways followed to obtain the final compounds with different nitrogen bi-heterocyclic scaffolds (Schemes 1-4 and 6) and the final pyrazole derivatives (Scheme 5). The most part of the new synthesized products have been recently published by our research group [Cantini, N. et al., 2020].

- **Schema 1:** 4-, 5-, 6-azaindole derivatives (**5a-f**)
- **Scheme 2:** 7-azaindazole derivatives (**13a-f**)
- **Scheme 3:** 5-azaindazole derivatives (**17a,b, 19a,b, 22a,b** and **27**)
- **Scheme 4:** pyrrolopyrazine derivatives (**31a,b** and **35a,b**)
- **Scheme 5:** pyrazole derivatives (**37a-d**)
- **Scheme 6:** pyrazolopyrimidine derivatives (**40a-h**)

In Scheme 1, starting from the commercial 4-,5- and 6-azaindoles **1a-c**, we performed a formylation at position 3 with HMTA in acetic acid at reflux, obtaining the corresponding formyl intermediates **2a-c** [**2a,b**: Bradbury, R. H. et al., 2009; **2c**: Nakano, H. et al., 2012]. They were firstly converted to the oxime derivatives **3a-c** [**3c**: Clark, B. A. J. et al., 1970] with hydroxylamine hydrochloride, and then dehydrated to the corresponding 3-cyano-azaindoles **4a-c** with POCl₃ [**4c**: Clark, B. A. J. et al., 1970]. The latter were acylated with m-toluoyl chloride or cyclopropanecarbonyl chloride and triethylamine in dichloromethane to afford the final compounds of type **5**.

In Scheme 2 is reported the procedure for the final 7-azaindazoles **13a-f** which have been obtained by acylation of the appropriate precursors **9a,b, 10** and **12**, synthesized as follow:

- 3-trifluoromethyl-7-azaindazole **9a** [Schirok, H. et al., 2005] has been obtained by treatment of the commercially available 2-fluoride pyridine **6** with LDA, ethyl trifluoroacetate and hydrazine monohydrate;
- 3-carbetoxy-7-azaindazole **9b** [Aranov, A. et al., 2005] starting from the same precursor **6** but in three steps: synthesis of the ethyl 2-(2-fluoropyridin-3-yl)-2-oxoacetate **7** [Aranov, A. et al., 2005], by reacting with LDA and diethyl oxalate, further treatment with hydrazine monohydrate (compound **8** [Aranov, A. et al., 2005]), followed by the cyclization to 3-carbetoxy 7-azaindazole **9b**;
- 3-CN intermediate **10** [Schirok, H. et al., 2005] has been obtained by reacting **9a** with aqueous ammonia 33% in microwave at high temperature;
- 3-nitro-7-azaindazole derivative **12** [Lynch, B. M. et al., 1988] has been obtained for treatment of 7-azaindazole **11**, commercially available, with a sulfonitric mixture in the classic conditions.

The acylation of nuclei **9a,b** and **10** was performed with *m*-toluoyl chloride or cyclopropanecarbonyl chloride and triethylamine in dichloromethane, as already illustrated in [Scheme 1](#), and have furnished the final **13a-e**; for compounds **13d-f** the reaction was carried out in THF using sodium hydride.

For the synthesis of final compounds with 5-azaindazoles structure ([Scheme 3](#)), we firstly treated 4-dimethylaminopyridine **14** with trifluoroacetic acid at 85°C providing compound **15** [Kawase, M. et al., 1999], which was then cyclized with hydrazine monohydrate at 200°C achieving the 3-trifluoromethyl-5-azaindazole nucleus **16** [Kawase, M. et al., 1999]. The latter was acylated at the nitrogen at position 1, using the procedure described in [Scheme 1](#), to obtain the final compounds **17a,b**. The reaction of **16** with 33% aqueous ammonia in reactor at high temperature gave the corresponding 3-CN-5-azaindazole **18** [Kawase, M. et al., 1999] that, in turn, was acylated to afford **19a,b**. The transformation of the cyano group in carboxylic acid (compound **20**) [Hert, J. et al., 2017] was carried out with potassium hydroxide in a mixture of water/ethanol in mini reactor; product **20** was esterified using thionyl chloride (ratio 1:1) in absolute ethanol at reflux to obtain intermediate **21** [Hert, J. et al., 2017] which was finally treated with *m*-toluoyl chloride or cyclopropanecarbonyl chloride and triethylamine in dichloromethane to afford the final compounds **22a,b**.

Moving to the second part of the scheme (**B**), the final compound 3-methyl-5-azaindazole **27** was obtained from the commercial 2-chloro-nicotinic acid **23** which, after activation with carbonyldiimidazole (CDI) and *N,O*-dimethylhydroxylamine hydrochloride (intermediate **24**) [Devita, R. J. et al., 2013] was transformed into 1-(4-chloropyridin-3-yl)ethan-1-one **25** [Lounsbury, N. et al., 2015] with methylmagnesium bromide in dry THF. This last one was then cyclized using hydrazine monohydrate and triethylamine in isopropanol, and the resulting **26** [Tucker, T. J. et al., 2008] was finally acylated to obtain the desired compound **27**.

The synthetic pathway for **31a,b** and **35a,b** is summarized in [Scheme 4](#). The commercially available 2-chloro-3-amino-pyrazine **28** was treated with tetrakis, CuI and trimethylsilylacetylene, leading to compound **29** [Johnson, T. W. et al., 2016], which was cyclized to the pyrrolopyrazine **30** [Clark, B. A. J. et al., 1976] in reactor with *tert*-butoxide at 80°C in anhydrous NMP. The following acylation in the usual conditions above describe led to final compounds **31a,b**. To obtain compounds **35a,b**, the CN group was inserted at position 3 as follows: formylation of compound **30** with HTMA and glacial acetic acid in **32** [Clark, B. A. J. et al., 1976]; transformation of formyl derivative **32** into the corresponding oxime **33**, and dehydration to compound **34**, which was finally subjected to acylation. Unfortunately, compounds **31a** and **35a**, both *N*1-*m*-toluoyl derivatives were not chemically stable and quickly turn into the precursors **30** and **34**, respectively.

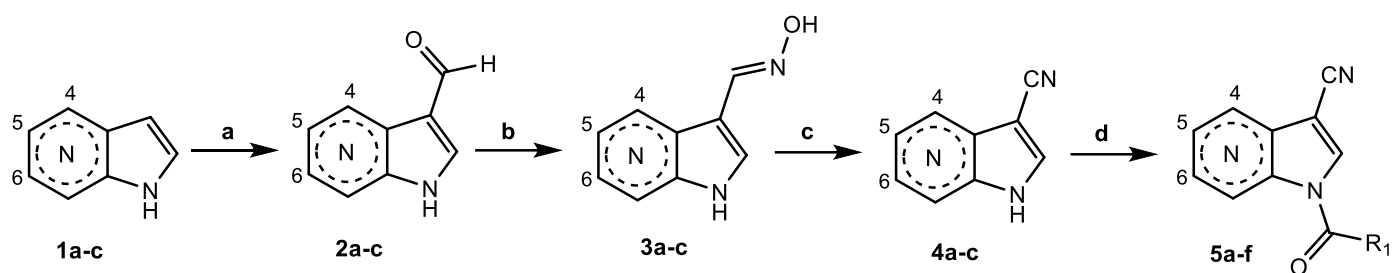
In [Scheme 5](#) are reported the final products **34a-d** which were obtained starting from the appropriate pyrazole **36a-c** [**36a**: Huang, D. S. et al., 2020; **36b**: Dos Santos, M. S. et al., 2012; **36c**: Al-Qalaf,

F. et al., 2008] through acylation reaction with m-toluoyl chloride, using triethylamine for **37a,b,d** and DIPEA for **37c**.

Scheme 6 shows the steps leading to the synthesis of the pyrazolopyrimidine derivatives **40a-h**. Part **a)** shows the synthesis of pyrazolopyrimidines bearing the amide function at position 6, while in part **b)** is reported the synthesis of the final compounds **40g,h** displaying the amide group at position 3 of the bicyclic scaffold. The already published compounds **38a,b** [Bruni, F. et al., 1995], **38d** [Bruni, F. et al., 1990], and the new product **38c**, which was obtained from **38b** through chlorination with N-chlorosuccinimide (NCS) and benzoyl peroxide in tetrachloromethane at reflux, have been hydrolyzed using 6N NaOH at reflux, resulting in the corresponding acids **39a-d** [**39a**: Bartroli, J. et al., 1998; **39b**: Kato, N. et al., 2011; **39d**: Goldfarb, D. S., 2009]. Compounds of type **39** were then treated with trichloroacetonitrile, triphenylphosphine and m-anisidine or 3-methoxybenzylamine to obtain the final **40a-h**.

4. Schemes

Scheme 1



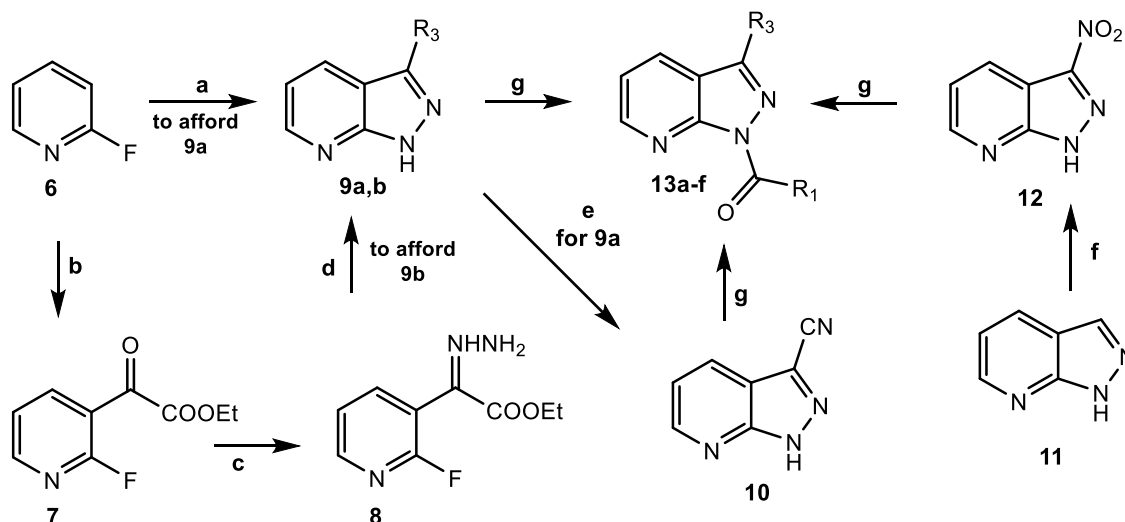
Reagents and conditions:

- a) HTMA, glacial CH_3COOH , reflux, 2h.
 b) $\text{NH}_2\text{OH}\cdot\text{HCl}$, H_2O , 60°C , 30 min, then NaHCO_3 , reflux, 4h.
 c) POCl_3 , reflux, 2h.
 d) $\text{R}_1\text{-COCl}$, Et_3N , dry CH_2Cl_2 , 0°C , 2h, then r.t., 2h.

1-4	N
a	4
b	5
c	6

5	N	R_1
a	4	m- $\text{CH}_3\text{-Ph}$
b	4	cC_3H_5
c	5	m- $\text{CH}_3\text{-Ph}$
d	5	cC_3H_5
e	6	m- $\text{CH}_3\text{-Ph}$
f	6	cC_3H_5

Scheme 2



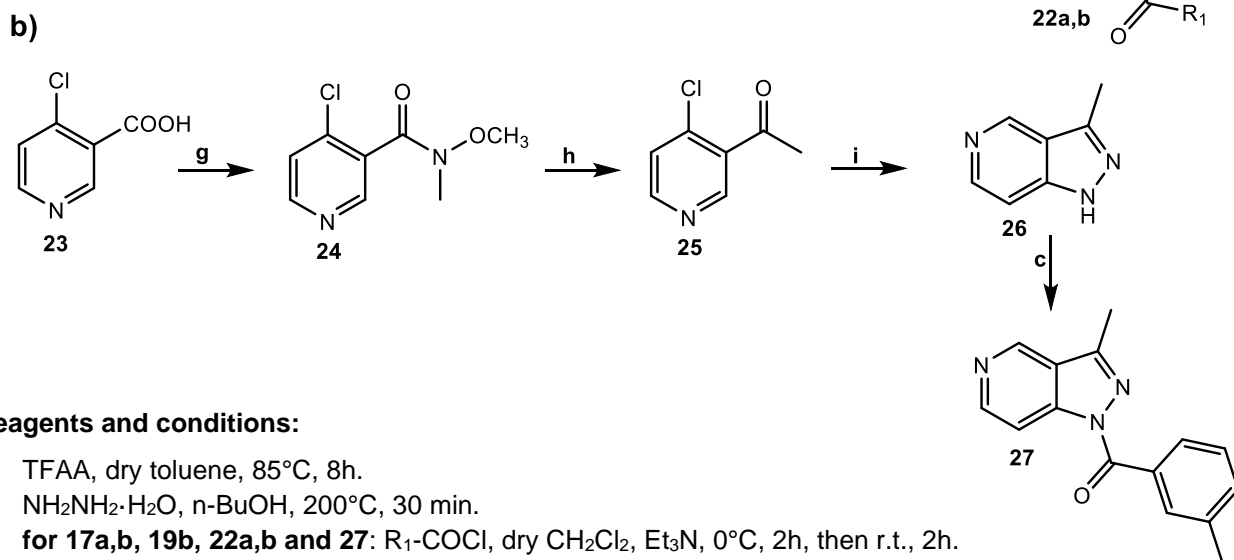
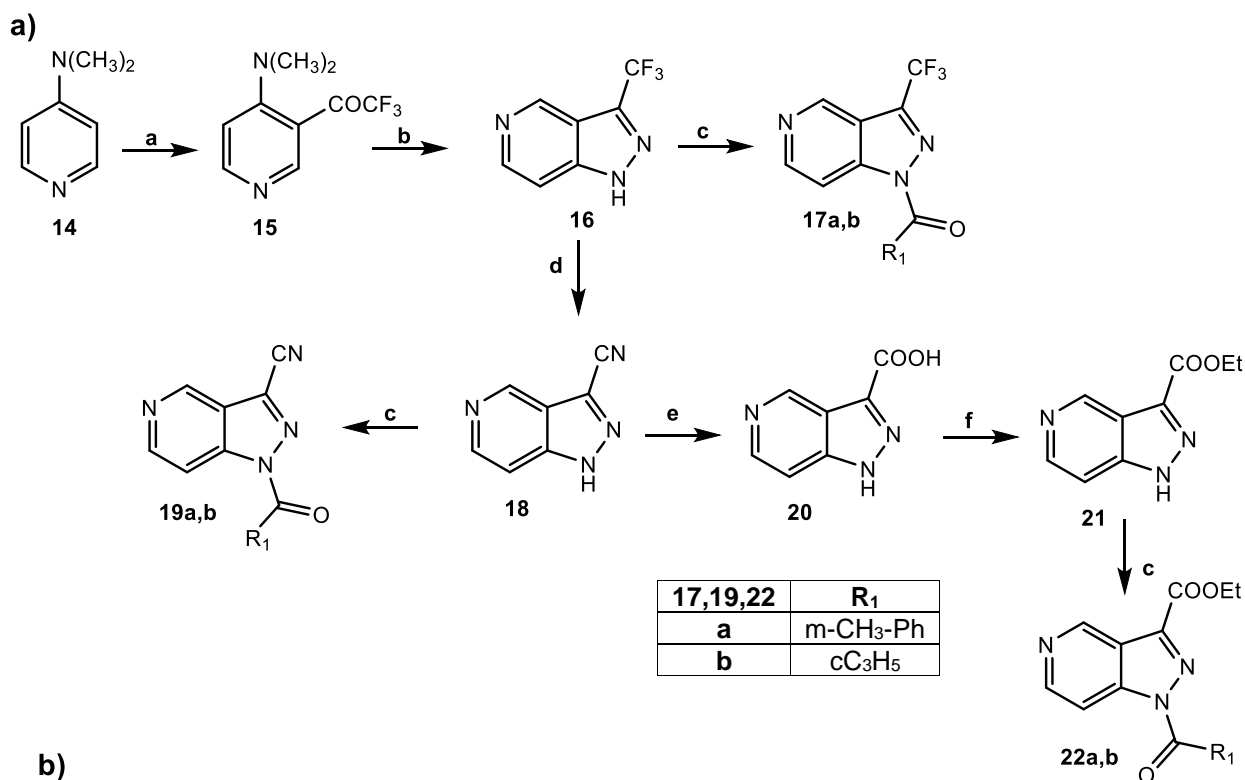
Reagents and conditions:

- a) LDA, dry THF, -78°C , 4h then CF_3COOEt , $\text{NH}_2\text{NH}_2\cdot\text{H}_2\text{O}$, reflux, 4h.
 b) LDA, dry THF, -78°C , 1.5h then diethyl oxalate, 1h.
 c) $\text{NH}_2\text{NH}_2\cdot\text{H}_2\text{O}$, dry CH_2Cl_2 , $\text{Ti}(\text{OiPr})_4$, r.t., 2.5h.
 d) Dry NMP, reactor, 250°C , 3h.
 e) NH_4OH 33%, microwave, 120°C , 30 min.
 f) H_2SO_4 96%, HNO_3 99.5%, reflux, 1h.
 g) **for 13a-c:** $\text{R}_1\text{-COCl}$, dry CH_2Cl_2 , Et_3N , 0°C , 2h, then r.t., 2h.
for 13d-f: NaH, dry THF, 0°C , 30 min, then $\text{R}_1\text{-COCl}$, r.t. 12h.

9	R_3
a	CF_3
b	COOEt

13	R_1	R_3
a	m- $\text{CH}_3\text{-Ph}$	CF_3
b	cC_3H_5	CF_3
c	m- $\text{CH}_3\text{-Ph}$	COOEt
d	m- $\text{CH}_3\text{-Ph}$	CN
e	cC_3H_5	CN
f	cC_3H_5	NO_2

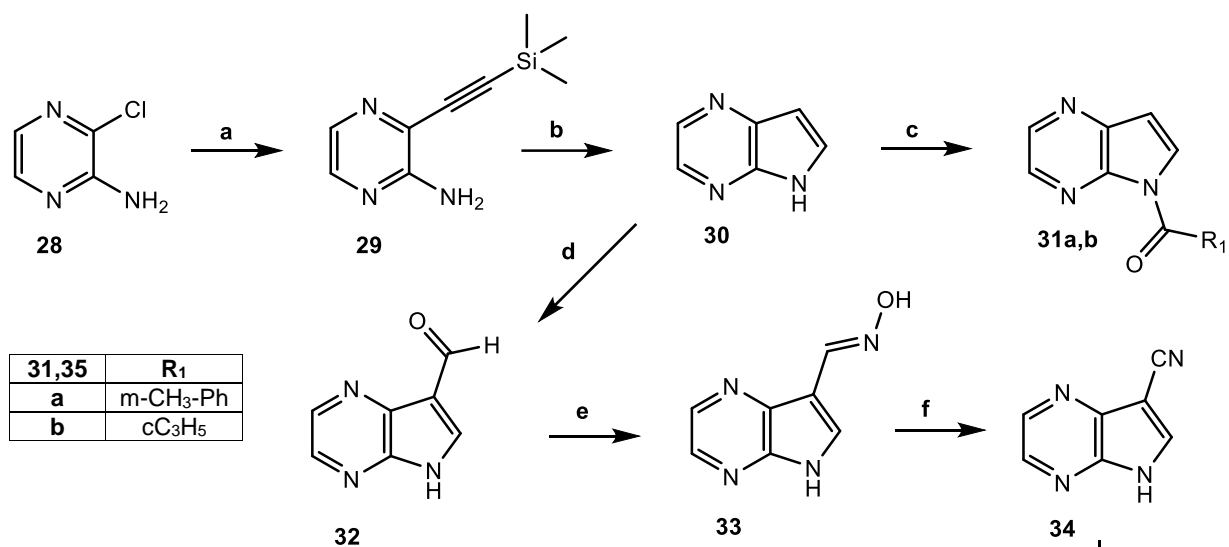
Scheme 3



Reagents and conditions:

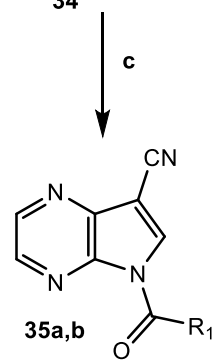
- TFAA, dry toluene, 85°C, 8h.
- NH₂NH₂·H₂O, n-BuOH, 200°C, 30 min.
- for **17a,b**, **19b**, **22a,b** and **27**: R₁-COCl, dry CH₂Cl₂, Et₃N, 0°C, 2h, then r.t., 2h.
for **19a**: NaH, dry THF, 0°C, 30 min, then R₁-COCl, r.t., 12h.
- NH₄OH 33%, reactor, 120°C.
- H₂O, EtOH 96%, KOH, reactor, 110°C, 6h.
- EtOH abs, SOCl₂, under N₂, reflux, 2h.
- Et₃N, dry CH₃CN, CDI, 80°C, 1.5h, then N,O-dimethylhydroxylamine hydrochloride, 80°C, 2h.
- CH₃MgBr, dry THF, under N₂, 0°C, 2h, then r.t., 12h.
- Et₃N, i-PrOH, NH₂NH₂·H₂O, reflux, 8h.

Scheme 4

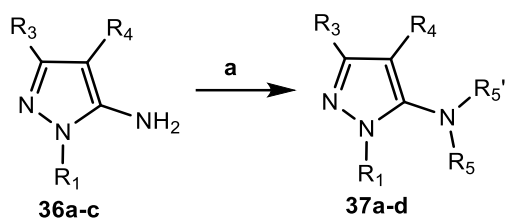


Reagents and conditions:

- a) Trimethylsilylacetylene, dry THF, CuI, Pd(PPh₃)₄, Et₃N, 0°C, then r.t., 12h.
 b) t-BuOK, dry NMP, reactor, 80°C, 1.5h.
 c) R₁-COCl, Et₃N, dry CH₂Cl₂, 0°C, 2 h, then r.t., 2h.
 d) HTMA, glacial CH₃COOH, reflux, 2 h.
 e) NH₂OH·HCl, H₂O, 60°C, 30 min, then NaHCO₃, reflux, 4h.
 f) POCl₃, reflux, 2h.



Scheme 5



36	R ₁	R ₃	R ₄
a	CH ₃	Ph	H
b	Ph	H	CN
c	H	Ph	CN

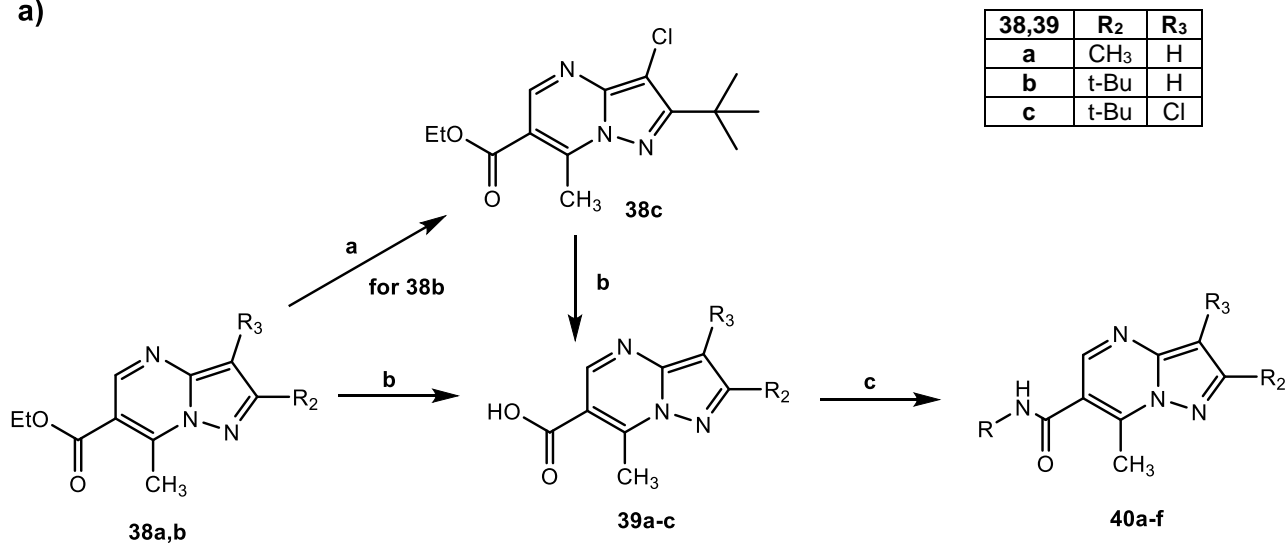
37	R ₁	R ₃	R ₄	R ₅	R ₅ '
a	CH ₃	Ph	H	CO-m-CH ₃ -Ph	H
b	CH ₃	Ph	H	CO-m-CH ₃ -Ph	CO-m-CH ₃ -Ph
c	Ph	H	CN	CO-m-CH ₃ -Ph	CO-m-CH ₃ -Ph
d	CO-m-CH ₃ -Ph	Ph	CN	H	H

Reagents and conditions:

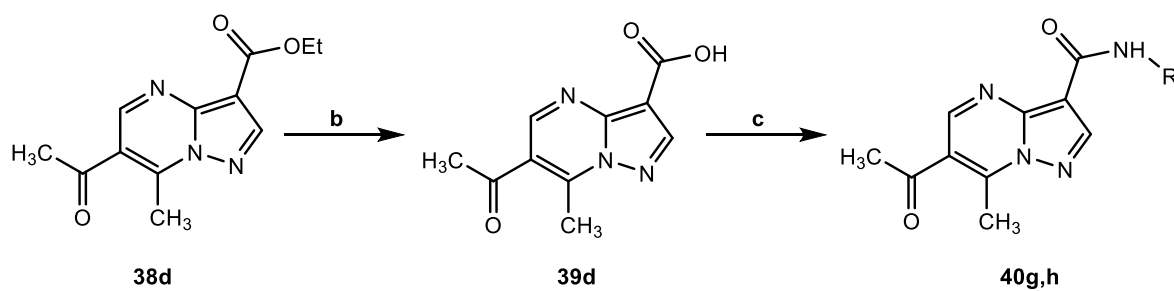
- a) for 37a,b,d: m-toluoyl chloride, dry CH₂Cl₂, Et₃N, 0°C, 2h, then r.t., 2h.
 for 37c: m-toluoyl chloride, dry CH₂Cl₂, DIPEA, 0°C, 2h, then r.t., 3h.

Scheme 6

a)



b)



Reagents and conditions:

- a) NCS, CCl₄, (PhCOO)₂, reflux, 12h.
 b) NaOH 6N, reflux, 2h.
 c) CCl₃CN, PPh₃, dry CH₂Cl₂, r.t., 4h, then R-NH₂, Et₃N, r.t., 12h.

40	R ₂	R ₃	R
a	CH ₃	H	m-(OCH ₃)-Ph
b	t-Bu	H	m-(OCH ₃)-Ph
c	t-Bu	Cl	m-(OCH ₃)-Ph
d	CH ₃	H	m-(OCH ₃)-Bn
e	t-Bu	H	m-(OCH ₃)-Bn
f	t-Bu	Cl	m-(OCH ₃)-Bn
g	-	-	m-(OCH ₃)-Ph
h	-	-	m-(OCH ₃)-Bn

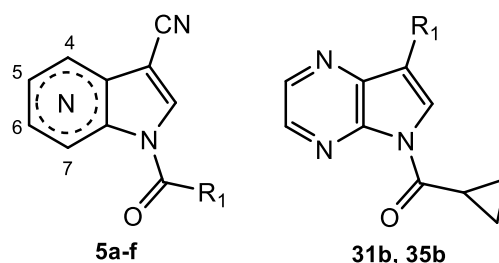
5. Results and discussion

5.1. Biological evaluation and structure-activity relationships (SARs) analysis

All compounds were evaluated for their ability to inhibit HNE by Prof. Quinn's group of Montana University. The results are presented in **Tables 1–4**, together with data of representative reference compounds from the previous series of 7-azaindoles [lead **A**: Crocetti, L. et al., 2018], N-benzoylindazoles [lead **B**: Crocetti, L. et al., 2013], and the drug Sivelestat.

Starting the discussion from those compounds which arise from the elaboration of the 7-azaindole nucleus of the lead compound **A** (4-, 5- and 6-azaindoles **5a-f** and the pyrrolopyrazines **31b** and **35b**, **Table 1**) we can observe that they are very powerful derivatives, with the only exception of pyrrolopyrazine **31b**. Specifically, movement of the nitrogen in the pyridine ring from position 7 to position 4 or 5 resulted in compounds with IC₅₀ values of 14-97 nM, with **5c** being the best term of this series. The shift of the nitrogen to position 6 (compounds **5e** and **5f**) led to reduced activity compared to the reference compound **A**, indicating that position 6 is the less suitable for the nitrogen displacement with respect to the other positions. The strong difference of potency between the two pyrrolopyrazines **31b** and **35b** (IC₅₀= 7.9 μM and 56 nM respectively) which differ only for the presence at position 3 of the CN group, is surely attributable to this last one, probably important for the interaction with the target.

Table 1. HNE inhibitory activity of compounds **5a-f**, **31b** and **35b**.



Compound	N	R ₁	IC ₅₀ (μM) ^a
5a	4	m-CH ₃ -Ph	0.089 ± 0.034
5b	4	cC ₃ H ₅	0.023 ± 0.004
5c	5	m-CH ₃ -Ph	0.014 ± 0.004
5d	5	cC ₃ H ₅	0.097 ± 0.01
5e	6	m-CH ₃ -Ph	0.194 ± 0.053
5f	6	cC ₃ H ₅	0.183 ± 0.044
31b	-	H	7.9 ± 2.5
35b	-	CN	0.056 ± 0.018
A	7	cC ₃ H ₅	0.087 ± 0.021
Sivelestat			0.050 ± 0.020

^aIC₅₀ values are presented as the mean ± SD of three independent experiments.

Moving to the azaindazoles series, arising from the insertion of a further nitrogen on the indazole scaffold of compound **B**, keeping the cyclopropanecarbonyl or the m-toluoyl fragment at N-1, we modified the substituents at position 3. Therefore, we inserted the cyano group as in the reference

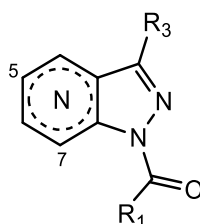
compound **B**, as well as other functions and groups selected from our previous publications or from the literature. Before analyzing the SARs of the compounds shown in **Table 2**, let us focus our attention on compounds **13d** and **19a**, which are the 7-aza and the 5-aza analogue respectively of the lead compound **B**. If the insertion of a nitrogen at position 7 (**13d**), afforded a 47-fold less potent compound with respect to **B** (**13d**: $IC_{50} = 330$ nM versus **B**: $IC_{50} = 7$ nM), the same additional nitrogen introduced in position 5 (**19a**) is responsible for the maintenance of activity, affording a compound as potent as the reference **B** (**19a**: $IC_{50} = 10$ nM versus **B**: $IC_{50} = 7$ nM).

Starting from the 7-azaindoles of type **13**, the replacement of the m-toluoyl fragment at N-1 in **13d** (which as above reported shows low potency) with the cyclopropanecarbonyl group, resulted in the very potent compound **13e** ($IC_{50} = 34$ nM). The replacement of the cyano group at position 3 with the carboxy function (**13c**) led to a moderately active inhibitor ($IC_{50} = 2.0$ μ M), while the introduction of a trifluoromethyl group (**13a,b**) gave different results depending on the fragment at N-1: in fact the cyclopropanecarbonyl derivative **13b**, showing $IC_{50} = 50$ nM is potent as the drug Sivelestat, while the m-toluoyl derivative **13a** is about one order of magnitude less potent.

Since also the introduction at position 3 of a nitro group (**13f**) gave a potent HNE inhibitor with an $IC_{50} = 21$ nM, we can identify for the series of 7-azaindoles two elements which seem important for HNE inhibitory activity: the presence of a strong electron withdrawing group at position 3 (i.e., CN, CF_3 , or NO_2) and the cyclopropyl at the amide function at N-1. In fact, the combination of these elements is present in the most powerful compounds of the series (**13b**, **13e** and **13f**).

Analysis of the 5-azaindazole derivatives (**17a,b**, **19a,b**, **22a,b** and **27**) revealed a slightly different trend with respect to the 7-indazoles. The presence of an electron withdrawing group is still important for activity and other than the strong CF_3 or CN groups (compounds **17a,b** and **19a,b**), also the weaker ester group (**22a,b**) afforded potent HNE inhibitors ($IC_{50} = 10$ -87 nM), and the confirmation of this is provided by the significant loss of activity of the 3-methyl derivative (**27**) ($IC_{50} = 760$ nM). In contrast to the 7-azaindole series, the group linked to the amide function appears not to affect the activity, since both N-cyclopropylcarbonyl and N-toluoyl derivatives show comparable potency as evident by comparing the pairs **17a/17b**, **19a/19b**, and **22a/22b**. As reported at the beginning of the discussion, compound **19a**, which is the 5-aza analogue of **B**, is the most potent compound of this series and had comparable activity with the lead **B** ($IC_{50} = 10$ nM).

Table 2. HNE inhibitory activity of compounds **13a-f**, **17a,b**, **19a,b**, **22a,b**, and **27**.



13a-f, **17a,b**, **19a,b**, **22a,b** **27**

Compound	N	R ₃	R ₁	IC ₅₀ (μM) ^a
13a	7	CF ₃	m-CH ₃ -Ph	0.42 ± 0.12
13b	7	CF ₃	cC ₃ H ₅	0.050 ± 0.01
13c	7	COOEt	m-CH ₃ -Ph	2.0 ± 0.44
13d	7	CN	m-CH ₃ -Ph	0.33 ± 0.03
13e	7	CN	cC ₃ H ₅	0.034 ± 0.012
13f	7	NO ₂	cC ₃ H ₅	0.021 ± 0.002
17a	5	CF ₃	m-CH ₃ -Ph	0.033 ± 0.011
17b	5	CF ₃	cC ₃ H ₅	0.087 ± 0.021
19a	5	CN	m-CH ₃ -Ph	0.010 ± 0.003
19b	5	CN	cC ₃ H ₅	0.079 ± 0.023
22a	5	COOEt	m-CH ₃ -Ph	0.016 ± 0.005
22b	5	COOEt	cC ₃ H ₅	0.069 ± 0.026
27	5	CH ₃	m-CH ₃ -Ph	0.760 ± 0.14
B	-	CN	m-CH ₃ -Ph	0.007 ± 0.0015
Sivelestat				0.050 ± 0.020

^aIC₅₀ values are presented as the mean ± SD of three independent experiments. ^bN.A.: no inhibitory activity was found at the highest concentration of compound tested (50 μM).

Table 3 showed the biological results of the pyrazole derivatives **37a-d**. Only compound **37d**, the only one presenting the N-1 involved in an amide function, showed some activity, although in the micromolar range (IC₅₀ = 1.1 μM). This result together with the inactivity of all other compounds (**37a-c**) which exhibit the amide function in the side chain at position 5, confirm the importance of the endocyclic amide for the activity.

Table 3. HNE inhibitory activity of compounds **37a-d**.



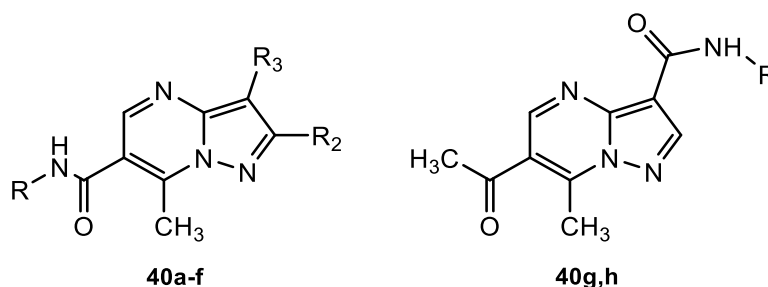
37a-d

Compound	R ₁	R ₃	R ₄	R ₅	R ₅ '	IC ₅₀ (μM) ^a
37a	CH ₃	Ph	H	CO-m-CH ₃ -Ph	H	N.A. ^b
37b	CH ₃	Ph	H	CO-m-CH ₃ -Ph	CO-m-CH ₃ -Ph	N.A. ^b
37c	Ph	H	CN	CO-m-CH ₃ -Ph	CO-m-CH ₃ -Ph	N.A. ^b
37d	CO-m-CH ₃ -Ph	Ph	CN	H	H	1.1 ± 0.4
Sivelestat						0.050 ± 0.020

^aIC₅₀ values are presented as the mean ± SD of three independent experiments. ^bN.A.: no inhibitory activity was found at the highest concentration of compound tested (50 μM).

Consistently, also the pyrazolopyrimidines **40a-h**, all bearing the amide function on a side chain at position 3 or 6, are inactive (**Table 4**).

Table 4. HNE inhibitory activity of compounds **40a-h**.



Compound	R	R ₂	R ₃	IC ₅₀ (μM) ^a
40a	m-(OCH ₃)-Ph	CH ₃	H	N.A. ^b
40b	m-(OCH ₃)-Ph	t-Bu	H	N.A. ^b
40c	m-(OCH ₃)-Ph	t-Bu	Cl	N.A. ^b
40d	m-(OCH ₃)-Bn	CH ₃	H	N.A. ^b
40e	m-(OCH ₃)-Bn	t-Bu	H	N.A. ^b
40f	m-(OCH ₃)-Bn	t-Bu	Cl	N.A. ^b
40g	m-(OCH ₃)-Ph	-	-	N.A. ^b
40h	m-(OCH ₃)-Bn	-	-	N.A. ^b
Sivelestat				0.050 ± 0.020

^aIC₅₀ values are presented as the mean ± SD of three independent experiments. ^bN.A.: no inhibitory activity was found at the highest concentration of compound tested (50 μM).

The 12 most potent HNE inhibitors (**5a-c**, **13b,f**, **17a,b**, **19a,b**, **22a,b** and **35b**) were evaluated for their chemical stability in aqueous buffer [Schepetkin, I. A. et al., 2007]. Spontaneous hydrolysis rates and reaction orders of the inhibitors were measured in phosphate buffer at pH 7.4 and 20 °C using spectrophotometry to detect compound hydrolysis. As examples, **Fig. 34** showed that the absorbance maxima at 305 nm decreased over time for compound **13f**, while a new peak appeared at 255 nm.

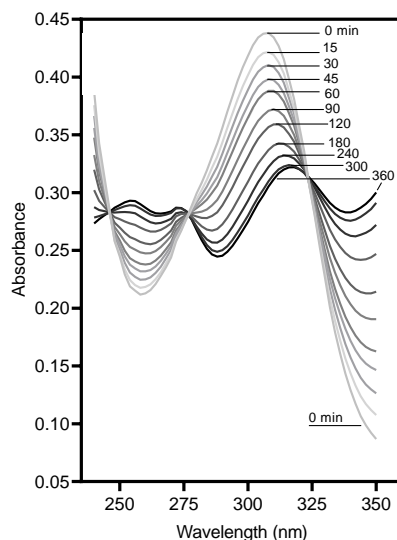


Figure 34. Analysis of changes in compound absorbance resulting from spontaneous hydrolysis of **13f**. The changes in absorbance spectra of the compounds (20 μ M in 0.05 M phosphate buffer, pH 7.4, 20 $^{\circ}$ C) were monitored over time in solution.

From data shown in **Table 5**, which exhibit as compounds **5b**, **13b**, **17b** and **22b** were the most stable with $t_{1/2} > 4$ h, we can obtain some information:

- generally, compounds containing a cyclopropanecarbonyl group at position 1 (compounds **5b** and **22b**) were more stable when compared to the analogs with a *m*-toluoyl substituent (compounds **5a** and **22a**, respectively);
- the azaindazole derivatives (compounds of type **13**, **17**, **19**, **22** and **27**) were more stable than the azaindoles (compounds of type **5**) and indazoles previously published [Crocetti, L. et al., 2013];
- the most stable compound **13b** had a CF_3 group at position 3, while molecules showing other electron-withdrawing substituents as CN and NO_2 (e.g., **5a**, **5c**, **13f**, **19a**, **19b**, **35b**), were unstable or moderately stable.

Table 5. Half-life ($t_{1/2}$) for the spontaneous hydrolysis of selected derivatives. LUMO energies of the compounds calculated by DFT B3LYP/6-31+G(d,p).

Compound	$t_{1/2}$ (min)	E(LUMO), eV
5a	76.6 ± 1.8	-2.414
5b	268.3 ± 29.3	-2.242
5c	163.3 ± 8.1	-2.484
13b	880.0 ± 77.5	-2.376
13f	93.8 ± 7.6	-3.374
17a	106.6 ± 2.4	-2.547
17b	386.1 ± 43.2	-2.386
19a	12.2 ± 4.0	-2.819
19b	79.0 ± 15.6	-2.743
22a	147.0 ± 12.3	-2.536
22b	436.8 ± 50.4	-2.418
35b	100.6 ± 5.2	-2.604

It is difficult to find a clear relationship between the spontaneous hydrolysis and a specific feature of our compounds (such as electronic or steric effects as of the heterocyclic scaffold and of the substituent). However, we found that the observed hydrolytic instability could be in part explained by the energies of the lowest unoccupied molecular orbital (LUMO) calculated for the optimized geometries of compounds **5a-c**, **13b,f**, **17a,b**, **19a,b**, **22a,b** and **35b** using density functional theory (DFT) (**Table 5**). The optimized structures of cyclopropyl-containing compounds, except for **5b**, have C_s symmetry with heterocyclic and cyclopropane groups lying in mutually perpendicular planes. For toluoyl-substituted derivatives, the angle between the planes of the heterocycle and m-tolyl group varied between 30° and 50°. Relatively stable compounds **13b**, **17b**, **22b**, and **5b** can be distinguished from hydrolytically unstable derivatives according to their LUMO energies E(LUMO) (**Fig. 35**).

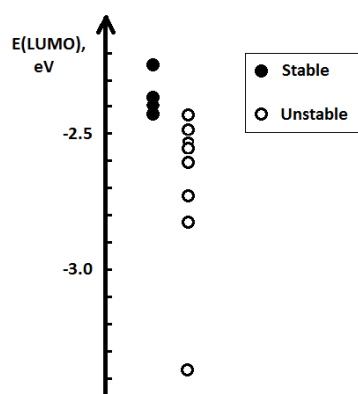


Figure 35. LUMO energies for hydrolytically stable and unstable compounds calculated by the DFT method at B3LYP/6-31+G(d,p) level of theory.

The unstable compounds had systematically lower values of E(LUMO) and, hence, were more prone to reactions with nucleophiles. This conclusion is in agreement with amide hydrolysis according to the well-known acyl substitution mechanism [Soderberg, T., 2019], which includes a nucleophilic

attack on the carbonyl carbon atom in the rate-limiting step. It should be noted that LUMO has a significant localization at the carbonyl carbon atom in both stable and unstable compounds (see examples in **Fig. 36**) and, thus, its energy can strongly affect electrophilicity of the carbonyl group. The relationship between $E(\text{LUMO})$ and hydrolytic stability is not quantitative (i.e., LUMO energy is not tightly correlated with $t_{1/2}$ or rate constant k'). Clearly, reactivity is determined not just by the electronic structure of a starting compound but it is also highly dependent on properties and stability of the tetrahedral intermediate formed on the addition of the hydroxide ion to the carbonyl group in the rate-limiting step.

Classification of stable and unstable compounds according to other calculated characteristics, such as energy of the highest occupied molecular orbital (HOMO), LUMO-HOMO energy gap, or some local indices of reactivity (e.g., atomic charges, Wiberg index for the amide bond) did not lead to a separation similar to the result presented in **Fig. 35** for LUMO energies.

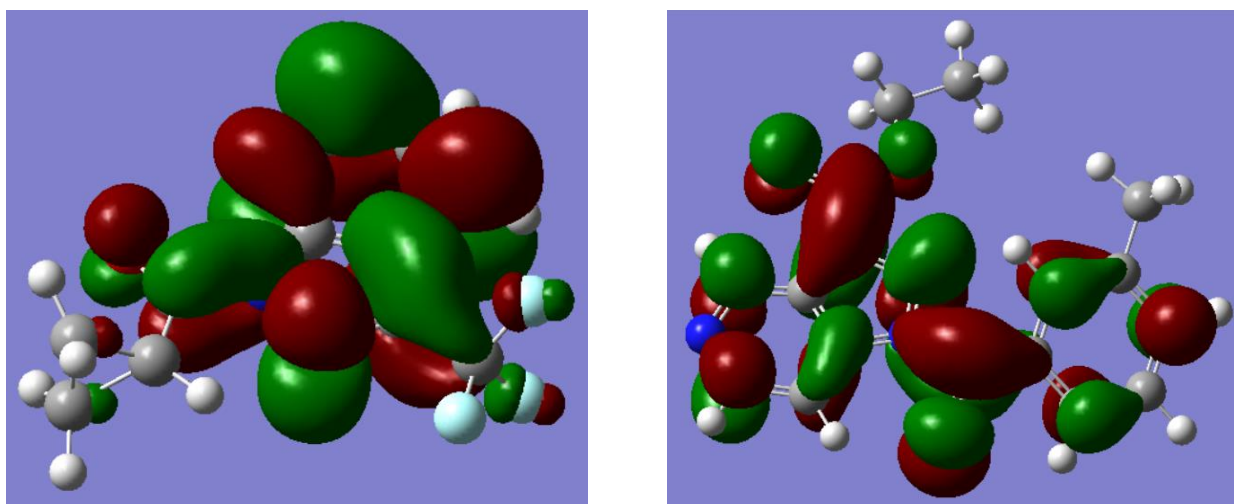


Figure 36. Surfaces of LUMO (isovalue 0.02) for compounds **13b** (A) and **22a** (B) calculated by the DFT method at B3LYP/6-31+G(d,p) level.

5.2. Molecular Modeling

We performed molecular modeling of selected compounds in the active site of HNE (1HNE entry of Protein Data Bank) using previously reported methods [Crocetti, L. et al., 2013; Crocetti, L. et al., 2018]. According to the literature [Ghose, A. K. et al., 1999], the inhibitors interact with HNE via a nucleophilic attack of the Ser195 hydroxyl oxygen atom onto a carbonyl carbon atom of the ligand, which leads to the formation of a Michaelis complex. This interaction is accompanied by a proton transfer from Ser195 to Asp102. For the docking poses obtained, we have evaluated the geometric parameters d_1 and α , which are important for Michaelis complex formation (**Fig. 37**). In addition, the length of the proton transfer channel within the catalytic triad from Ser195 to Asp102 through His57 was calculated using d_2 and d_3 distances between the key atoms (see *Methods*).

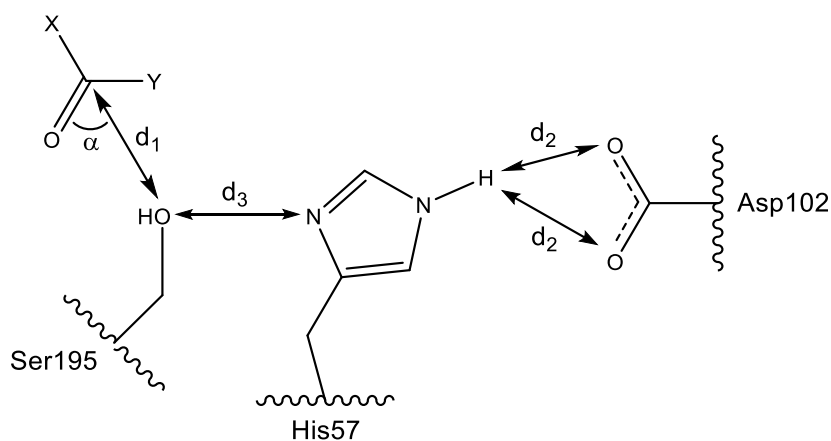


Figure 37. Interaction of a carbonyl-containing ligand XC(O)Y with the HNE catalytic triad (Ser195, His57, and Asp102). Distance d_1 and angle α determine conditions for the Michaelis complex formation. The value of α was measured as an angle between $\text{C}(\text{carbonyl})\cdots\text{O}(\text{Ser195})$ axis and $\text{C}=\text{O}$ bond. Distances d_2 and d_3 influence on the proton transfer from Ser195 to Asp102. Length of the proton transfer channel was calculated as $L = \min(d_2) + d_3$.

The comparison between azaindoles, **5a**, **5c**, and **5e** and the reference compound **C** [Crocetti, L. et al., 2018], showing a *m*-toluoyl fragment at the nitrogen at position 1, highlighted a similar orientation within the binding site (**Fig. 38A**). Both heterocyclic and *m*-toluoyl group were located approximately in the same corresponding regions of space inside the enzyme. Some features of their interactions with the HNE amino acids should be mentioned and are illustrated in **Fig. 38**. Compounds of this series form H-bonds with Gly193 involving participation of the amide oxygen atom (**5e** and **5c**, see **Fig. 38B** and **38D**), or with Ser195 involving participation of the oxygen and nitrogen atoms of the amide function (**5e** and **5a**, see **Fig. 38B** and **38C**). In addition, compound **5a** is H-bonded to Val216 via the nitrogen atom at position 4 of the heterocycle. A comparison of the docking poses of compounds **5c** and **19a**, of which the latter has an additional nitrogen atom in the five-membered ring instead of the CH group, showed a slight difference in orientation of the molecules within the binding site (not shown).

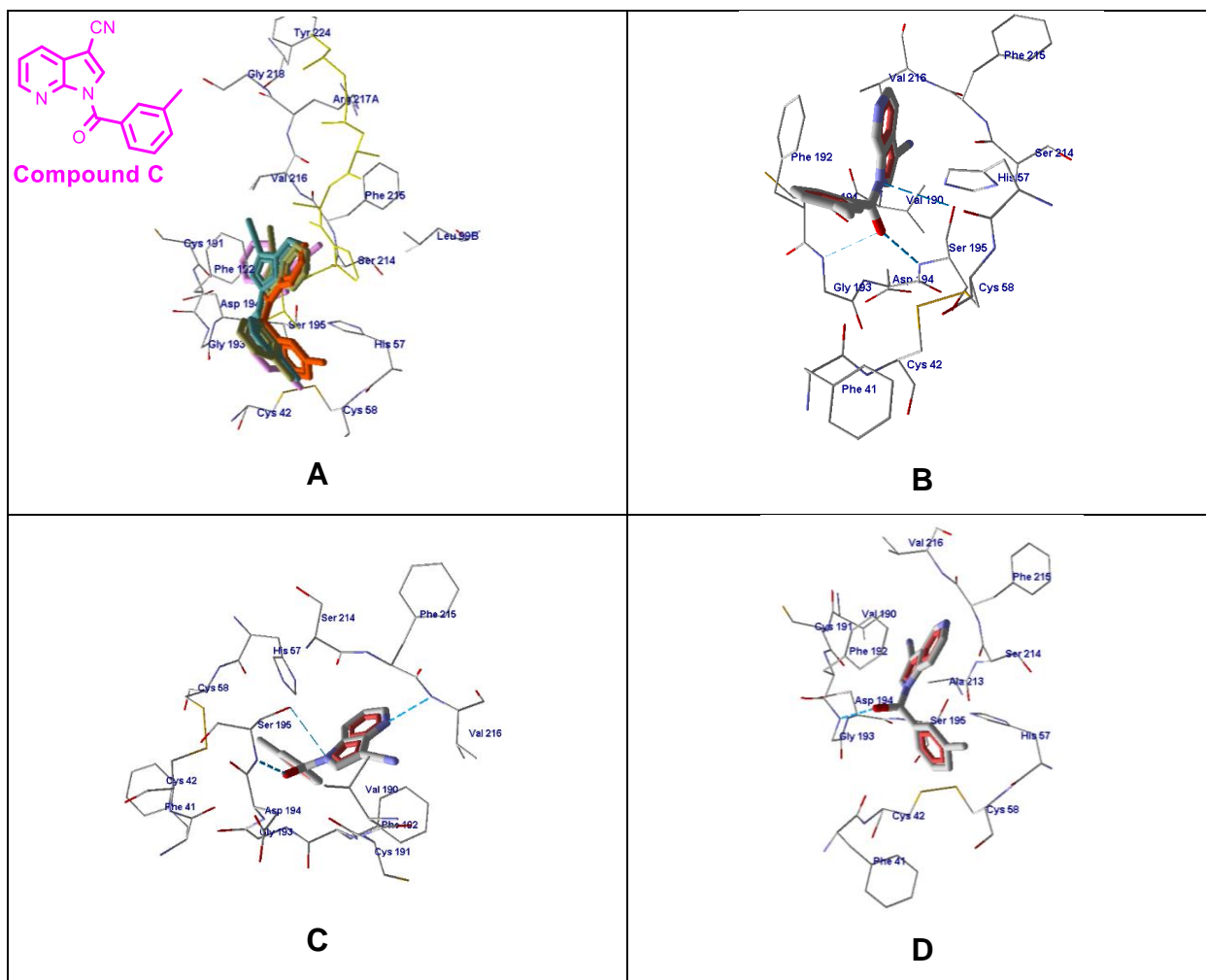


Figure 38. Docking poses of **5a**, **5c**, **5e**, and reference compound **C**. **Panel A.** Docking poses of compounds **C** (magenta), **5e** (dark green), **5a** (light blue), and **5c** (orange). Co-crystallized MSACK is shown in yellow sticks. Residues within 4 Å of the co-crystallized ligand are visible. **Panel B.** Docking pose of compound **5e**. **Panel C.** Docking pose of compound **5a**. **Panel D.** Docking pose of compound **5c**. For **Panels B-D** residues within 4 Å of the pose are visible.

Although the carbonyl groups of **5c** and **19a** have the same orientation and can engage a hydrogen bond with Asp194 (**19a** also with Gly193, see **Fig. 39c**), the bicyclic ring and the *m*-toluoyl fragments do not mutually coincide since they are oriented oppositely. Despite this different arrangement of the **19a** with respect **5c** the HNE inhibitory activity is comparable (0.010 μM and 0.014 μM respectively) Compounds **13d** ($\text{IC}_{50} = 330 \text{ nM}$) and **19a** ($\text{IC}_{50} = 10 \text{ nM}$) contain an additional nitrogen atom at different positions of the fused aromatic ring compared to compound **B**. The docking poses of these molecules are shown in **Fig. 39**. Although these three molecules are isosteres, the presence of an additional nitrogen atom in the heterocycle of compounds **13d** and **19a** favors arrangement of their bicyclic fragments among polar amino acid residues versus compound **B** with an indazole heterocycle. Molecule **13d** forms a H-bond with Val216 via participation of the nitrogen atom at position 7 of the heterocycle, while compound **19a** is H-bonded to Ser195 with two nitrogen atoms of the five-membered ring. In addition, strong H-bonds are formed between the carbonyl oxygen of

19a and Gly193 and Ser195. Note that the nitrogen atom at position 5 of the heterocycle in **19a** is located near an electropositive (blue) region of the binding site surface (**Fig. 39D**), which should, along with the H-bonds, stabilize the molecule in the obtained docking pose.

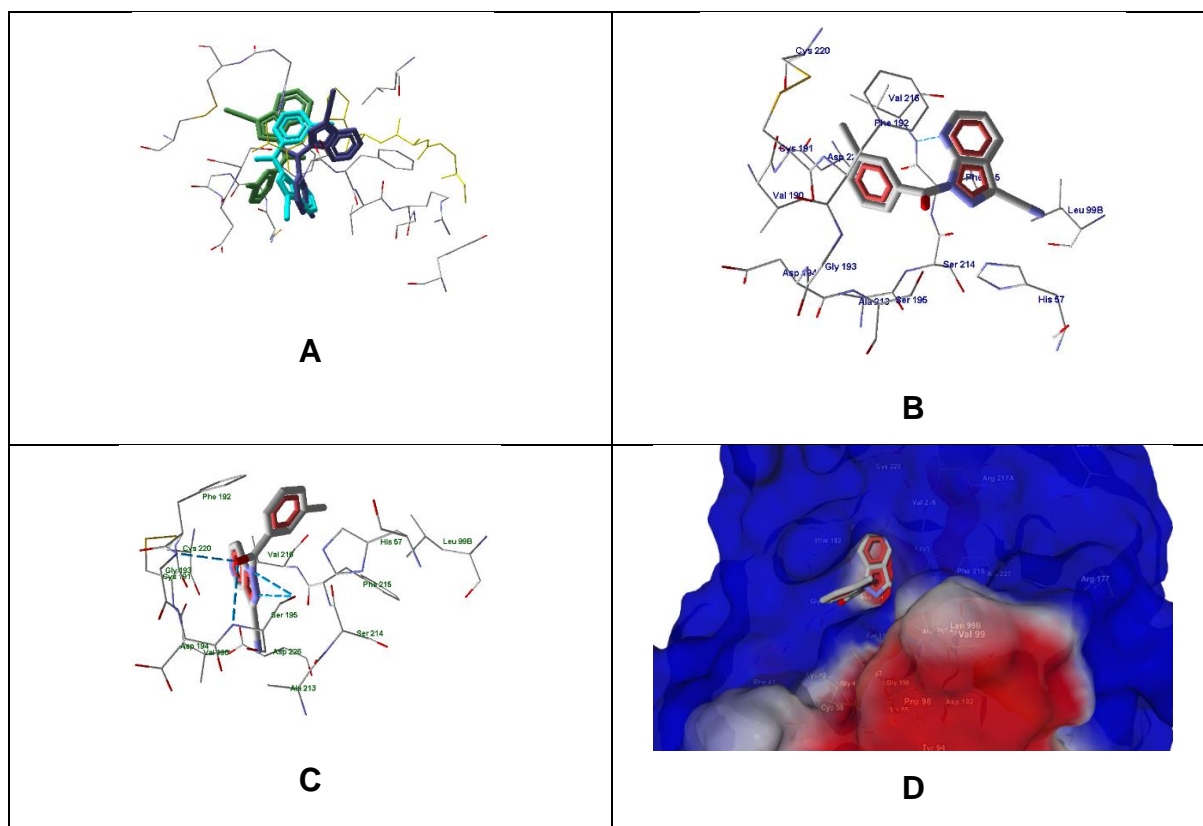


Figure 39. Docking poses of **13d**, **19a** and reference compound **B**. **Panel A.** Docking poses of **13d** (violet), **19a** (light blue), and reference compound **B** (green). Co-crystallized methoxysuccinyl-Ala-Ala-Pro-Ala chloromethyl ketone (MSACK) is shown in yellow sticks. Residues within 4 Å from the co-crystallized ligand are visible. **Panel B.** Docking pose of compound **13d**. **Panel C.** Docking pose of compound **19a**. For **Panels B** and **C**, residues within 4 Å of the pose are visible. **Panel D.** Docking pose of compound **19a**. The semi-transparent surface of HNE is shown.

Compound **13f** containing nitro and cyclopropanecarbonyl group is anchored in the HNE binding site due to H-bonds with Val216 (with the participation of the nitro group), Gly193, and Ser195 (with the participation of the carbonyl oxygen atom of the amide) (**Fig. 40A**). Compound **22a** has two potential centers for nucleophilic attack by Ser195 (i.e., carbonyl oxygen atoms of the amide and ester groups). The three H-bonds engaged by the carbonyl oxygen atom of amide and the N-2 of the five-membered ring with Gly193 play a role in anchoring **22a** inside the binding site (**Fig. 40B**). The d_1 distances $O=C\cdots O(\text{Ser195})$ in the pose obtained for compound **22a** are 2.946 and 3.817 Å for the carbonyl carbon atoms of the ester and amide groups, respectively (**Table 6**). From this point of view, nucleophilic attack on the ester group is more likely. In addition, the angle α in this case is 86.7°, being in the range of 80-120°, which is favorable for the formation of the Michaelis complex

[Burgi, H. B. et al., 1974; Vergely, I. et al., 1996; Peters, M. B. et al., 2006], which is in contrast to $\alpha = 132.9^\circ$ obtained for the amide C=O bond.

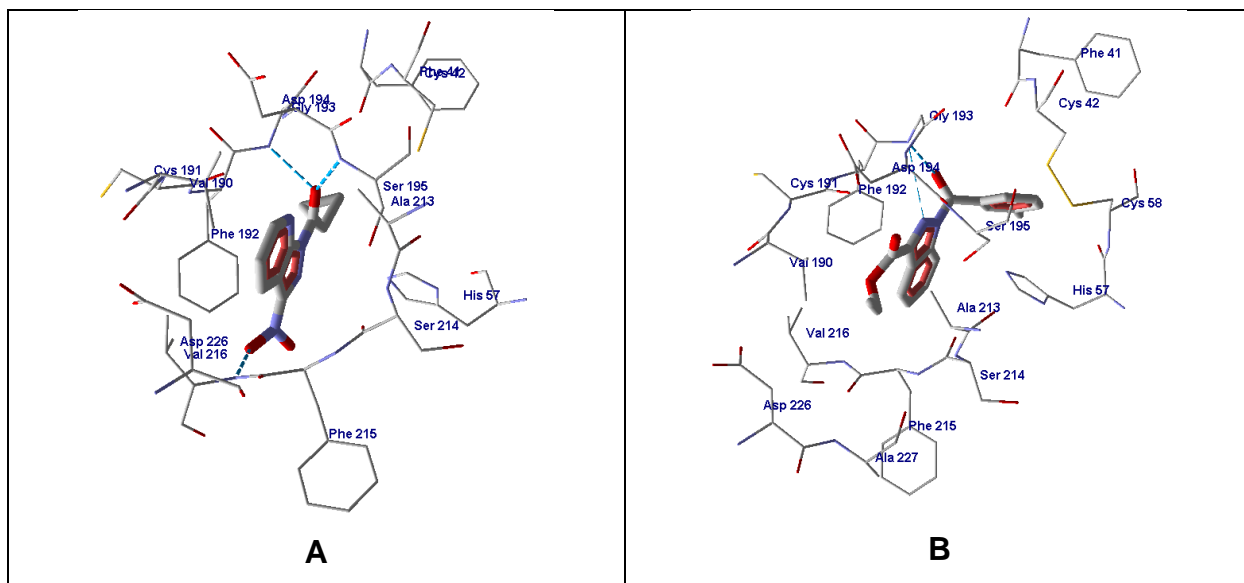


Figure 40. Docking pose of compound **13f** (Panel A) and **22a** (Panel B). For both panels, residues within 4 Å of the pose are visible.

Table 6 shows the geometric parameters (distance d_1 and angle α) for the docking poses, as well as the distances d_2 and d_3 between the key atoms of the catalytic triad of Ser195, His57, and Asp102 (**Fig. 37**), which determine the length L of the proton transfer channel. Values of α for most of the compounds evaluated were between 80° to 120° and are optimal for formation of the Michaelis complex. The exceptions were the less active compounds **13d** and **5e**. The pose of another compound with reduced activity (**5a**) is characterized by an angle α close to 80° ; however, the proton transfer channel L for this molecule has a rather high value due to mutual displacements of the residues of the catalytic triad upon binding of **5c** to HNE.

Table 6. HNE inhibitory activity of selected compounds and geometric parameters of the enzyme–inhibitor complexes predicted by molecular modeling^a.

Compound	IC ₅₀ (nM)	α (°)	d_1	d_2	d_3	L
			Å			
5a	89	79.7	3.256	4.852, 5.345	2.478	7.330
5c	14	140.0	4.324	1.790, 3.334	2.815	4.605
5e	194	64.9	3.622	1.857, 3.396	2.872	4.729
13d	330	76.3	3.620	2.196, 3.606	3.291	5.487
13f	21	85.2	3.298	2.349, 3.883	3.294	5.643
19a	10	89.8	3.001	1.790, 3.334	2.826	4.616
22a	16	86.7	2.946 ^b	1.769, 3.340	2.856	4.625

^aGeometric parameters correspond to the formation of Michaelis complex with the ester carbonyl group.

^bThe indicated d_1 value corresponds to the carbonyl carbon atom of the ester function of compound **22a**. For amide carbon atom of this compound, the d_1 distance equals 3.817 Å.

5.3. ADMET assessment

To improve the knowledge and to facilitate the selection of lead compounds for in vivo studies, we also performed *in silico* absorption, distribution, metabolism, and excretion-toxicity (ADMET) pharmacokinetics evaluation. The *in silico* assessment was generated through the evaluation of pharmacokinetic profiles and possible adverse side effects for compounds **5a-f**, **13a-f**, **17a,b**, **19a,b**, **22a,b**, **27**, **31**, and **35**. ADMET molecular studies were conducted using SwissADME (<http://swissadme.ch>) [Daina, A. et al., 2017] and pkCSM (<http://biosig.unimelb.edu.au/pkcsml/>) [Pires, D. E. V. et al., 2015] (see **Tables 1S-11S** in experimental section). Most of the compounds were predicted to be orally available, with high gastrointestinal absorption and high-water solubility (see **Table 2S, 3S**). Compounds with predicted moderate solubility (10^{-5} mol/L range) were **13a**, **13c**, **17a** and **22a**. Only compound **17b** was predicted to be P-glycoprotein substrates, whereas most of the compounds were predicted to be inhibitors of the CYP1A2. Some compounds were also predicted to inhibit CYP2C19/CYP2C9, but no inhibition was predicted for CYP3A4 and CYP2D6. Otherwise, most of the compounds were predicted to be CYP3A4 substrates but should not be metabolized by CYP2D6 (see **Table 7S**). Interestingly, none of the compounds violated the Lipinski rule of 5, nor did they violate the other drug-likeness rules (Ghose, Egan, Veber, and Muegee) [Lipinski, C. A. et al., 1997; Ghose, A. K. et al., 1999; Egan, W. J. et al., 2000; Veber, D. F. et al., 2002; Muegge, I. et al., 2001].

The absorption and distribution calculated parameters are shown in an Egan–Egg model (**Fig. 41**) (Brain or Intestinal Estimated, BOILED-Egg). The Egan–Egg model highlights that most of the compounds were predicted to passively permeate the blood-brain barrier, whereas compounds **13e**, **13f**, **19b**, **22b** and **35** are only able to be passively absorbed by the gastrointestinal tract pkCSM calculated absorption properties showed > 95 % intestinal absorption (aside from molecule **6** with 77.3%), due to the calculated optimal (> 0.90) Caco-2 cell permeability (see **Table 5S**). Moreover, most of the compounds are predicted to be adsorbed by the skin (exploitable for transdermal drug delivery) as shown by the Log Kp < -2.5 (see skin permeability, **Table 5S**).

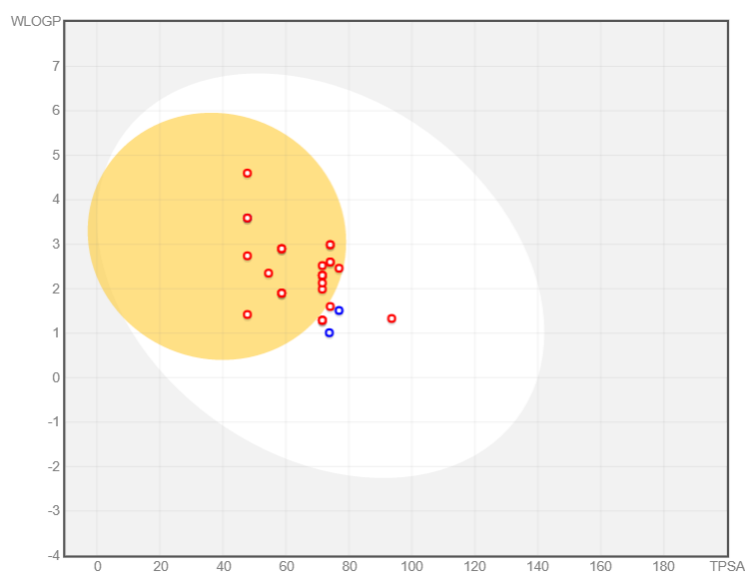


Figure 41. BOILED-Egg plot. Points located in the BOILED-Egg's yellow are the compounds predicted to permeate the BBB passively, differently the ones in the white are the molecules predicted to be only passively absorbed by the gastrointestinal tract. Blue dots indicate molecules expected to be refluxed from the central nervous system (CNS) by the P-glycoprotein, whereas the red ones are not transported by the P-glycoprotein.

The calculated values of steady state volume of distribution are relatively low for some compounds (Log VD_{ss} < -0.15, see **Table 6S** in experimental section), but most of the compounds were predicted to have a significant unbound fraction in the plasma, thus becoming available for interaction with the pharmacological target (see **Table 7S**). The calculated values of the total clearance (see **Table 8S**) indicate that most of the compounds were predicted to have good renal elimination (0.20 - 0.84 mL/min/kg), and no compounds were predicted to be substrates of the renal organic cation transporter 2. pkCSM calculated toxicity properties indicated concerns about the AMES test, the *T. pyriformis* toxicity and hepatotoxicity. On the other hand, the compounds did not have skin sensitization properties and were not predicted to be inhibitors of hERG I and II (see **Table 9S**). Due to the toxicology concerns indicated by pkCSM, toxicology was also evaluated with Datawarrior (v. 5.2.1 <http://www.openmolecules.org/datawarrior/>). In this case, all compounds were predicted to be non-mutagenic, non-tumorigenic, and not irritants. A low risk for reproductive system effects was associated with molecules **13c**, **17a** and **22a,b** (see **Table 16**). *In silico* toxicity evaluations were also performed with preadmet (<https://preadmet.bmdrc.kr/toxicity/>) and admetsar1 (<http://lmmd.ecust.edu.cn/admetsar1>). The results for preadmet are presented in **Table 11S**, which considered most of the compounds mutagenic in the same test. Despite this result, most of the compounds were considered non-carcinogenic for mouse or rat, with a medium to low risk for their hERG inhibition in both *in silico* evaluations. Further biological evaluation is needed due to the somewhat contrasting test results, but the ADMET general profile was good for our set of compounds (see **Table 7**), particularly the most potent compounds **5b**, **5c**, **13f**, **19a** and **22a**, which had excellent ADMET profiles and shouldn't have any particular toxicity issues. The IC₅₀ measured potency,

together with the ADMET profile will be of fundamental importance for the future selection of compounds for *in vivo* evaluation.

Table 7. Predicted ADME properties for selected compounds **5b**, **5c**, **13b**, **13f**, **17b**, **19a** and **22a,b**.

Mol	Water solubility	Caco2 permeability	Skin Permeability	Clearance	Consensus Log P	IC₅₀ (nM)
5b	-2.62	1.30	-2.75	0.54	1.52	23
5c	-3.59	2.35	-2.42	0.41	2.50	14
13b	-3.88	1.35	-2.90	0.31	2.54	50
13f	-3.03	0.52	-2.82	0.49	0.91	21
17b	-3.97	1.37	-2.78	0.31	2.35	87
19a	-3.18	0.96	-2.42	0.23	2.20	10
22a	-3.23	1.23	-2.56	0.62	2.70	16
22b	-2.83	1.27	-2.66	0.64	1.66	69

6. Conclusions

The modifications of effective compounds previously synthesized by our research group [Crocetti, L. et al., 2013; Crocetti, L. et al., 2018] have allowed us to identify new potent HNE inhibitors with different nitrogen heterocyclic scaffolds. The biological results indicated that the change of position of the nitrogen, as well as the insertion of an additional nitrogen atom in the nuclei of reference compounds **A** and **B** is compatible with biological activity, since most of the new products exhibited potent HNE inhibitory activity with IC₅₀ values in the nanomolar range. The most potent compounds were found in the series of 5- and 7-azaindazoles (**13f**, **19a** and **22a**, with IC₅₀ = 21, 10, and 16 nM, respectively) and 4- and 5-azaindoles (**5b**, **5c** with IC₅₀ = 23 and 14 nM, respectively). The chemical stability of the new inhibitors is generally good, with a half-life ($t_{1/2}$) > 1 h and for compounds **5b**, **13b**, **17b** and **22b**, $t_{1/2}$ > 4 h. With the only exception of **19a** ($t_{1/2}$ = 12.2 min), the new azaindazole derivatives were more stable than the previously described indazoles (i.e., reference compound **B**, $t_{1/2}$ = 21.7 min) [Crocetti, L. et al., 2013], suggesting that this new scaffold improves chemical stability against spontaneous hydrolysis. However, the chemical stability also seems to be related to the substituent at position 3 of the scaffold, since both the azaindazole **19a** and the indazole **B**, showing a CN group at position 3 are compounds chemically unstable in aqueous buffer.

The relatively stable compounds **5b**, **13b**, **17b** and **22b** were well separated from unstable derivatives by considering their LUMO energies E(LUMO). Indeed, the unstable compounds had overall lower values of E(LUMO) and, hence, were more prone to reactions with nucleophilic species. Molecular modeling studies confirmed the importance of the Michaelis complex formation for the interaction with the enzyme pocket, and we found that highly active HNE inhibitors were characterized by geometries favorable for acyl-inhibitor complex formation and by relatively short lengths of the proton transfer channel via the catalytic triad. Finally, *in silico* ADMET calculations predicted that most of the new compounds would be optimally absorbed, distributed, metabolized and excreted. Particularly, compounds **5b**, **5c**, **13f**, **19a** and **22a** had excellent predicted ADMET profiles and no noted toxicity problems. Moreover, many of our compounds seem to be well adsorbed by the skin, opening to a new potential and easier route of administration for *in vivo* studies of these new HNE inhibitors.

Section II

7. Background and aims of the work

As second main project of this thesis, the following three new scaffolds have been investigated: 1,5,6,7-tetrahydro-4H-indazol-4-one (**D**), 5,6-dihydrocyclopenta[c]pyrazol-4(1H)-one (**E**) and 5,6,7,8-tetrahydrocyclohepta[c]pyrazol-4(1H)-one (**F**).

SCAFFOLD D

The idea to expand the research on HNE inhibitors has recently come from a promising series of molecules patented by Boehringer Ingelheim [Oost, T. et al., 2016b; Peters, S. et al., 2016; Gnam, C. et al., 2017]. These are molecular complications of potent pyrimidines synthesized by Bayer, of which **BAY 85-8501** [Von Nussbaum, F. et al., 2015b] is currently the most interesting, being in phase II clinical trials for the treatment of bronchiectasis. These compounds present a 4,6,7,8-tetrahydroquinazolin-2,5(1H,3H)-dione structure, with the pyrimidine ring condensed with a cyclohexanone (**Fig. 42**).

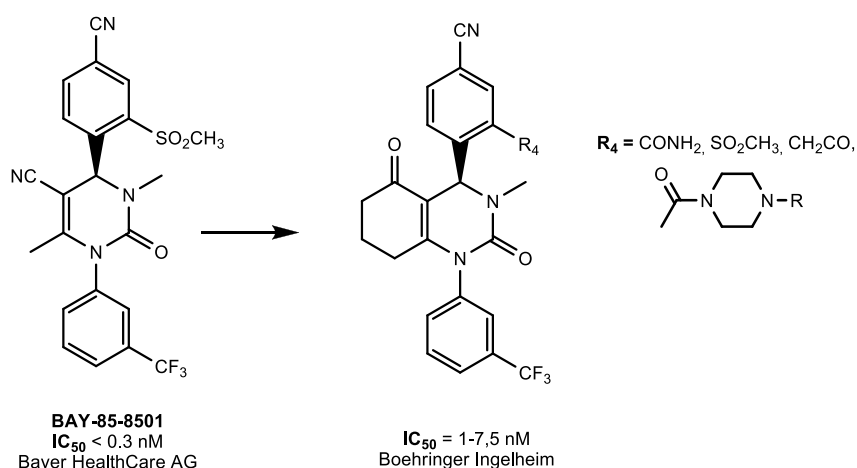


Figure 42. Compounds reported in the literature developed by Bayer HealthCare and Boehringer Ingelheim.

Therefore, we followed a similar strategy on our indazole scaffold, and as first step we replaced the benzene of indazole with the cyclohexanone ring, by obtaining the 1,5,6,7-tetrahydro-4H-indazol-4-one nucleus (**D**) (**Fig. 43**).

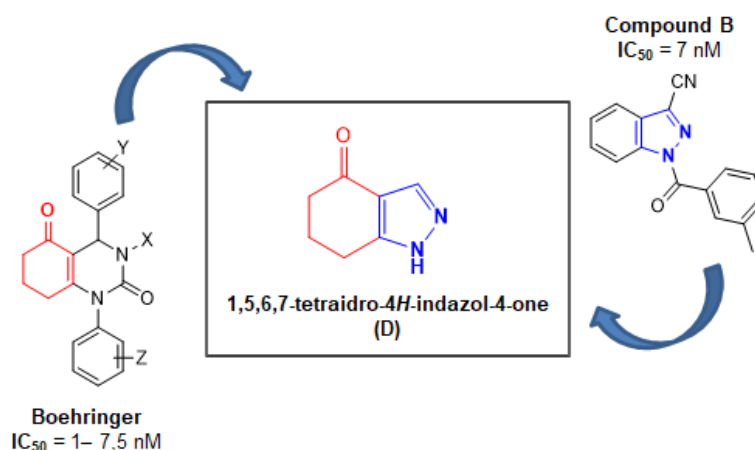
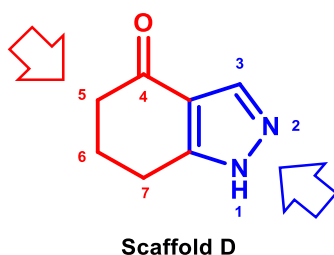


Figure 43

On **D** we planned to insert those groups that gave the best results in the indazole derivatives, but also to insert a basic center (piperazine chain) in analogy to Boehringer's products. Finally, we synthesized some products bearing the amide function on a side chain, to understand if also for this nucleus is necessary the endocyclic N-CO function for the activity.

In undertaking synthetic work, we then designed some modifications outlined below:



Pyrazole

- Synthesis of N-CO derivatives by introducing the best substituents of the indazole series, in particular cyclocarbonyl or m-tolouyl groups.
- Elimination of the N-CO function by insertion of a benzyl or phenyl group.
- Introduction of basic groups and simultaneous displacement of amide function outside the scaffold.

Cyclohexanone

- The shift of the amide group from the pyrazole nucleus to position 4 of the bicycle.
- Insertion of 1/2 bromine atoms at position 5 of the scaffold, maintaining the amide group on the pyrazole.
- Insertion of basic chain at position 5.

SCAFFOLD E AND F

Given the promising results obtained by studying the scaffold **D**, we decided to operate as a contraction and an enlargement of the cyclohexanone ring, thus obtaining 5,6-dihydrocyclopenta[c]pyrazol-4(1H)-one (**E**) and 5,6,7,8-tetrahydrocyclohepta[c]pyrazol-4(1H)-one respectively (**F**) (**Fig. 44**) Both these scaffolds have been investigated by repeating the same modifications and elaborations made on the pyrazolecyclohexanone nucleus.

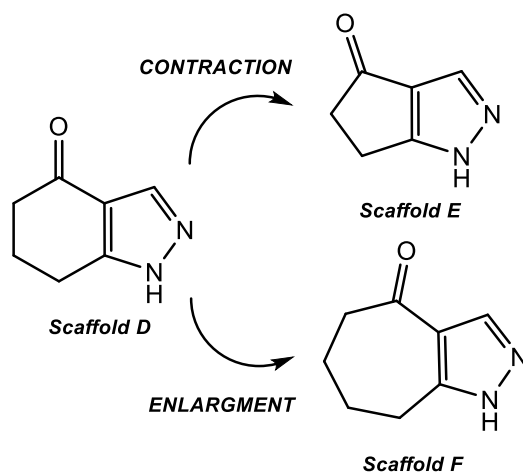


Figure 44

Stability and gas chromatographic studies have been performed on compounds with scaffolds **D** and **E**, and, in addition, molecular modeling and crystallographic investigations have also been carried out on the 5,6-dihydrocyclopenta[c]pyrazol-4(1H)-one (**E**), which allowed us to assign the correct structures of the new compounds.

Finally, we synthesized a new 4,6,7,8-tetrahydropyrazolo[4,3-b]azepin-5(1H)-one scaffold, exhibiting a lactam moiety within the heptacycle, in order to obtain final compounds offering two different points of attach for Ser-OH. (**Fig. 45**).

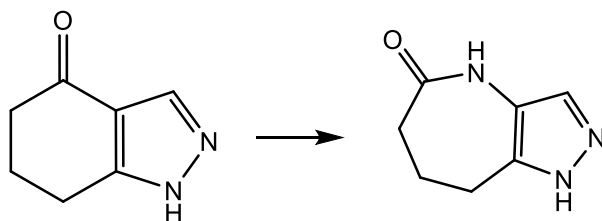


Figure 45

8. Chemistry

In the [Schemes 7-13](#) are reported the synthetic procedures to obtain the final compounds showing the three scaffolds 1,5,6,7-tetrahydro-4H-indazol-4-one (**D**), 5,6-dihydrocyclopenta[*c*]pyrazol-4(1H)-one (**E**) and 5,6,7,8-tetrahydrocyclohepta[*c*]pyrazol-4(1H)-one (**F**).

- **Schema 7:** 2-iodo-1-(4-phenylpiperazin-1-yl)ethan-1-one (**43**)
- **Scheme 8:** 1,5,6,7-dihydro-1H-indazol-4(5H)-one derivatives (**47a-e** and **48a-e**)
- **Scheme 9:** 5-bromo-6,7-dihydro-1H-indazol-4(5H)-one derivatives (**50a** and **51a,c**) and 5,5-dibromo-6,7-dihydro-1H-indazol-4(5H)-one derivatives (**50b** and **51b,d**)
- **Scheme 10:** 4,5,6,7-tetrahydro-1H-indazol-4-amine derivatives (**55a-c**)
- **Scheme 11:** 5,6-dihydrocyclopenta[*c*]pyrazol-4(1H)-one derivatives (**60a-c** and **61a-d**)
- **Scheme 12:** 5,6,7,8-tetrahydrocyclohepta[*c*]pyrazol-4(1H)-one derivatives (**65a-c** and **66a,b**)
- **Scheme 13:** 4,6,7,8-tetrahydropyrazolo[4,3-*b*]azepin-5(1H)-one derivatives (**71** and **74**)

Before starting the description of the schemes, it should be noted that the three scaffolds **D-E** present two possible tautomeric forms, according to the literature [**46:** Claramunt, R. M. et al., 2006; **59:** Lauffer, D. J. et al., 2019; **64:** Maynard, G. et al., 2003], and the hydrogen may be at both the nitrogen atoms of the pyrazole (see **Fig. 46**). The presence of one or the other form in solution depends on the type of solvent, its polarity, reaction medium, type of reactive used, and during alkylation and acylation reactions it was possible to observe the formation of a mixture of the two isomers, often widely unbalanced in favor of one form. For each scaffold, an *in-depth* study of this aspect will be dealt in detail in the corresponding scheme as well as the use of different techniques for the characterization and separation of the pair of isomers.

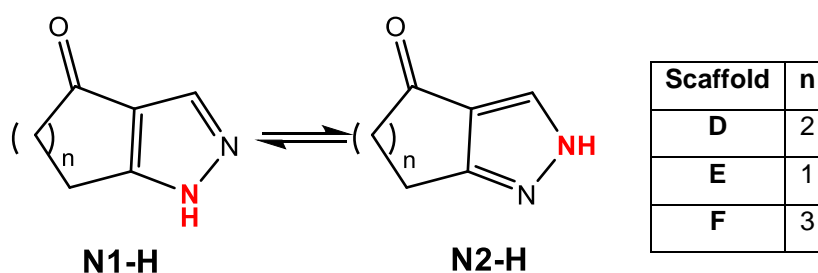


Figure 46. Tautomerism of scaffolds **D**, **E** and **F**.

Going now to the description of the synthetic procedures, in [Scheme 7](#) is reported the synthesis of the reactive **43** used in the following schemes. The commercial 1-phenyl-piperazine **41** was firstly treated with chloroacetyl chloride and DIEA to afford the intermediate **42** [Sharma, R. K. et al., 2015] and then transformed into the corresponding iodinated reagent **43** with sodium iodide in acetone at room temperature.

In [Scheme 8](#) is described the synthetic pathway leading to the final compounds of type **47** and **48**. The commercial 1,3-cyclohexandione **44**, treated with DMF-DMA at reflux afforded the 2-[(dimethylamino)methylene]cyclohexane-1,3-dione **45** [Claramunt, R. M. et al., 2006], which was then cyclized with hydrazine to the key intermediate **46**, without isolating the open intermediate. As above mentioned, studies performed through NMR and crystallographic analysis by Claramunt et al., demonstrated that the tautomerism of 1,5,6,7-tetrahydro-4H-indazol-4-one **46**, is strongly influenced by the polarity of the solvent. In particular in polar solvents the N1-H form prevails on the N2-H (**Fig. 46**, scaffold **D**), consistent with the dipolar moment value of the tautomer N1-H, which is about 2.5-fold higher than the value of the tautomer N2-H. Therefore, as expected, the acylation reaction performed using m-toluoyl chloride or cyclopropanecarbonyl chloride in dichloromethane and triethylamine led to a pair of isomers (**47a/48a** and **47b/48b** respectively). It is possible to observe the same trend in the alkylation reactions carried out in standard condition and using various reagents (**47c/48c** and **47d/48d**) as well as in coupling reaction with 3-(trifluoromethyl)phenylboronic acid, copper(II) acetate and triethylamine in dichloromethane (**47e** [Guo, S. et al., 2010]/**48e**).

Once we found that we obtained the pairs of the two isomers, we focused our efforts on understanding the course of the reactions, in particular which one is the most favorite. ¹H-NMR spectra proved to be very similar, even if it was possible to highlight a difference of the 3-CH pyrazole chemical shift for each couple of isomers. This gap was more marked in the acyl derivatives (about 0.7 ppm) compared to the alkylates (about 0.1 ppm), while an intermediate value difference was measured for the coupling derivatives **47e/48e** (0.3 ppm).

Since these chemical shift differences did not allow us to uniquely identify the exact structure of the isomers, we used more sophisticated 2D-NMR techniques, such as HSQC (Heteronuclear Single Quantum Correlation) and HMBC (Heteronuclear Multiple Bond Correlation), which turned out to be decisive for our purpose. The HSQC provided important information, since each signal indicates the coupling between a proton and its α carbon. This information, combined with the HMBC technique, which highlights the ¹H-¹³C couplings in the long range, allowed us to establish the structure of the studied compounds.

So, we were able to characterize the alkylated derivatives (**47c/48c** and **47d/48d**) since the presence of the coupling between the pyrazole 3-CH and the CH₂ (CH₂-Ph or CH₂CO-phenylpiperazine) is possible only for the N2 isomers **48c** and **48d**, while it is missing in the N1 isomers **47c** and **47d**. Similarly, for compounds **47b** and **48b**, it was possible to point out the coupling between the pyrazole 3-CH and the carbonyl carbon of the cyclopropanecarbonyl chain and the assignment of the structure for the couple of N-cyclopropanecarbonyl isomers **47b/48b**, was done by extrapolation of the data of compounds **47a/48a**.

2D-NMR spectra weren't resolvable for the couple of isomers **47e/48e** since it wasn't possible to identify any significant correlation. The exact structures for these compounds were assigned

performing the unique synthesis shown in Scheme 10 (see below) by reacting the intermediate **45** with m-trifluoromethyl-phenyl hydrazine, and obtaining the only N1 form, thus **47e**.

In addition, using Gas Chromatography (GC) coupled with a single quadrupole mass spectrometer with electronic ionization source (EI) on the benzylated isomers **47c/48c**, we further confirmed the structures assignment.

Once we identified the structures of the isomers, we realized the course of our reactions are not completely in agreement with results reported by Claramunt et al., since only for the cyclopropanecarbonyl derivative the N1 form prevails, (ratio N1/N2 about 4:1), while for all other compounds the N2 form is the most abundant (ratio N1/N2 1:3).

In Scheme 9 is reported the synthesis of the 5-mono and 5,5-dibromo derivatives of type **50** and **51**. The key intermediate **46** was treated with trimethylphenylammonium tribromide to afford a mixture of mono-bromo (**49a**) [Bolea, C. et al., 2014] and di-bromo (**49b**) derivatives, which were separated by flash chromatography. It was not possible to achieve a single compound also modulating the reaction conditions but we managed to obtain one compound predominantly over the other by varying the molar ratio between substrate and reactive. The best molar ratio substrate/reactive to obtain the mono-bromo derivative **49a** in higher yield was 1:1 (**49a/49b** 4:1), while a ratio 1:1.5 afforded a mixture of **49a/49b** in equivalent amount (**49a/49b** 1:1).

The next acylation on intermediates **49a,b** using the appropriate acyl/aroyl chloride in the same conditions reported above, showed a different trend. In fact, we observed the formation of a pair of isomers using cyclopropanecarbonyl chloride as reactive (**50a,b** and **51a,b**), while using m-toluoyl chloride we obtained only the N2 form, as for the mono-bromo and for the di-bromo (compounds **51c,d**). As for compounds of type **47** and **48**, a spectroscopic study was carried out on products **50** and **51**, affording the same results. Furthermore, we also elaborated 5-bromo-1,5,6,7-tetrahydro-4H-indazol-4-one (**49a**) by replacing the bromine atom with methylpiperazine group and obtaining compound **52**, which is unstable, therefore not suitable for further study.

In Scheme 10 is described the synthesis of the final **55a-c** starting from compound **45** [Claramunt, R. M. et al., 2006] that was cyclized to 1-phenyl-pyrazolocyclohexanone **53** [Spanò, V. et al., 2015] which, in turn, was subjected to a reductive amination using ammonium acetate and sodium cyanoborohydride affording the 4-aminoderivative **54** [Lain, S. et al., 2017]. The final compounds **55a,b** were obtained by reacting the intermediate **54** under the classic conditions with cyclopropanecarbonyl chloride and triethylamine in anhydrous dichloromethane, while to obtain product **55c**, compound **54** and triethylamine were added to 3-methylbenzoyl chloride prepared *in situ* with triphenylphosphine and trichloroacetonitrile in anhydrous dichloromethane at room temperature.

In [Scheme 11](#) is described the synthetic pathway leading to the final products of type **60** and **61**. Starting from the commercial product 1,3-cyclopentanedione (**56**), for treatment with DMF-DMA was obtained 2-[(dimethylamino)methylen]cyclopentan-1,3-dione **57** [Liverton, N. J. et al., 2012], which then was converted with p-toluensulfonyl hydrazide in methanol to the corresponding hydrazide **58** [Liverton, N. J. et al., 2012]. The following cyclization with HCl 37% and n-BuOH led to the desired 5,6-dihydrocyclopentan[c]pyrazol-4(1H)-one (**59**) [Lauffer, D. J. et al., 2019]. As previously reported, it can exist in two tautomer forms (see [Fig 46](#) scaffold **E**) which we were able to clearly observe in ¹H-NMR spectra recorded in DMSO-d₆ (about 1:1 ratio), while in CDCl₃ only one form is visible. The tautomerism and the reactivity of the pyrazolocyclopentanone (**59**) is described in 5 different patents [D'Alessio, R. et al, 2003; Liverton, N. J. et al., 2012a; Liverton, Nigel J. et al., 2012b; Veits, G. K. et al., 2019; Lauffer, D. J. et al., 2019], which gave different information, sometimes conflicting. Nevertheless, we performed both acylation and alkylation reactions, using the same conditions reported in [Scheme 8](#) for scaffold **D**, and obtaining in most cases a mixture of the isomers (**60a-c** and **61a-c**), often widely unbalanced in favor of N2 form (in ratio 2:1). The only exception was observed when m-toluoyl chloride was used as reactive; in this case we obtained only the N2 form (**61d**), as previously seen for the mono- and di-bromo derivatives **51c** and **51d** reported in [Scheme 9](#). Once again, NMR techniques (mono- and bi-dimensional) helped us to determine the exact structures of the isomers, highlighting the numerous analogies between the pyrazolocyclopentanone (scaffold **E**) and the pyrazolocyclohexanone (scaffold **D**) nuclei, in particular the different chemical shift of the pyrazole 3-CH for the two isomers. As well, HMBC showed for the alkylated compounds **60a,b** and **61a,b** a correlation between the CH₂ (CH₂-Ph or CH₂CO-phenylpiperazine) and the 3-CH of the nucleus only for the N2-isomers. Additionally, also for this class of compounds, we have chosen the pair of benzyl isomers **60a/61a** to perform a gas chromatography analysis that will be discussed below.

The use of 2D-NMR techniques has not been useful for the correct structure assignment of the isomers **60c/61c** (N-cyclopropancarbonyl derivatives), so, as first approach, we hypothesized their structures by extrapolating the results of the series of 1,5,6,7-tetrahydro-4H-indazol-4-one (see [Scheme 8](#)), and taking into account the chemical shift of pyrazole 3-CH. To verify if our assignments were correct, single crystal X-ray diffraction of the acyl derivative **60c** was performed. At the same time, we also studied the key intermediate pyrazolocyclopentanone (**59**). The results obtained and reported in the figure hereunder, allowed us to correctly assign the unambiguous structure to the acyl derivative **60c**, which turns out to be the N1 isomer, confirming the validity of our processing ([Fig. 47](#)). Moreover, we can affirm that the precursor **59** in solid state shows the hydrogen on the nitrogen more distant from the fusion carbon (see result and discussion section for more details).

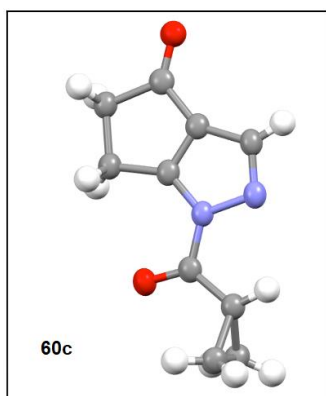


Figure 47. X-ray crystallography of compound **60c** (E).

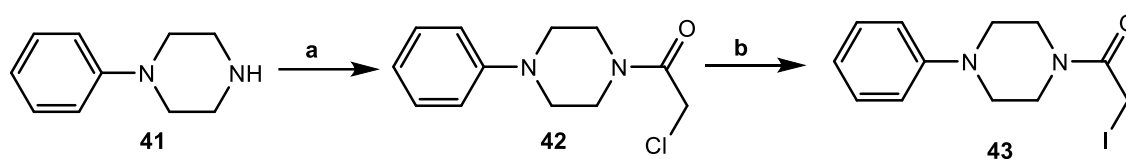
Taking all this information into account, we can conclude that when the acylation/alkylation reactions afford a mixture of products, the N-2 isomer is always the most abundant one; in some case it is even the only product formed, as for example for the compounds **51c**, **51d** and **61d**.

In the [Scheme 12](#), the synthesis of compounds with pyrazolocycloheptanone scaffold (**F**) is illustrated. The steps to afford the key intermediate **64** were the same described in [Scheme 8](#) for 1,5,6,7-tetrahydro-4H-indazol-4-one derivative. Therefore, the commercial cycloheptanedione **62** was reacted with DMF-DMA to afford the intermediate **63** [Maynard, G. et al., 2003] which was cyclized with hydrazine monohydrate to 5,6,7,8-tetrahydrocyclohepta[c]pyrazol-4(1H)-one **64** [Maynard, G. et al., 2003]. Similarly to pyrazolocyclohexanone (**46**) and (**59**) nuclei, compound **64** exhibits two tautomeric forms (**Fig. 46** scaffold **F**), and the acylation or alkylation reactions provided in the most cases a couple of isomers with a ratio of about 1:3 (compounds **65a-c** and **66a,b**). The acylation reaction with m-toluoyl chloride afforded only a compound, but differently from 1,5,6,7-dihydro-1H-indazol-4(5H)-one and 5,6-dihydrocyclopenta[c]pyrazol-4(1H)-one derivatives, the N-1 isomer is the only one formed (**65c**).

Finally, in [Scheme 13](#) is showed the synthesis of the two isomers **71** and **74**. In part a), the methylation of the intermediate **46** [Claramunt, R. M. et al., 2006] with methyl iodide and sodium carbonate in acetonitrile, gave the mixture of the two isomers **67** and **68** [Spanò, V. et al., 2015], separated by flash chromatography. The low yield of the isomer **68** prompted us to follow an alternative route, described in the part **b**), which allowed us to obtain **68** in 86% yield by cyclizing **45** with methylhydrazine. Afterwards, both isomers **67** and **68** were treated with hydroxylamine monohydrate in water to afford the corresponding oxime derivatives **69** and **72** [Yoshinaga, H. et al., 2020], which were treated with p-toluensulfonyl chloride to obtain compounds **70** and **73**. These were then converted to the corresponding lactams **71** [Estrada, A. A. et al., 2017] and **74** [Yoshinaga, H. et al., 2020] performing an enlargement of the cyclohexane ring with sodium acetate in ethanol/water at reflux.

9. Schemes

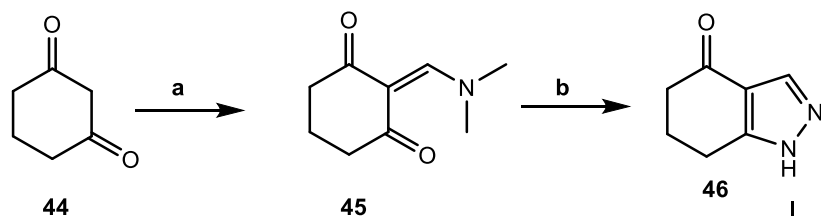
Scheme 7



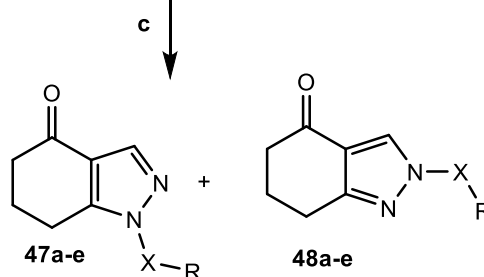
Reagents and conditions:

- a) ClCH_2COCl , dry CH_2Cl_2 , DIEA, r.t., 4h.
 b) Acetone, NaI, r.t., 16h.

Scheme 8



47,48	X	R
a	CO	m- CH_3 -Ph
b	CO	c- C_3H_5
c	CH_2	m- CF_3 -Ph
d	CH_2CO	N,N-piperazine-Ph
e	-	m- CF_3 -Ph

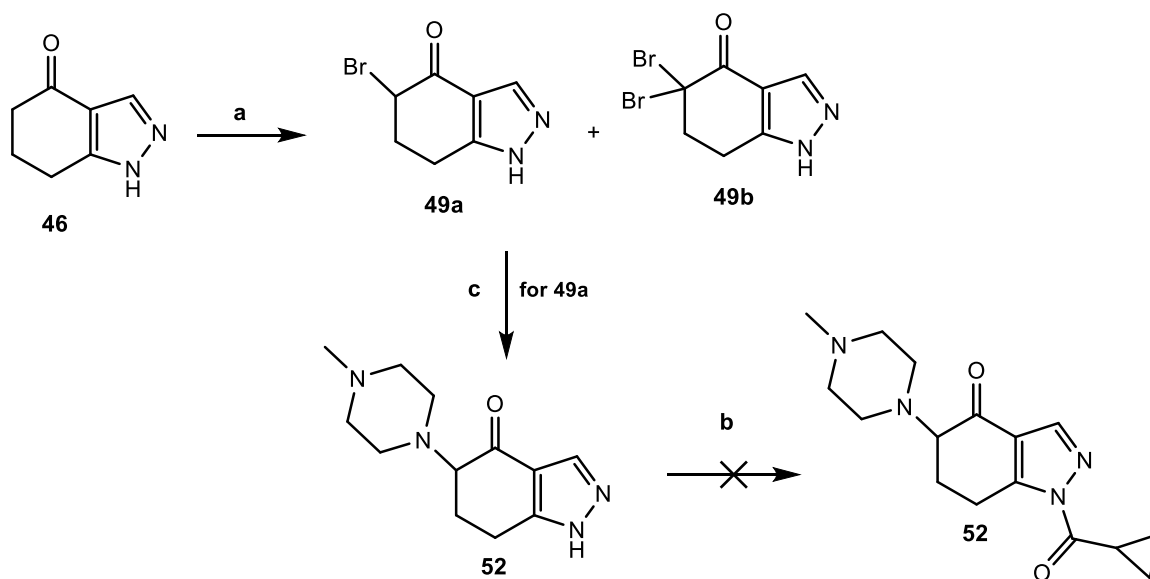


Reagents and conditions:

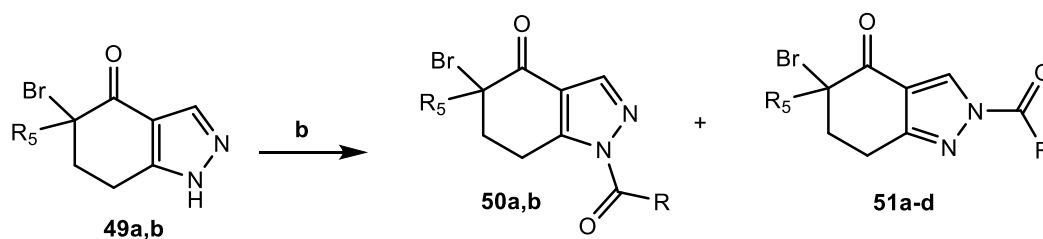
- a) DMF-DMA, reflux, 1h.
 b) $\text{MeOH}/\text{H}_2\text{O}$, $\text{NH}_2\text{NH}_2 \cdot \text{H}_2\text{O}$, NaOH, reflux, 2h, then $\text{AcOH}/\text{H}_2\text{O}$, 110°C , 1.5h.
 c) for 47a,b and 48a,b: R-COCl , Et_3N , dry CH_2Cl_2 , 0°C , 2h, then r.t., 2h.
 for 47c,d and 48c,d: 3-(trifluoromethyl)benzyl bromide or 43, dry CH_3CN , K_2CO_3 , reflux, 3h.
 for 47e and 48e: $(\text{CH}_3\text{COO})_2\text{Cu}$, dry CH_2Cl_2 , 3-(trifluoromethyl)phenylboronic acid, Et_3N , r.t., 12h.

Scheme 9

a)



b)



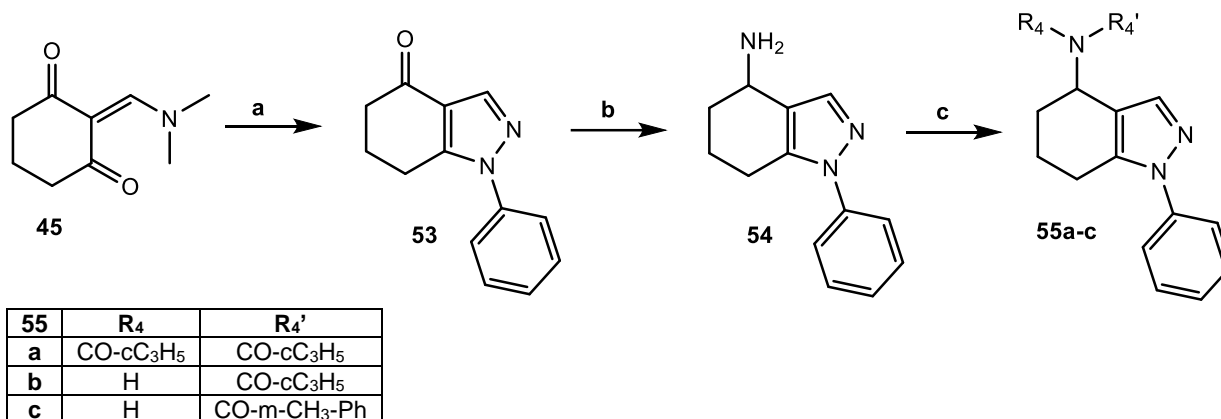
Reagents and conditions:

- a) $[\text{PhNMe}_3][\text{Br}]_3$, dry CH_2Cl_2 , 100°C , 3h.
 b) R-COCl , dry CH_2Cl_2 , Et_3N , 0°C , 2h, then r.t., 2h.
 c) Methylpiperazine, dry DMF, r.t., 24h.

50	R	R ₅
a	cC ₃ H ₅	H
b	cC ₃ H ₅	Br

51	R	R ₅ '
a	cC ₃ H ₅	H
b	cC ₃ H ₅	Br
c	m-CH ₃ -Ph	H
d	m-CH ₃ -Ph	Br

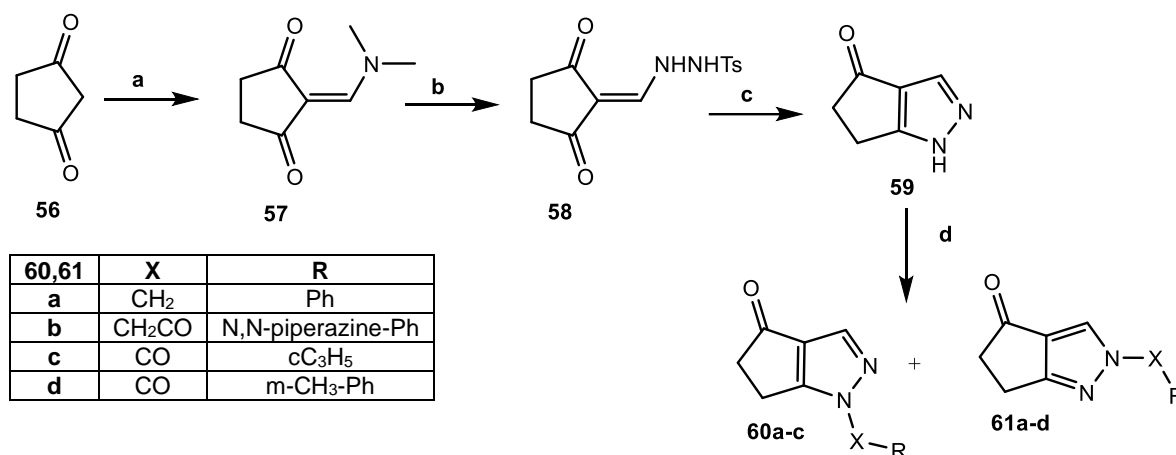
Scheme 10



Reagents and conditions:

- a) MeOH/H₂O, PhNHNH₂, NaOH, reflux, 2h, then AcOH/H₂O, 110°C, 1.5h.
 b) i-PrOH, CH₃COONH₄, molecular sieves, NaBH₃CN, 70°C, 24h.
 c) **for 55a,b**: cyclopropanecarbonyl chloride, dry CH₂Cl₂, Et₃N, 0°C, 2h, then r.t., 2h.
for 55c: 3-methylbenzoic acid, CCl₃CN, dry CH₂Cl₂, PPh₃, r.t., 4h, then Et₃N, r.t., 12h.

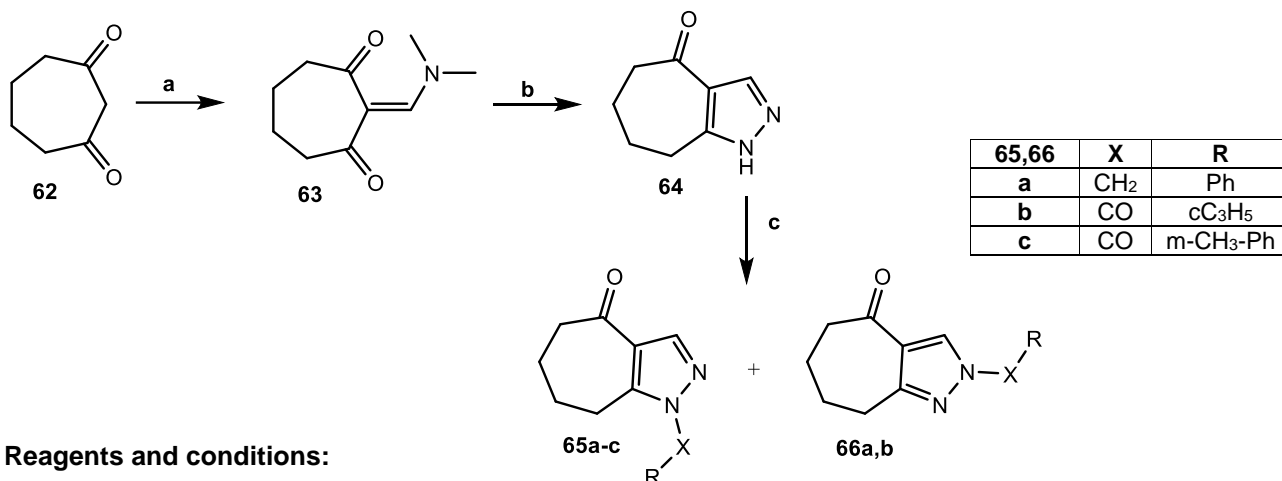
Scheme 11



Reagents and conditions:

- a) DMF-DMA, reflux, 1h.
 b) MeOH, p-toluensulfonyl hydrazide, r.t., 40 min.
 c) HCl 37%, n-BuOH, 110°C, 1h.
 d) **for 60a,b and 61a,b**: benzyl bromide or **43**, dry CH₃CN, K₂CO₃, reflux, 3h.
for 60c and 61c,d: R-COCl, Et₃N, dry CH₂Cl₂, 0°C, 2h, then r.t., 2h.

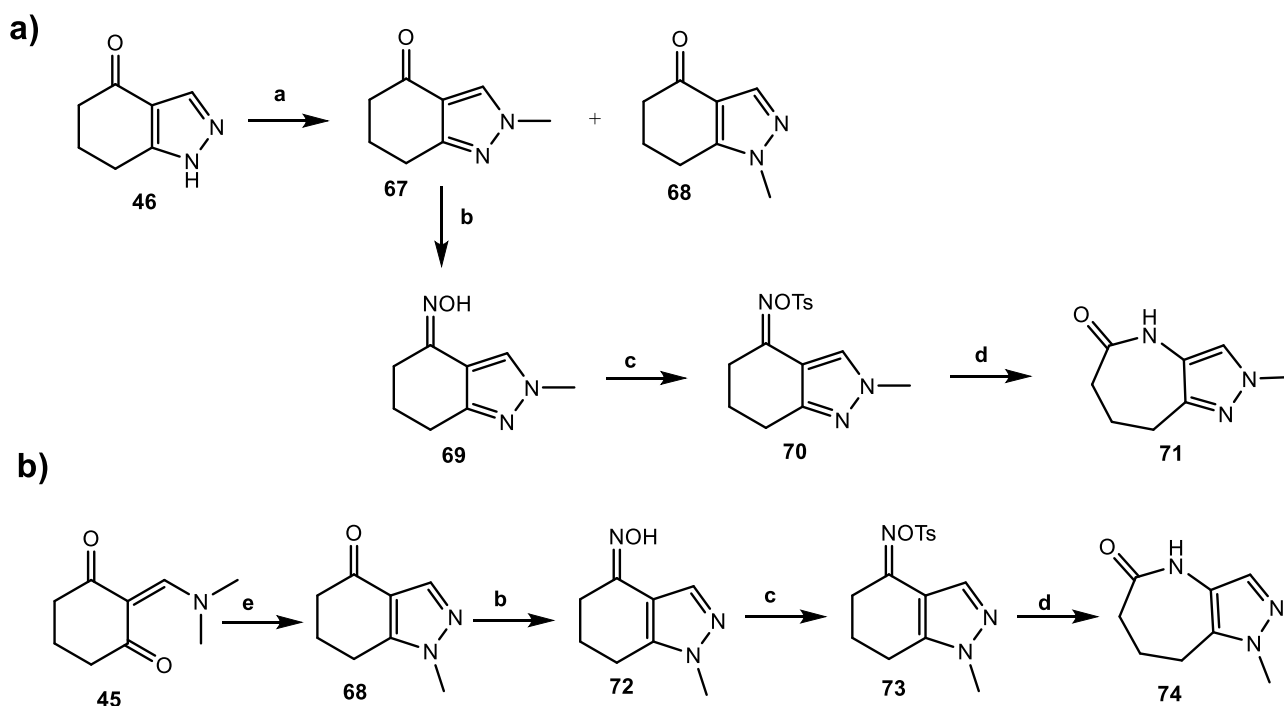
Scheme 12



Reagents and conditions:

- a) DMF-DMA, reflux, 1h.
 b) MeOH/H₂O, NH₂NH₂·H₂O, NaOH, reflux, 2h, then AcOH/H₂O, 110°C, 1.5h.
 c) for **65a** and **66a**: benzyl bromide, dry CH₃CN, K₂CO₃, reflux, 3h.
 for **65b,c** and **66b**: R-COCl, Et₃N, dry CH₂Cl₂, 0°C, 2h, then r.t., 2h.

Scheme 13



Reagents and conditions:

- a) CH₃I, Na₂CO₃, dry CH₃CN, 80°C, 6h.
 b) NH₂OH·HCl, H₂O, 60°C, 30 min, then NaHCO₃, reflux, 4h.
 c) DMAP, p-toluenesulfonyl chloride, pyridine, r.t., 16h.
 d) H₂O, EtOH, NaOAc, reflux, 3h.
 e) MeOH/H₂O, CH₃NHNH₂·H₂O, NaOH, reflux, 2h, then AcOH/H₂O, 110°C, 1.5h.

10. Results and discussion

10.1. Biological evaluation and structure-activity relationship (SAR) analysis

The biological results of all new synthesized compounds are shown in **Tables 8-9** with the reference drug Sivelestat.

Starting the discussion from the 1,5,6,7-tetrahydro-4H-indazol-4-one derivatives (**Table 8**) we can see that the newly synthesized compounds are very potent HNE inhibitors, with IC_{50} in the nanomolar range ($IC_{50} = 12-74$ nM). In all the most active products the N-CO function, already proved to be the point of attack of Ser-OH, involves a pyrazole nitrogen, consistently with our previous results.

Looking at compounds of type **47** and **48**, the insertion of a cyclopropanecarbonyl (**47b/48b**) or a m-toluoyl (**47a/48a**) group, resulted in very potent compounds, as the N-1 and N-2 isomers (**Table 8**). In general, the N-2 isomers are slightly more potent, as for example for the m-toluoyl derivatives **47a/48a** where the N2 isomer (**48a**) showed an IC_{50} value 3 times lower than N1 (**48a**: 24 nM versus **47a**: 74 nM). Instead, for the cyclopropyl derivatives **47b/48b**, there is no marked difference between the two isomers both showing similar IC_{50} values.

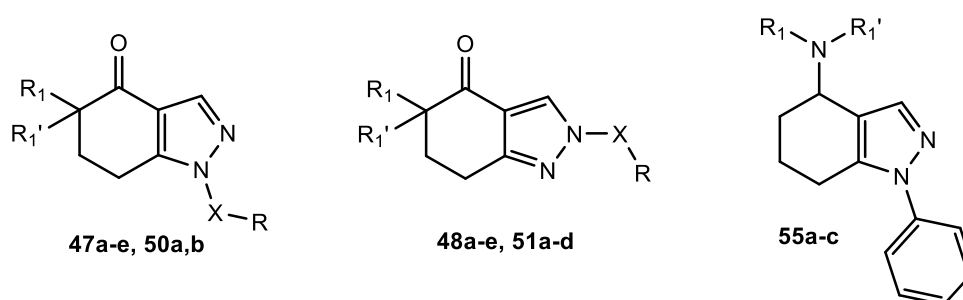
The importance of the N-CO function is confirmed again by the complete inactivity of **47c/48c** (N-benzyl derivatives) and **47e/48e** (N-aryl derivatives) in which the amide bond was removed.

Interestingly, the two isomers **47d/48d**, bearing a basic chain, as in the compounds developed by Boehringer, and an amide function on the same chain, showed a certain ability to inhibit HNE ($IC_{50} = 27.5$ μ M for **47d** and 41.5 μ M for **48d**). This result, although mediocre, opens a new field of investigation which will be further developed.

Also compounds bearing at position 5 one bromine (compounds **50a** and **51a,c**), or two bromine (**50b** and **51b,d**), are potent HNE inhibitors with $IC_{50} = 12-37$ nM (**Table 8**). Comparing the potency of 5-bromo or 5,5'-dibromo derivatives with the corresponding 5-unsubstituted compounds, we can observe that the introduction of the bromine led to a general improvement of activity (i.e., **48b** and **51b**, $IC_{50} = 53$ nM and 23 nM, respectively). Conversely, there is no significant difference in activity between the mono- and di-bromo derivatives, as demonstrated by the couples **50a/50b**, **51a/51b** and **51c/51d**. In this series, the most potent HNE inhibitors are the m-toluoyl derivative **51c** ($IC_{50} = 13$ nM) and **51d** ($IC_{50} = 12$ nM).

Finally, products **55a-c** showing the amide function shifted to position 4 of the cyclohexanone, are completely inactive.

Table 8. HNE inhibitory activity of compounds **47a-e**, **48a-e**, **50a,b**, **51a-d** and **55a-c**.



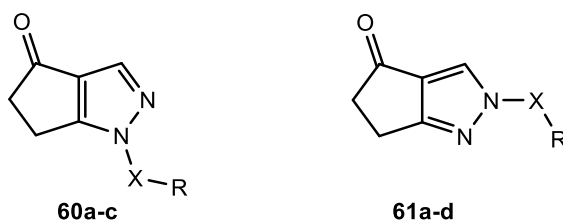
Compound	X	R	R ₁	R ₁ '	IC ₅₀ (μM) ^a
47a	CO	m-CH ₃ -Ph	H	H	0.074 ± 0.023
47b	CO	cC ₃ H ₅	H	H	0.055 ± 0.009
47c	CH ₂	m-CF ₃ -Ph	H	H	N.A. ^b
47d	CH ₂ CO	N,N-piperazine-Ph	H	H	27.5 ± 4.6
47e	-	m-CF ₃ -Ph	H	H	N.A. ^b
48a	CO	m-CH ₃ -Ph	H	H	0.024 ± 0.07
48b	CO	cC ₃ H ₅	H	H	0.053 ± 0.006
48c	CH ₂	m-CF ₃ -Ph	H	H	N.A. ^b
48d	CH ₂ CO	N,N-piperazine-Ph	H	H	41.5 ± 5.3
48e	-	m-CF ₃ -Ph	H	H	N.A. ^b
50a	CO	cC ₃ H ₅	Br	H	0.037 ± 0.007
50b	CO	cC ₃ H ₅	Br	Br	0.030 ± 0.006
51a	CO	cC ₃ H ₅	Br	H	0.035 ± 0.005
51b	CO	cC ₃ H ₅	Br	Br	0.023 ± 0.001
51c	CO	m-CH ₃ -Ph	Br	H	0.013 ± 0.003
51d	CO	m-CH ₃ -Ph	Br	Br	0.012 ± 0.002
55a	-	-	cC ₃ H ₅	cC ₃ H ₅	N.A. ^b
55b	-	-	H	cC ₃ H ₅	N.A. ^b
55c	-	-	H	m-CH ₃ -Ph	N.A. ^b
Sivelestat					0.050 ± 0.020

^aIC₅₀ values are presented as the mean ± SD of three independent experiments. ^bN.A.: no inhibitory activity was found at the highest concentration of compound tested (50 μM).

As regard the biological results concerning the 5,6-dihydrocyclopenta[*c*]pyrazol-4(1H)-one of type **60** and **61**, they are shown in **Table 9**. Starting the discussion from the acylated products, the only pair of isomers obtained in this series, the N-cyclopropyl **60c** and **61c**, showed good inhibitory HNE activity in the nanomolar range, IC₅₀ = 26 nM for the N1 isomer (**60c**) and 67 nM for the N2 isomer (**61c**) respectively. Compound **61d**, with a *m*-toluoyl fragment in the N2 position, maintained nanomolar activity values (IC₅₀ = 71 nM) comparable to those of compound (**61c**).

Concerning the N-benzylated derivatives (**60a/61a**), we obtained conflicting results as reported in **Table 9**. In fact, while the N1-benzylated isomer (**60a**) lacking the N-CO function follows the trend mentioned above for pyrazolocyclohexanone, thus it's completely inactive, the N2-benzylated (**61a**) shows a certain HNE inhibitory activity even if in the micromolar range (IC₅₀ = 2.4 μM). This information opens to the hypothesis of a different mechanism of action that needs further investigation.

Finally, compounds bearing the piperazine ring (**60b/61b**), differently from the corresponding 1,5,6,7-tetrahydro-4H-indazol-4-one derivatives **47d** and **48d**, are completely inactive.

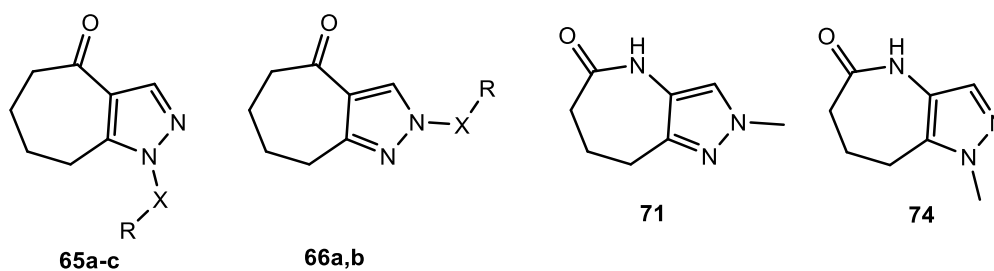
Table 9. HNE inhibitory activity of compounds **60a-c**, **61a-d**, **65a-c**, **66a,b**.

Compound	X	R	IC ₅₀ (μM) ^a
60a	CH ₂	Ph	N.A. ^b
60b	CH ₂ CO	N,N-piperazine-Ph	N.A. ^b
60c	CO	cC ₃ H ₅	0.026 ± 0.012
61a	CH ₂	Ph	2.4 ± 0.72
61b	CH ₂ CO	N,N-piperazine-Ph	N.A. ^b
61c	CO	cC ₃ H ₅	0.067 ± 0.015
61d	CO	m-CH ₃ -Ph	0.071 ± 0.032
Sivelestat			0.050 ± 0.020

^aIC₅₀ values are presented as the mean ± SD of three independent experiments. ^bN.A.: no inhibitory activity was found at the highest concentration of compound tested (50 μM).

The inhibitory activities of the 5,6,7,8-tetrahydrocyclohepta[c]pyrazol-4(1H)-one of type **65** and **66** and 4,6,7,8-tetrahydropyrazolo[4,3-b]azepin-5(1H)-one derivatives **71** and **74** are shown in **Table 10**. Looking at the results obtained for compounds of type **65** and **66**, as expected the benzyl derivatives **65a** and **66a** are inactive, while both the N1 acyl derivatives, as compound **65c** showing the m-toluyyl and compound **65b** showing the cyclopropyl group, are very potent HNE inhibitors (IC₅₀ = 20 and 38 nM respectively). Finally, differently from the previously described bicycles of type **D** and **E**, a marked difference in activity (about one order of magnitude) was measured between the N1 (**65b**) and the N2 isomer (**66b**, IC₅₀ = 240 nM), suggesting that the heptacycle influences the interaction with the target.

In **Table 10** are also reported the intermediates **71** and **74**, which for reasons of time have not been further elaborated and are completely inactive.

Table 10 HNE inhibitory activity of compounds **65a-c**, **66a,b**, **71**, **74**.

Compound	X	R	IC ₅₀ (μM) ^a
65a	CH ₂	Ph	N.A. ^b
65b	CO	cC ₃ H ₅	0.038 ± 0.012
65c	CO	m-CH ₃ -Ph	0.020 ± 0.006
66a	CH ₂	Ph	N.A. ^b
66b	CO	cC ₃ H ₅	0.240 ± 0.021
71			N.A. ^b
74			N.A. ^b
Sivelestat			0.050 ± 0.020

^aIC₅₀ values are presented as the mean ± SD of three independent experiments. ^bN.A.: no inhibitory activity was found at the highest concentration of compound tested (50 μM).

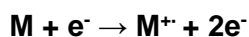
The stability in aqueous buffer for some products was also evaluated and the results are reported in **Table 11**. The most stable compound results **51b**, i.e., 5,5-dibromo-2-(cyclopropanecarbonyl)-2,5,6,7-tetrahydro-4H-indazol-4-one, with $t_{1/2}$ = 4h, followed by compounds **61c** and **61d** which also exhibit excellent $t_{1/2}$ of about 3h. Comparing the half-life of the mono-bromo **50a/51a** with di-bromo derivatives **50b/51b**, we can hypothesize that the increased lipophilicity due to the additional bromine enhances the time required for hydrolysis. In addition, if we observe the isomer pairs **50a/51a** ($t_{1/2}$ = 53.88 and 57.06 min, respectively), **50b/51b** ($t_{1/2}$ = 114.74 and 234.84 min, respectively), and **60c/61c** ($t_{1/2}$ = 68.47 and 157.57 min, respectively), we can affirm that the N1-acylated are more susceptible to hydrolysis than the corresponding N2.

Table 11. Half-life ($t_{1/2}$) for the spontaneous hydrolysis of selected derivatives.

Compound	$t_{1/2}$ (min)
47a	98.13 ± 3.53
50a	53.88
50b	114.74 ± 6.7
51a	57.06 ± 1.65
51b	234.84 ± 18.15
60c	68.47 ± 7.08
61c	157.57 ± 3.60
61d	187.57 ± 5.11

10.2. Gas chromatography-mass spectrometry (GC-MS)

In order to unambiguously confirm the information obtained from the mono and bi-dimensional NMR spectra, two pairs of N-benzylated isomers **47c/48c**, with 1,5,6,7-tetrahydro-4H-indazol-4-one scaffold, and **60a/61a**, with 5,6-dihydrocyclopenta[c]pyrazol-4(1H)-one core, were analyzed using the GC-MS technique, in collaboration with Prof. Bartolucci. Through Gas Chromatography (GC) coupled to a single quadrupole mass spectrometer with electronic ionization source (EI), the sample was subjected to an interaction with high energetic electron (70 eV) that causes large fluctuations in the electric field around the neutral molecules and induces their ionization and fragmentation. The electron ionization process can be described as follows:



where M is the analyte molecule being ionized, e⁻ is the electron and M⁺ is the resulting molecular ion. The electron ionization process, due to the high energy involved, often leads to predictable cleavage reactions that give rise to fragment ions which, following detection and signal processing, convey structural information about the analyte. Therefore, using this approach, it was possible to acquire the chromatogram and respective fragmentation spectra of the two pairs of isomers, which gave similar trends. Starting from the chromatographic study, the outcome was not significant regarding the assignment of the structures, as the retention time between **47c/48c** (Fig. 47), and **60a/61a** (Fig. 48) respectively, was not sufficiently different to be considered discriminatory.

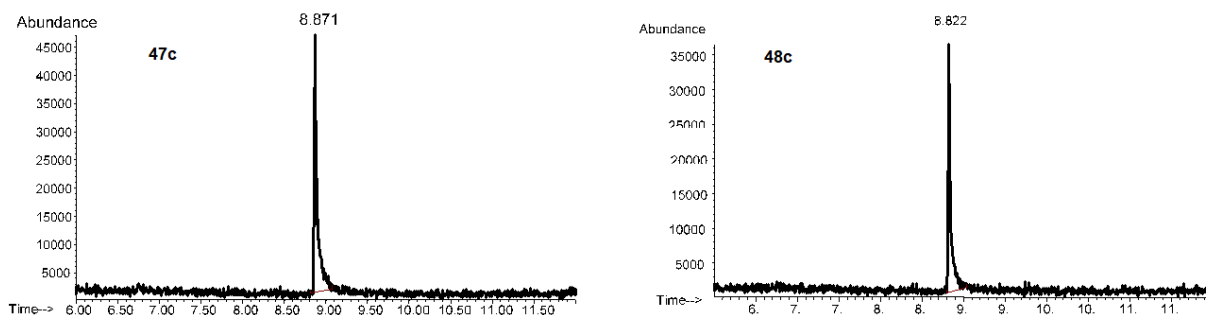


Figure 47. Chromatogram isomers **47c/48c**.

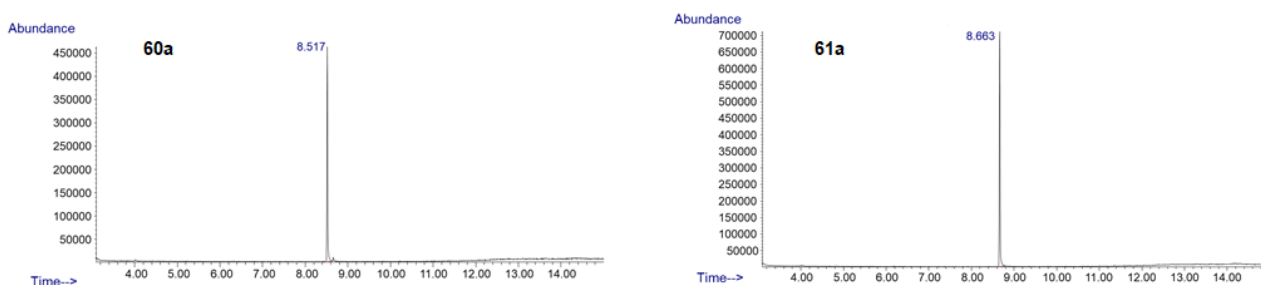


Figure 48. Chromatogram isomers **60a/61a**.

Each chromatographic peak corresponds to a mass spectrum that is different between the two isomers, and it allowed us to confirm their structure. Starting from the first couple **47c/48c** (Fig. 49), we can see that the isomer (**47c**) shows as principal peak the value of 294 m/z corresponding to the radical molecular ion, while the other isomer (**48c**) shows more abundant fragments within that range, including 294 m/z itself, but the most intense lies at 293 m/z. If we assume that the latter is the N2-benzylated, it may be hypothesized that the signal at 293 m/z is due to the formation of a very stable fragmented ion, which is the result of the radical proton leaving from position 3 of the pyrazole resulting in the re-arrangement showed in Fig.50. On the contrary, such rearrangement is much less predictable for N1-benzylated. As a result of this first divergence, it could be supposed that the fragment at 293 m/z is in competition with the 135 m/z ion formation, which is likely to represent the nucleus without the m-CF₃-phenyl moiety. On the other hand, **47c**, which does not possess this stable intermediate, shows a very intense peak at 135 m/z. In common, the two isomers share the peak at 159 m/z corresponding to the 3-CF₃-tropylium cation.

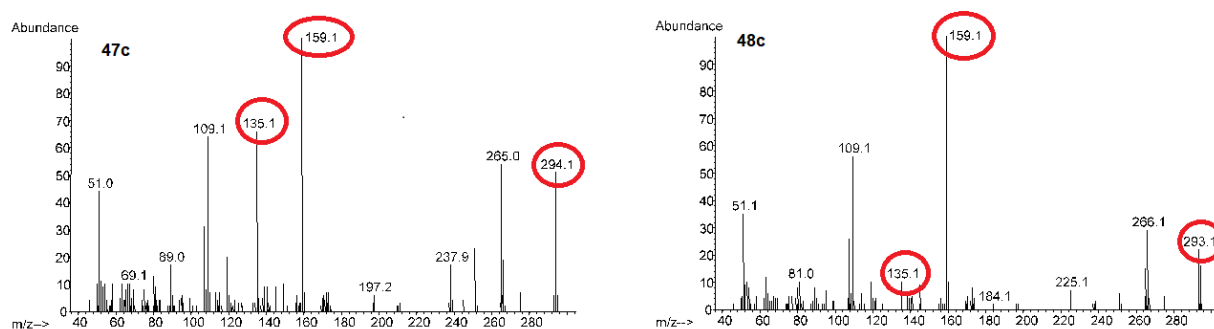


Figure 49. Mass spectrum of isomers **47c/48c**.

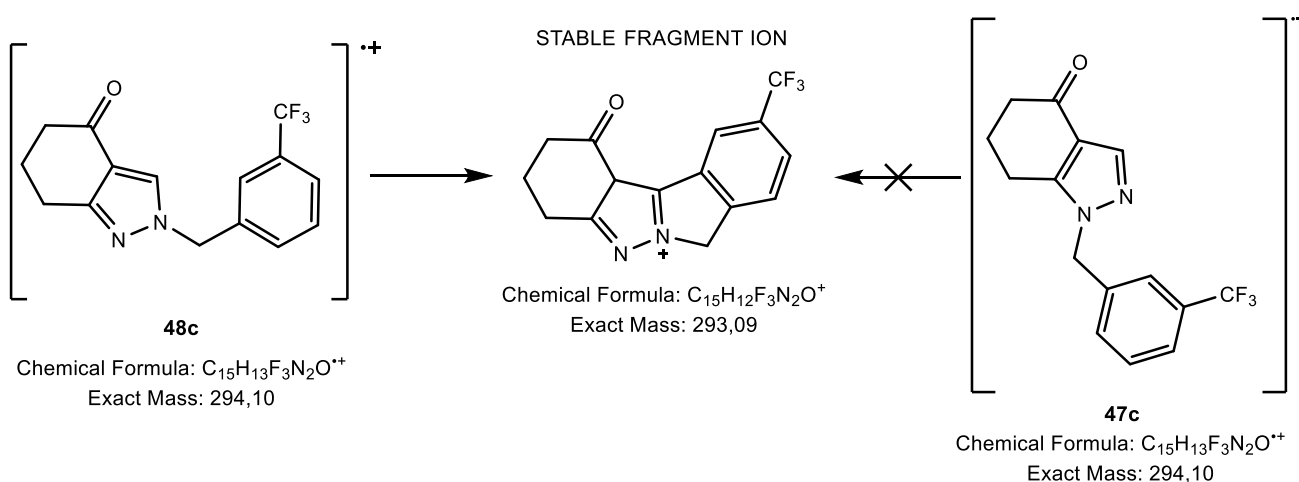


Figure 50. Different rearrangement of isomers **47c/48c**.

Now we proceed to examine the mass spectrum of the pair with 5,6-dihydrocyclopenta[c]pyrazol-4(1H)-one nucleus (**60a/61a**, Fig. 51).

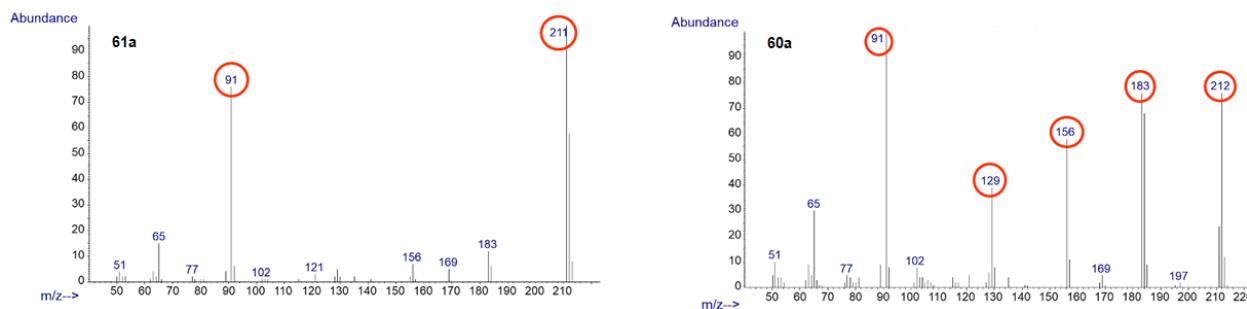


Figure 51. Mass spectrum of isomers **60a/61a**.

Similarly to the aforementioned compounds, the two isomers have two different molecular peaks; in fact, while for **61a** the higher peak is at 212 m/z, for **60a** the more significant is at 211 m/z. Also in this case the difference can be explained by the formation of a very stable transition intermediate, presented in **Fig. 52**.

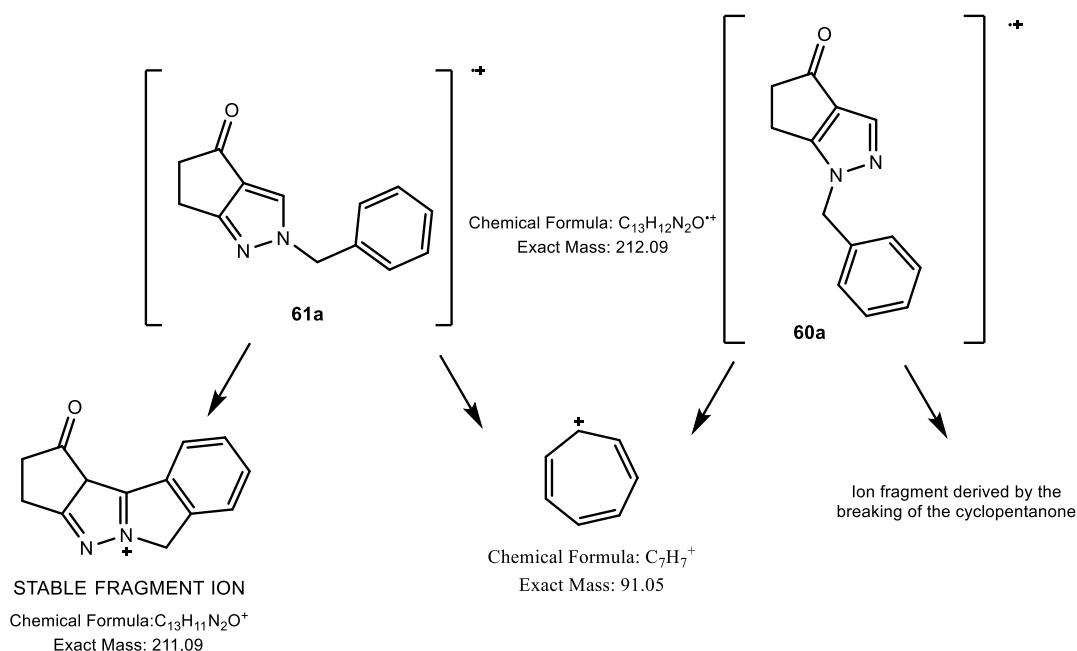


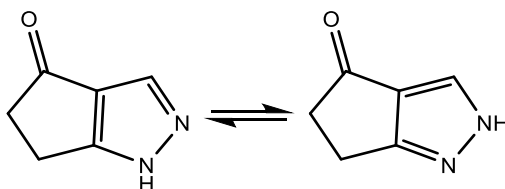
Figure 52. Different rearrangement of isomers **60a/61a**.

Compared to the previous nucleus, there is not a fragment lacking of benzyl moiety alone, but it is possible to highlight only for N1-alkylate (**60a**) the formation of fragments at the values of 183 m/z, 156 m/z and 129 m/z, probably due to the lack of formation of the intermediate at 211 m/z (**Fig. 52**). However, both isomers present the tropylium fragment at 91 m/z.

In conclusion, given the similarity of the data obtained from gas chromatography on both pairs of isomers **47c/48c** and **60a/61a**, it can be stated that the isomers forming the stable intermediate (**48c** and **61a**) are those with the benzyl moiety linked to nitrogen at position 2 (N2), while **47c** and **60a** are the corresponding N1 isomers.

10.3. X-ray crystallography

To unequivocally assigned the structure of key intermediate **59**, (5,6-dihydrocyclopenta[*c*]pyrazol-4(1H)-one) that can exist in the two isomers (tautomers), an X-ray crystallographic study was carried out by Prof. Paola Paoli and Prof. Patrizia Rossi of Florence University.



The analysis of Fourier map differences permitted to identify the hydrogen atoms bound to C2, C3 and C6 while the position of the last hydrogen that can be bound to N1 or N2 was not simple to detect. In fact, close to both nitrogen atoms there is low electron density at a distance compatible with the presence of a hydrogen atom. Moreover, the investigation of the bonding distances inside the five-term loop helps us verify where the double bonds were located and which nitrogen atom was protonated.

To support our investigations was searched for a compound with a similar structure in the Cambridge Structural Database (v5.38) [Groom, C. R. et al., 2016] and was found the compound 6,6-dimethyl-1(2),5,6,7-tetrahydro-4H-indazol-4-one (refcode PESLEF) [Claramunt, R. M. et al., 2006]. In the asymmetric unit of PESLEF there are six molecules, four of which correspond to tautomer **A** and two to **B** (Fig. 53).

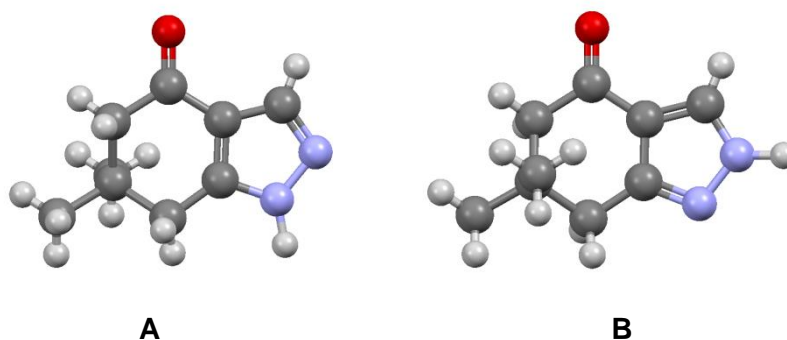


Figure 53. Tautomers **A** and **B** in the asymmetric unit of PESLEF compound.

From the comparison of the bonding distances found in the intermediate **59** (Fig. 54) to that of compound PESLEF tautomer **B**, can be seen likeness, as reported in **Table 12**.

Table 12. Bonds distances in tautomers **A** and **B** of PESFEL compound, and of the intermediate **59**. The labels refer to the **Fig. 53A**.

	Intermediate 59	PESLEF	
		B	A
C4-C5	1.394(9)	1.390(6)-1.395(6)	1.371(6)-1.384(6)
C5-C6	1.402(9)	1.365(7)-1.378(8)	1.365(8)-1.394(7)
C6-N1	1.332(8)	1.331(8)-1.335(8)	1.316(6)-1.346(8)
N1-N2	1.382(8)	1.368(7)-1.378(7)	1.369(6)-1.394(6)
N2-C4	1.326(8)	1.324(6)-1.340(6)	1.322(7)-1.367(6)

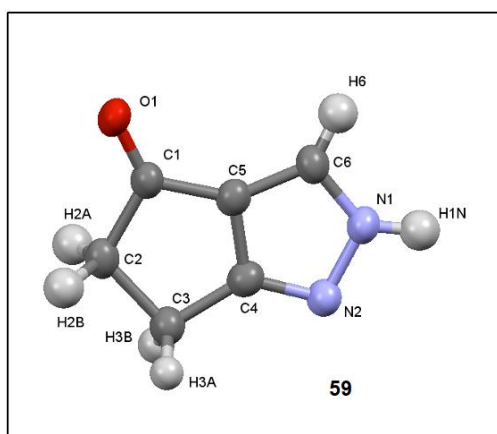


Figure 54

Compound **59** crystallizes in the space group P21 and in the asymmetric unit only one molecule is present. The molecule is planar with bonding distances and angles in the expected range.

The analysis of the interactions within the crystal lattice of the compound shows that at 2.801(7) Å from the nitrogen atom N1 is present the oxygen atom O1 of another molecule reported by symmetry (1+x, 1+y, z). This fact suggests the presence of a strong hydrogen bond between the molecules, inside the crystal. Therefore, among the low intensity peaks present in the Fourier differences map, the highest peak near N1 was chosen, this peak was assigned as a hydrogen atom and the refining procedure was performed as reported in the experimental part.

In **Fig. 55** is reported the chain of **59** that is formed due to the strong hydrogen bond above reported (N1...O1' = 2.801(7) Å; H1N...O1' = 1.88(9) Å; N1-H1N...O1' = 173(8)°, ' = 1+x, 1+y, z).

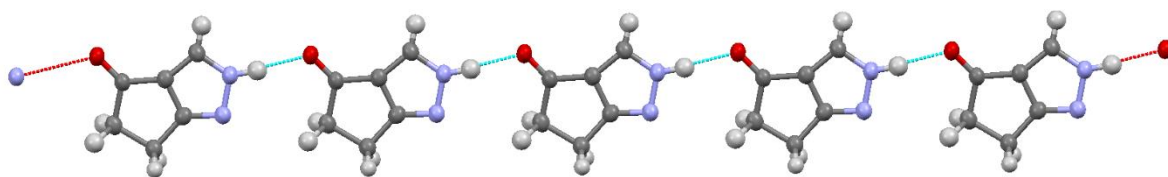


Figure 55. Ball and stick representation of **59** molecules chain.

This chain propagates along the diagonal ab (see **Fig. 56**). Inside the crystal, the chains of **59** are held together by weak interactions.

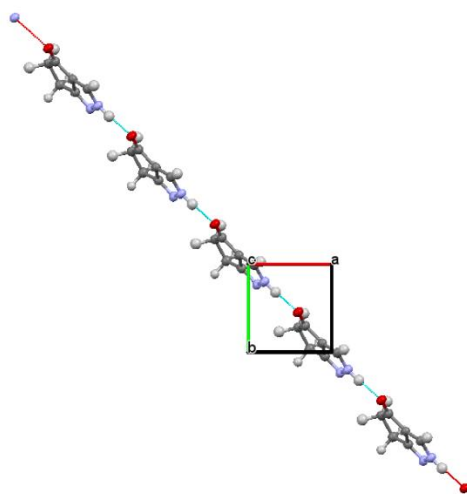
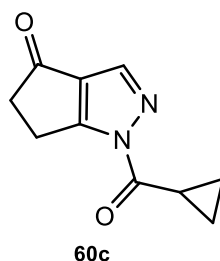


Figure 56. Ball and stick representation of the chain of molecules of **59**, viewed along the c axis.

10.4. Molecular Modeling

Prof. Andrei Khlebnikov of Tomsk State University conducted preliminary studies of molecular modeling on the compound **60c**, shown below, the most active of this new series ($IC_{50} = 26$ nM), whose amide bond at position 1 could be a possible point of attack by the Ser195 of HNE catalytic site (PDB code: 1HNE).



The structure of the **60c** compound was realized using the program ChemOffice 2016 and imported into the Molegro Virtual Docker 6.0 program. The docking of **60c** follows the interaction model developed by Prof. Khlebnikov for the N-benzopyrazole, already discussed in molecular modeling of the first section, and used for other molecules synthesized in this thesis laboratory [Crocetti, L. et al., 2018].

The docking of **60c** shows that the molecule establishes strong hydrogen bonds with both Ser195 and Gly193 by means pyrazole nitrogen atoms (**Fig. 57A**). **Figure 57B**, displays **60c** in the catalytic triad (Ser195-His57-Asp102) and appear the hydrogen bond interactions engaged with the two nitrogen atoms of the heterocycle. Moreover, the molecule **60c** creates also a hydrogen bond with Asp194, even if weaker than the others.

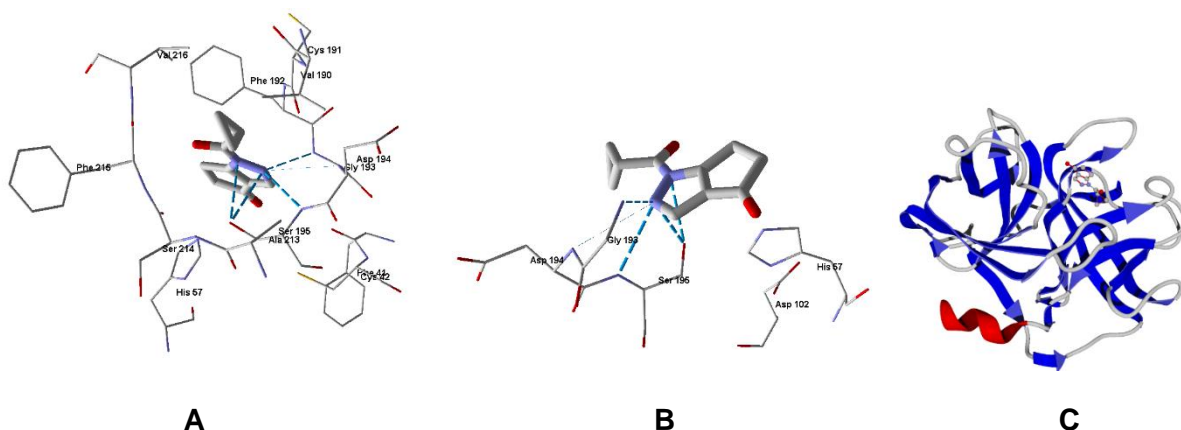


Figure 57. Lower energy docking pose of **60c** (**A**). Hydrogen bonds are represented as dashed lines. Docking pose of 1-(cyclopropanecarbonyl)-5,6-dihydrocyclopenta[c]pyrazol-4(1H)-one (**60c**) inside the catalytic triad (**B**) and inside the protein (**C**).

The orientation of the molecule is favorable to the formation of the Michaelis complex, but the distance d_1 between the Ser195 hydroxyl oxygen and the carbonyl of **60c** is 3.443 Å, a value that exceeds the optimal range of 1.8-2.6 Å. On the contrary, the angle α between O(Ser195)....C=O

amidic of **60c** is 100.9° , which is within the optimal range. Another important parameter for this interaction model is the distance L , equal to 6.333 \AA , given by the combination of $d_3= 3.196 \text{ \AA}$ and $d_2= (3.137, 4.315 \text{ \AA})$. These values are consistent with the good inhibitory activity of the compound **60c** against HNE.

11. Conclusions

In conclusion, the results obtained indicate that the three nuclei **D**, **E** and **F** were suitable for the synthesis of new potent HNE inhibitors with IC_{50} s in the nanomolar range (IC_{50} s =12 - 74 nM). The pirazolocyclohexanone scaffold was the best, affording the most potent HNE inhibitor obtained in this work (compound **51d**, $IC_{50} = 12 \text{ nM}$).

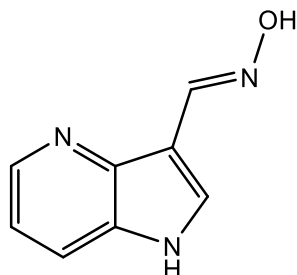
Of great importance were the spectroscopic, GC-MS and crystallographic studies, which allowed us to assign the correct structures to the pairs of isomers obtained. In terms of inhibitory activity, for all three nuclei **D**, **E** and **F** the two isomers N1 and N2 were very similar, with comparable potency. The only exceptions to this trend are represented by the couple of pyrazolocycloheptanones **65b/66b**, where the N1 isomer is about 10 fold more potent than N2 (**65b**, $IC_{50} = 38 \text{ nM}$; **66b**, $IC_{50} = 240 \text{ nM}$). Finally, the stability in aqueous buffer resulted satisfactory, with $t_{1/2} > 1 \text{ h}$ for almost all compounds and generally the N2 is more stable than the corresponding N1 isomer.

12. Experimental section

All melting points were determined on a Büchi apparatus (New Castle, DE) and are uncorrected. Extracts were dried over Na_2SO_4 , and the solvents were removed under reduced pressure. Merck F-254 commercial plates (Merck, Durham, NC) were used for analytical TLC to follow the course of reactions. Silica gel 60 (Merck 70-230 mesh, Merck, Durham, NC) was used for column chromatography. $^1\text{H-NMR}$ and $^{13}\text{C-NMR}$ spectra were recorded on an Avance 400 instrument (Bruker Biospin Version 002 with SGU, Bruker Inc., Billerica, MA). Chemical shifts (δ) are reported in ppm to the nearest 0.01 ppm using the solvent as an internal standard. Coupling constants (J values) are given in Hz and were calculated using TopSpin 4.0.8 software (Nicolet Instrument Corp., Madison, WI) and are rounded to the nearest 0.1 vHz. High resolution mass spectrometry (HRMS) analysis was performed with a Thermo Finnigan LTQ Orbitrap mass spectrometer equipped with an electrospray ionization source (ESI). The solvents used in HRMS were acetonitrile (Chromasolv grade) purchased from Sigma-Aldrich (Milan, Italy) and mQ water 18 M Ω cm, obtained from Millipore's Simplicity system (Milan, Italy). The accurate mass measure was performed by introducing sample solution (1.0 $\mu\text{g mL}^{-1}$ in mQ water: acetonitrile 50:50) via syringe pump at 10 $\mu\text{L min}^{-1}$, and the signal of the positive ions was acquired. The experimental conditions allowed monitoring of the protonated molecules ($[\text{M}+\text{H}]^+$ species) with a proper dwell time to achieve 60.000 units of resolution at full width at half maximum (FWHM). As for atoms presenting an isotopic cluster in the measurement, the average value was taken. Microanalyses indicated by the symbols of the elements or functions were performed with a Perkin–Elmer 260 elemental analyzer (PerkinElmer, Inc., Waltham, MA) for C, H, and N, and the results were within $\pm 0.4\%$ of the theoretical values, unless otherwise stated. Reagents and starting material were commercially available.

General procedure for compounds (3a,b). A mixture of the appropriate 1H-pyrrolo[3,2-b]pyridine-3-carbaldehyde **2a,b** [Bradbury, R. H. et al., 2009] (0.78 mmol) and hydroxylamine hydrochloride (2.35 mmol) in 2 mL of water was heated at 60°C for 30 min. Afterwards, 2.35 mmol of sodium bicarbonate was added and the reaction mixture was stirred at reflux for 4h. After cooling to room temperature, the solid obtained was filtered, washed with an excess of ice-cold water and dried.

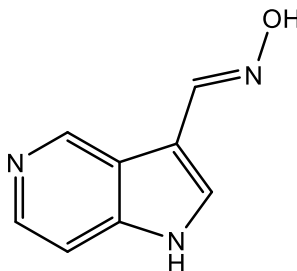
1H-pyrrolo[3,2-b]pyridine-3-carbaldehyde oxime (3a)



Obtained from 1H-pyrrolo[3,2-b]pyridine-3-carbaldehyde (**2a**) [Bradbury, R. H. et al., 2009] following the general procedure. The compound was purified by crystallization from ethanol.

Yield = 65%; mp = 221-222°C (EtOH). ¹H-NMR (400 MHz, DMSO-d₆) δ 7.14-7.19 (m, 1H, Ar), 7.81 (d, 1H, Ar, *J* = 8.0), 7.84 (s, 1H, CH=N-OH), 8.38 (d, 1H, Ar, *J* = 4.4), 8.43 (s, 1H, Ar), 11.31 (exch br s, 1H, CH=N-OH), 11.73 (exch br s, 1H, NH). ESI-MS calcd. for C₈H₇N₃O, 161.16; found: *m/z* 162.06 [M+H]⁺. Anal. C₈H₇N₃O (C, H, N).

1H-pyrrolo[3,2-c]pyridine-3-carbaldehyde oxime (3b)

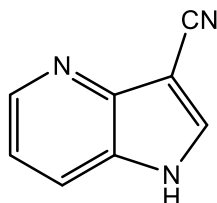


Obtained from 1H-pyrrolo[3,2-c]pyridine-3-carbaldehyde (**2b**) [Bradbury, R. H. et al., 2009] following the general procedure. The compound was purified by crystallization from ethanol.

Yield = 91%; mp = 227-228°C (EtOH). ¹H-NMR (400 MHz, DMSO-d₆) δ 7.39 (d, 1H, Ar, *J* = 5.6), 7.86 (s, 1H, CH=N-OH), 8.21 (d, 2H, Ar, *J* = 7.2), 9.15 (s, 1H, Ar), 11.38 (exch br s, 1H, CH=N-OH), 11.88 (exch br s, 1H, NH). ESI-MS calcd. for C₈H₇N₃O, 161.16; found: *m/z* 162.06 [M+H]⁺. Anal. C₈H₇N₃O (C, H, N).

General procedure for compounds (4a,b). A mixture of intermediate **3a** or **3b** (0.92 mmol) and 4 mL of POCl₃ was stirred at reflux for 2h. After cooling, ice-cold water was slowly added (20 mL), and the precipitate was filtered under vacuum and washed with abundant cold water to obtain the desired compound.

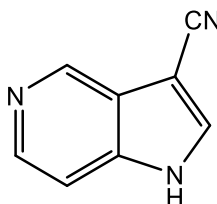
1H-pyrrolo[3,2-b]pyridine-3-carbonitrile (4a)



Obtained from 1H-pyrrolo[3,2-b]pyridine-3-carbaldehyde oxime (**3a**) following the general procedure. The compound was purified by crystallization from ethanol.

Yield = 86%; mp > 300°C (EtOH). ¹H-NMR (400 MHz, DMSO-d₆) δ 7.25-7.30 (m, 1H, Ar), 7.93 (d, 1H, Ar, *J* = 7.2), 8.46 (d, 2H, Ar, *J* = 3.2), 12.36 (exch br s, 1H, NH). IR = 2240 cm⁻¹ (CN). ESI-MS calcd. for C₈H₅N₃, 143.15; found: *m/z* 144.05 [M+H]⁺. Anal. C₈H₅N₃ (C, H, N).

1H-pyrrolo[3,2-c]pyridine-3-carbonitrile (4b)

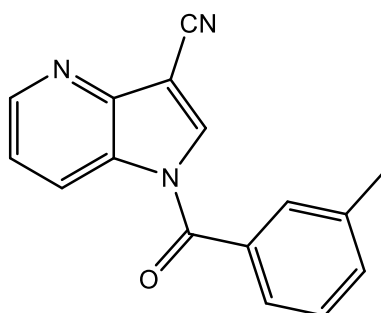


Obtained from 1H-pyrrolo[3,2-c]pyridine-3-carbaldehyde oxime (**3b**) following the general procedure. The compound was purified by crystallization from ethanol.

Yield = 46%; mp = 262-263°C dec. (EtOH). ¹H-NMR (400 MHz, DMSO-d₆) δ 7.53 (d, 1H, Ar, *J* = 5.2), 8.34 (d, 1H, Ar, *J* = 5.6), 8.37 (s, 1H, Ar), 8.92 (s, 1H, Ar), 12.51 (exch br s, 1H, NH). IR = 2240 cm⁻¹ (CN). ESI-MS calcd. for C₈H₅N₃, 143.15; found: *m/z* 144.05 [M+H]⁺. Anal. C₈H₅N₃ (C, H, N).

General procedure for compounds (5a-f). To a cooled (0°C) suspension of the appropriate substrate **4a-c** [4c: Clark, B. A. J. et al., 1970] (0.32 mmol) in anhydrous dichloromethane (2 mL), 0.64 mmol of triethylamine and 0.96 mmol of the appropriate acyl/aroyl chloride were added. The mixture was stirred at 0°C for 2h and then at room temperature for additional 2h. After evaporation of the solvent, cold water was added (20 mL) and pH was neutralized with 0.5 N NaOH. The suspension was extracted with CH₂Cl₂ (3 x 15 mL), dried over sodium sulfate and evaporated under vacuum.

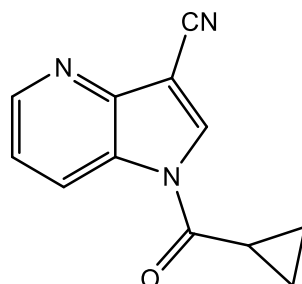
1-(3-methylbenzoyl)-1H-pyrrolo[3,2-b]pyridine-3-carbonitrile (5a)



Obtained from 1H-pyrrolo[3,2-b]pyridine-3-carbonitrile (**4a**) and using m-toluoyl chloride as reactive, following the general procedure. The compound was purified by crystallization from ethanol.

Yield = 55%; mp = 190-191°C (EtOH). ¹H-NMR (400 MHz, CDCl₃) δ 2.48 (s, 3H, CH₃), 7.41-7.46 (m, 1H, Ar), 7.49-7.56 (m, 4H, Ar), 8.09 (s, 1H, Ar), 8.61 (d, 1H, Ar, *J* = 8.0), 8.74 (d, 1H, Ar, *J* = 4.8). ¹³C-NMR (100 MHz, CDCl₃) δ 21.4 (CH₃), 94.8 (C), 112.5 (C), 121.3 (CH), 124.3 (CH), 126.7 (CH), 128.9 (C), 129.1 (CH), 130.0 (CH), 131.6 (C), 134.4 (CH), 136.8 (CH), 139.5 (C), 145.7 (C), 148.2 (CH), 167.8 (C). IR = 1726 cm⁻¹ (CO), 2222 cm⁻¹ (CN). ESI-MS calcd. for C₁₆H₁₁N₃O, 261.28; found: *m/z* 262.09 [M+H]⁺. Anal. C₁₆H₁₁N₃O (C, H, N).

1-(cyclopropanecarbonyl)-1H-pyrrolo[3,2-b]pyridine-3-carbonitrile (5b)

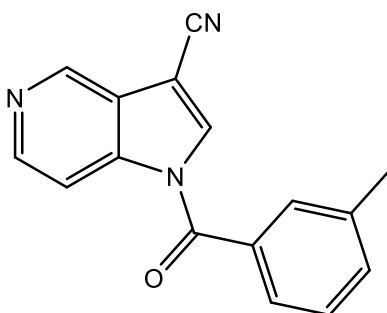


Obtained from 1H-pyrrolo[3,2-b]pyridine-3-carbonitrile (**4a**) and using cyclopropanecarbonyl chloride as reactive, following the general procedure. The compound was purified by crystallization from ethanol.

Yield = 34%; mp = 134-135°C (EtOH). ¹H-NMR (400 MHz, CDCl₃) δ 1.22-1.27 (m, 2H, CH₂), 1.38-1.43 (m, 2H, CH₂), 2.24-2.29 (m, 1H, CH), 7.37-7.42 (m, 1H, Ar), 8.47 (s, 1H, Ar), 8.67 (d, 2H, Ar, *J* = 8.4). ¹³C-NMR (100 MHz, CDCl₃) δ 11.2 (CH₂), 13.7 (CH), 95.2 (C), 112.6 (C), 121.3 (CH), 124.6

(CH), 128.5 (C), 134.2 (CH), 145.4 (C), 147.9 (CH), 171.7 (C). IR = 1718 cm⁻¹ (CO), 2231 cm⁻¹ (CN). ESI-MS calcd. for C₁₂H₉N₃O, 211.22; found: *m/z* 212.08 [M+H]⁺. Anal. C₁₂H₉N₃O (C, H, N).

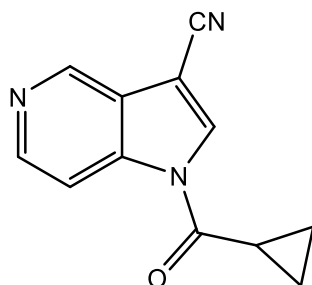
1-(3-methylbenzoyl)-1H-pyrrolo[3,2-c]pyridine-3-carbonitrile (5c)



Obtained from 1H-pyrrolo[3,2-c]pyridine-3-carbonitrile (**4b**) and using *m*-toluoyl chloride as reactive, following the general procedure. The compound was purified by crystallization from ethanol.

Yield = 40%; mp = 180-181°C (EtOH). ¹H-NMR (400 MHz, CDCl₃) δ 2.48 (s, 3H, CH₃), 7.50-7.57 (m, 4H, Ar), 7.99 (s, 1H, Ar), 8.23 (d, 1H, Ar, *J* = 4.8), 8.69 (d, 1H, Ar, *J* = 4.8), 9.16 (s, 1H, Ar). ¹³C-NMR (100 MHz, CDCl₃) δ 21.4 (CH₃), 92.1 (C), 111.2 (CH), 112.6 (C), 126.7 (CH), 129.2 (CH), 130.0 (CH), 131.5 (C), 134.7 (CH), 135.8 (CH), 139.6 (C), 139.9 (C), 142.4 (CH), 145.7 (CH), 167.6 (C). IR = 1707 cm⁻¹ (CO), 2233 cm⁻¹ (CN). ESI-MS calcd. for C₁₆H₁₁N₃O, 261.28; found: *m/z* 262.09 [M+H]⁺. Anal. C₁₆H₁₁N₃O (C, H, N).

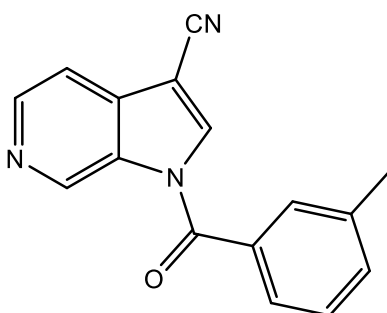
1-(cyclopropanecarbonyl)-1H-pyrrolo[3,2-c]pyridine-3-carbonitrile (5d)



Obtained from 1H-pyrrolo[3,2-c]pyridine-3-carbonitrile (**4b**) and using cyclopropanecarbonyl chloride as reactive, following the general procedure. The compound was purified by flash chromatography using cyclohexane/ethyl acetate 1:1 as eluent.

Yield = 24%; mp = 139-140°C (EtOH). ¹H-NMR (400 MHz, CDCl₃) δ 1.25-1.30 (m, 2H, CH₂), 1.41-1.46 (m, 2H, CH₂), 2.23-2.28 (m, 1H, CH), 8.32 (d, 2H, Ar, *J* = 4.8), 8.56 (s, 1H, Ar), 9.12 (s, 1H, Ar). ¹³C-NMR (100 MHz, CDCl₃) δ 11.4 (CH₂), 14.3 (CH), 92.6 (C), 111.4 (CH), 112.7 (C), 124.1 (C), 133.2 (CH), 139.2 (C), 142.5 (CH), 146.1 (CH), 171.6 (C). IR = 1710 cm⁻¹ (CO), 2232 cm⁻¹ (CN). ESI-MS calcd. for C₁₂H₉N₃O, 211.22; found: *m/z* 212.08 [M+H]⁺. Anal. C₁₂H₉N₃O (C, H, N).

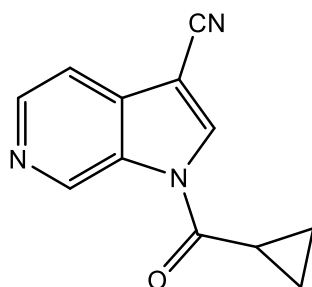
1-(3-methylbenzoyl)-1H-pyrrolo[2,3-c]pyridine-3-carbonitrile (5e)



Obtained from 1H-pyrrolo[2,3-c]pyridine-3-carbonitrile (**4c**) [Clark, B. A. J. et al., 1970] and using *m*-toluoyl chloride as reactive, following the general procedure. The compound was purified by flash chromatography using cyclohexane/ethyl acetate 1:1 as eluent.

Yield = 14%; mp = 157-159°C (EtOH). ¹H-NMR (400 MHz, CDCl₃) δ 2.51 (s, 3H, CH₃), 7.51-7.62 (m, 4H, Ar), 8.08 (s, 1H, Ar), 8.35 (d, 1H, Ar, *J* = 12.0), 8.71 (d, 1H, Ar, *J* = 5.6), 9.79 (s, 1H, Ar). ¹³C-NMR (100 MHz, CDCl₃) δ 21.4 (CH₃), 92.7 (C), 112.8 (C), 114.2 (CH), 126.7 (CH), 129.1 (CH), 130.0 (CH), 131.6 (C), 132.1 (C), 133.2 (C), 134.0 (CH), 137.1 (CH), 138.9 (CH), 139.6 (C), 144.3 (CH), 167.7 (C). IR = 1709 cm⁻¹ (CO), 2231 cm⁻¹ (CN). ESI-MS calcd. for C₁₆H₁₁N₃O, 261.28; found: *m/z* 262.09 [M+H]⁺. Anal. C₁₆H₁₁N₃O (C, H, N).

1-(cyclopropanecarbonyl)-1H-pyrrolo[2,3-c]pyridine-3-carbonitrile (5f)

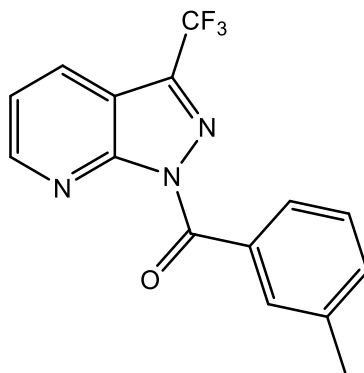


Obtained from 1H-pyrrolo[2,3-c]pyridine-3-carbonitrile (**4c**) [Clark, B. A. J. et al., 1970] and using cyclopropanecarbonyl chloride as reactive, following the general procedure. The compound was purified by crystallization from ethanol.

Yield = 61%; mp = 188-189°C (EtOH). ¹H-NMR (400 MHz, CDCl₃) δ 1.31-1.36 (m, 2H, CH₂), 1.48-1.53 (m, 2H, CH₂), 2.26-2.31 (m, 1H, CH), 7.87 (d, 1H, Ar, *J* = 5.2), 8.54 (s, 1H, Ar), 8.64 (d, 1H, Ar, *J* = 5.2), 9.79 (s, 1H, Ar). ¹³C-NMR (100 MHz, CDCl₃) δ 11.4 (CH₂), 14.1 (CH), 92.9 (C), 112.9 (C), 114.0 (CH), 131.6 (C), 133.7 (C), 134.6 (CH), 139.1 (CH), 144.0 (CH), 171.2 (C). IR = 1722 cm⁻¹ (CO), 2233 cm⁻¹ (CN). ESI-MS calcd. for C₁₂H₉N₃O, 211.22; found: *m/z* 212.08 [M+H]⁺. Anal. C₁₂H₉N₃O (C, H, N).

General procedure for compounds (13a-c). Compounds **13a-c** were obtained using the general procedure followed for compounds **5a-f**, starting from intermediate **9a,b** [**9a**: Schirok, H. et al., 2005; **9b**: Aranov, A. et al., 2005].

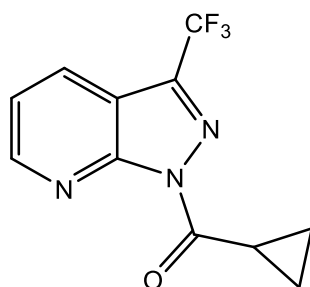
m-tolyl-[3-(trifluoromethyl)-1H-pyrazolo[3,4-b]pyridin-1-yl]methanone (13a)



Obtained from 3-(trifluoromethyl)-1H-pyrazolo[3,4-b]pyridine (**9a**) [Schirok, H. et al., 2005] and using m-toluoyl chloride as reactive, following the general procedure for compound of type **5**. The final compound was purified by flash chromatography using cyclohexane/ethyl acetate 3:1 as eluent.

Yield = 26%; mp = 67-69°C (EtOH). ¹H-NMR (400 MHz, CDCl₃) δ 2.43 (s, 3H, CH₃), 7.38-7.49 (m, 3H, Ar), 7.80 (d, 1H, Ar, *J* = 7.2), 7.85 (s, 1H, Ar), 8.26 (d, 1H, Ar, *J* = 8.0), 8.89 (d, 1H, Ar, *J* = 3.2). ¹³C-NMR (100 MHz, CDCl₃) δ 21.3 (CH₃), 117.7 (C), 121.0 (CH), 122.8 (C), 128.1 (CH), 128.8 (CH), 129.7 (CH), 130.4 (C), 131.9 (CH), 134.4 (CH), 138.2 (C), 142.1 (C), 152.1 (CH), 159.1 (C), 165.0 (C). ESI-MS calcd. for C₁₅H₁₀F₃N₃O, 305.26; found: *m/z* 306.08 [M+H]⁺. Anal. C₁₅H₁₀F₃N₃O (C, H, N).

Cyclopropyl-[3-(trifluoromethyl)-1H-pyrazolo[3,4-b]pyridin-1-yl]methanone (13b)

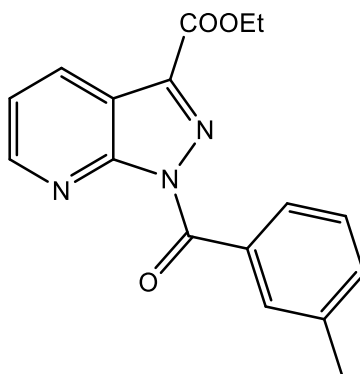


Obtained from 3-(trifluoromethyl)-1H-pyrazolo[3,4-b]pyridine (**9a**) [Schirok, H. et al., 2005] and using cyclopropanecarbonyl chloride as reactive, following the general procedure for compound of type **5**. The final compound was purified by flash chromatography using cyclohexane/ethyl acetate 3:1 as eluent.

Yield = 23%; oil. ¹H-NMR (400 MHz, CDCl₃) δ 1.16-1.23 (m, 2H, CH₂), 1.38-1.44 (m, 2H, CH₂), 3.31-3.36 (m, 1H, CH), 7.43-7.48 (m, 1H, Ar), 8.24 (d, 1H, Ar, *J* = 8.0), 8.85 (d, 1H, Ar, *J* = 2.8). ¹³C-NMR (100 MHz, CDCl₃) δ 11.9 (CH₂), 13.6 (CH), 114.3 (C), 118.8 (C), 120.9 (CH), 121.9 (C), 129.7 (CH),

151.6 (C), 152.1 (CH), 172.5 (C). ESI-MS calcd. for $C_{11}H_8F_3N_3O$, 255.20; found: m/z 256.07 $[M+H]^+$.
Anal. $C_{11}H_8F_3N_3O$ (C, H, N).

ethyl 1-(3-methylbenzoyl)-1H-pyrazolo[3,4-b]pyridine-3-carboxylate (13c)

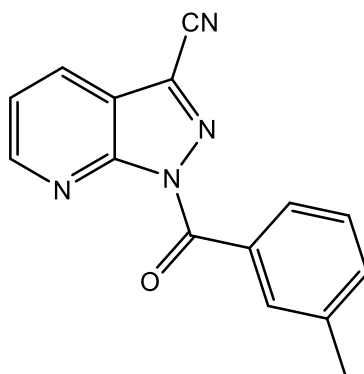


Obtained from ethyl 1H-pyrazolo[3,4-b]pyridine-3-carboxylate (**9b**) [Aranov, A. et al., 2005] and using m-toluoyl chloride as reactive, following the general procedure for compound of type **5**. The compound was purified by crystallization from ethanol.

Yield = 30%; mp = 185-187°C (EtOH). 1H -NMR (400 MHz, $CDCl_3$) δ 1.47 (t, 3H, OCH_2CH_3 , $J = 6.8$), 2.44 (s, 3H, m- CH_3 -Ph), 4.52 (q, 2H, OCH_2CH_3 , $J = 6.8$), 7.40-7.48 (m, 3H, Ar), 7.83 (d, 1H, Ar, $J = 7.2$), 7.88 (s, 1H, Ar), 8.60 (d, 1H, Ar, $J = 8.0$), 8.83 (d, 1H, Ar, $J = 4.0$). ^{13}C -NMR (100 MHz, $CDCl_3$) δ 14.3 (CH_3), 21.3 (CH_3), 62.0 (CH_2), 108.0 (C), 121.1 (CH), 128.1 (CH), 128.9 (CH), 130.5 (C), 131.8 (CH), 132.1 (CH), 133.0 (C), 134.3 (CH), 136.7 (C), 138.1 (C), 151.4 (CH), 159.1 (C), 165.0 (C). ESI-MS calcd. for $C_{17}H_{15}N_3O_3$, 309.33; found: m/z 310.11 $[M+H]^+$. Anal. $C_{17}H_{15}N_3O_3$ (C, H, N).

General procedure for compounds (13d-f). To a suspension of the appropriate substrate **10** [Schirok, H. et al., 2005] or **12** [Lynch, B. M. et al., 1988] (0.86 mmol) and 1.72 mmol of sodium hydride (60% oil dispersion) in 10 mL of anhydrous THF, 1.03 mmol of the appropriate acyl/aroyl chloride were added. The mixture was stirred at room temperature overnight. The solvent was evaporated, cold water was added, and the mixture was neutralized with 2.5 N NaOH. The precipitate was recovered by vacuum filtration.

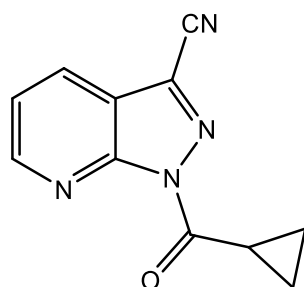
1-(3-methylbenzoyl)-1H-pyrazolo[3,4-b]pyridine-3-carbonitrile (13d)



Obtained from 1H-pyrazolo[3,4-b]pyridine-3-carbonitrile (**10**) [Schirok, H. et al., 2005] and using m-toluoyl chloride as reactive, following the general procedure for compound of type **5**. The compound was purified by crystallization from ethanol.

Yield = 25%; mp = 210-213°C (EtOH). ¹H-NMR (400 MHz, CDCl₃) δ 2.46 (s, 3H, CH₃), 7.41-7.55 (m, 3H, Ar), 7.77-7.82 (m, 2H, Ar), 8.31 (d, 1H, Ar, *J* = 8.0), 8.92 (d, 1H, Ar, *J* = 2.8). ¹³C-NMR (100 MHz, CDCl₃) δ 21.7 (CH₃), 105.0 (C), 110.5 (C), 114.2 (C), 119.6 (CH), 127.3 (CH), 128.4 (CH), 129.8 (CH), 130.4 (C), 130.7 (CH), 133.0 (C), 134.4 (CH), 138.9 (C), 150.2 (CH), 165.7 (C). IR = 2241 cm⁻¹ (CN). ESI-MS calcd. for C₁₅H₁₀N₄O, 262.27; found: *m/z* 263.09 [M+H]⁺. Anal. C₁₅H₁₀N₄O (C, H, N).

1-(cyclopropanecarbonyl)-1H-pyrazolo[3,4-b]pyridine-3-carbonitrile (13e)

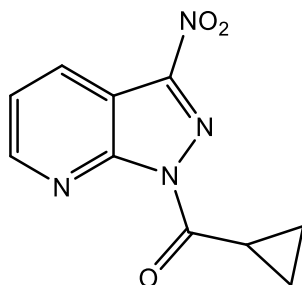


Obtained from 1H-pyrazolo[3,4-b]pyridine-3-carbonitrile (**10**) [Schirok, H. et al., 2005] and using cyclopropanecarbonyl chloride as reactive, following the general procedure for compound of type **5**. The compound was purified by crystallization from ethanol.

Yield = 34%; mp = 147-149°C (EtOH). ¹H-NMR (400 MHz, CDCl₃) δ 1.24-1.29 (m, 2H, CH₂), 1.45-1.50 (m, 2H, CH₂), 3.32-3.37 (m, 1H, CH), 7.48-7.53 (m, 1H, Ar), 8.27 (d, 1H, Ar, *J* = 8.0), 8.88 (d, 1H, Ar, *J* = 4.4). ¹³C-NMR (100 MHz, CDCl₃) δ 12.3 (CH₂), 13.7 (CH), 105.0 (C), 110.4 (C), 114.1

(C), 121.4 (CH), 129.2 (CH), 133.0 (C), 152.5 (CH), 173.6 (C). IR = 2243 cm⁻¹ (CN). ESI-MS calcd. for C₁₁H₈N₄O, 212.21; found: *m/z* 213.07 [M+H]⁺. Anal. C₁₁H₈N₄O (C, H, N).

Cyclopropyl-(3-nitro-1H-pyrazolo[3,4-b]pyridin-1-yl)methanone (13f)

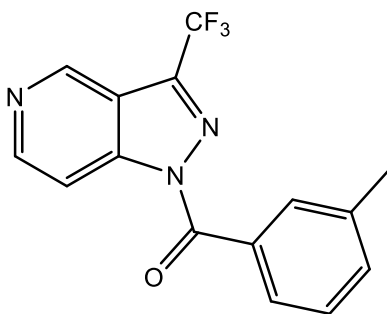


Obtained from 3-nitro-1H-pyrazolo[3,4-b]pyridine (**12**) [Lynch, B. M. et al., 1988] and using cyclopropanecarbonyl chloride as reactive, following the general procedure for compound of type **5**. The compound was purified by crystallization from ethanol.

Yield = 30%; mp = 137-139°C (EtOH). ¹H-NMR (400 MHz, CDCl₃) δ 1.28-1.33 (m, 2H, CH₂), 1.47-1.52 (m, 2H, CH₂), 3.29-3.35 (m, 1H, CH), 7.58-7.63 (m, 1H, Ar), 8.68 (dd, 1H, Ar, *J*₁ = 1.4 and *J*₂ = 8.0), 8.90 (d, 1H, Ar, *J* = 4.4). ¹³C-NMR (100 MHz, CDCl₃) δ 12.6 (CH₂), 13.8 (CH), 110.6 (C), 122.7 (CH), 131.2 (CH), 142.6 (C), 151.8 (C), 152.9 (CH), 172.2 (C). ESI-MS calcd. for C₁₀H₈N₄O₃, 232.20; found: *m/z* 233.06 [M+H]⁺. Anal. C₁₀H₈N₄O₃ (C, H, N).

General procedure for compounds (17a,b, 19b, 22a,b and 27). Compounds **17a,b**, **19b**, **22a,b** and **27** were obtained using the general procedure followed for compounds of type **5**, starting from intermediates **16** [Kawase, M. et al., 1999], **18** [Kawase, M. et al., 1999], **21** [Hert, J. et al., 2017] and **26** [Tucker, T. J. et al., 2008] respectively.

m-tolyl-[3-(trifluoromethyl)-1H-pyrazolo[4,3-c]pyridin-1-yl]methanone (17a)

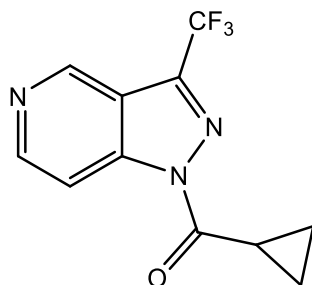


Obtained from 3-(trifluoromethyl)-1H-pyrazolo[4,3-c]pyridine (**16**) [Kawase, M. et al., 1999] and using *m*-toluoyl chloride as reactive, following the general procedure for compounds of type **5**. The final compound was purified by flash chromatography using cyclohexane/ethyl acetate 3:1 as eluent.

Yield = 66%; mp = 79-81°C (EtOH). ¹H-NMR (400 MHz, CDCl₃) δ 2.46 (s, 3H, CH₃), 7.41-7.49 (m, 2H, Ar), 7.92 (d, 2H, Ar, *J* = 6.4), 8.42 (d, 1H, Ar, *J* = 5.6), 8.80 (d, 1H, Ar, *J* = 6.0), 9.29 (s, 1H, Ar). ¹³C-NMR (100 MHz, CDCl₃) δ 21.4 (CH₃), 110.4 (CH), 116.6 (C), 118.9 (C), 121.7 (C), 128.2 (CH), 128.8 (CH), 130.7 (C), 131.9 (CH), 134.5 (CH), 138.3 (C), 144.2 (CH), 145.0 (C), 148.4 (CH), 167.6

(C). ESI-MS calcd. for $C_{15}H_{10}F_3N_3O$, 305.26; found: m/z 306.08 $[M+H]^+$. Anal. $C_{15}H_{10}F_3N_3O$ (C, H, N).

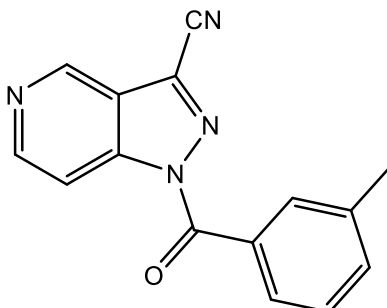
Cyclopropyl-[3-(trifluoromethyl)-1H-pyrazolo[4,3-c]pyridin-1-yl]methanone (17b)



Obtained from 3-(trifluoromethyl)-1H-pyrazolo[4,3-c]pyridine (**16**) [Kawase, M. et al., 1999] and using cyclopropanecarbonyl chloride as reactive, following the general procedure for compounds of type **5**. The compound was purified by crystallization from ethanol.

Yield = 30%; mp = 93-94°C (EtOH). 1H -NMR (400 MHz, $CDCl_3$) δ 1.25-1.30 (m, 2H, CH_2), 1.39-1.44 (m, 2H, CH_2), 3.18-3.24 (m, 1H, CH), 8.37 (d, 1H, Ar, $J = 6.0$), 8.75 (d, 1H, Ar, $J = 5.6$), 9.28 (s, 1H, Ar). ^{13}C -NMR (100 MHz, $CDCl_3$) δ 12.0 (CH_2), 12.9 (CH), 110.1 (CH), 119.0 (C), 121.7 (C), 143.4 (C), 144.1 (CH), 148.3 (CH), 174.3 (C). ESI-MS calcd. for $C_{11}H_8F_3N_3O$, 255.20; found: m/z 256.07 $[M+H]^+$. Anal. $C_{11}H_8F_3N_3O$ (C, H, N).

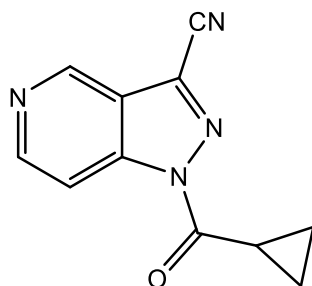
1-(3-methylbenzoyl)-1H-pyrazolo[4,3-c]pyridine-3-carbonitrile (19a)



Obtained from 1H-pyrazolo[4,3-c]pyridine-3-carbonitrile (**18**) [Kawase, M. et al., 1999] and using *m*-toluoyl chloride as reactive, following the general procedure for compounds **13d-f**. The compound was purified by crystallization from ethanol.

Yield = 47%; mp = 192-194°C (EtOH). 1H -NMR (400 MHz, $CDCl_3$) δ 2.48 (s, 3H, CH_3), 7.46 (t, 1H, Ar, $J = 7.6$), 7.52 (d, 1H, Ar, $J = 7.2$), 7.88 (d, 2H, Ar, $J = 6.8$), 8.45 (d, 1H, Ar, $J = 6.0$), 8.84 (d, 1H, Ar, $J = 6.0$), 9.34 (s, 1H, Ar). ^{13}C -NMR (100 MHz, $CDCl_3$) δ 21.4 (CH_3), 110.5 (CH), 111.2 (C), 122.1 (C), 124.0 (C), 128.4 (CH), 128.8 (CH), 130.3 (C), 131.9 (CH), 134.9 (CH), 138.5 (C), 143.7 (CH), 144.2 (C), 148.8 (CH), 167.3 (C). IR = 2241 cm^{-1} (CN). ESI-MS calcd. for $C_{15}H_{10}N_4O$, 262.27; found: m/z 263.09 $[M+H]^+$. Anal. $C_{15}H_{10}N_4O$ (C, H, N).

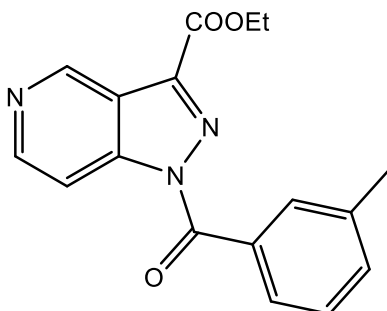
1-(cyclopropanecarbonyl)-1H-pyrazolo[4,3-c]pyridine-3-carbonitrile (19b)



Obtained from 1H-pyrazolo[4,3-c]pyridine-3-carbonitrile (**18**) [Kawase, M. et al., 1999] and using cyclopropanecarbonyl chloride as reactive, following the general procedure for compounds of type **5**. The compound was purified by crystallization from ethanol.

Yield = 44%; mp = 152-154°C (EtOH). ¹H-NMR (400 MHz, CDCl₃) δ 1.30-1.35 (m, 2H, CH₂), 1.42-1.47 (m, 2H, CH₂), 3.14-3.20 (m, 1H, CH), 8.41 (d, 1H, Ar, *J* = 6.0), 8.78 (d, 1H, Ar, *J* = 5.6), 9.34 (s, 1H, Ar). ¹³C-NMR (100 MHz, CDCl₃) δ 12.4 (CH₂), 12.9 (CH), 110.2 (CH), 111.2 (C), 122.2 (C), 123.7 (C), 142.6 (C), 143.7 (CH), 148.8 (CH), 173.9 (C). IR = 2243 cm⁻¹ (CN). ESI-MS calcd. for C₁₁H₈N₄O, 212.21; found: *m/z* 213.07 [M+H]⁺. Anal. C₁₁H₈N₄O (C, H, N).

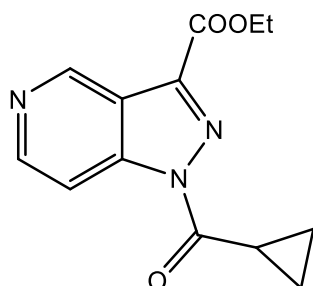
ethyl 1-(3-methylbenzoyl)-1H-pyrazolo[4,3-c]pyridine-3-carboxylate (22a)



Obtained from ethyl 1H-pyrazolo[4,3-c]pyridine-3-carboxylate (**21**) [Hert, J. et al., 2017] and using *m*-toluoyl chloride as reactive, following the general procedure for compounds of type **5**. The final compound was purified by flash chromatography using dichloromethane/methanol 9:1 as eluent.

Yield = 49%; mp = 87-89°C (EtOH). ¹H-NMR (400 MHz, CDCl₃) δ 1.48 (t, 3H, OCH₂CH₃, *J* = 7.2), 2.44 (s, 3H, *m*-CH₃-Ph), 4.55 (q, 2H, OCH₂CH₃, *J* = 7.2), 7.39-7.46 (m, 2H, Ar), 7.94 (d, 2H, Ar, *J* = 7.2), 8.36 (d, 1H, Ar, *J* = 6.0), 8.74 (d, 1H, Ar, *J* = 5.6), 9.58 (s, 1H, Ar). ¹³C-NMR (100 MHz, CDCl₃) δ 14.3 (CH₃), 21.4 (CH₃), 62.3 (CH₂), 110.1 (CH), 120.8 (C), 128.3 (CH), 129.0 (CH), 131.1 (C), 132.1 (CH), 134.4 (CH), 138.3 (C), 141.0 (C), 145.3 (C), 146.3 (CH), 147.8 (CH), 160.8 (C), 168.0 (C). ESI-MS calcd. for C₁₇H₁₅N₃O₃, 309.33; found: *m/z* 310.11 [M+H]⁺. Anal. C₁₇H₁₅N₃O₃ (C,H,N).

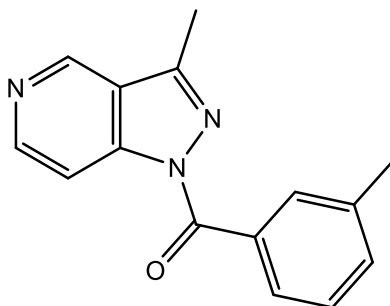
ethyl 1-(cyclopropanecarbonyl)-1H-pyrazolo[4,3-c]pyridine-3-carboxylate (22b)



Obtained from ethyl 1H-pyrazolo[4,3-c]pyridine-3-carboxylate (**21**) [Hert, J. et al., 2017] and using cyclopropanecarbonyl chloride as reactive, following the general procedure for compounds of type **5**. The final compound was purified by flash chromatography using cyclohexane/ethyl acetate 1:1 as eluent.

Yield = 44%; mp = 94-96°C (EtOH). ¹H-NMR (400 MHz, CDCl₃) δ 1.23 (m, 2H, CH₂ cC₃H₅), 1.36 (m, 2H, CH₂ cC₃H₅), 1.50 (t, 3H, CH₃, *J* = 7.2), 3.25-3.31 (m, 1H, CH cC₃H₅), 4.57 (q, 2H, CH₂CH₃, *J* = 7.2), 8.25 (d, 1H, Ar, *J* = 5.6), 8.67 (d, 1H, Ar, *J* = 5.6), 9.52 (s, 1H, Ar). ¹³C-NMR (100 MHz, CDCl₃) δ 8.8 (CH), 12.2 (CH₂), 14.1 (CH₃), 60.9 (CH₂), 105.3 (C), 113.7 (CH), 126.2 (C), 136.7 (C), 143.1 (CH), 148.0 (CH), 160.6 (C), 172.3 (C). ESI-MS calcd. for C₁₃H₁₃N₃O₃, 259.27; found: *m/z* 260.10 [M+H]⁺. Anal. C₁₃H₁₃N₃O₃ (C,H,N).

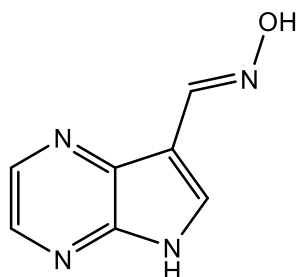
(3-methyl-1H-pyrazolo[4,3-c]pyridin-1-yl)(m-tolyl)methanone (27)



Obtained from 3-methyl-1H-pyrazolo[4,3-c]pyridine (**26**) [Tucker, T. J. et al., 2008] and using *m*-toluoyl chloride as reactive, following the general procedure for compounds of type **5**. The final compound was purified by flash chromatography using cyclohexane/ethyl acetate 1:1 as eluent.

Yield = 43%; mp = 104-105°C (EtOH). ¹H-NMR (400 MHz, CDCl₃) δ 2.45 (s, 3H, *m*-CH₃-Ph), 2.67 (s, 3H, 3-CH₃), 7.39-7.45 (m, 2H, Ar), 7.89 (d, 2H, Ar, *J* = 8.8), 8.38 (d, 1H, Ar, *J* = 6.6), 8.70 (d, 1H, Ar, *J* = 5.6), 9.11 (s, 1H, Ar). ¹³C-NMR (100 MHz, CDCl₃) δ 12.4 (CH₃), 21.4 (CH₃), 102.9 (C), 110.3 (CH), 122.8 (C), 127.9 (CH), 128.4 (CH), 131.5 (CH), 132.4 (C), 133.5 (CH), 138.9 (C), 144.0 (CH), 144.8 (C), 147.9 (CH), 148.5 (C), 168.1 (C). ESI-MS calcd. for C₁₅H₁₃N₃O, 251.28; found: *m/z* 252.11 [M+H]⁺. Anal. C₁₅H₁₃N₃O (C, H, N).

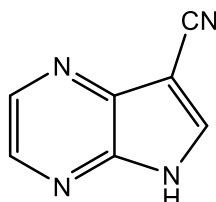
5H-pyrrolo[2,3-b]pyrazine-7-carbaldehyde oxime (33)



Compound **33** was obtained using the general procedure followed for compounds **3a,b**, starting from intermediate **32** [Clark, B. A. J. et al., 1976].

Yield = 90%; mp = 239-240°C dec. (EtOH). ¹H-NMR (400 MHz, DMSO-d₆) δ 8.12 (s, 1H, Ar), 8.27 (s, 2H, Ar), 8.43 (s, 1H, CH=N), 10.85 (exch br s, 1H, OH), 12.38 (exch br s, 1H, NH). ESI-MS calcd. for C₇H₆N₄O, 162.15; found: *m/z* 163.05 [M+H]⁺. Anal. C₇H₆N₄O (C,H,N).

5H-pyrrolo[2,3-b]pyrazine-7-carbonitrile (34)

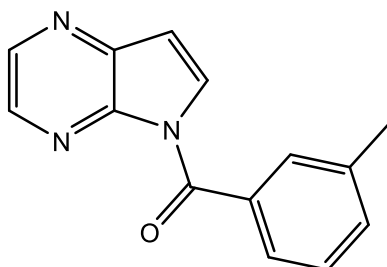


Compound **34** was obtained using the general procedure followed for compounds **4a,b**, starting from intermediate **33**. The desired compound was purified by flash chromatography using dichloromethane/methanol 9:1 as eluent.

Yield = 20%; mp > 300°C (EtOH). ¹H-NMR (400 MHz, DMSO-d₆) δ 8.44 (d, 1H, Ar, *J* = 2.4), 8.56 (d, 1H, Ar, *J* = 2.4), 8.75 (s, 1H, Ar), 13.20 (exch br s, 1H, NH). IR = 2227 cm⁻¹ (CN), 3390 cm⁻¹ (NH). ESI-MS calcd. for C₇H₄N₄, 144.13; found: *m/z* 145.07 [M+H]⁺. Anal. C₇H₄N₄ (C,H,N).

General procedure for compounds (31a,b and 35a,b). Compounds **31a,b** and **35a,b** were obtained using the general procedure followed for compounds of type **5**, starting from intermediate **30** [Clark, B. A. J. et al., 1976] and **34**.

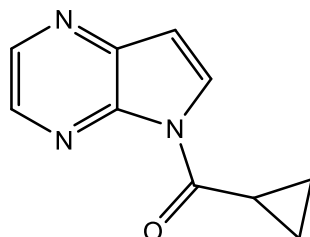
(5H-pyrrolo[2,3-b]pyrazin-5-yl)(m-tolyl)methanone (31a)



Obtained from 5H-pyrrolo[2,3-b]pyrazine-7-carbonitrile (**30**) and using m-toluoyl chloride as reactive, following the general procedure for compounds of type **5**. The final compound was purified by flash chromatography using dichloromethane/methanol 98:2 as eluent.

Yield = 19%; mp = 108-110°C (EtOH). ¹H-NMR (400 MHz, CDCl₃) δ 2.40 (s, 3H, CH₃), 6.87 (d, 1H, Ar, *J* = 4.0), 7.40 (t, 1H, Ar, *J* = 7.6), 7.49 (d, 1H, Ar, *J* = 7.6), 7.55 (d, 1H, Ar, *J* = 7.6), 7.60 (s, 1H, Ar), 8.13 (d, 1H, Ar, *J* = 4.0), 8.24 (d, 1H, Ar, *J* = 2.4), 8.62 (d, 1H, Ar, *J* = 2.4). ¹³C-NMR (100 MHz, CDCl₃) δ 21.2 (CH₃), 100.8 (CH), 106.7 (CH), 127.8 (CH), 128.7 (CH), 130.5 (C), 131.6 (CH), 133.5 (C), 134.3 (CH), 137.2 (CH), 138.3 (C), 138.5 (CH), 141.7 (C), 167.8 (C). ESI-MS calcd. for C₁₄H₁₁N₃O, 237.26; found: *m/z* 238.09 [M+H]⁺. Anal. C₁₄H₁₁N₃O (C,H,N).

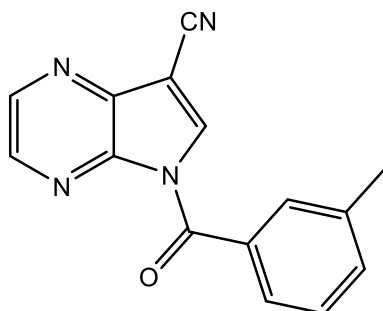
cyclopropyl(5H-pyrrolo[2,3-b]pyrazin-5-yl)methanone (31b)



Obtained from 5H-pyrrolo[2,3-b]pyrazine-7-carbonitrile (**30**) and using cyclopropanecarbonyl chloride as reactive, following the general procedure for compounds of type **5**. The final compound was purified by flash chromatography using cyclohexane/ethyl acetate 3:1 as eluent.

Yield = 25%; mp = 117-119°C (EtOH). ¹H-NMR (400 MHz, CDCl₃) δ 1.21-1.29 (m, 2H, CH₂), 1.37-1.42 (m, 2H, CH₂), 4.00 (quin, 1H, CH, *J* = 4.0), 6.85 (d, 1H, Ar, *J* = 4.0), 8.33 (m, 2H, Ar), 8.53 (d, 1H, Ar, *J* = 2.4). ¹³C-NMR (100 MHz, CDCl₃) δ 11.8 (CH₂), 14.6 (CH), 106.3 (CH), 130.0 (CH), 137.4 (CH), 140.5 (CH), 141.7 (C), 143.1 (C), 172.7 (C). ESI-MS calcd. for C₁₀H₉N₃O, 187.20; found: *m/z* 188.07 [M+H]⁺. Anal. C₁₀H₉N₃O (C,H,N).

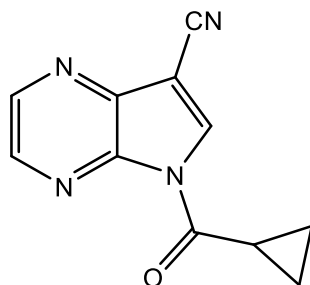
5-(3-methylbenzoyl)-5H-pyrrolo[2,3-b]pyrazine-7-carbonitrile (35a)



Obtained from 5H-pyrrolo[2,3-b]pyrazine-7-carbonitrile (**34**) and using m-toluoyl chloride as reactive, following the general procedure for compounds of type **5**. The final compound was purified by flash chromatography using dichloromethane/methanol 98:2 as eluent.

Yield = 4%; mp = 140-141°C (EtOH). ¹H-NMR (400 MHz, CDCl₃) δ 2.45 (s, 3H, CH₃), 7.38-7.48 (m, 1H, Ar), 7.53-7.58 (m, 2H, Ar), 7.65 (s, 1H, Ar), 8.42 (d, 1H, Ar, *J* = 2.4), 8.52 (s, 1H, Ar), 8.68 (d, 1H, Ar, *J* = 2.4). ¹³C-NMR (100 MHz, CDCl₃) δ 20.9 (CH₃), 83.6 (C), 113.6 (C), 119.4 (CH), 120.7 (C), 128.1 (CH), 129.2 (CH), 130.1 (CH), 130.5 (C), 134.8 (CH), 138.9 (C), 144.3 (CH), 145.8 (CH), 147.8 (C), 167.8 (C). ESI-MS calcd. for C₁₅H₁₀N₄O, 262.27; found: *m/z* 263.09 [M+H]⁺. Anal. C₁₅H₁₀N₄O (C,H,N).

5-(cyclopropanecarbonyl)-5H-pyrrolo[2,3-b]pyrazine-7-carbonitrile (35b)

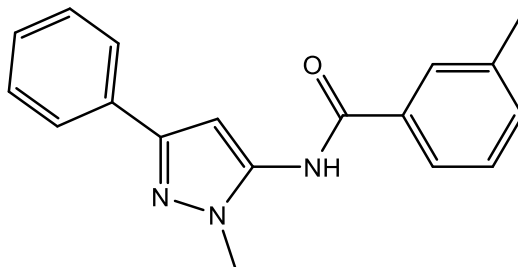


Obtained from 5H-pyrrolo[2,3-b]pyrazine-7-carbonitrile (**34**) and using cyclopropanecarbonyl chloride as reactive, following the general procedure for compounds of type **5**. The final compound was purified by flash chromatography using cyclohexane/ethyl acetate 3:1 as eluent.

Yield = 20%; mp = 158-159°C (EtOH). ¹H-NMR (400 MHz, CDCl₃) δ 1.33 (m, 2H, CH₂), 1.46 (m, 2H, CH₂), 3.93 (m, 1H, CH), 8.49 (s, 1H, Ar), 8.69 (s, 1H, Ar), 8.75 (s, 1H, Ar). ¹³C-NMR (100 MHz, CDCl₃) δ 11.4 (CH), 12.6 (CH₂), 83.7 (C), 113.5 (C), 119.5 (CH), 120.7 (C), 144.2 (CH), 145.9 (CH), 147.9 (C), 172.8 (C). ESI-MS calcd. for C₁₁H₈N₄O, 212.21; found: *m/z* 213.07 [M+H]⁺. Anal. C₁₁H₈N₄O (C,H,N).

General procedure for compounds (37a,b,d). Compounds **37a,b,d** were obtained using the general procedure followed for compounds of type **5**, starting from intermediate **36a,c** [**36a**: Huang, D. S. et al., 2020; **36c**: Al-Qalaf, F. et al., 2008], and using *m*-toluoyl chloride as reactive.

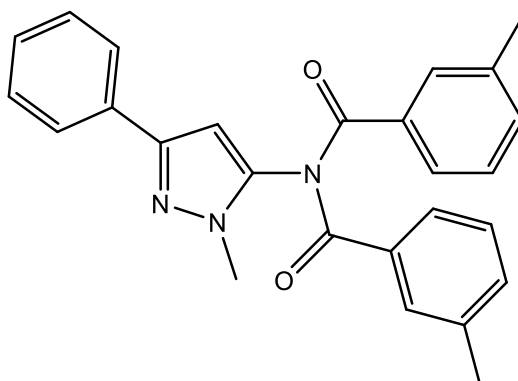
3-methyl-N-(1-methyl-3-phenyl-1H-pyrazol-5-yl)benzamide (37a)



It was synthesized starting from 1-methyl-3-phenyl-1H-pyrazol-5-amine (**36a**) [Huang, D. S. et al., 2020] following the general procedure for compounds of type **5**. The product **37a** was obtained in mixture with the N-disubstituted **37b** and they were separated by flash chromatography using cyclohexane/ethyl acetate 3:1 as eluent.

Yield = 24%; mp = 146-147°C (EtOH). ¹H-NMR (400 MHz, DMSO-d₆) δ 2.39 (s, 3H, *m*-CH₃-Ph), 3.73 (s, 3H, N-CH₃), 6.69 (s, 1H, pyrazole), 7.27 (t, 1H, Ar, *J* = 7.4), 7.38 (t, 2H, Ar, *J* = 7.6), 7.43 (m, 2H, Ar), 7.75-7.80 (m, 4H, Ar), 10.34 (exch br s, 1H, NH). ¹³C-NMR (100 MHz, DMSO-d₆) δ 21.4 (CH₃), 35.8 (CH₃), 98.0 (CH), 124.4 (CH), 125.4 (CH), 127.7 (CH), 128.2 (CH), 128.6 (CH), 128.8 (CH), 132.9 (C), 133.3 (CH), 136.4 (C), 138.9 (C), 150.1 (C), 166.3 (C). ESI-MS calcd. for C₁₈H₁₇N₃O, 291.35; found: *m/z* 292.14 [M+H]⁺. Anal. C₁₈H₁₇N₃O (C,H,N).

3-methyl-N-(1-methyl-3-phenyl-1H-pyrazol-5-yl)-N-(3-methylbenzoyl)benzamide (37b)

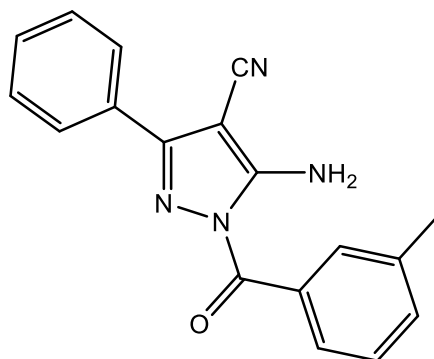


It was synthesized starting from 1-methyl-3-phenyl-1H-pyrazol-5-amine (**36a**) [Huang, D. S. et al., 2020] following the general procedure for compounds of type **5**. The product **37b** was obtained in mixture with the N-monosubstituted **37a** and they were separated by flash chromatography using cyclohexane/ethyl acetate 3:1 as eluent.

Yield = 30%; mp = 161-163°C (EtOH). ¹H-NMR (400 MHz, DMSO-d₆) δ 2.30 (s, 6H, 2 x *m*-CH₃-Ph), 3.76 (s, 3H, N-CH₃), 6.80 (s, 1H, pyrazole), 7.24-7.29 (m, 7H, Ar), 7.58 (d, 4H, Ar, *J* = 8.8), 7.67 (d, 2H, Ar, *J* = 8.8). ¹³C-NMR (100 MHz, DMSO-d₆) δ 21.3 (CH₃), 36.1 (CH₃), 101.6 (CH), 125.3 (CH),

126.1 (CH), 127.9 (CH), 128.6 (CH), 128.6 (CH), 129.8 (CH), 133.0 (C), 133.4 (C), 134.0 (CH), 138.1 (C), 138.8 (C), 150.5 (C), 172.0 (C). ESI-MS calcd. for $C_{26}H_{23}N_3O_2$, 409.49; found: m/z 410.18 $[M+H]^+$. Anal. $C_{26}H_{23}N_3O_2$ (C,H,N).

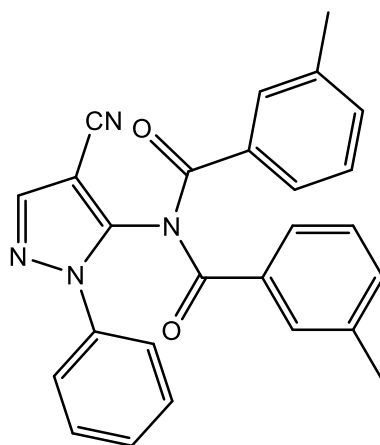
5-amino-1-(3-methylbenzoyl)-3-phenyl-1H-pyrazole-4-carbonitrile (37d)



It was obtained from 5-amino-3-phenyl-1H-pyrazole-4-carbonitrile (**36c**) [Al-Qalaf, F. et al., 2008] following the general procedure for compounds of type **5**. The compound was purified by flash chromatography using cyclohexane/ethyl acetate 4:1 as eluent.

Yield = 24%; mp = 171-172°C (EtOH). 1H -NMR (400 MHz, $CDCl_3$) δ 2.45 (s, 3H, CH_3), 6.66 (exch br s, 2H, NH_2), 7.38-7.45 (m, 5H, Ar), 7.94-7.99 (m, 4H, Ar). ^{13}C -NMR (100 MHz, $CDCl_3$) δ 21.4 (CH_3), 73.4 (C), 114.2 (C), 127.0 (CH), 127.9 (CH), 128.8 (CH), 128.8 (CH), 130.0 (C), 130.3 (CH), 131.5 (C), 131.9 (CH), 134.2 (CH), 138.0 (C), 152.3 (C), 157.4 (C), 170.3 (C). ESI-MS calcd. for $C_{18}H_{14}N_4O$, 302.34; found: m/z 303.12 $[M+H]^+$. Anal. $C_{18}H_{14}N_4O$ (C,H,N).

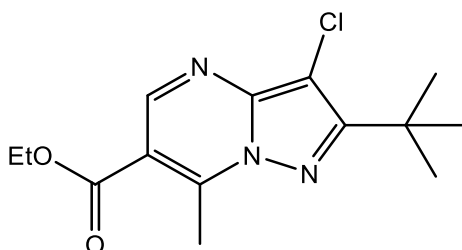
N-(4-cyano-1-phenyl-1H-pyrazol-5-yl)-3-methyl-N-(3-methylbenzoyl)benzamide (37c)



To a cooled suspension (0°C) of 5-amino-1-phenyl-1H-pyrazole-4-carbonitrile (**36b**) [Dos Santos, M. S. et al., 2012] (0.54 mmol) in anhydrous dichloromethane (2 mL), 1.03 mmol of DIPEA and 0.76 mmol of *m*-tolyl chloride were added. The mixture was kept stirring at room temperature for 3h. After evaporation of the solvent, cold water was added (20 mL), and the mixture was extracted with CH_2Cl_2 (3 x 15 mL), dried over sodium sulfate and evaporated under vacuum. The compound was finally purified by flash chromatography using cyclohexane/ethyl acetate 3:1 as eluent.

Yield = 20%; mp = 106-108°C (EtOH). ¹H-NMR (400 MHz, CDCl₃) δ 2.25 (s, 6H, 2 x CH₃), 7.14 (t, 2H, Ar, *J* = 7.6), 7.22-7.28 (m, 4H, Ar), 7.30 (t, 4H, Ar, *J* = 7.2), 7.37-7.43 (m, 3H, Ar), 7.98 (s, 1H, pyrazole). ¹³C-NMR (100 MHz, CDCl₃) δ 21.2 (CH₃), 94.2 (C), 111.6 (C), 124.1 (CH), 125.1 (CH), 128.4 (CH), 129.5 (CH), 129.6 (CH), 129.9 (CH), 133.0 (C), 134.1 (CH), 136.5 (C), 138.6 (C), 142.2 (CH), 142.5 (C), 171.4 (C). IR = 1699 cm⁻¹ (CO), 1714 cm⁻¹ (CO), 2233 cm⁻¹ (CN). ESI-MS calcd. for C₂₆H₂₀N₄O₂, 420.47; found: *m/z* 421.16 [M+H]⁺. Anal. C₂₆H₂₀N₄O₂ (C,H,N).

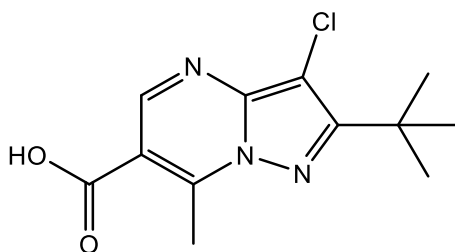
Ethyl 2-tert-butyl-3-chloro-7-methylpyrazolo[1,5-a]pyrimidine-6-carboxylate (**38c**)



To a solution of the pyrazolo[1,5-a]pyrimidine (**38b**) [Bruni, F. et al.] (0.50 mmol) in anhydrous dichloromethane (10 mL), N-chlorosuccinimide (NCS) (0.75 mmol) and a catalytic amount of benzoyl peroxide (0.05 mmol) were added. The reaction mixture was stirred at reflux for 12h. The solution was evaporated, and the product was obtained through trituration with diisopropyl ether.

Yield = 70%; mp = 59-60°C (EtOH). ¹H-NMR (400 MHz, DMSO-d₆) δ 1.41 (s, 9H, C-(CH₃)₃), 1.44 (t, 3H, OCH₂CH₃, *J* = 7.2), 3.10 (s, 3H, CH₃), 4.41 (q, 2H, OCH₂CH₃, *J* = 7.2), 8.87 (s, 1H, Ar). ESI-MS calcd. for C₁₄H₁₈ClN₃O₂, 295.76; found: *m/z* 296.18 [M+H]⁺. Anal. C₁₄H₁₈ClN₃O₂ (C,H,N).

2-(tert-butyl)-3-chloro-7-methylpyrazolo[1,5-a]pyrimidine-6-carboxylic acid (**39c**)

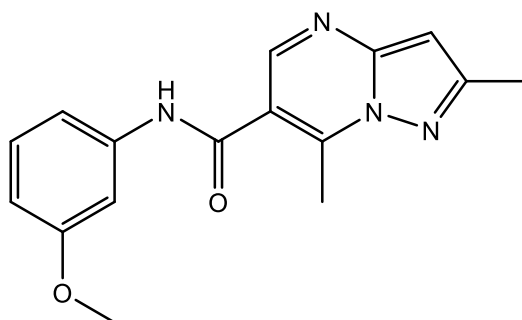


To a suspension of ethyl 2-(tert-butyl)-3-chloro-7-methylpyrazolo[1,5-a]pyrimidine-6-carboxylate (**38c**) (1.01 mmol) in 5 mL of sodium hydroxide 40%, the minimum volume of ethanol needed to solubilize the solid was added. The reaction was kept stirring at reflux for 1h. The mixture was cooled to 0°C and acidified with HCl 6N up to pH=2. The solid was filtered under vacuum and crystallized from ethanol to obtain the pure product.

Yield = 96%; mp = 269-270°C (EtOH). ¹H-NMR (400 MHz, DMSO-d₆) δ 1.45 (s, 9H, C-(CH₃)₃), 3.04 (s, 3H, CH₃), 8.85 (s, 1H, Ar). ESI-MS calcd. for C₁₂H₁₄ClN₃O₂, 267.71; found: *m/z* 268.08 [M+H]⁺. Anal. C₁₂H₁₄ClN₃O₂ (C,H,N).

General procedure for compounds (40a-h). To a solution of the appropriate acid of type **39** [**39a**: Bartroli, J. et al., 1998; **39b**: Kato, N. et al., 2011; **39d**: Goldfarb, D. S., 2009] (0.37 mmol) in 3 mL of anhydrous dichloromethane, in order were added 1.87 mmol of trichloro acetonitrile and, after 5 minutes, 0.71 mmol of triphenylphosphine, maintaining the suspension under stirring at room temperature. After 4h, 0.37 mmol of m-anisidine or 3-methoxybenzylamine and 1.12 mmol of triethylamine were added, and the mixture, which was stirred for further 12h at room temperature. The solvent was evaporated, cold water was added (20 mL), and the mixture was extracted with CH₂Cl₂ (3 x 15 mL). The organic solvent was dried over sodium sulfate and evaporated under vacuum.

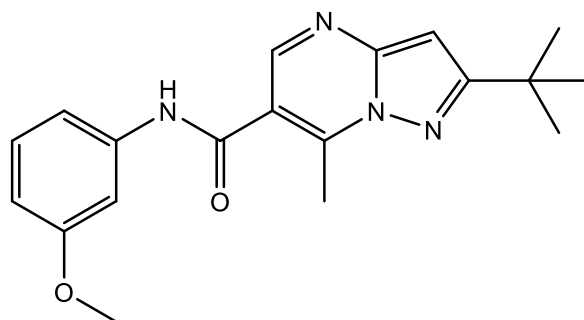
N-(3-methoxyphenyl)-2,7-dimethylpyrazolo[1,5-a]pyrimidine-6-carboxamide (40a)



Obtained from 2,7-dimethylpyrazolo[1,5-a]pyrimidine-6-carboxylic acid (**39a**) [Bartroli, J. et al., 1998] and using m-anisidine as reactive, following the general procedure for compounds of type **40**. The compound was purified by flash chromatography using cyclohexane/ethyl acetate 1:1 as eluent.

Yield = 19%; mp = 128-129°C (EtOH). ¹H-NMR (400 MHz, CDCl₃) δ 2.49 (s, 3H, 2-CH₃), 2.90 (s, 3H, 7-CH₃), 3.79 (s, 3H, OCH₃), 6.40 (s, 1H, Ar), 6.71 (dd, 1H, Ar, *J*₁ = 2.4 and *J*₂ = 8.8), 7.11 (d, 1H, Ar, *J* = 7.6), 7.23 (t, 1H, Ar, *J* = 8.2), 7.36 (s, 1H, Ar), 8.44 (s, 1H, Ar), 8.45 (exch br s, 1H, NH). ¹³C-NMR (100 MHz, CDCl₃) δ 14.8 (CH₃), 14.9 (CH₃), 55.4 (CH₃), 97.2 (CH), 106.0 (CH), 110.9 (CH), 112.3 (CH), 115.9 (C), 129.9 (CH), 138.8 (C), 146.3 (CH), 147.1 (C), 148.6 (C), 156.9 (C), 160.3 (C), 163.6 (C). ESI-MS calcd. for C₁₆H₁₆N₄O₂, 296.33; found: *m/z* 297.13 [M+H]⁺. Anal. C₁₆H₁₆N₄O₂ (C,H,N).

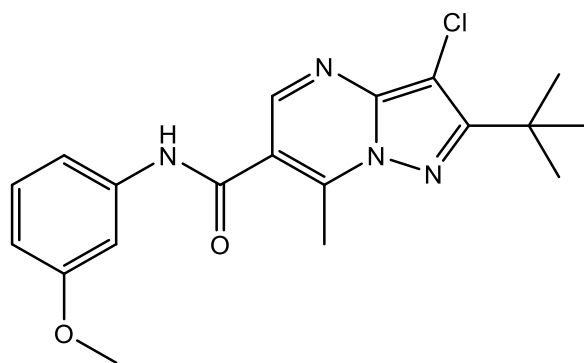
2-(tert-butyl)-N-(3-methoxyphenyl)-7-methylpyrazolo[1,5-a]pyrimidine-6-carboxamide (40b)



Obtained from 2-(tert-butyl)-7-methylpyrazolo[1,5-a]pyrimidine-6-carboxylic acid (**39b**) [Kato, N. et al., 2011] and using m-anisidine as reactive, following the general procedure for compounds of type **40**. The compound was purified by flash chromatography using petroleum ether/ethyl acetate 5:2 as eluent.

Yield = 14%; mp = 114-115°C (EtOH). ¹H-NMR (400 MHz, CDCl₃) δ 1.40 (s, 9H, C-(CH₃)₃), 2.99 (s, 3H, CH₃), 3.79 (s, 3H, OCH₃), 6.54 (s, 1H, Ar), 6.72 (dd, 1H, Ar, *J*₁ = 2.0 and *J*₂ = 8.2), 7.10 (d, 1H, Ar, *J* = 7.6), 7.25 (t, 1H, Ar, *J* = 8.2), 7.39 (exch br s, 1H, NH), 8.09 (s, 1H, Ar), 8.54 (s, 1H, Ar). ¹³C-NMR (100 MHz, CDCl₃) δ 14.8 (CH₃), 30.3 (CH₃), 33.1 (C), 55.4 (CH₃), 93.8 (CH), 106.0 (CH), 110.8 (CH), 112.3 (CH), 115.6 (C), 129.9 (CH), 138.9 (C), 145.9 (CH), 147.7 (C), 148.3 (C), 160.3 (C), 163.7 (C), 169.6 (C). ESI-MS calcd. for C₁₉H₂₂N₄O₂, 338.41; found: *m/z* 339.17 [M+H]⁺. Anal. C₁₉H₂₂N₄O₂ (C,H,N).

2-(tert-butyl)-3-chloro-N-(3-methoxyphenyl)-7-methylpyrazolo[1,5-a]pyrimidine-6-carboxamide (40c)

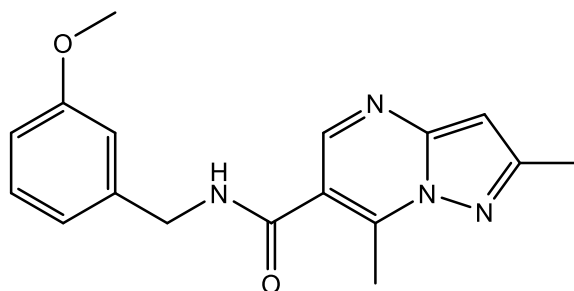


Obtained from 2-(tert-butyl)-3-chloro-7-methylpyrazolo[1,5-a]pyrimidine-6-carboxylic acid (**39c**) and using m-anisidine as reactive, following the general procedure for compounds of type **40**. The compound was purified by flash chromatography using dichloromethane/methanol 98:2 as eluent.

Yield = 7%; mp = 164-166°C (EtOH). ¹H-NMR (400 MHz, CDCl₃) δ 1.51 (s, 9H, C-(CH₃)₃), 2.98 (s, 3H, CH₃), 3.83 (s, 3H, OCH₃), 6.74 (dd, 1H, Ar, *J*₁ = 2.0 and *J*₂ = 8.0), 7.10 (d, 1H, Ar, *J* = 7.6), 7.27 (t, 1H, Ar, *J* = 8.4), 7.38 (s, 1H, Ar), 7.91 (exch br s, 1H, NH), 8.59 (s, 1H, Ar). ¹³C-NMR (100 MHz, CDCl₃) δ 14.2 (CH₃), 28.5 (CH₃), 34.1 (C), 55.4 (CH₃), 98.2 (C), 111.0 (CH), 112.3 (CH), 129.9 (CH),

138.7 (C), 144.3 (C), 146.8 (CH), 148.1 (C), 160.3 (C), 162.7 (C). ESI-MS calcd. for $C_{19}H_{21}ClN_4O_2$, 372.85; found: m/z 373.14 $[M+H]^+$. Anal. $C_{19}H_{21}ClN_4O_2$ (C,H,N).

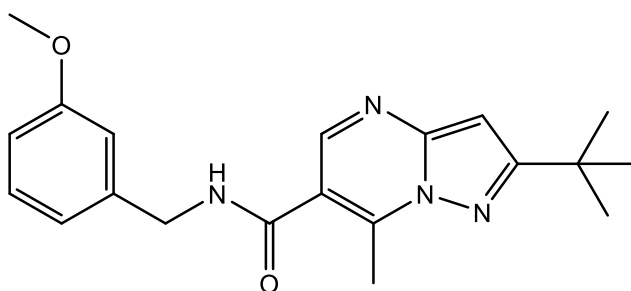
N-(3-methoxybenzyl)-2,7-dimethylpyrazolo[1,5-a]pyrimidine-6-carboxamide (40d)



Obtained from 2,7-dimethylpyrazolo[1,5-a]pyrimidine-6-carboxylic acid (**39a**) [Bartroli, J. et al., 1998] and using 3-methoxybenzylamine as reactive, following the general procedure for compounds of type **40**. The compound was purified by flash chromatography using cyclohexane/ethyl acetate 2:1 as eluent.

Yield = 6%; mp = 125-127°C (EtOH). 1H -NMR (400 MHz, $CDCl_3$) δ 2.52 (s, 3H, 2- CH_3), 2.95 (s, 3H, 7- CH_3), 3.79 (s, 3H, OCH_3), 4.60 (d, 2H, CH_2 , $J = 5.6$), 6.46 (m, 2H, Ar + NH), 6.83 (d, 1H, Ar, $J = 8.0$), 6.88 (s, 1H, Ar), 6.92 (d, 1H, Ar, $J = 7.6$), 7.26 (m, 1H, Ar), 8.43 (s, 1H, Ar). ^{13}C -NMR (100 MHz, $CDCl_3$) δ 14.9 (CH_3), 44.4 (CH_2), 55.3 (CH_3), 97.2 (CH), 113.2 (CH), 113.6 (CH), 115.3 (C), 120.1 (CH), 130.0 (CH), 139.1 (C), 146.4 (CH), 156.7 (C), 165.3 (C). ESI-MS calcd. for $C_{17}H_{18}N_4O_2$, 310.36; found: m/z 311.14 $[M+H]^+$. Anal. $C_{17}H_{18}N_4O_2$ (C,H,N).

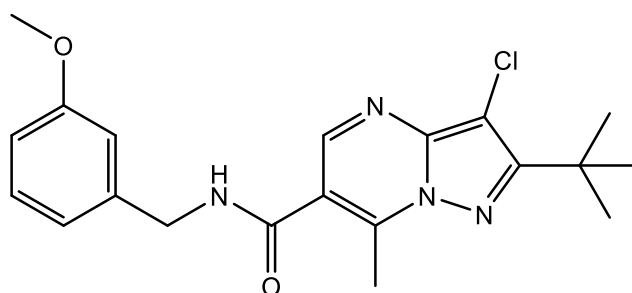
2-(tert-butyl)-N-(3-methoxybenzyl)-7-methylpyrazolo[1,5-a]pyrimidine-6-carboxamide (40e)



Obtained from 2-(tert-butyl)-7-methylpyrazolo[1,5-a]pyrimidine-6-carboxylic acid (**39b**) [Kato, N. et al., 2011] and using 3-methoxybenzylamine as reactive, following the general procedure for compounds of type **40**. The compound was purified by flash chromatography using hexane/ethyl acetate 3:2 as eluent.

Yield = 13%; oil. 1H -NMR (400 MHz, $CDCl_3$) δ 1.39 (s, 9H, C-(CH_3)₃), 2.98 (s, 3H, CH_3), 3.80 (s, 3H, OCH_3), 4.62 (d, 2H, CH_2 , $J = 5.6$), 6.38 (exch br s, 1H, NH), 6.52 (s, 1H, Ar), 6.81-6.94 (m, 3H, Ar), 7.27 (m, 1H, Ar), 8.44 (s, 1H, Ar). ^{13}C -NMR (100 MHz, $CDCl_3$) δ 14.9 (CH_3), 30.3 (CH_3), 33.2 (C), 44.3 (CH_2), 55.3 (CH_3), 93.8 (CH), 113.2 (CH), 113.5 (CH), 120.0 (CH), 126.8 (C), 130.0 (CH), 139.2 (C), 141.8 (C), 145.9 (CH), 147.6 (C), 150.8 (C), 153.5 (C), 160.1 (C), 165.3 (C). ESI-MS calcd. for $C_{20}H_{24}N_4O_2$, 352.44; found: m/z 353.19 $[M+H]^+$. Anal. $C_{20}H_{24}N_4O_2$ (C,H,N).

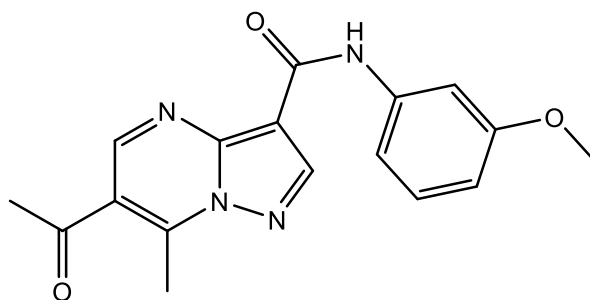
2-(tert-butyl)-3-chloro-N-(3-methoxybenzyl)-7-methylpyrazolo[1,5-a]pyrimidine-6-carboxamide (40f)



Obtained from 2-(tert-butyl)-3-chloro-7-methylpyrazolo[1,5-a]pyrimidine-6-carboxylic acid (**39c**) and using 3-methoxybenzylamine as reactive, following the general procedure for compounds of type **40**. The compound was purified by flash chromatography using cyclohexane/ethyl acetate 2:1 as eluent.

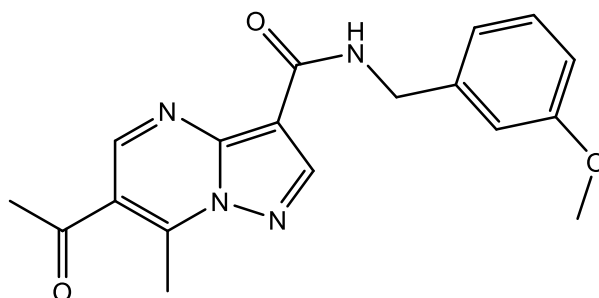
Yield = 21%; mp = 140-141°C (EtOH). ¹H-NMR (400 MHz, CDCl₃) δ 1.50 (s, 9H, C-(CH₃)₃), 2.97 (s, 3H, CH₃), 3.81 (s, 3H, OCH₃), 4.63 (d, 2H, CH₂, J = 5.6), 6.20 (exch br s, 1H, NH), 6.85 (dd, 1H, Ar, J₁ = 2.4 and J₂ = 8.0), 6.90 (d, 1H, Ar, J = 2.0), 6.93 (d, 1H, Ar, J = 7.6), 7.83 (t, 1H, Ar, J = 7.8), 8.51 (s, 1H, Ar). ¹³C-NMR (100 MHz, CDCl₃) δ 14.2 (CH₃), 28.5 (CH₃), 44.4 (CH₂), 55.3 (CH₃), 98.2 (C), 113.3 (CH), 113.6 (CH), 115.9 (C), 120.0 (CH), 130.0 (CH), 139.0 (CH), 144.5 (C), 146.9 (CH), 147.9 (C), 160.1 (C), 162.5 (C), 164.9 (C). ESI-MS calcd. for C₂₀H₂₃ClN₄O₂, 386.88; found: m/z 387.15 [M+H]⁺. Anal. C₂₀H₂₃ClN₄O₂ (C,H,N).

6-acetyl-N-(3-methoxyphenyl)-7-methylpyrazolo[1,5-a]pyrimidine-3-carboxamide (40g)



Obtained from 6-acetyl-7-methylpyrazolo[1,5-a]pyrimidine-3-carboxylic acid (**39d**) [Goldfarb, D. S., 2009] and using m-anisidine as reactive, following the general procedure for compounds of type **40**. The compound was purified by flash chromatography using cyclohexane/ethyl acetate 1:1 as eluent. Yield = 7%; mp = 178-179°C (EtOH). ¹H-NMR (400 MHz, CDCl₃) δ 2.76 (s, 3H, CH₃), 3.21 (s, 3H, COCH₃), 3.85 (s, 3H, OCH₃), 6.68 (m, 1H, Ar), 7.16 (m, 1H, Ar), 7.22-7.27 (m, 1H, Ar), 7.53 (s, 1H, Ar), 8.83 (s, 1H, Ar), 9.04 (s, 1H, Ar), 9.83 (exch br s, 1H, NH). ¹³C-NMR (100 MHz, CDCl₃) δ 15.5 (CH₃), 29.9 (CH₃), 55.3 (CH₃), 90.7 (C), 105.4 (CH), 110.0 (CH), 112.0 (CH), 119.8 (C), 129.6 (CH), 138.9 (C), 142.5 (C), 145.4 (C), 148.8 (CH), 150.7 (CH), 152.4 (C), 159.9 (C), 196.6 (C). ESI-MS calcd. for C₁₇H₁₆N₄O₃, 324.34; found: m/z 325.12 [M+H]⁺. Anal. C₁₇H₁₆N₄O₃ (C,H,N).

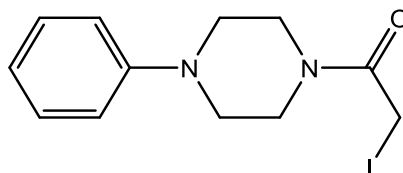
6-acetyl-N-(3-methoxybenzyl)-7-methylpyrazolo[1,5-a]pyrimidine-3-carboxamide (40h)



Obtained from 6-acetyl-7-methylpyrazolo[1,5-a]pyrimidine-3-carboxylic acid (**39d**) [Goldfarb, D. S., 2009] and using 3-methoxybenzylamine as reactive, following the general procedure for compounds of type **40**. The compound was purified by flash chromatography using cyclohexane/ethyl acetate 1:1 as eluent.

Yield = 5%; mp = 164-166°C (EtOH). ¹H-NMR (400 MHz, CDCl₃) δ 2.71 (s, 3H, CH₃), 3.20 (s, 3H, COCH₃), 3.79 (s, 3H, OCH₃), 4.71 (d, 2H, CH₂, J = 6.0), 6.82 (dd, 1H, Ar, J₁ = 2.4 and J₂ = 8.4), 6.94 (m, 1H, Ar), 6.98 (d, 1H, Ar, J = 7.2), 7.26 (t, 1H, Ar, J = 7.6), 8.24 (exch br s, 1H, NH), 8.81 (s, 1H, Ar), 8.92 (s, 1H, Ar). ¹³C-NMR (100 MHz, CDCl₃) δ 16.6 (CH₃), 29.1 (CH₃), 43.9 (CH₂), 55.9 (CH₃), 105.1 (C), 111.0 (CH), 112.3 (CH), 119.2 (CH), 119.7 (C), 129.5 (CH), 138.3 (C), 142.6 (C), 145.5 (CH), 145.8 (C), 156.2 (CH), 160.4 (C), 167.9 (C), 196.7 (C). ESI-MS calcd. for C₁₈H₁₈N₄O₃, 338.37; found: m/z 339.14 [M+H]⁺. Anal. C₁₈H₁₈N₄O₃ (C,H,N).

2-iodo-1-(4-phenylpiperazin-1-yl)ethan-1-one (43)

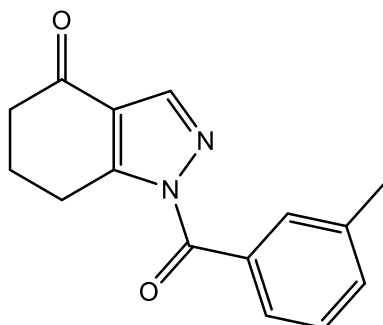


A mixture of 2-chloro-1-(4-phenyl-1,4-diazepan-1-yl)ethan-1-one (**42**) [Sharma, R. K. et al., 2015] (2.25 mmol) and NaI (6.67 mmol) in 21 mL of acetone was stirred at room temperature for 16h. After evaporation of the solvent, cold water was added and the mixture was extracted with CH₂Cl₂ (3 x 15 mL), dried over sodium sulfate and evaporated under vacuum.

Yield = 89%; oil. ¹H-NMR (400 MHz, CDCl₃) δ 3.16 (t, 2H, CH₂ piperazine, J = 5.0), 3.25 (t, 2H, CH₂ piperazine, J = 5.0), 3.61 (t, 2H, CH₂ piperazine, J = 5.0), 3.75-3.80 (m, 4H, CH₂ piperazine + CO-CH₂-I), 6.90-6.95 (m, 3H, Ar), 7.25-7.30 (m, 2H, Ar). ESI-MS calcd. for C₁₂H₁₅IN₂O, 330.17; found: m/z 331.02 [M+H]⁺. Anal. C₁₂H₁₅IN₂O (C,H,N).

General procedure for compounds (47a,b) and (48a,b). Compounds **47a,b** and **48a,b** were obtained using the general procedure followed for compounds of type **5**, starting from the intermediate **46** [Claramunt, R. M. et al., 2006].

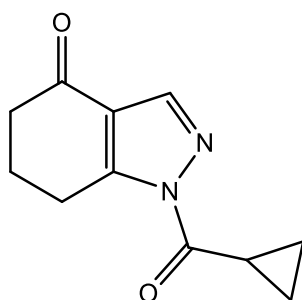
2-(3-methylbenzoyl)-2,5,6,7-tetrahydro-4H-indazol-4-one (47a)



It was synthesized using m-toluoyl chloride as reactive and following the general procedure for compounds of type **5**. The final compound **47a** was obtained in mixture with the N-2 isomer **48a** and they were separated by flash chromatography using cyclohexane/ethyl acetate 3:1 as eluent.

Yield = 2%; oil. $^1\text{H-NMR}$ (400 MHz, CDCl_3) δ 2.17 (t, 2H, CH_2 , $J = 6.0$), 2.43 (s, 3H, CH_3), 2.58 (t, 2H, CH_2 , $J = 6.0$), 2.92 (t, 2H, CH_2 , $J = 6.0$), 7.37-7.46 (m, 2H, Ar), 7.87 (d, 2H, Ar, $J = 9.2$), 8.75 (s, 1H, pyrazole). $^{13}\text{C-NMR}$ (100 MHz, CDCl_3) δ 21.4 (CH_3), 23.0 (CH_2), 23.3 (CH_2), 39.2 (CH_2), 121.2 (C), 128.2 (CH), 128.8 (CH), 130.6 (C), 131.0 (CH), 131.9 (CH), 134.5 (CH), 138.3 (C), 159.4 (C), 166.4 (C), 194.6 (C). ESI-MS calcd. for $\text{C}_{15}\text{H}_{14}\text{N}_2\text{O}_2$, 254.29; found: m/z 255.11 $[\text{M}+\text{H}]^+$. Anal. $\text{C}_{15}\text{H}_{14}\text{N}_2\text{O}_2$ (C,H,N).

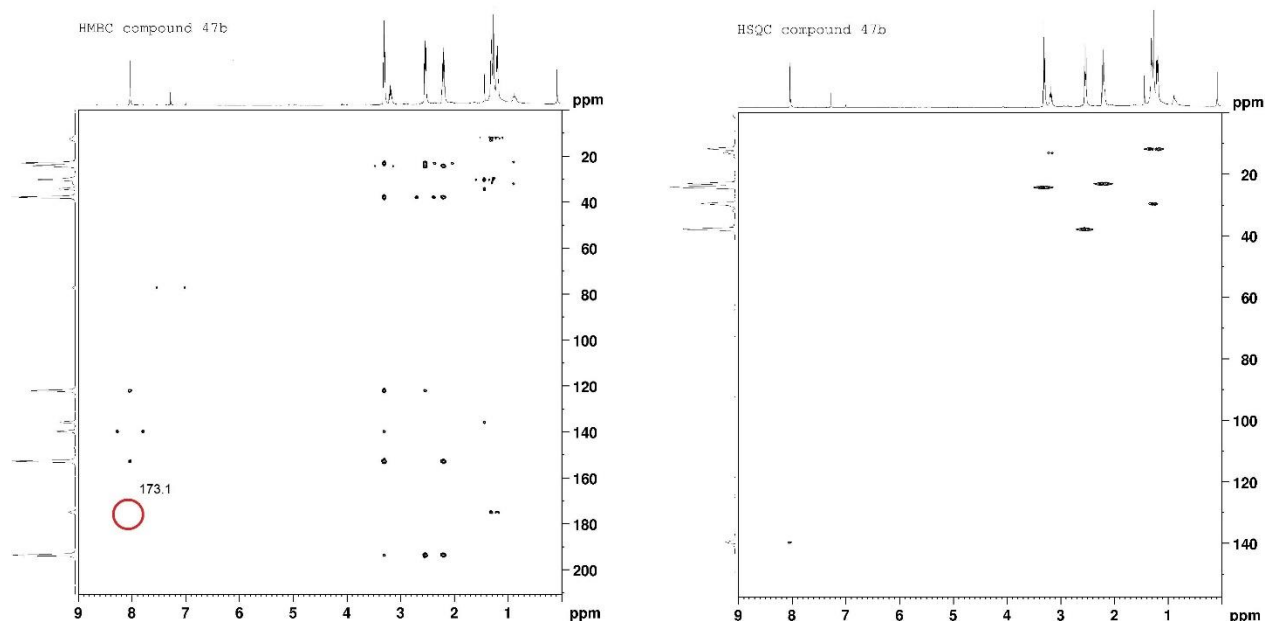
1-(cyclopropanecarbonyl)-1,5,6,7-tetrahydro-4H-indazol-4-one (47b)



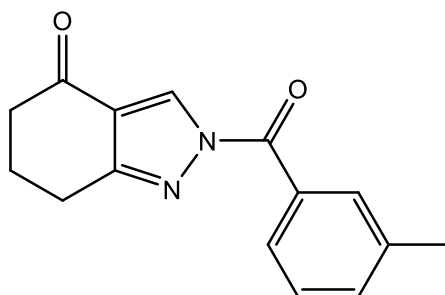
It was synthesized using cyclopropanecarbonyl chloride as reactive and following the general procedure for compounds of type **5**. The final compound **47b** was obtained in mixture with the N-2 isomer **48b** and they were separated by flash chromatography using petroleum ether/ethyl acetate 5:2 as eluent.

Yield = 30%; oil. $^1\text{H-NMR}$ (400 MHz, CDCl_3) δ 1.17-1.22 (m, 2H, CH_2 cC_3H_5), 1.27-1.33 (m, 2H, CH_2 cC_3H_5), 2.16 (quin, 2H, CH_2 , $J = 6.4$), 2.55 (t, 2H, CH_2 , $J = 6.4$), 2.91 (t, 2H, CH_2 , $J = 6.2$), 3.06-3.12 (quin, 1H, CH cC_3H_5 , $J = 4.0$), 8.62 (s, 1H, pyrazole). $^{13}\text{C-NMR}$ (100 MHz, CDCl_3) δ 12.2 (CH_2), 12.3 (CH), 23.0 (CH_2), 23.2 (CH_2), 39.2 (CH_2), 112.1 (C), 121.4 (C), 128.0 (CH), 159.1 (C), 173.1 (C),

194.6 (C). ESI-MS calcd. for $C_{11}H_{12}N_2O_2$, 204.23; found: m/z 205.09 $[M+H]^+$. Anal. $C_{11}H_{12}N_2O_2$ (C,H,N).



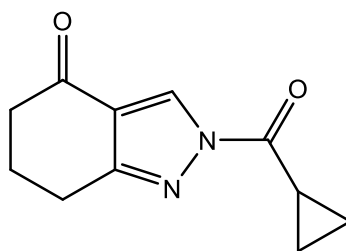
1-(3-methylbenzoyl)-1,5,6,7-tetrahydro-4H-indazol-4-one (48a)



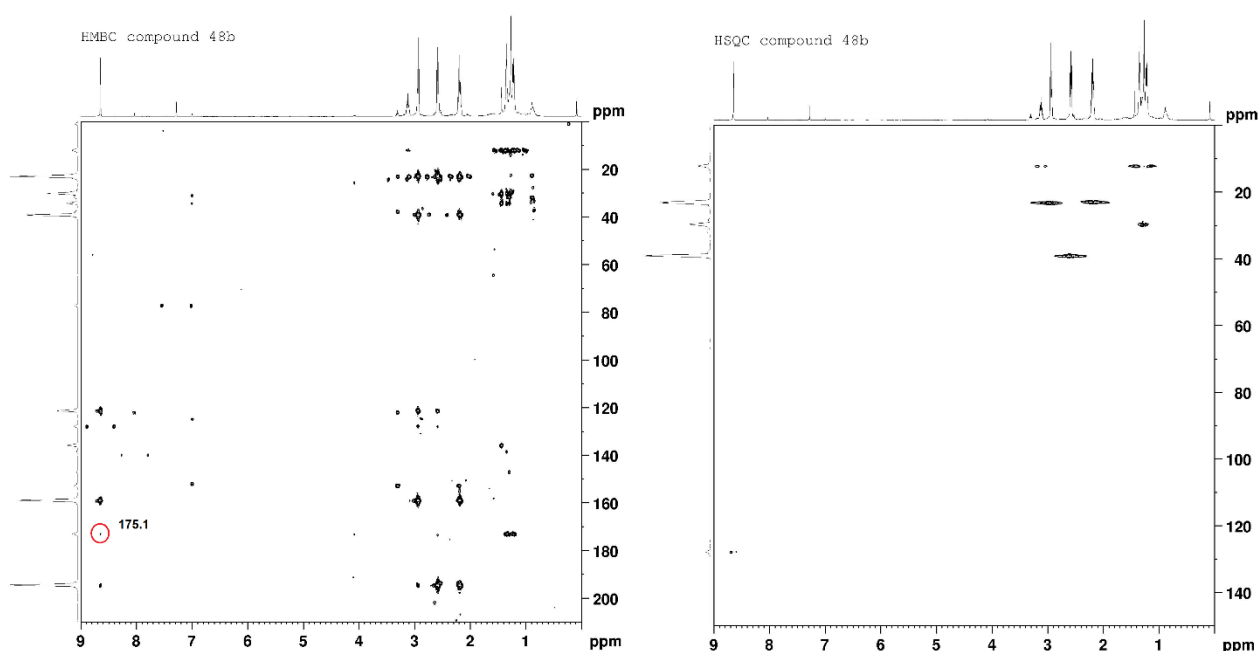
It was synthesized using *m*-toluoyl chloride as reactive and following the general procedure for compounds of type **5**. The final compound **48a** was obtained in mixture with the *N*-1 isomer **47a** and they were separated by flash chromatography using cyclohexane/ethyl acetate 3:1 as eluent.

Yield = 6%; mp = 136-138°C (EtOH). $^1\text{H-NMR}$ (400 MHz, CDCl_3) δ 2.25 (quin, 2H, CH_2 , $J = 6.0$), 2.43 (s, 3H, CH_3), 2.58 (t, 2H, CH_2 , $J = 6.8$), 3.38 (t, 2H, CH_2 , $J = 6.4$), 7.37-7.45 (m, 2H, Ar), 7.80 (s, 2H, Ar), 8.04 (s, 1H, pyrazole). $^{13}\text{C-NMR}$ (100 MHz, CDCl_3) δ 21.4 (CH_3), 23.3 (CH_2), 24.4 (CH_2), 38.0 (CH_2), 112.0 (C), 123.1 (C), 128.1 (CH), 128.7 (C), 131.6 (C), 131.8 (CH), 134.3 (CH), 138.1 (C), 140.0 (CH), 154.7 (C), 193.6 (C). ESI-MS calcd. for $C_{15}H_{14}N_2O_2$, 254.29; found: m/z 255.11 $[M+H]^+$. Anal. $C_{15}H_{14}N_2O_2$ (C,H,N).

2-(cyclopropanecarbonyl)-2,5,6,7-tetrahydro-4H-indazol-4-one (48b)

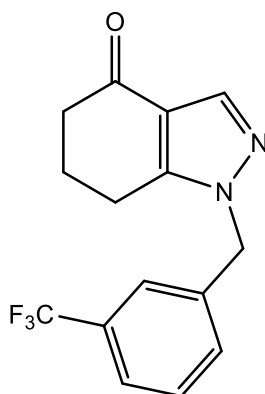


It was synthesized using cyclopropanecarbonyl chloride as reactive and following the general procedure for compounds of type **5**. The final compound **48b** was obtained in mixture with the N-1 isomer **47b** and they were separated by flash chromatography using petroleum ether/ethyl acetate. Yield = 7%; oil. $^1\text{H-NMR}$ (400 MHz, CDCl_3) δ 1.14-1.19 (m, 2H, CH_2 cC_3H_5), 1.26-1.31 (m, 2H, CH_2 cC_3H_5), 2.17 (quin, 2H, CH_2 , $J = 6.4$), 2.51 (t, 2H, CH_2 , $J = 6.6$), 3.16 (quin, 1H, CH cC_3H_5 , $J = 4.0$), 3.29 (t, 2H, CH_2 , $J = 6.2$), 8.01 (s, 1H, pyrazole). $^{13}\text{C-NMR}$ (100 MHz, CDCl_3) δ 11.9 (CH_2), 13.2 (CH), 23.1 (CH_2), 24.3 (CH_2), 37.9 (CH_2), 122.1 (C), 139.9 (CH), 152.9 (C), 175.1 (C), 193.7 (C). ESI-MS calcd. for $\text{C}_{11}\text{H}_{12}\text{N}_2\text{O}_2$, 204.23; found: m/z 205.09 $[\text{M}+\text{H}]^+$. Anal. $\text{C}_{11}\text{H}_{12}\text{N}_2\text{O}_2$ (C,H,N).



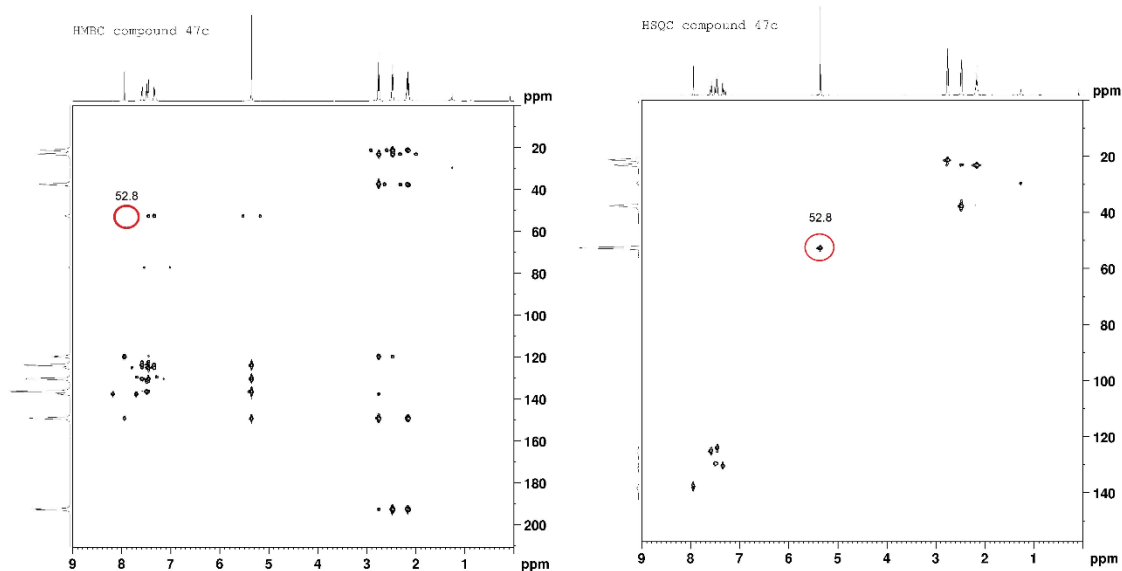
General procedure for compounds (47c,d and 48c,d). To a suspension of the intermediate **46** [Claramunt, R. M. et al., 2006] (0.42 mmol) and 0.50 mmol of potassium carbonate in anhydrous acetonitrile (2 mL), 0.84 mmol of 3-(trifluoromethyl)benzyl bromide or alternatively **43** were added. The mixture was stirred at reflux for 4h. After evaporation of the solvent, cold water was added (20 mL), and the pH was neutralized with 1N HCl. The suspension was extracted with CH_2Cl_2 (3 x 15 mL), dried over sodium sulfate and evaporated under vacuum.

1-(3-(trifluoromethyl)benzyl)-1,5,6,7-tetrahydro-4H-indazol-4-one (47c)

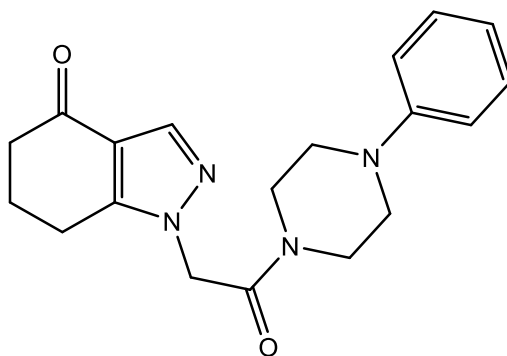


It was synthesized using 3-(trifluoromethyl)benzyl bromide as reactive and following the general procedure above reported. The final compound **47c** was obtained in mixture with the N-2 isomer **47c** and they were separated by flash chromatography using toluene/ethyl acetate/acetic acid 9:1:0.5 as eluent.

Yield = 14%; oil. $^1\text{H-NMR}$ (400 MHz, CDCl_3) δ 2.15 (quin, 2H, CH_2 , $J = 6.4$), 2.42 (t, 2H, CH_2 , $J = 6.4$), 2.73 (t, 2H, CH_2 , $J = 6.4$), 5.33 (s, 2H, $\text{CH}_2\text{-Ph}$), 7.31 (d, 1H, Ar, $J = 7.6$), 7.43-7.48 (m, 2H, Ar), 7.56 (d, 1H, Ar, $J = 7.6$), 7.92 (s, 1H, pyrazole). $^{13}\text{C-NMR}$ (100 MHz, CDCl_3) δ 21.3 (CH_2), 23.2 (CH_2), 37.7 (CH_2), 52.8 (CH_2), 119.9 (C), 122.4 (C), 123.9 (CH), 125.1 (CH), 129.6 (CH), 130.5 (CH), 131.3 (C), 136.6 (C), 137.8 (CH), 149.3 (C), 192.8 (C). ESI-MS calcd. for $\text{C}_{15}\text{H}_{13}\text{F}_3\text{N}_2\text{O}$, 294.28; found: m/z 295.10 $[\text{M}+\text{H}]^+$. Anal. $\text{C}_{15}\text{H}_{13}\text{F}_3\text{N}_2\text{O}$ (C,H,N).

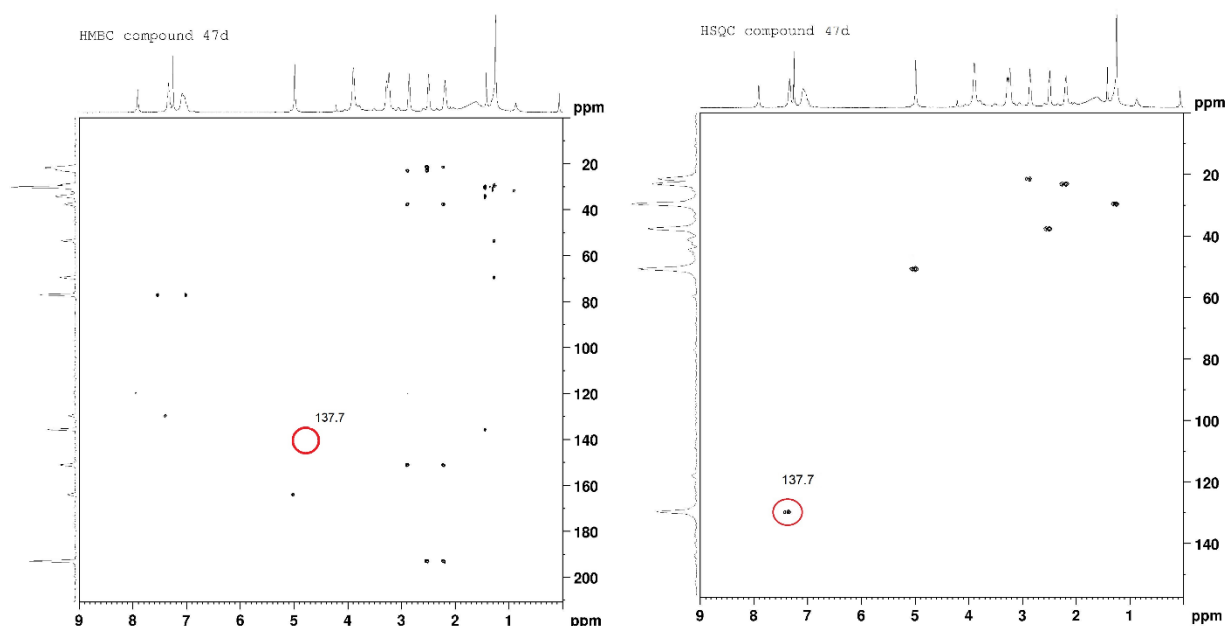


1-[2-Oxo-2-(4-phenylpiperazine-1-yl)ethyl]-1,5,6,7-tetrahydro-4H-indazol-4-one (47d)

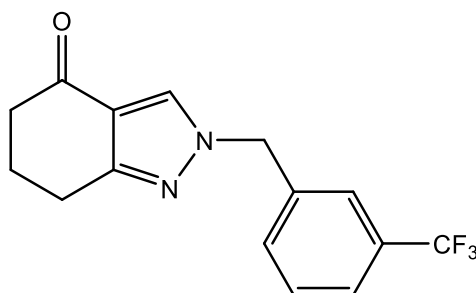


It was synthesized using **43** as reactive and following the general procedure above reported. The final compound **47d** was obtained in mixture with the N-2 isomer **48d** and they were separated by flash chromatography using toluene/ethyl acetate/ethanol 8:2:2 as eluent.

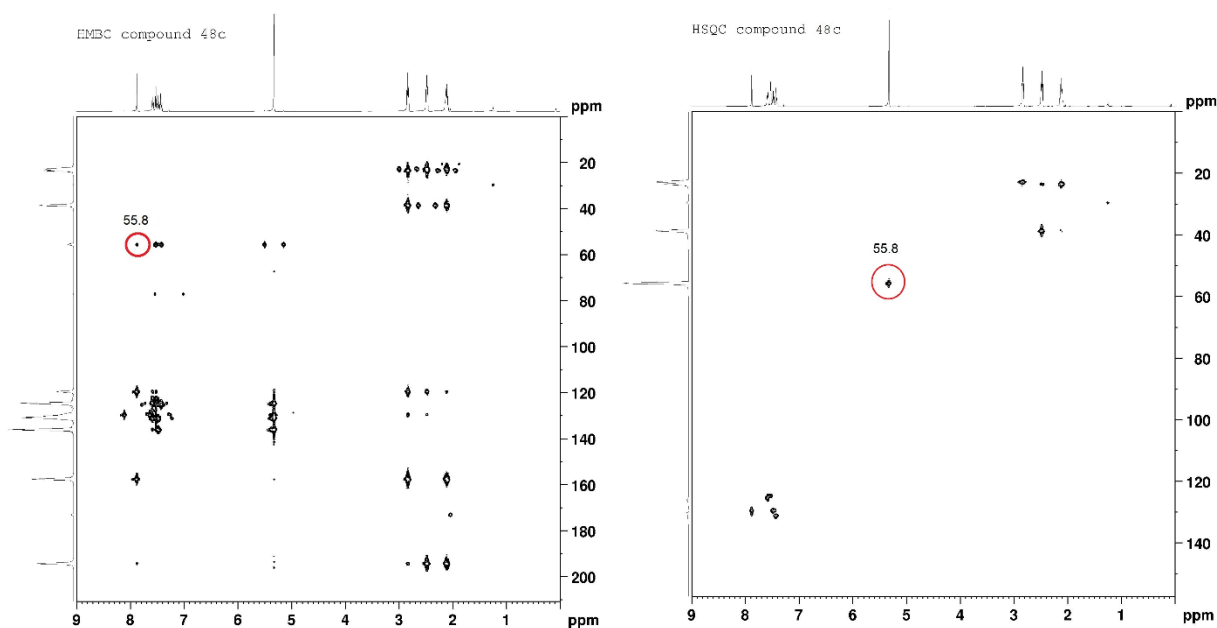
Yield = 3%; oil. $^1\text{H-NMR}$ (400 MHz, CDCl_3) δ 2.13-2.18 (m, 2H, CH_2), 2.44-2.49 (m, 2H, CH_2), 2.81-2.86 (m, 2H, CH_2), 3.22-3.28 (m, 4H, 2 x CH_2 piperazine), 3.84-3.89 (m, 4H, 2 x CH_2 piperazine), 4.98 (s, 2H, N- CH_2 -CO), 6.98-7.08 (m, 3H, Ar), 7.31-7.36 (m, 2H, Ar), 7.91 (s, 1H, pyrazole). $^{13}\text{C-NMR}$ (100 MHz, CDCl_3) δ 21.3 (CH_2), 23.2 (CH_2), 37.8 (CH_2), 45.1 (CH_2), 50.69 (CH_2), 51.1 (CH_2), 114.3 (CH), 118.1 (CH), 119.6 (C), 129.8 (CH), 137.7 (CH), 149.6 (C), 151.4 (C), 164.0 (C), 193.6 (C). ESI-MS calcd. for $\text{C}_{19}\text{H}_{22}\text{N}_4\text{O}_2$, 338.41; found: m/z 339.17 $[\text{M}+\text{H}]^+$. Anal. $\text{C}_{19}\text{H}_{22}\text{N}_4\text{O}_2$ (C,H,N).



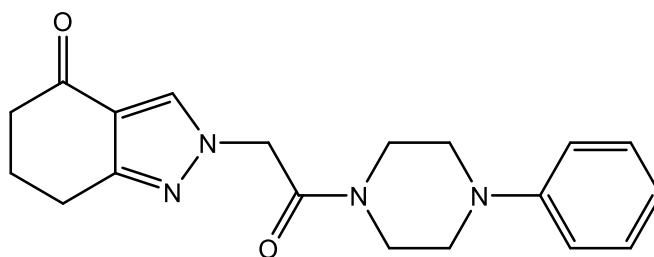
2-(3-(trifluoromethyl)benzyl)-2,5,6,7-tetrahydro-4H-indazol-4-one (48c)



It was synthesized using 3-(trifluoromethyl)benzyl bromide as reactive and following the general procedure above reported. The final compound **48c** was obtained in mixture with the N-1 isomer **47c** and they were separated by flash chromatography using toluene/ethyl acetate/acetic acid Yield = 42%; mp = 100-102°C (EtOH). $^1\text{H-NMR}$ (400 MHz, CDCl_3) δ 2.10 (quin, 2H, CH_2 , $J = 6.4$), 2.47 (t, 2H, CH_2 , $J = 6.4$), 2.82 (t, 2H, CH_2 , $J = 6.4$), 5.30 (s, 2H, $\text{CH}_2\text{-Ph}$), 7.40 (d, 1H, Ar, $J = 7.6$), 7.45-7.50 (m, 2H, Ar), 7.57 (d, 1H, Ar, $J = 7.6$), 7.84 (s, 1H, CH pyrazole). $^{13}\text{C-NMR}$ (100 MHz, CDCl_3) δ 22.9 (CH_2), 23.6 (CH_2), 38.8 (CH_2), 55.8 (CH_2), 119.7 (C), 124.8 (CH), 125.1 (C), 125.4 (CH), 129.6 (CH), 129.7 (CH), 131.3 (CH), 131.6 (C), 136.2 (C), 157.7 (C), 194.5 (C). ESI-MS calcd. for $\text{C}_{15}\text{H}_{13}\text{F}_3\text{N}_2\text{O}$, 294.28; found: m/z 295.10 $[\text{M}+\text{H}]^+$. Anal. $\text{C}_{15}\text{H}_{13}\text{F}_3\text{N}_2\text{O}$ (C,H,N).

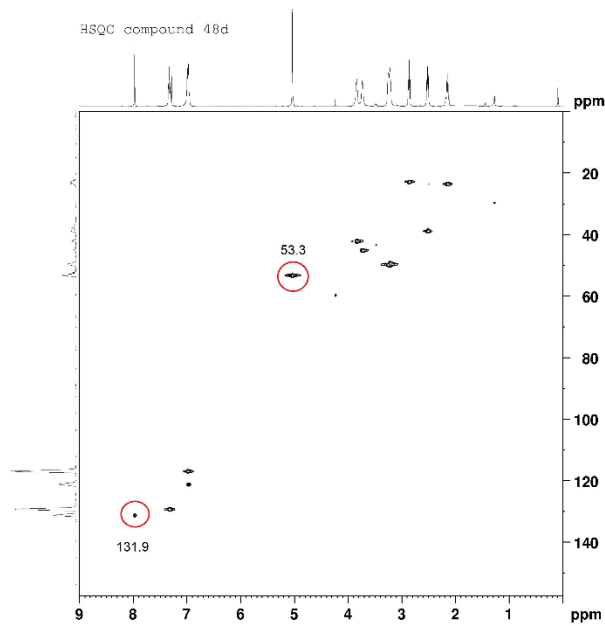
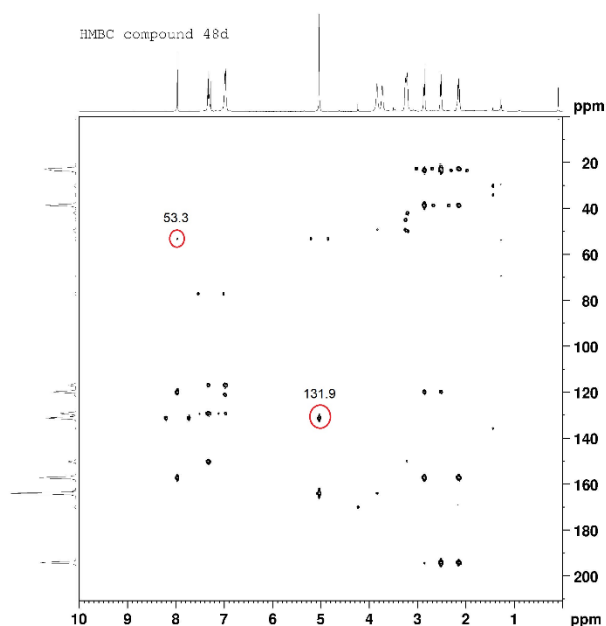


2-(2-oxo-2-(4-phenylpiperazin-1-yl)ethyl)-2,5,6,7-tetrahydro-4H-indazol-4-on (48d)

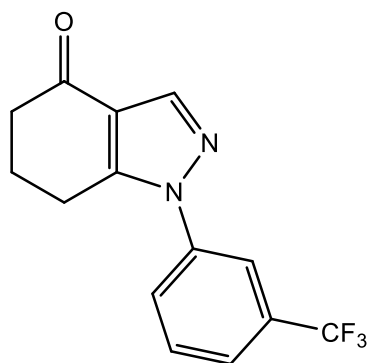


It was synthesized using **43** as reactive and following the general procedure above reported. The final compound **48d** was obtained in mixture with the N-1 isomer **47d** and they were separated by flash chromatography using toluene/ethyl acetate/ethanol 8:2:2 as eluent.

Yield = 5%; oil. ¹H-NMR (400 MHz, CDCl₃) δ 2.10-2.15 (m, 2H, CH₂), 2.45-2.50 (m, 2H, CH₂), 2.83-2.88 (m, 2H, CH₂), 3.19-3.25 (m, 4H, 2 x CH₂ piperazine), 3.69-3.74 (m, 2H, CH₂ piperazine), 3.75-3.80 (m, 2H, CH₂ piperazine), 5.00 (s, 2H, N-CH₂-CO), 6.92-6.98 (m, 3H, Ar), 7.28-7.33 (m, 2H, Ar), 7.94 (s, 1H, pyrazole). ¹³C-NMR (100 MHz, CDCl₃) δ 22.9 (CH₂), 23.5 (CH₂), 38.8 (CH₂), 42.1 (CH₂), 45.1 (CH₂), 49.5 (CH₂), 49.9 (CH₂), 53.3 (CH₂), 117.0 (CH), 120.0 (C), 121.5 (CH), 129.4 (CH), 131.4 (CH), 150.9 (C), 157.3 (C), 164.1 (C), 194.3 (C). ESI-MS calcd. for C₁₉H₂₂N₄O₂, 338.41; found: *m/z* 339.17 [M+H]⁺. Anal. C₁₉H₂₂N₄O₂ (C,H,N).



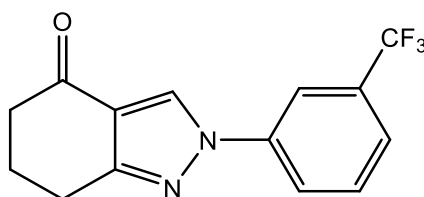
1-(3-(trifluoromethyl)phenyl)-1,5,6,7-tetrahydro-4H-indazol-4-one (47e) [Guo, S. et al., 2010]



A solution of 1,5,6,7-tetrahydro-4H-indazol-4-one (**46**) [Claramunt, R. M. et al., 2011] (0.73 mmol), 1.10 mmol of copper(II) acetate monohydrate, 1.46 mmol of triethylamine and 1.46 mmol of 3-(trifluoromethyl)phenylboronic in 5 mL anhydrous dichloromethane was stirred at room temperature for 12h. The mixture was washed with a saturated solution of ammonium chloride (3 x 15 mL) to remove copper salts and then with cold water (20 mL). The organic solvent was recovered, dried over sodium sulfate and evaporated under vacuum to afford a crude solid which contains **47e** and the N-2 isomer **48e**. The mixture was separated by flash chromatography using petroleum ether/ethyl acetate 5:2 as eluent.

Yield = 2%; oil. ¹H-NMR (400 MHz, CDCl₃) δ 2.20 (quin, 2H, CH₂, *J* = 6.4), 2.57 (t, 2H, CH₂, *J* = 6.4), 3.01 (t, 2H, CH₂, *J* = 6.0), 7.63-7.70 (m, 2H, Ar), 7.73 (d, 1H, Ar, *J* = 7.6), 7.82 (s, 1H, Ar), 8.10 (s, 1H, pyrazole). ¹³C-NMR (100 MHz, CDCl₃) δ 23.3 (CH₂), 23.6 (CH₂), 37.8 (CH₂), 114.6 (C), 120.5 (CH), 124.1 (C), 124.8 (CH), 130.1 (CH), 131.7 (C), 134.9 (C), 139.1 (CH), 140.1 (C), 196.9 (C). ESI-MS calcd. for C₁₄H₁₁F₃N₂O, 280.25; found: *m/z* 281.08 [M+H]⁺. Anal. C₁₄H₁₁F₃N₂O (C,H,N).

2-(3-(trifluoromethyl)phenyl)-2,5,6,7-tetrahydro-4H-indazol-4-one (48e)

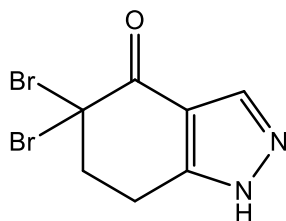


A solution of 1,5,6,7-tetrahydro-4H-indazol-4-one (**46**) [Claramunt, R. M. et al., 2011] (0.73 mmol), 1.10 mmol of copper(II) acetate monohydrate, 1.46 mmol of triethylamine and 1.46 mmol of 3-(trifluoromethyl)phenylboronic in 5 mL anhydrous dichloromethane was stirred at room temperature for 12h. The mixture was washed with a saturated solution of ammonium chloride (3 x 15 mL) to remove copper salts and then with cold water (20 mL). The organic solvent was recovered, dried over sodium sulfate and evaporated under vacuum to afford a crude solid which contains **48e** and the N-1 isomer **47e**. The mixture was separated by flash chromatography using petroleum ether/ethyl acetate 5:2 as eluent.

Yield = 5%; mp = 159-161°C (EtOH). ¹H-NMR (400 MHz, CDCl₃) δ 2.19 (quin, 2H, CH₂, *J* = 6.4), 2.56 (t, 2H, CH₂, *J* = 6.4), 2.95 (t, 2H, CH₂, *J* = 6.4), 7.61 (d, 2H, Ar, *J* = 4.8), 7.85 (s, 1H, Ar), 8.02

(s, 1H, Ar), 8.39 (s, 1H, pyrazole). $^{13}\text{C-NMR}$ (100 MHz, CDCl_3) δ 23.0 (CH_2), 23.4 (CH_2), 38.9 (CH_2), 114.7 (C), 116.9 (CH), 121.3 (C), 122.4 (CH), 124.1 (CH), 124.9 (C), 126.7 (CH), 130.3 (CH), 139.7 (C), 158.5 (C), 194.4 (C). ESI-MS calcd. for $\text{C}_{14}\text{H}_{11}\text{F}_3\text{N}_2\text{O}$, 280.25; found: m/z 281.08 $[\text{M}+\text{H}]^+$. Anal. $\text{C}_{14}\text{H}_{11}\text{F}_3\text{N}_2\text{O}$ (C,H,N).

5,5-dibromo-1,5,6,7-tetrahydro-4H-indazol-4-one (49b)

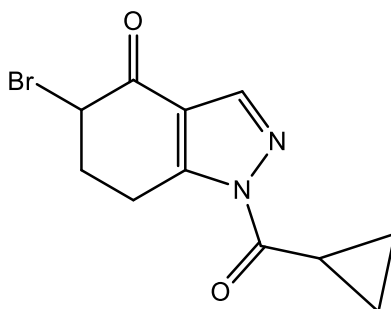


To a solution of 1,5,6,7-tetrahydro-4H-indazol-4-one (**46**) [Claramunt, R. M. et al., 2011] (2.94 mmol) in 5 mL of anhydrous dichloromethane, 4.41 mmol of $[\text{PhNMe}_3][\text{Br}]_3$ were added and the reaction was kept stirring at 100°C for 3h. After evaporation of the solvent, cold water was added (20 mL) and the suspension was extracted with CH_2Cl_2 (3 x 15 mL), dried over sodium sulfate and evaporated under vacuum. Compound **49b** was obtained in mixture with the monobromo derivative **49a** [Bolea, C. et al., 2014] and they were separated by flash chromatography using hexane/ethyl acetate 1:3 as eluent.

Yield = 24%; mp = 170°C (EtOH). $^1\text{H-NMR}$ (400 MHz, CDCl_3) δ 3.03-3.08 (m, 2H, CH_2), 3.10-3.15 (m, 2H, CH_2), 8.17 (s, 1H, pyrazole). ESI-MS calcd. for $\text{C}_7\text{H}_6\text{Br}_2\text{N}_2\text{O}$, 294.95; found: m/z 295.88 $[\text{M}+\text{H}]^+$. Anal. $\text{C}_7\text{H}_6\text{Br}_2\text{N}_2\text{O}$ (C,H,N).

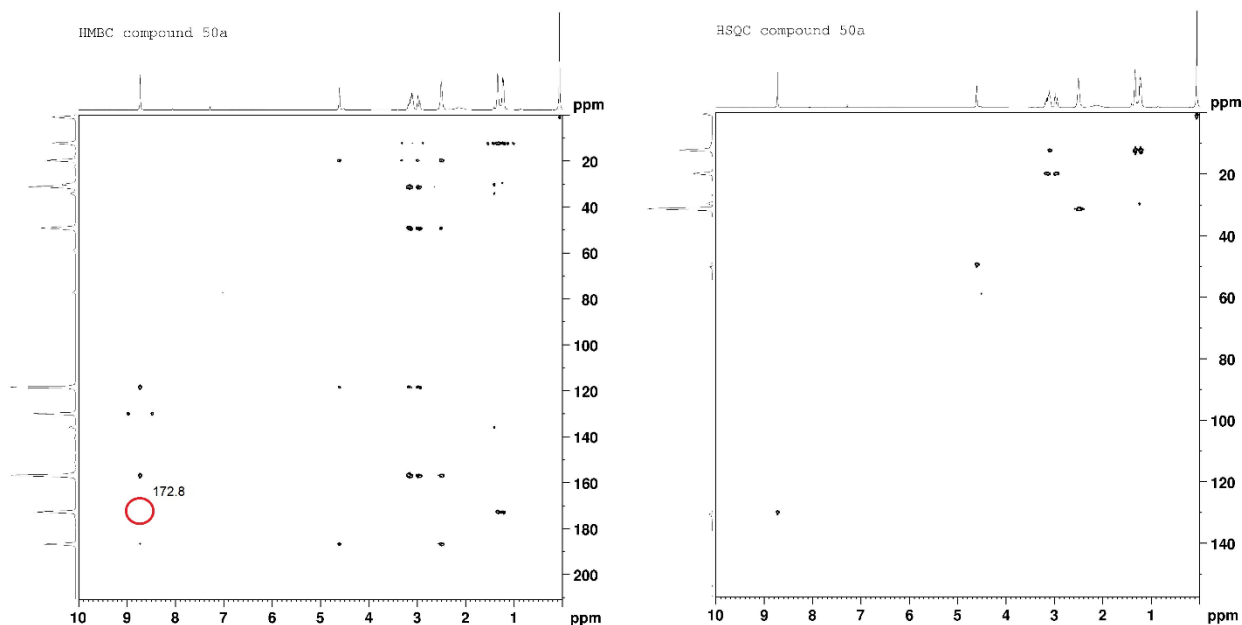
General procedure for compounds (50a,b and 51a-d). Compounds **50a,b** and **51a-d** were obtained using the general procedure followed for compounds of type **5**, starting from the intermediates **49a,b** [**49a**: Bolea, C. et al., 2014].

5-bromo-1-(cyclopropanecarbonyl)-1,5,6,7-tetrahydro-4H-indazol-4-one (50a)

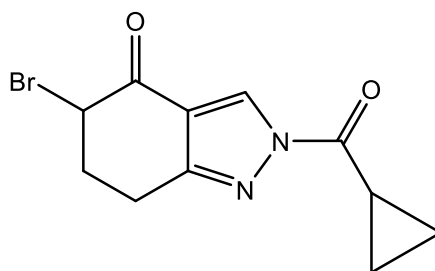


It was obtained from 5-bromo-1,5,6,7-tetrahydro-4H-indazol-4-one (**49a**) [Bolea, C. et al., 2014] using cyclopropanecarbonyl chloride as reactive, and following the general procedure for compounds of type **5**. The final compound **50a** was obtained in mixture with the N-2 isomer **51a** and they were separated by flash chromatography using cyclohexane/ethyl acetate 4:1 as eluent.

Yield = 13%; oil. $^1\text{H-NMR}$ (400 MHz, CDCl_3) δ 1.20-1.25 (m, 2H, CH_2 cC_3H_5), 1.28-1.33 (m, 2H, CH_2 cC_3H_5), 2.49-2.54 (m, 2H, CH_2), 2.93-2.98 (m, 1H, CH cC_3H_5), 3.09-3.17 (m, 2H, CH_2), 4.59-4.65 (m, 1H, CH-Br), 8.72 (s, 1H, pyrazole). $^{13}\text{C-NMR}$ (100 MHz, CDCl_3) δ 9.5 (CH), 12.3 (CH_2), 12.4 (CH_2), 19.9 (CH_2), 31.3 (CH_2), 49.5 (CH), 118.5 (C), 130.1 (CH), 157.0 (C), 172.8 (C), 186.8 (C). ESI-MS calcd. for $\text{C}_{11}\text{H}_{11}\text{BrN}_2\text{O}_2$, 283.13; found: m/z 283.00 $[\text{M}+\text{H}]^+$. Anal. $\text{C}_{11}\text{H}_{11}\text{BrN}_2\text{O}_2$ (C,H,N).

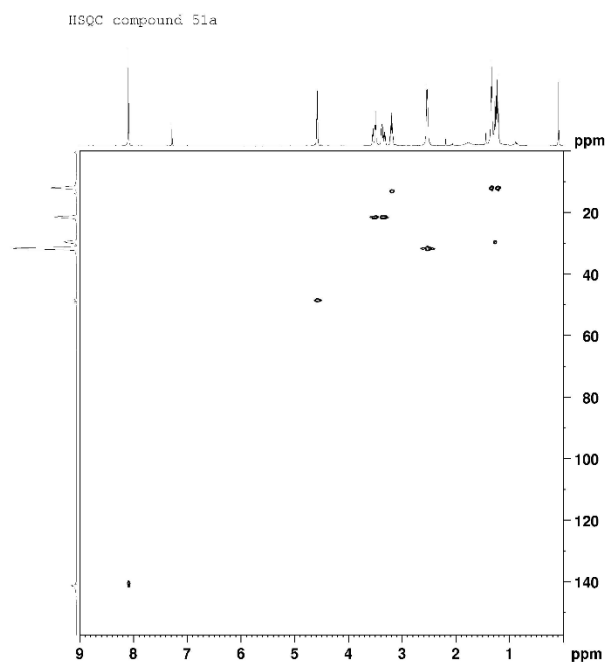
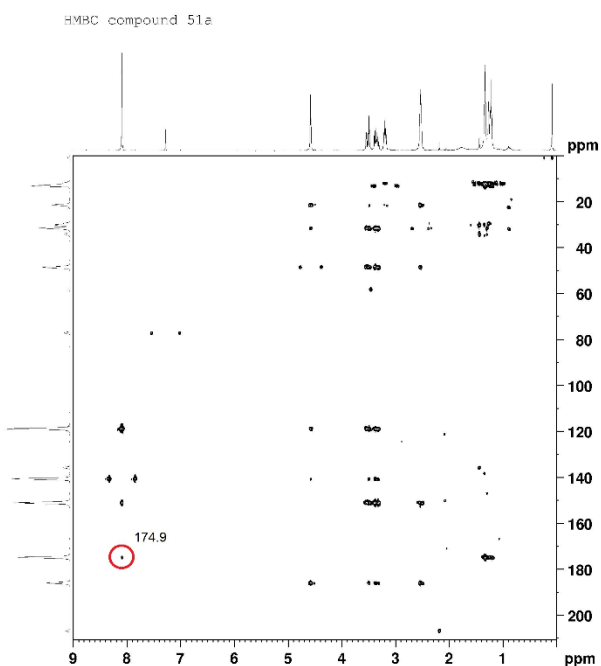


5-bromo-2-(cyclopropanecarbonyl)-2,5,6,7-tetrahydro-4H-indazol-4-one (51a)

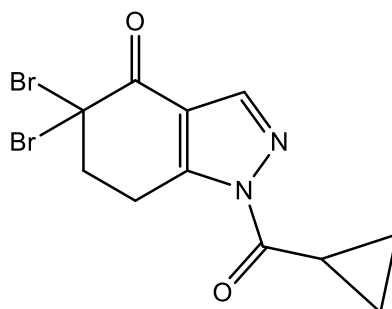


It was obtained from 5-bromo-1,5,6,7-tetrahydro-4H-indazol-4-one (**49a**) [Bolea, C. et al., 2014] using cyclopropanecarbonyl chloride as reactive, and following the general procedure for compounds of type **5**. The final compound **51a** was obtained in mixture with the N-1 isomer **50a** and they were separated by flash chromatography using cyclohexane/ethyl acetate 4:1 as eluent.

Yield = 15%; mp = 103-106°C (EtOH). $^1\text{H-NMR}$ (400 MHz, CDCl_3) δ 1.18-1.24 (m, 2H, CH_2 cC_3H_5), 1.31-1.36 (m, 2H, CH_2 cC_3H_5), 2.50-2.55 (m, 2H, CH_2), 3.15-3.20 (m, 1H, CH cC_3H_5), 3.29-3.36 (m, 1H, CH-H), 3.46-3.51 (m, 1H, CH-H), 4.55-4.60 (m, 1H, CH-Br), 8.07 (s, 1H, pyrazole). $^{13}\text{C-NMR}$ (100 MHz, CDCl_3) δ 12.0 (CH_2), 12.1 (CH_2), 13.2 (CH), 21.6 (CH_2), 31.7 (CH_2), 48.6 (CH), 119.0 (C), 140.8 (CH), 151.2 (C), 174.9 (C), 186.6 (C). ESI-MS calcd. for $\text{C}_{11}\text{H}_{11}\text{BrN}_2\text{O}_2$, 283.13; found: m/z 283.00 $[\text{M}+\text{H}]^+$. Anal. $\text{C}_{11}\text{H}_{11}\text{BrN}_2\text{O}_2$ (C,H,N).

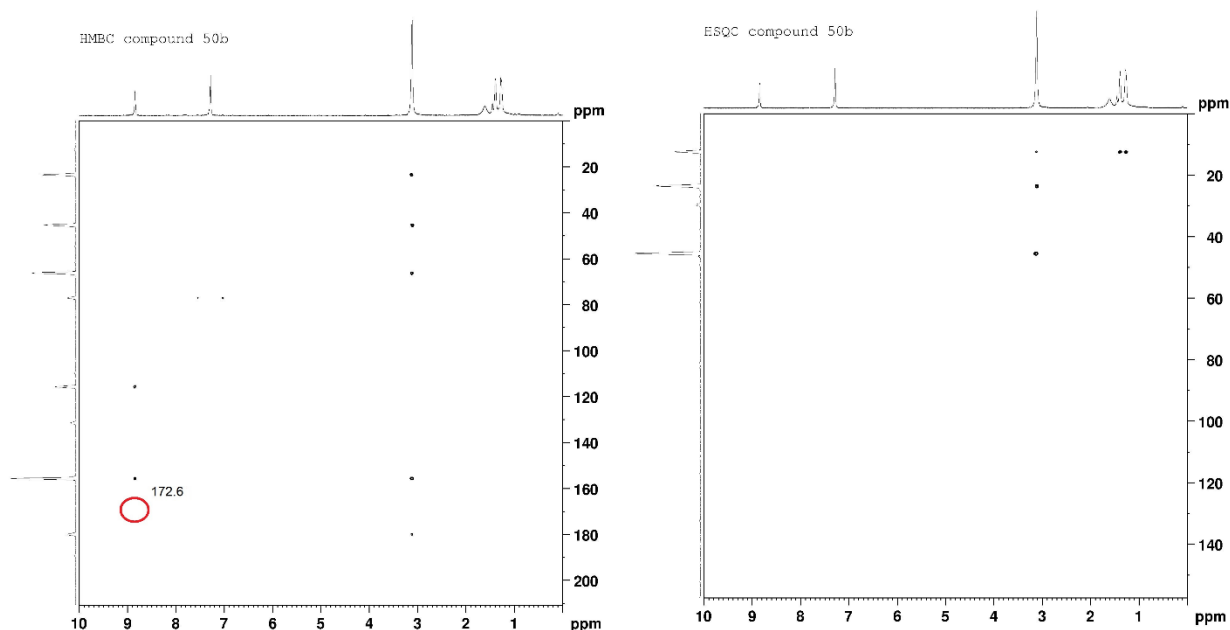


5,5-dibromo-1-(cyclopropanecarbonyl)-1,5,6,7-tetrahydro-4H-indazol-4-one (50b)

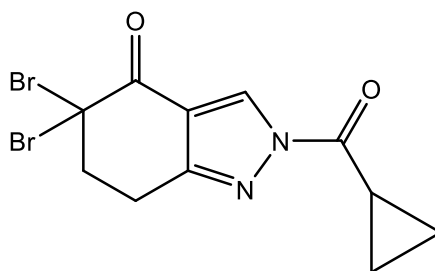


It was obtained from 5,5-dibromo-1,5,6,7-tetrahydro-4H-indazol-4-one (**49b**) using cyclopropanecarbonyl chloride as reactive, and following the general procedure for compounds of type **5**. The final compound **50b** was obtained in mixture with the N-2 isomer **51b** and they were separated by flash chromatography using cyclohexane/ethyl acetate 6:1 as eluent.

Yield = 37%; mp = 163-166°C (EtOH). $^1\text{H-NMR}$ (400 MHz, CDCl_3) δ 1.24-1.35 (m, 4H, 2 x CH_2 cC_3H_5), 3.05-3.15 (m, 5H, 2 x CH_2 + CH cC_3H_5), 8.81 (s, 1H, pyrazole). $^{13}\text{C-NMR}$ (100 MHz, CDCl_3) δ 12.4 (CH), 12.5 (CH_2), 23.6 (CH_2), 45.5 (CH_2), 66.4 (C), 115.9 (C), 131.6 (CH), 155.7 (C), 172.6 (C), 180.1 (C). ESI-MS calcd. for $\text{C}_{11}\text{H}_{10}\text{Br}_2\text{N}_2\text{O}_2$, 362.02; found: m/z 360.91 $[\text{M}+\text{H}]^+$. Anal. $\text{C}_{11}\text{H}_{10}\text{Br}_2\text{N}_2\text{O}_2$ (C,H,N).

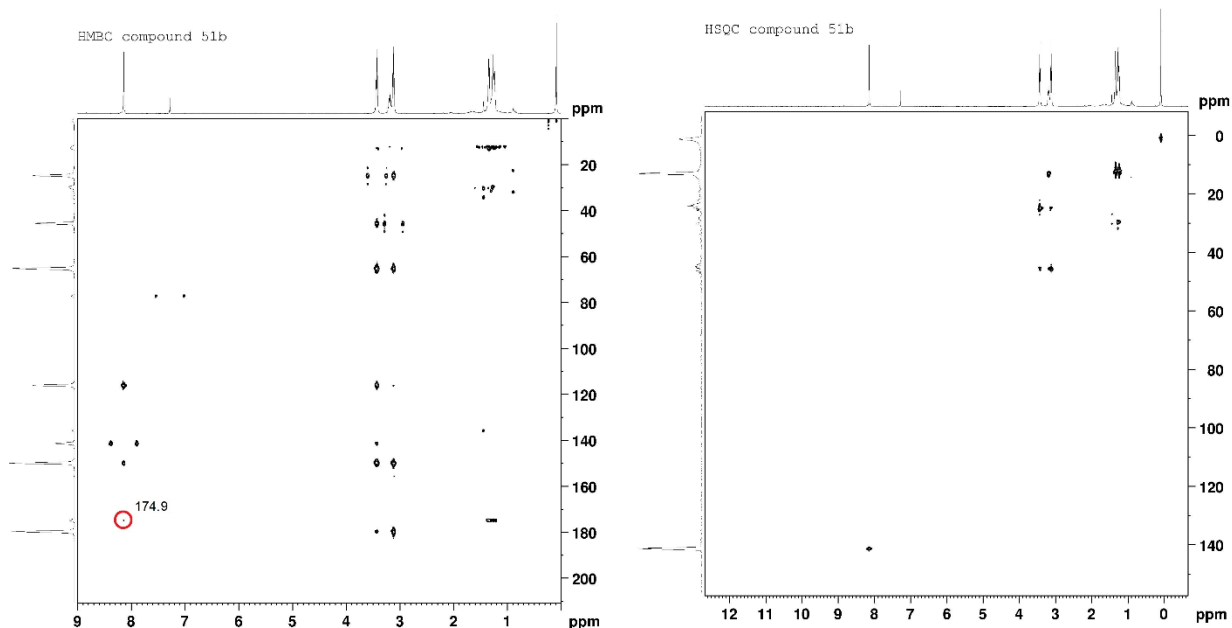


5,5-dibromo-2-(cyclopropanecarbonyl)-2,5,6,7-tetrahydro-4H-indazol-4-one (51b)

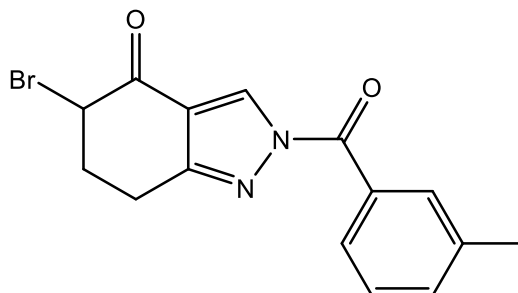


It was obtained from 5,5-dibromo-1,5,6,7-tetrahydro-4H-indazol-4-one (**49b**) using cyclopropanecarbonyl chloride as reactive, and following the general procedure for compounds of type **5**. The final compound **51b** was obtained in mixture with the N-1 isomer **50b** and they were separated by flash chromatography using cyclohexane/ethyl acetate 6:1 as eluent.

Yield = 8%; mp = 133-136°C (EtOH). ¹H-NMR (400 MHz, CDCl₃) δ 1.20-1.31 (m, 4H, 2 x CH₂ cC₃H₅), 3.07-3.12 (m, 3H, CH₂ + CH cC₃H₅), 3.34-3.39 (m, 2H, CH₂), 8.11 (s, 1H, pyrazole). ¹³C-NMR (100 MHz, CDCl₃) δ 12.3 (CH₂), 13.2 (CH), 25.0 (CH₂), 45.7 (CH₂), 65.3 (C), 116.3 (C), 141.5 (CH), 150.0 (C), 174.9 (C), 179.7 (C). ESI-MS calcd. for C₁₁H₁₀Br₂N₂O₂, 362.02; found: *m/z* 360.91 [M+H]⁺. Anal. C₁₁H₁₀Br₂N₂O₂ (C,H,N).



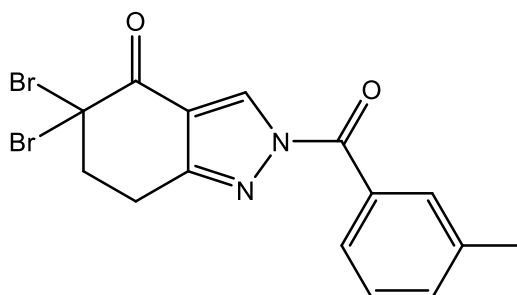
5-bromo-2-(3-methylbenzoyl)-2,5,6,7-tetrahydro-4H-indazol-4-one (51c)



It was obtained from 5-bromo-1,5,6,7-tetrahydro-4H-indazol-4-one (**49a**) [Bolea, C. et al., 2014] using *m*-toluoyl chloride as reactive, and following the general procedure for compounds of type **5**. The final compound was purified by flash chromatography using cyclohexane/ethyl acetate 4:1 as eluent.

Yield = 10%; oil. ¹H-NMR (400 MHz, CDCl₃) δ 2.43 (s, 3H, CH₃), 2.55-2.60 (m, 2H, CH₂), 3.48-3.54 (m, 2H, CH₂), 4.61 (t, 1H, CH, *J* = 3.6), 7.40-7.45 (m, 2H, Ar), 7.76-7.83 (m, 2H, Ar), 8.09 (s, 1H, pyrazole). ¹³C-NMR (100 MHz, CDCl₃) δ 20.0 (CH₃), 21.6 (CH₂), 31.9 (CH₂), 48.6 (CH), 119.0 (C), 128.1 (CH), 128.7 (CH), 131.3 (C), 131.9 (CH), 134.5 (CH), 138.2 (C), 140.9 (CH), 153.1 (C), 168.3 (C), 186.2 (C). ESI-MS calcd. for C₁₅H₁₃BrN₂O₂, 333.19; found: *m/z* 333.02 [M+H]⁺. Anal. C₁₅H₁₃BrN₂O₂ (C,H,N).

5,5-dibromo-2-(3-methylbenzoyl)-2,5,6,7-tetrahydro-4H-indazol-4-one (51d)

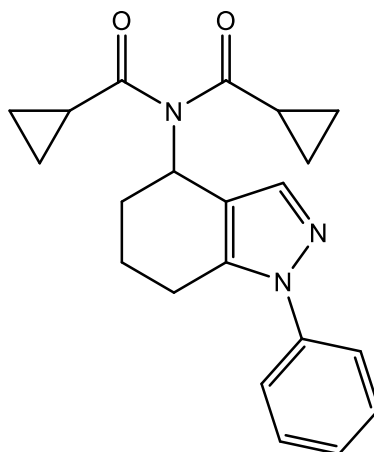


It was obtained from 5,5-dibromo-1,5,6,7-tetrahydro-4H-indazol-4-one (**49b**) using m-toluoyl chloride as reactive, and following the general procedure for compounds of type **5**. The final compound was purified by flash chromatography using cyclohexane/ethyl acetate 4:1 as eluent.

Yield = 10%; oil. $^1\text{H-NMR}$ (400 MHz, CDCl_3) δ 2.43 (s, 3H, CH_3), 3.16 (t, 2H, CH_2 , $J = 6.2$), 3.51 (t, 2H, CH_2 , $J = 6.2$), 7.38-7.47 (m, 2H, Ar), 7.80-7.85 (m, 2H, Ar), 8.14 (s, 1H, pyrazole). $^{13}\text{C-NMR}$ (100 MHz, CDCl_3) δ 21.4 (CH_3), 25.0 (CH_2), 45.8 (CH_2), 65.2 (C), 116.1 (C), 128.2 (CH), 128.8 (CH), 131.0 (C), 131.9 (CH), 134.7 (CH), 138.3 (C), 141.5 (CH), 152.0 (C), 168.1 (C), 179.7 (C). ESI-MS calcd. for $\text{C}_{15}\text{H}_{12}\text{Br}_2\text{N}_2\text{O}_2$, 412.08; found: m/z 410.93 $[\text{M}+\text{H}]^+$. Anal. $\text{C}_{15}\text{H}_{12}\text{Br}_2\text{N}_2\text{O}_2$ (C,H,N).

Synthesis of compounds (55a,b). Compounds **55a** and **55b** were obtained using the general procedure followed for compounds of type **5**, starting from intermediate **54** [Lain, S. et al., 2017] and using cyclopropanecarbonyl chloride as reactive. They were obtained in mixture and separated by flash chromatography using cyclohexane/ethyl acetate 2:1 as eluent.

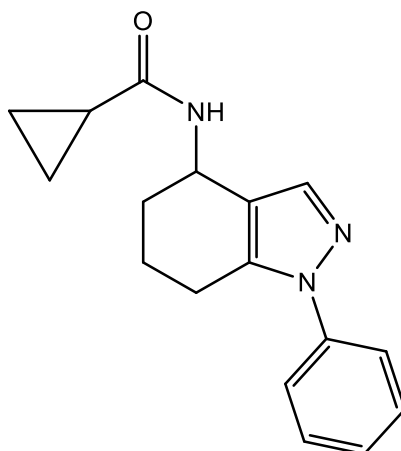
N-(cyclopropanecarbonyl)-N-(1-phenyl-4,5,6,7-tetrahydro-1H-indazol-4-yl)cyclopropanecarboxamide (55a)



Yield = 19%; mp = 94-95°C (EtOH). $^1\text{H-NMR}$ (400 MHz, CDCl_3) δ 0.89-0.98 (m, 4H, 2 x CH_2 cC_3H_5), 1.13-1.24 (m, 4H, 2 x CH_2 cC_3H_5), 1.69-1.76 (m, 1H, CH cC_3H_5), 2.09-2.24 (m, 5H, 2 x CH_2 + CH cC_3H_5), 2.67-2.84 (m, 2H, CH_2), 5.76-5.80 (m, 1H, N-CH), 7.30 (t, 1H, Ar, $J = 7.2$), 7.40-7.49 (m, 5H, Ar + pyrazole). $^{13}\text{C-NMR}$ (100 MHz, CDCl_3) δ 11.1 (CH_2), 11.6 (CH_2), 18.2 (CH), 23.0 (CH_2), 23.2 (CH_2), 28.5 (CH_2), 50.2 (CH), 118.5 (C), 123.1 (CH), 126.9 (CH), 129.1 (CH), 136.9 (CH), 139.2 (C),

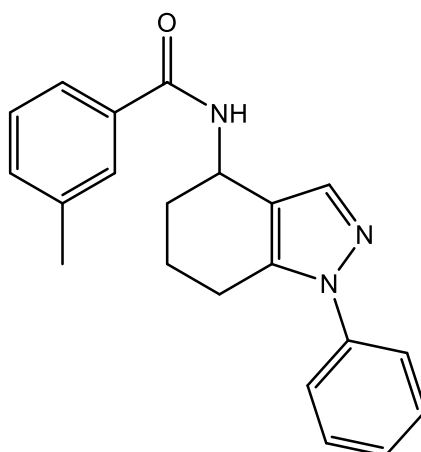
139.8 (C), 178.2 (C). ESI-MS calcd. for $C_{21}H_{23}N_3O_2$, 349.43; found: m/z 350.18 $[M+H]^+$. Anal. $C_{21}H_{23}N_3O_2$ (C,H,N).

N-(1-phenyl-4,5,6,7-tetrahydro-1H-indazol-4-yl)cyclopropanecarboxamide (55b)



Yield = 36%; mp = 148-151°C (EtOH). 1H -NMR (400 MHz, DMSO- d_6) δ 0.60-0.70 (m, 4H, 2 x CH_2 cC_3H_5), 1.53-1.58 (m, 2H, CH_2), 1.68-1.73 (m, 1H, CH cC_3H_5), 1.79-1.84 (m, 2H, CH_2), 2.71-2.76 (m, 2H, CH_2), 4.88-4.93 (m, 1H, N-CH), 7.33-7.38 (m, 1H, Ar), 7.46-7.52 (m, 5H, Ar + pyrazole), 8.30 (exch br d, 1H, NH, $J = 8.0$). ^{13}C -NMR (100 MHz, DMSO- d_6) δ 6.7 (CH_2), 14.0 (CH), 20.3 (CH_2), 23.2 (CH_2), 30.0 (CH_2), 41.9 (CH), 119.8 (C), 123.2 (CH), 127.3 (CH), 129.7 (CH), 139.0 (CH), 139.5 (C), 140.0 (C), 172.4 (C). ESI-MS calcd. for $C_{17}H_{19}N_3O$, 281.36; found: m/z 282.15 $[M+H]^+$. Anal. $C_{17}H_{19}N_3O$ (C,H,N).

3-methyl-N-(1-phenyl-4,5,6,7-tetrahydro-1H-indazol-4-yl)benzamide (55c)



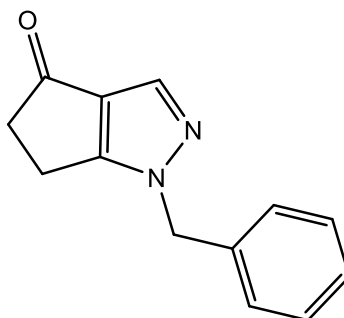
Compound **55c** was obtained using the general procedure followed for compounds of type **40**, and by treatment of 1-phenyl-4,5,6,7-tetrahydro-1H-indazol-4-amine (**54**) [Lain, S. et al., 2017] with toluylic acid. The compound was purified by flash chromatography using cyclohexane/ethyl acetate 2:1.

Yield = 15%; mp = 151-153°C (EtOH). 1H -NMR (400 MHz, DMSO- d_6) δ 1.73-1.78 (m, 2H, CH_2), 1.92-1.97 (m, 2H, CH_2), 2.29 (s, 3H, CH_3), 2.69-2.74 (m, 2H, CH_2), 5.09-5.14 (m, 1H, N-CH), 7.30-

7.35 (m, 3H, Ar), 7.48-7.53 (m, 5H, Ar + pyrazole), 7.60-7.65 (m, 2H, Ar), 8.55 (exch br s, 1H, NH). ¹³C-NMR (100 MHz, DMSO-d₆) δ 20.7 (CH₂), 21.3 (CH₃), 23.1 (CH₂), 29.6 (CH₂), 42.8 (CH), 119.7 (C), 123.2 (CH), 125.0 (CH), 127.6 (CH), 128.3 (CH), 128.7 (CH), 129.8 (CH), 132.4 (CH), 134.6 (C), 138.2 (C), 138.8 (CH), 139.7 (C), 140.0 (C), 167.2 (C). ESI-MS calcd. for C₂₁H₂₁N₃O, 331.42; found: *m/z* 332.17 [M+H]⁺. Anal. C₂₁H₂₁N₃O (C,H,N).

General procedure for compounds (60a,b, 61a,b, 65a and 66a). To a suspension of the intermediate **59** [Liverton, N. J. et al., 2012] or **64** [Maynard, G. et al., 2003] (0.42 mmol) and 0.50 mmol of potassium carbonate in anhydrous acetonitrile (2 mL), 0.84 mmol of benzyl bromide or alternatively **43** were added. The mixture was stirred at reflux for 4h. After evaporation of the solvent, cold water was added (20 mL), and the pH was neutralized with 1N HCl. The suspension was extracted with CH₂Cl₂ (3 x 15 mL), dried over sodium sulfate and evaporated under vacuum.

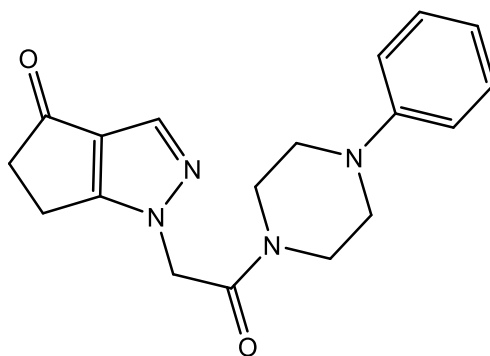
1-benzyl-5,6-dihydrocyclopenta[c]pyrazol-4(1H)-one (60a)



It was synthesized starting from 5,6-dihydrocyclopenta[c]pyrazol-4(1H)-one (**59**) [[Liverton, N. J. et al., 2012]] and using benzyl bromide as reactive, following the general procedure above reported. Compound **60a** was obtained in mixture with the N-2 isomer **61a** and they were separated by flash chromatography using dichloromethane/methanol 99:1 as eluent.

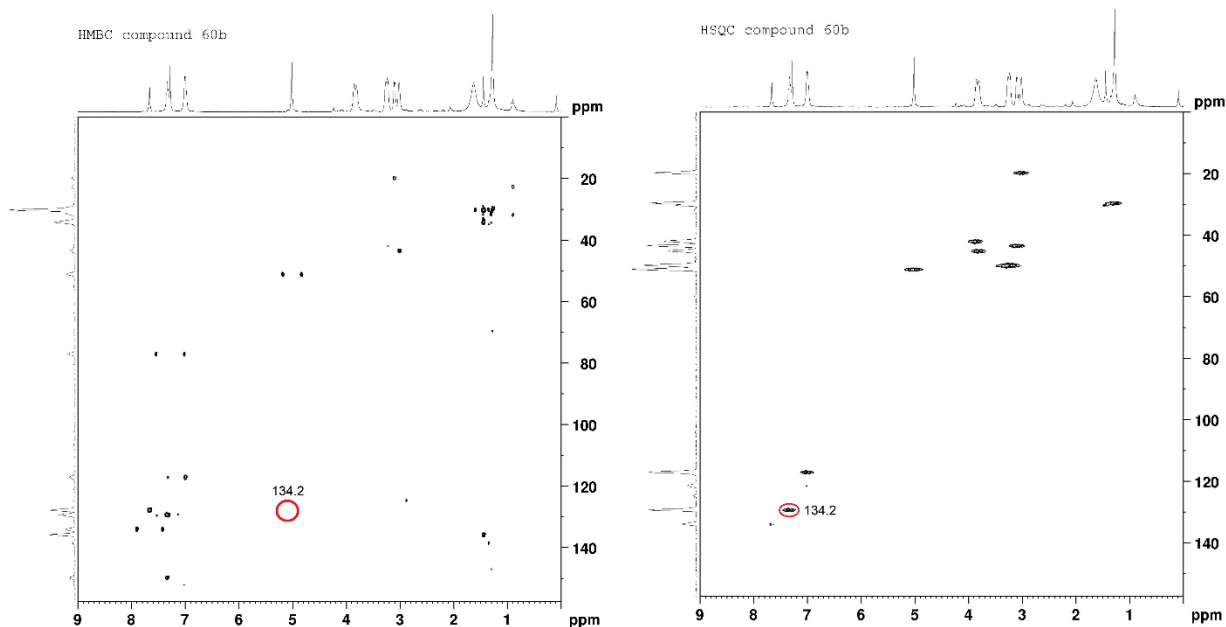
Yield = 8%; mp = 92-94°C (EtOH). ¹H-NMR (400 MHz, CDCl₃) δ 2.68-2.73 (m, 2H, CH₂), 2.95-3.00 (m, 2H, CH₂), 5.28 (s, 2H, CH₂-Ph), 7.25-7.30 (m, 2H, Ar), 7.33-7.40 (m, 3H, Ar), 7.64 (s, 1H, pyrazole). ¹³C-NMR (100 MHz, CDCl₃) δ 18.7 (CH₂), 42.9 (CH₂), 54.3 (CH₂), 125.1 (C), 128.1 (CH), 128.6 (CH), 129.1 (CH), 133.3 (CH), 135.0 (C), 159.3 (C), 197.5 (C). ESI-MS calcd. for C₁₃H₁₂N₂O, 212.25; found: *m/z* 213.09 [M+H]⁺. Anal. C₁₃H₁₂N₂O (C,H,N).

1-(2-oxo-2-(4-phenylpiperazin-1-yl)ethyl)-5,6-dihydrocyclopenta[c]pyrazol-4(1H)-one (60b)

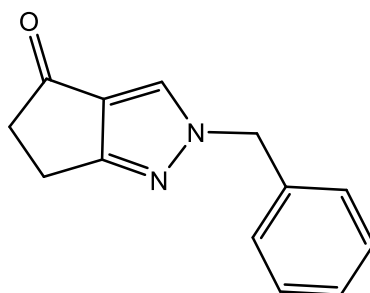


It was synthesized starting from 5,6-dihydrocyclopenta[c]pyrazol-4(1H)-one (**59**) [Liverton, N. J. et al., 2012] and using the iododerivative **43** as reactive, following the general procedure above reported. Compound **60b** was obtained in mixture with the N-2 isomer **61b** and they were separated by flash chromatography using toluene/ethyl acetate/methanol/NH₃ 8:2:2:0.1 as eluent.

Yield = 13%; oil. ¹H-NMR (400 MHz, CDCl₃) δ 2.95-3.00 (m, 2H, CH₂), 3.05-3.10 (m, 2H, CH₂), 3.15-3.25 (m, 4H, 2 x CH₂ piperazine), 3.70-3.85 (m, 4H, 2 x CH₂ piperazine), 4.98 (s, 2H, N-CH₂-CO), 6.90-7.00 (m, 3H, Ar), 7.23-7.30 (m, 2H, Ar), 7.63 (s, 1H, pyrazole). ¹³C-NMR (100 MHz, CDCl₃) δ 19.8 (CH₂), 41.9 (CH₂), 43.5 (CH₂), 45.1 (CH₂), 50.0 (CH₂), 50.4 (CH₂), 51.2 (CH₂), 117.4 (CH), 118.0 (C), 124.7 (CH), 129.5 (CH), 134.2 (CH), 150.1 (C), 164.0 (C), 166.7 (C), 194.1 (C). ESI-MS calcd. for C₁₈H₂₀N₄O₂, 324.38; found: *m/z* 325.16 [M+H]⁺. Anal. C₁₈H₂₀N₄O₂ (C,H,N).

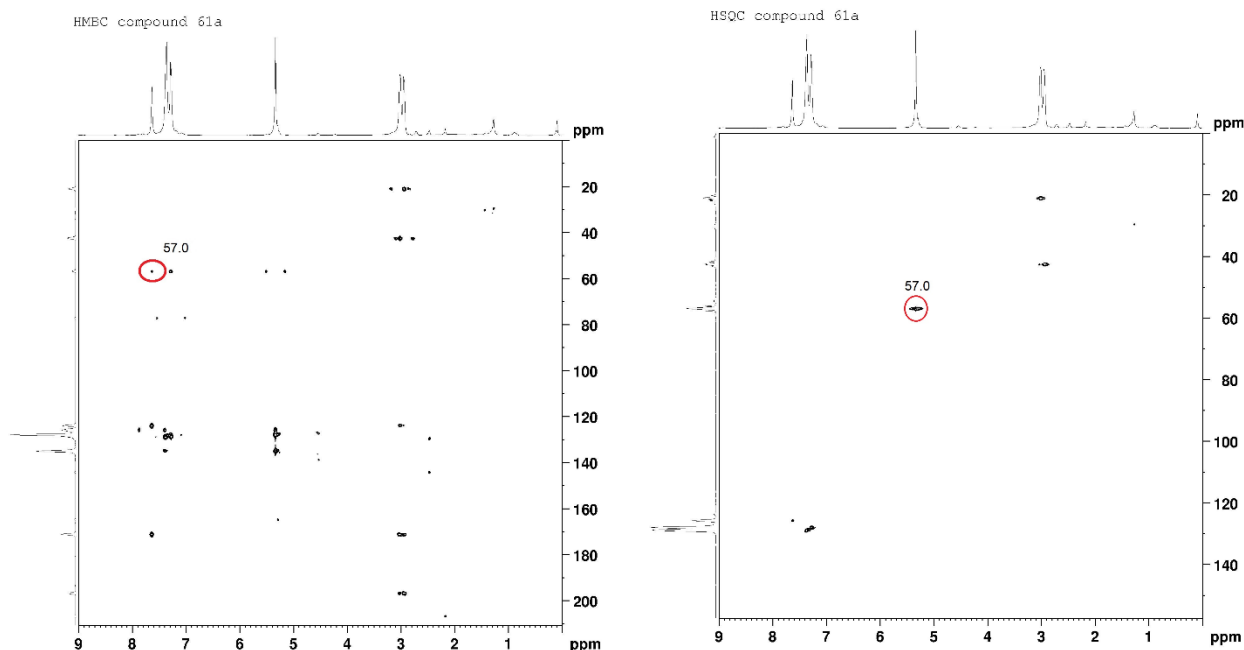


2-benzyl-5,6-dihydrocyclopenta[c]pyrazol-4(2H)-one (61a)

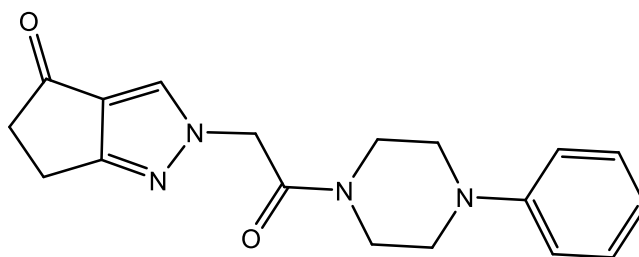


It was synthesized starting from 5,6-dihydrocyclopenta[c]pyrazol-4(1H)-one (**59**) [Liverton, N. J. et al., 2012] and using benzyl bromide as reactive, following the general procedure above reported. Compound **61a** was obtained in mixture with the N-1 isomer **60a** and they were separated by flash chromatography using dichloromethane/methanol 99:1 as eluent.

Yield = 16%; mp = 135-137°C (EtOH). $^1\text{H-NMR}$ (400 MHz, CDCl_3) δ 2.89-2.94 (m, 2H, CH_2), 2.95-3.00 (m, 2H, CH_2), 5.30 (s, 2H, $\text{CH}_2\text{-Ph}$), 7.24 (d, 2H, Ar, $J = 6.4$), 7.30-7.35 (m, 3H, Ar), 7.61 (s, 1H, pyrazole). $^{13}\text{C-NMR}$ (100 MHz, CDCl_3) δ 21.1 (CH_2), 42.6 (CH_2), 57.0 (CH_2), 125.1 (C), 125.9 (CH), 128.1 (CH), 128.6 (CH), 129.1 (CH), 135.0 (C), 171.3 (C), 197.4 (C). ESI-MS calcd. for $\text{C}_{13}\text{H}_{12}\text{N}_2\text{O}$, 212.25; found: m/z 213.09 $[\text{M}+\text{H}]^+$. Anal. $\text{C}_{13}\text{H}_{12}\text{N}_2\text{O}$ (C,H,N).

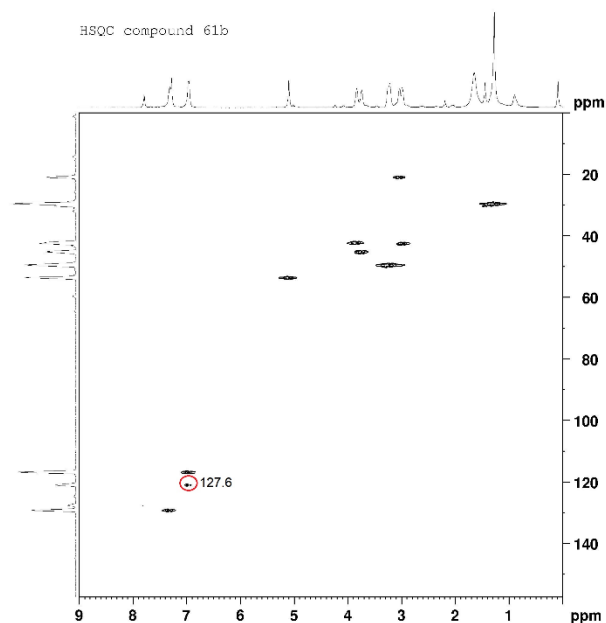
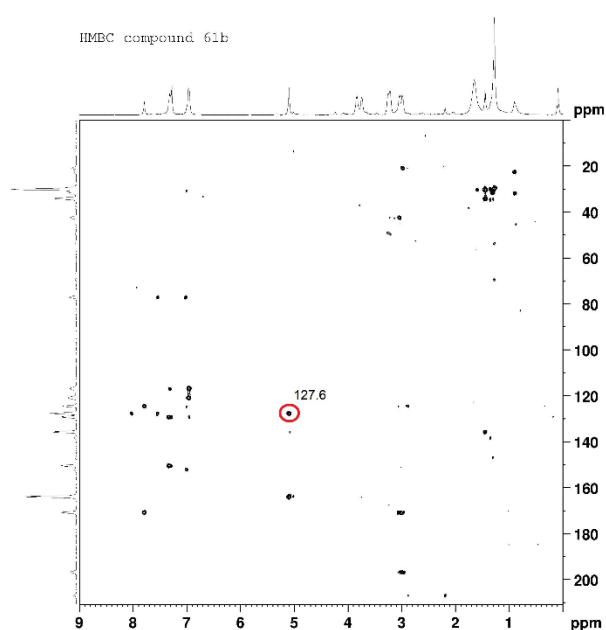


2-(2-oxo-2-(4-phenylpiperazin-1-yl)ethyl)-5,6-dihydrocyclopenta[c]pyrazol-4(2H)-one (61b)

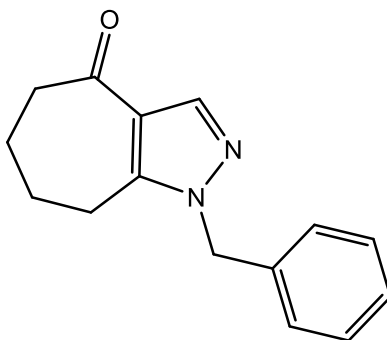


It was synthesized starting from 5,6-dihydrocyclopenta[c]pyrazol-4(1H)-one (**59**) [Liverton, N. J. et al., 2012] and using the iododerivative **43** as reactive, following the general procedure above reported. Compound **61b** was obtained in mixture with the N-1 isomer **60b** and they were separated by flash chromatography using toluene/ethyl acetate/methanol/NH₃ 8:2:2:0.1 as eluent.

Yield = 13%; oil. ¹H-NMR (400 MHz, CDCl₃) δ 2.92-2.98 (m, 2H, CH₂), 3.00-3.05 (m, 2H, CH₂), 3.10-3.20 (m, 4H, 2 x CH₂ piperazine), 3.70-3.80 (m, 4H, 2 x CH₂ piperazine), 5.07 (s, 2H, N-CH₂-CO), 6.90-6.95 (m, 3H, Ar), 7.25-7.35 (m, 2H, Ar), 7.76 (s, 1H, pyrazole). ¹³C-NMR (100 MHz, CDCl₃) δ 21.0 (CH₂), 42.3 (CH₂), 42.6 (CH₂), 45.4 (CH₂), 49.3 (CH₂), 49.8 (CH₂), 53.7 (CH₂), 116.9 (CH), 121.0 (CH), 127.6 (CH), 129.3 (CH), 150.0 (C), 164.6 (C), 171.3 (C), 196.05 (C). ESI-MS calcd. for C₁₈H₂₀N₄O₂, 324.38; found: *m/z* 325.16 [M+H]⁺. Anal. C₁₈H₂₀N₄O₂ (C,H,N).



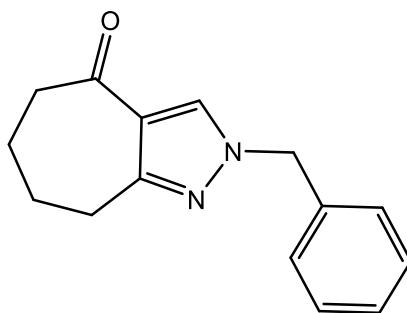
1-benzyl-5,6,7,8-tetrahydrocyclohepta[c]pyrazol-4(1H)-one (65a)



It was synthesized starting from 5,6,7,8-tetrahydrocyclohepta[c]pyrazol-4(1H)-one (**64**) [Maynard, G. et al., 2003] and using benzyl bromide as reactive, following the general procedure above reported. Compound **65a** was obtained in mixture with the N-2 isomer **66a** and they were separated by flash chromatography using toluene/ethyl acetate/methanol 9:1:0.5 as eluent.

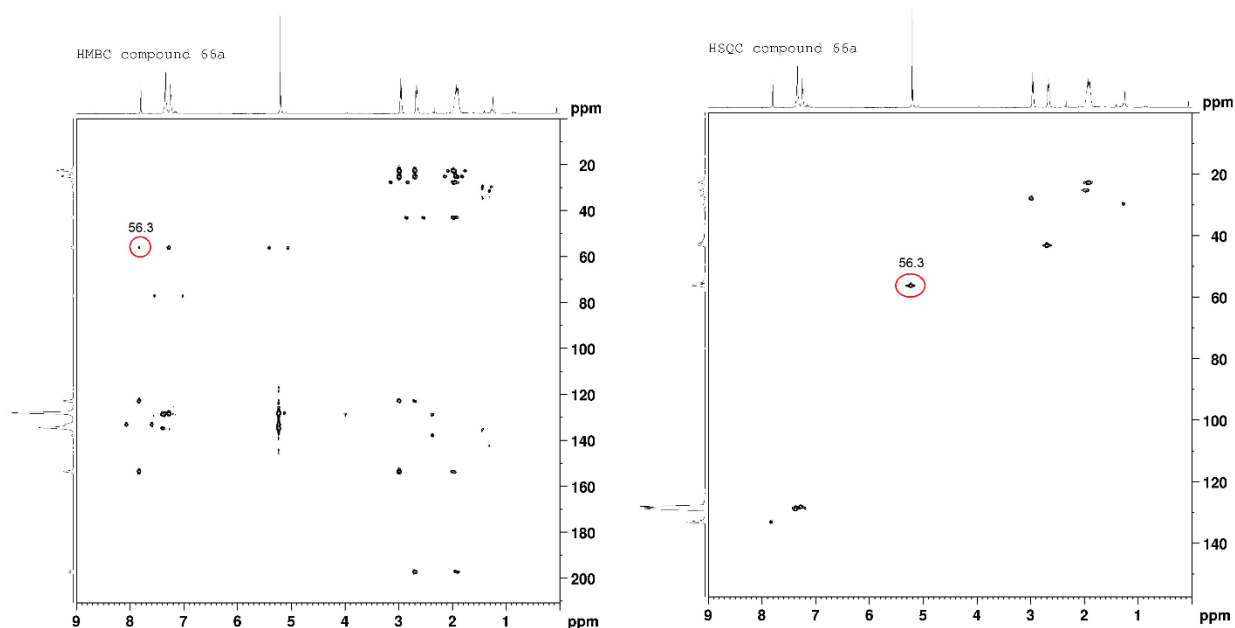
Yield = 2%; oil. $^1\text{H-NMR}$ (400 MHz, CDCl_3) δ 1.85-1.90 (m, 2H, CH_2), 1.92-1.97 (m, 2H, CH_2), 2.68-2.73 (m, 2H, CH_2), 2.79-2.84 (m, 2H, CH_2), 5.30 (s, 2H, $\text{CH}_2\text{-Ph}$), 7.09 (d, 2H, Ar, $J = 7.2$), 7.28-7.34 (m, 3H, Ar), 8.00 (s, 1H, pyrazole). $^{13}\text{C-NMR}$ (100 MHz, CDCl_3) δ 20.3 (CH_2), 28.2 (CH_2), 31.6 (CH_2), 40.2 (CH_2), 56.0 (CH_2), 112.4 (C), 125.7 (CH), 127.6 (CH), 128.6 (CH), 136.2 (C), 139.0 (C), 142.1 (CH), 200.3 (C). ESI-MS calcd. for $\text{C}_{15}\text{H}_{16}\text{N}_2\text{O}$, 240.31; found: m/z 241.13 [$\text{M}+\text{H}$] $^+$. Anal. $\text{C}_{15}\text{H}_{16}\text{N}_2\text{O}$ (C, H, N).

2-benzyl-5,6,7,8-tetrahydrocyclohepta[c]pyrazol-4(2H)-one (66a)



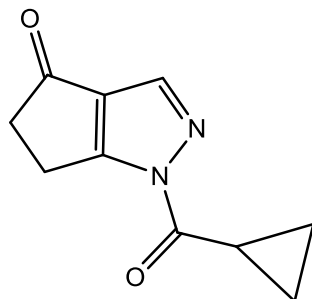
It was synthesized starting from 5,6,7,8-tetrahydrocyclohepta[c]pyrazol-4(1H)-one (**64**) [Maynard, G. et al., 2003] and using benzyl bromide as reactive, following the general procedure above reported. Compound **66a** was obtained in mixture with the N-1 isomer **65a** and they were separated by flash chromatography using toluene/ethyl acetate/methanol 9:1:0.5 as eluent.

Yield = 7%; mp = 88-89°C (EtOH). $^1\text{H-NMR}$ (400 MHz, CDCl_3) δ 1.87-1.98 (m, 4H, 2 x CH_2), 2.67 (m, 2H, CH_2), 2.96 (m, 2H, CH_2), 5.20 (s, 2H, $\text{CH}_2\text{-Ph}$), 7.22-7.27 (m, 2H, Ar), 7.32-7.38 (m, 3H, Ar), 7.80 (s, 1H, pyrazole). $^{13}\text{C-NMR}$ (100 MHz, CDCl_3) δ 22.8 (CH_2), 25.3 (CH_2), 27.9 (CH_2), 43.2 (CH_2), 56.3 (CH_2), 123.0 (C), 128.2 (CH), 128.6 (CH), 129.0 (CH), 133.3 (CH), 135.0 (C), 153.8 (C), 197.4 (C). ESI-MS calcd. for $\text{C}_{15}\text{H}_{16}\text{N}_2\text{O}$, 240.31; found: m/z 241.13 [$\text{M}+\text{H}$] $^+$. Anal. $\text{C}_{15}\text{H}_{16}\text{N}_2\text{O}$ (C, H, N).

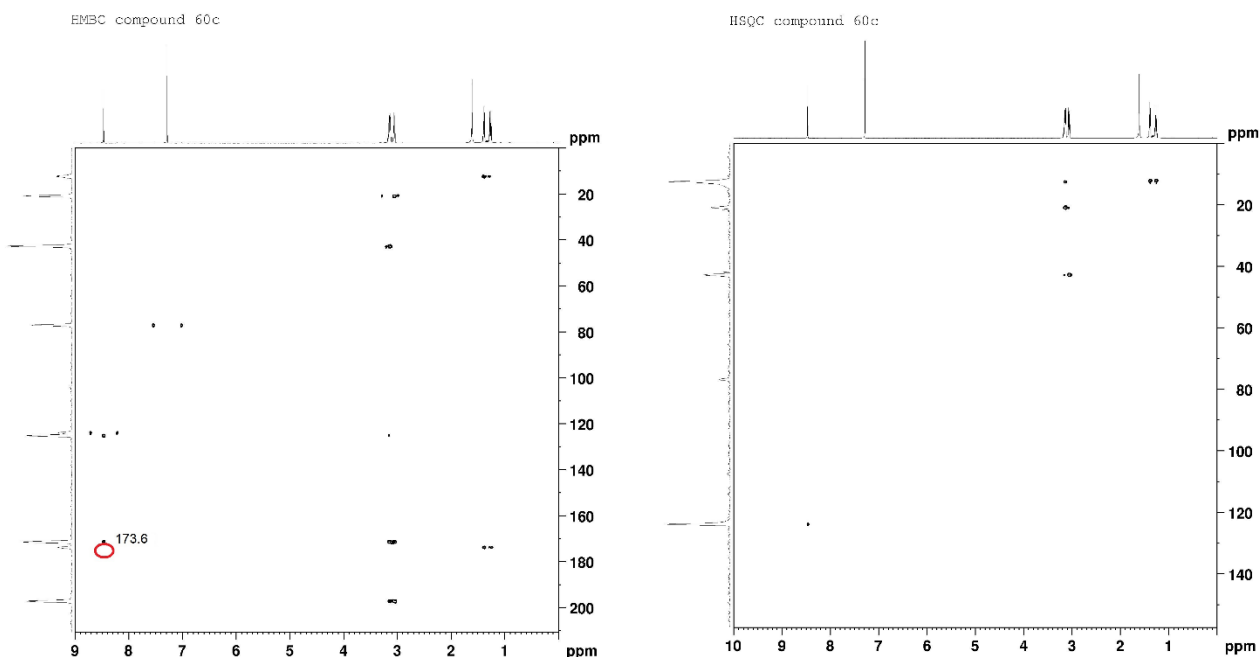


General procedure for compounds (60c, 61c,d, 65b,c and 66b). Compounds **60c**, **61c,d**, **65b,c** and **66b** were obtained using the general procedure followed for compounds of type **5**, starting from intermediate **59** [Liverton, N. J. et al., 2012] or **64** [Maynard, G. et al., 2003].

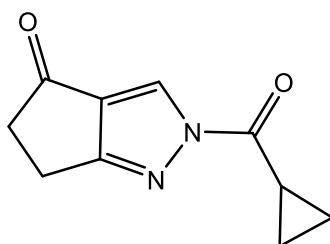
1-(cyclopropanecarbonyl)-5,6-dihydrocyclopenta[c]pyrazol-4(1H)-one (**60c**)



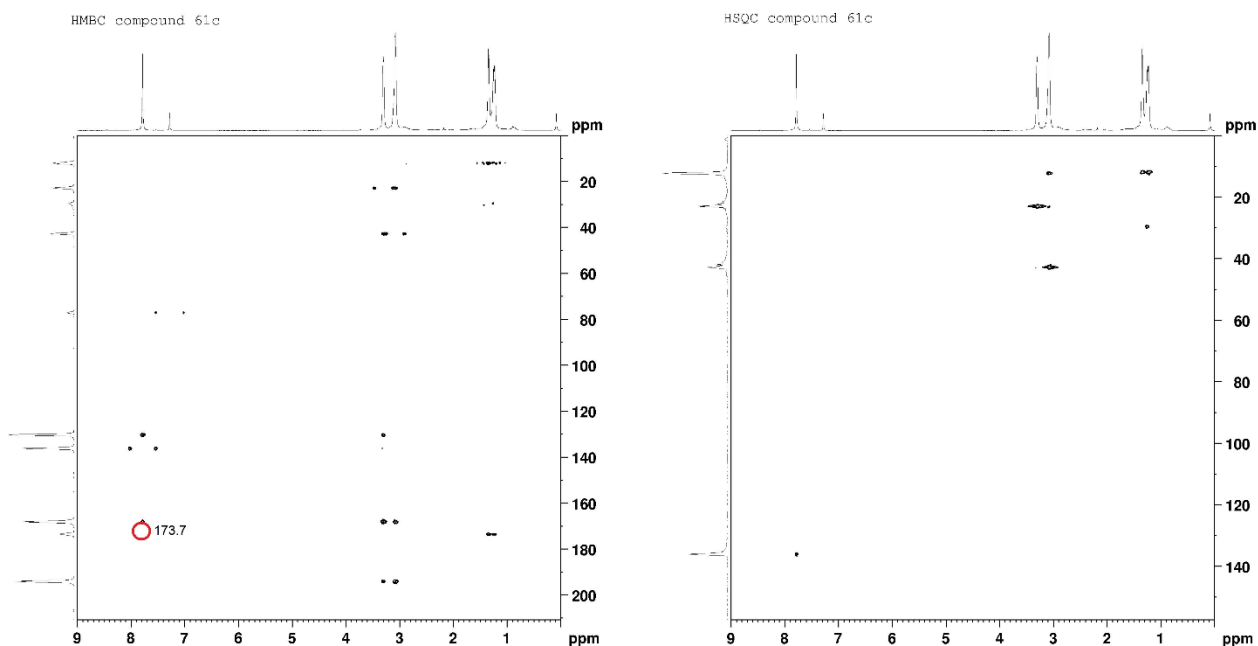
It was synthesized starting from 5,6-dihydrocyclopenta[c]pyrazol-4(1H)-one (**59**) [Liverton, N. J. et al., 2012] and using cyclopropanecarbonyl chloride as reactive, following the general procedure reported for compounds of type **5**. Compound **60c** was obtained in mixture with the N-2 isomer **61c** and they were separated by flash chromatography using dichloromethane/methanol 99:1 as eluent. Yield = 8%; mp = 113-115°C (EtOH). **¹H-NMR** (400 MHz, CDCl₃) δ 1.21-1.26 (m, 2H, CH₂ cC₃H₅), 1.33-1.39 (m, 2H, CH₂ cC₃H₅), 3.00-3.05 (m, 2H, CH₂), 3.09-3.14 (m, 3H, CH₂ + CH cC₃H₅), 8.44 (s, 1H, pyrazole). **¹³C-NMR** (100 MHz, CDCl₃) δ 12.0 (CH₂), 12.4 (CH), 23.0 (CH₂), 42.9 (CH₂), 130.4 (C), 136.3 (CH), 168.3 (C), 173.6 (C), 194.4 (C). ESI-MS calcd. for C₁₀H₁₀N₂O₂, 190.20; found: *m/z* 191.07 [M+H]⁺. Anal. C₁₀H₁₀N₂O₂ (C,H,N).



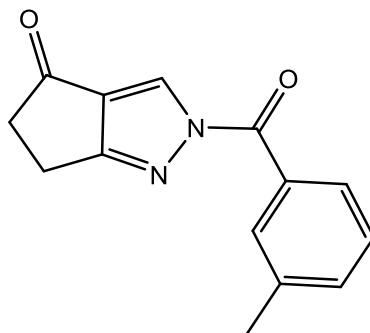
2-(cyclopropanecarbonyl)-5,6-dihydrocyclopenta[c]pyrazol-4(2H)-one (61c)



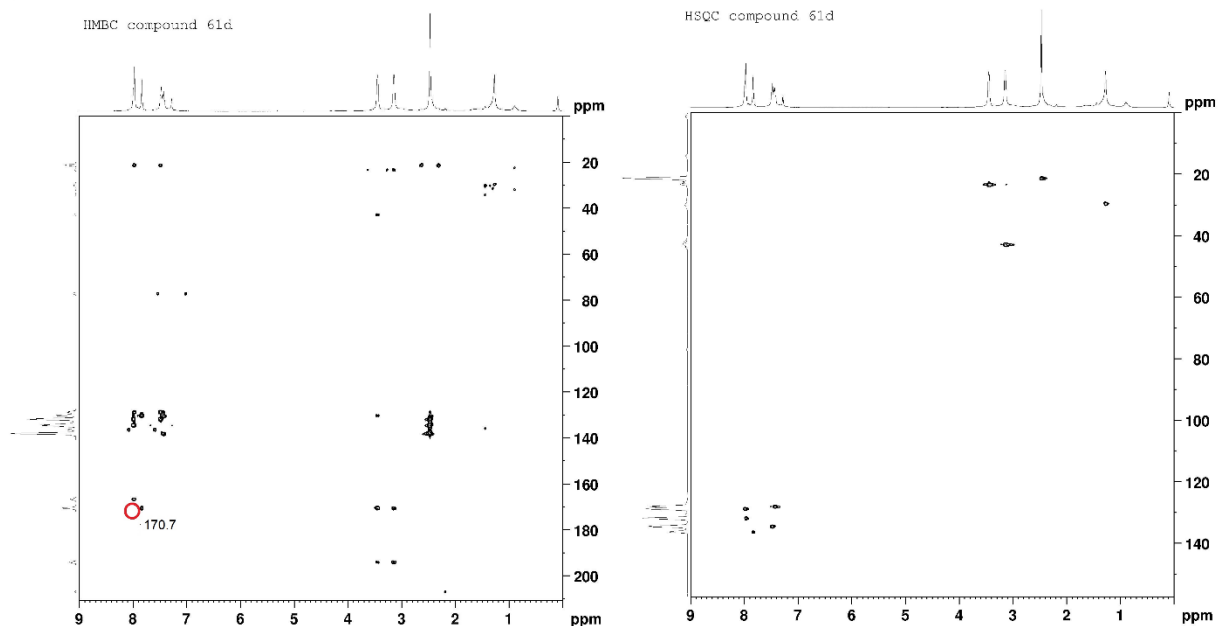
It was synthesized starting from 5,6-dihydrocyclopenta[c]pyrazol-4(1H)-one (**59**) [Liverton, N. J. et al., 2012] and using cyclopropanecarbonyl chloride as reactive, following the general procedure reported for compounds of type **5**. Compound **61c** was obtained in mixture with the N-1 isomer **60c** and they were separated by flash chromatography using dichloromethane/methanol 99:1 as eluent. Yield = 23%; mp = 109-111°C (EtOH). ¹H-NMR (400 MHz, CDCl₃) δ 1.19-1.25 (m, 2H, CH₂ cC₃H₅), 1.30-1.35 (m, 2H, CH₂ cC₃H₅), 3.04-3.10 (m, 3H, CH₂ + CH cC₃H₅), 3.25-3.30 (m, 2H, CH₂), 7.76 (s, 1H, pyrazole). ¹³C-NMR (100 MHz, CDCl₃) δ 12.0 (CH₂), 12.4 (CH), 23.0 (CH₂), 42.9 (CH₂), 130.4 (C), 136.3 (CH), 168.2 (C), 173.7 (C), 194.2 (C). ESI-MS calcd. for C₁₀H₁₀N₂O₂, 190.20; found: *m/z* 191.07 [M+H]⁺. Anal. C₁₀H₁₀N₂O₂ (C,H,N).



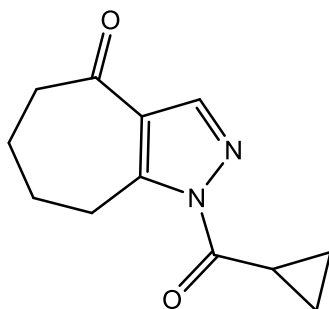
2-(3-methylbenzoyl)-5,6-dihydrocyclopenta[c]pyrazol-4(2H)-one (61d)



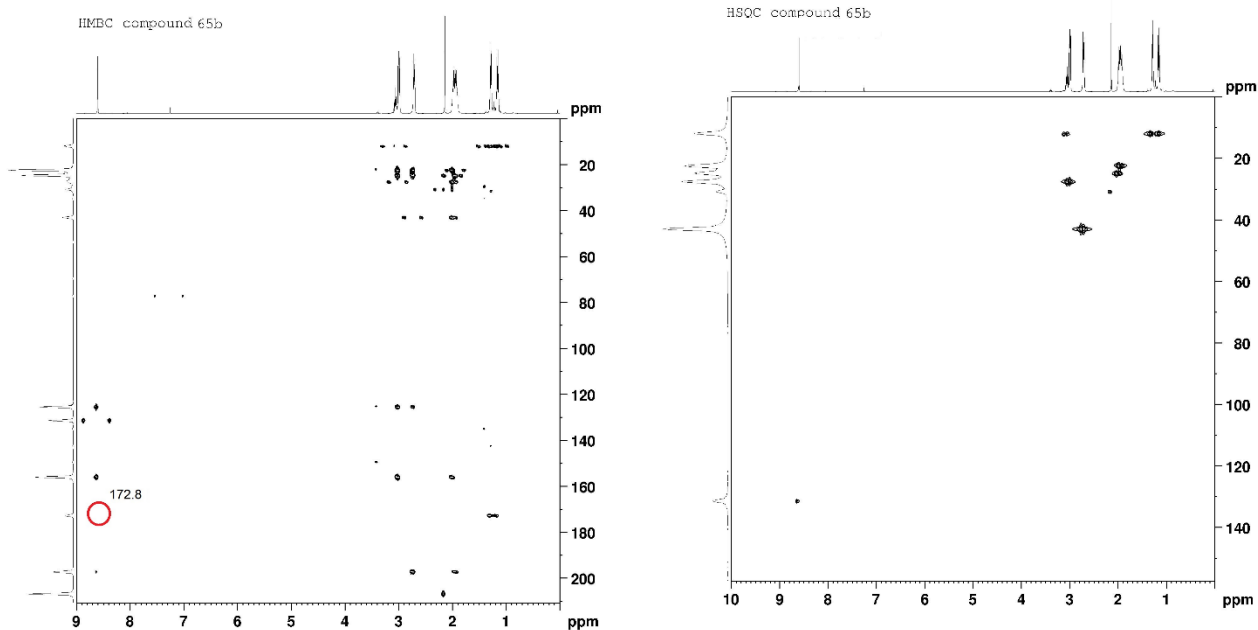
Obtained from 5,6-dihydrocyclopenta[c]pyrazol-4(1H)-one (**59**) [Liverton, N. J. et al., 2012] and using *m*-toluoyl chloride as reactive, following the general procedure for compounds of type **5**. The final compound was purified by flash chromatography using dichloromethane/methanol 99:1 as eluent. Yield = 5%; mp = 121-123°C (EtOH). ¹H-NMR (400 MHz, CDCl₃) δ 2.44 (s, 3H, CH₃), 3.10-3.15 (m, 2H, CH₂), 3.40-3.45 (m, 2H, CH₂), 7.41 (t, 1H, Ar, *J* = 7.2), 7.46 (d, 1H, Ar, *J* = 7.2), 7.81 (s, 1H, pyrazole), 7.96 (d, 2H, Ar, *J* = 8.8). ¹³C-NMR (100 MHz, CDCl₃) δ 21.4 (CH₃), 23.4 (CH₂), 43.0 (CH₂), 128.2 (CH), 128.9 (CH), 130.3 (C), 130.5 (C), 132.0 (CH), 134.5 (CH), 136.5 (CH), 138.2 (C), 166.8 (C), 170.7 (C), 194.2 (C). ESI-MS calcd. for C₁₄H₁₂N₂O₂, 240.26; found: *m/z* 241.09 [M+H]⁺. Anal. C₁₄H₁₂N₂O₂ (C,H,N).



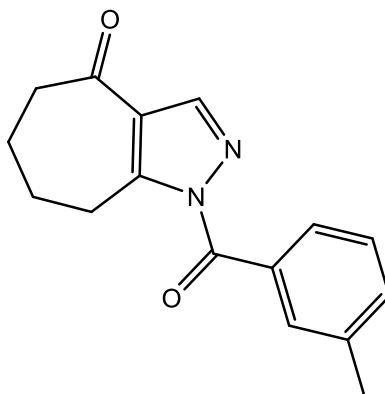
1-(cyclopropanecarbonyl)-5,6,7,8-tetrahydrocyclohepta[c]pyrazol-4(1H)-one (65b)



It was synthesized starting from 5,6,7,8-tetrahydrocyclohepta[c]pyrazol-4(1H)-one (**64**) [Maynard, G. et al., 2003] and using cyclopropanecarbonyl chloride as reactive, following the general procedure reported for compounds of type **5**. Compound **65b** was obtained in mixture with the N-2 isomer **66b** and they were separated by flash chromatography using petroleum ether/ethyl acetate 5:1 as eluent. Yield = 27%; oil. $^1\text{H-NMR}$ (400 MHz, CDCl_3) δ 1.13-1.18 (m, 2H, CH_2 cC_3H_5), 1.25-1.30 (m, 2H, CH_2 cC_3H_5), 1.89-2.04 (m, 4H, 2 x CH_2), 2.69-2.74 (m, 2H, CH_2), 2.98-3.07 (m, 3H, CH_2 + CH cC_3H_5), 8.60 (s, 1H, pyrazole). $^{13}\text{C-NMR}$ (100 MHz, CDCl_3) δ 12.0 (CH_2), 12.1 (CH), 22.5 (CH_2), 24.9 (CH_2), 27.6 (CH_2), 43.1 (CH_2), 125.5 (C), 131.5 (CH), 156.1 (C), 172.8 (C), 197.4 (C). ESI-MS calcd. for $\text{C}_{12}\text{H}_{14}\text{N}_2\text{O}_2$, 218.26; found: m/z 219.11 $[\text{M}+\text{H}]^+$. Anal. $\text{C}_{12}\text{H}_{14}\text{N}_2\text{O}_2$ (C, H, N).



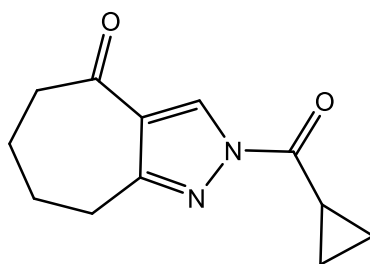
1-(3-methylbenzoyl)-5,6,7,8-tetrahydrocyclohepta[c]pyrazol-4(1H)-one (65c)



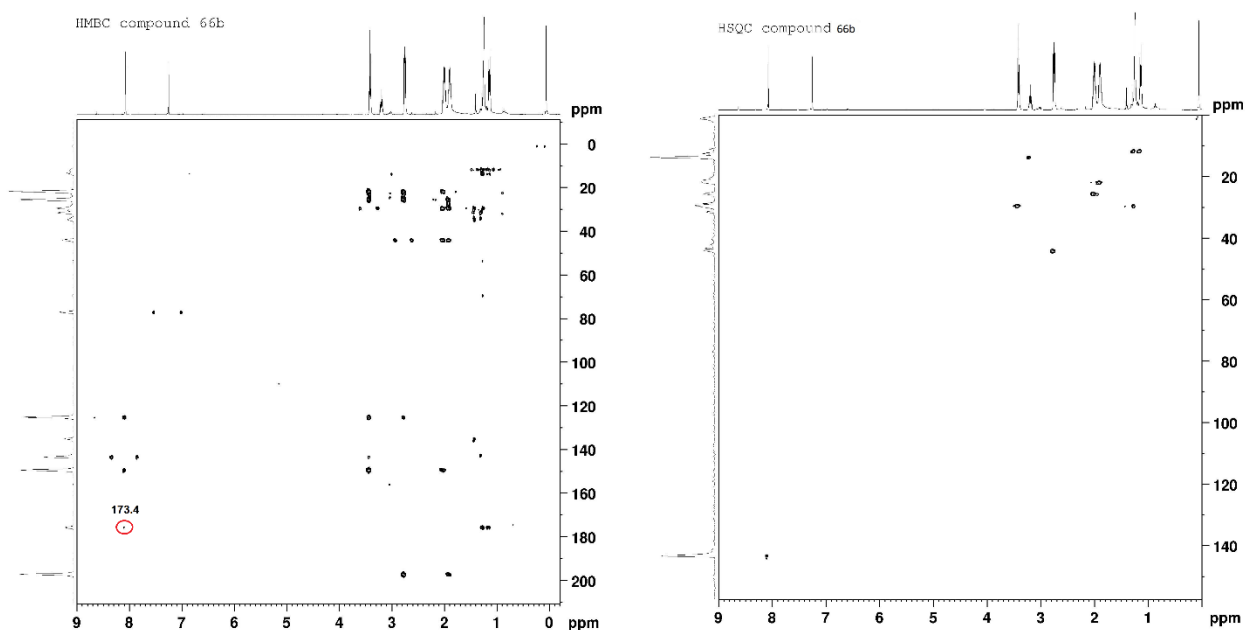
Obtained from 5,6,7,8-tetrahydrocyclohepta[c]pyrazol-4(1H)-one (**64**) [Maynard, G. et al., 2003] and using m-toluoyl chloride as reactive, following the general procedure for compounds of type **5**. The final compound was purified by flash chromatography using petroleum ether/ethyl acetate 5:2 as eluent.

Yield = 34%; oil. ¹H-NMR (400 MHz, CDCl₃) δ 1.95-2.00 (m, 4H, 2 x CH₂), 2.42 (s, 3H, CH₃), 2.72-2.77 (m, 2H, CH₂), 3.00-3.05 (m, 2H, CH₂), 7.38-7.44 (m, 3H, Ar), 7.87 (d, 2H, Ar, *J* = 9.2), 8.73 (s, 1H, pyrazole). ¹³C-NMR (100 MHz, CDCl₃) δ 21.4 (CH₃), 22.5 (CH₂), 24.9 (CH₂), 27.8 (CH₂), 43.1 (CH₂), 125.3 (C), 128.2 (CH), 128.8 (CH), 130.6 (C), 131.7 (CH), 134.4 (CH), 138.3 (C), 156.5 (C), 166.1 (C), 197.4 (C). ESI-MS calcd. for C₁₆H₁₆N₂O₂, 268.32; found: *m/z* 269.12 [M+H]⁺. Anal. C₁₆H₁₆N₂O₂ (C, H, N).

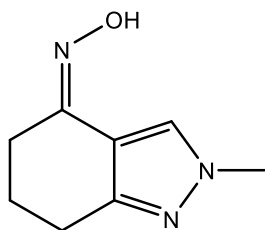
2-(cyclopropanecarbonyl)-5,6,7,8-tetrahydrocyclohepta[c]pyrazol-4(2H)-one (66b)



It was synthesized starting from 5,6,7,8-tetrahydrocyclohepta[c]pyrazol-4(1H)-one (**64**) [Maynard, G. et al., 2003] and using cyclopropanecarbonyl chloride as reactive, following the general procedure reported for compounds of type **5**. Compound **66b** was obtained in mixture with the N-1 isomer **65b** and they were separated by flash chromatography using petroleum ether/ethyl acetate 5:1 as eluent. Yield = 3%; mp = 99-100°C (EtOH). $^1\text{H-NMR}$ (400 MHz, CDCl_3) δ 1.11-1.16 (m, 4H, 2 x CH_2 C_3H_5), 1.86-2.03 (m, 4H, 2 x CH_2), 2.72-2.77 (m, 2H, CH_2), 3.16-3.23 (m, 1H, CH C_3H_5), 3.41 (m, 2H, CH_2), 8.07 (s, 1H, pyrazole). $^{13}\text{C-NMR}$ (100 MHz, CDCl_3) δ 11.8 (CH_2), 13.8 (CH), 21.9 (CH_2), 25.7 (CH_2), 29.6 (CH_2), 44.2 (CH_2), 112.0 (C), 143.6 (CH), 144.5 (C), 173.4 (C), 197.0 (C). ESI-MS calcd. for $\text{C}_{12}\text{H}_{14}\text{N}_2\text{O}_2$, 218.26; found: m/z 219.11 $[\text{M}+\text{H}]^+$. Anal. $\text{C}_{12}\text{H}_{14}\text{N}_2\text{O}_2$ (C, H, N).



2-methyl-2,5,6,7-tetrahydro-4H-indazol-4-one oxime (69)

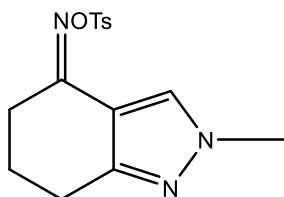


A mixture of 2-methyl-2,5,6,7-tetrahydro-4H-indazol-4-one (**67**) [Spanò, V. et al., 2015] (0.78 mmol) and hydroxylamine hydrochloride (2.35 mmol) in 2 mL of water was heated at 60°C for 30 min. Afterwards, 2.35 mmol of sodium bicarbonate was added and the reaction mixture was stirred at reflux for 4h. After cooling to room temperature, the solid obtained was filtered, washed with an excess of ice-cold water and dried.

Yield = 86%; mp = 160-165°C (EtOH). ¹H-NMR (400 MHz, DMSO-d₆) δ 1.79-1.84 (m, 2H, CH₂), 2.32-2.37 (m, 2H, CH₂), 2.58-2.63 (m, 2H, CH₂), 3.77 (s, 3H, CH₃), 8.17 (s, 1H, pyrazole), 10.55 (exch br s, 1H, OH). ESI-MS calcd. for C₈H₁₁N₃O, 165.20; found: *m/z* 166.09 [M+H]⁺. Anal. C₈H₁₁N₃O (C, H, N).

General procedure for compounds (70, 73). To a cooled (0°C) solution of **69** or **72** [Yoshinaga, H. et al., 2020] (1.21 mmol) and DMAP (0.12 mmol) in pyridine (3 mL), 0.96 mmol of tosyl chloride were added in portion. The mixture was stirred at room temperature for 16h. After the evaporation of the solvent, cold water was added (20 mL), and the pH was neutralized with 1N HCl. The suspension was extracted with CH₂Cl₂ (3 x 15 mL), dried over sodium sulfate and evaporated under vacuum

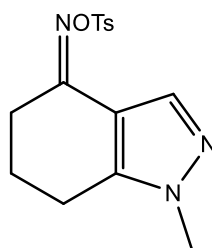
2-methyl-2,5,6,7-tetrahydro-4H-indazol-4-one O-tosyl oxime (70)



Obtained from 2-methyl-2,5,6,7-tetrahydro-4H-indazol-4-one oxime (**69**) following the general procedure. The final compound was purified by flash chromatography using hexane/ethyl acetate 1:2 as eluent.

Yield = 23%; mp = 141-142°C (EtOH). ¹H-NMR (400 MHz, CDCl₃) δ 1.97 (t, 2H, CH₂, *J* = 6.0), 2.40-2.45 (m, 5H, CH₃ tosyl + CH₂), 2.67 (t, 2H, CH₂, *J* = 6.0), 3.75 (s, 3H, N-CH₃), 7.29 (d, 2H, Ar, *J* = 7.6), 7.85 (d, 2H, Ar, *J* = 8.0), 8.09 (s, 1H, pyrazole). ESI-MS calcd. for C₁₅H₁₇N₃O₃S, 319.38; found: *m/z* 320.10 [M+H]⁺. Anal. C₁₅H₁₇N₃O₃S (C, H, N).

1-methyl-1,5,6,7-tetrahydro-4H-indazol-4-one O-tosyl oxime (73)

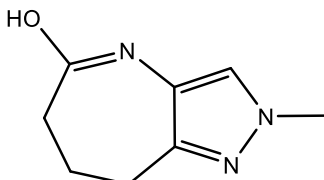


Obtained from 1-methyl-1,5,6,7-tetrahydro-4H-indazol-4-one oxime (**72**) [Yoshinaga, H. et al., 2020] following the general procedure. The final compound was purified by flash chromatography using hexane/ethyl acetate 1:2 as eluent.

Yield = 57%; mp = 128-130°C (EtOH). ¹H-NMR (400 MHz, CDCl₃) δ 2.00 (t, 2H, CH₂, *J* = 6.2), 2.42 (s, 3H, CH₃ tosyl), 2.46 (t, 2H, CH₂, *J* = 6.2), 2.46 (quin, 2H, CH₂, *J* = 6.6), 3.78 (s, 3H, N-CH₃), 7.31 (d, 2H, Ar, *J* = 8.0), 7.89 (d, 2H, Ar, *J* = 8.0), 8.12 (s, 1H, pyrazole). ESI-MS calcd. for C₁₅H₁₇N₃O₃S, 319.38; found: *m/z* 320.10 [M+H]⁺. Anal. C₁₅H₁₇N₃O₃S (C, H, N).

General procedure for compounds (71) and (74). To a solution of **70** or **73** (0.28 mmol) in a mixture water/ethanol 2:1 (9 mL), 0.28 mmol of sodium acetate were added. The mixture was stirred at reflux for 3h. After evaporation of the solvent, cold water was added (20 mL), and the pH was neutralized with 1N HCl. The suspension was extracted with CH₂Cl₂ (3 x 15 mL), dried over sodium sulfate and evaporated under vacuum.

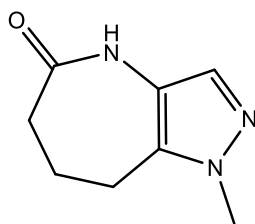
2-methyl-2,6,7,8-tetrahydropyrazolo[4,3-b]azepin-5-ol (71) [Estrada, A. A., 2017]



Obtained from 2-methyl-2,5,6,7-tetrahydro-4H-indazol-4-one O-tosyl oxime (**70**) following the general procedure above reported. The final compound was purified by flash chromatography using dichloromethane/methanol 9:1 as eluent

Yield = 31%; mp = 153-154°C (EtOH). ¹H-NMR (400 MHz, DMSO-d₆) δ 1.84-1.89 (m, 2H, CH₂), 2.80 (t, 2H, CH₂, *J* = 6.6), 3.14 (q, 2H, CH₂, *J* = 4.8), 3.74 (s, 3H, CH₃), 7.49 (exch br s, 1H, OH), 7.97 (s, 1H, pyrazole). ¹³C-NMR (100 MHz, DMSO-d₆) δ 26.7 (CH₂), 28.3 (CH₂), 38.9 (CH₃), 42.1 (CH₂), 116.6 (C), 136.1 (CH), 149.4 (C), 165.3 (C). ESI-MS calcd. for C₈H₁₁N₃O, 165.20; found: *m/z* 166.09 [M+H]⁺. Anal. C₈H₁₁N₃O (C, H, N).

1-methyl-4,6,7,8-tetrahydropyrazolo[4,3-b]azepin-5(1H)-one (74) [Yoshinaga, H. et al., 2020]



Obtained from 1-methyl-1,5,6,7-tetrahydro-4H-indazol-4-one O-tosyl oxime (**73**) following the general procedure above reported. The final compound was purified by flash chromatography using toluene/ethyl acetate/methanol/NH₃ 9:1:1.5:0.1.

Yield = 14%; mp = 200-202°C (EtOH). ¹H-NMR (400 MHz, DMSO-d₆) δ 1.85-1.91 (m, 2H, CH₂), 2.38-2.43 (m, 2H, CH₂), 2.75 (t, 2H, CH₂, *J* = 6.2), 3.60 (s, 3H, CH₃), 7.00 (s, 1H, pyrazole), 9.34 (exch br s, 1H, NH). ¹³C-NMR (100 MHz, CDCl₃) δ 19.3 (CH₂), 25.7 (CH₂), 36.0 (CH₂), 36.7 (CH₃), 119.8 (C), 129.2 (C), 129.3 (CH), 173.5 (C). ESI-MS calcd. for C₈H₁₁N₃O, 165.20; found: *m/z* 166.09 [M+H]⁺. Anal. C₈H₁₁N₃O (C, H, N).

12.1. Methods

• HNE inhibition assay

All compounds were dissolved in 100% DMSO at 5 mM stock concentrations. The final concentration of DMSO in the reactions was 1%, and this level of DMSO had no effect on enzyme activity. The HNE inhibition assay was performed in black flat-bottom 96-well microtiter plates. Briefly, a buffer solution containing 200 mM Tris–HCl, pH 7.5, 0.01% bovine serum albumin, and 0.05% Tween-20 and 20 mU/mL of HNE (Calbiochem) was added to wells containing different concentrations of each compound. The reaction was initiated by addition of 25 μ M elastase substrate (N-methylsuccinyl-Ala-Ala-Pro-Val-7-amino-4-methylcoumarin, Calbiochem) in a final reaction volume of 100 μ L/well. Kinetic measurements were obtained every 30 s for 10 min at 25 °C using a Fluoroskan Ascent FL fluorescence microplate reader (Thermo Electron, MA) with excitation and emission wavelengths of 355 and 460 nm, respectively. For all compounds tested, the concentration of inhibitor that caused 50% inhibition of the enzymatic reaction (IC_{50}) was calculated by plotting % inhibition versus logarithm of inhibitor concentration (at least six points). The data are presented as the mean values of at least three independent experiments with relative standard deviations of <15%.

• Analysis of Compound Stability

Spontaneous hydrolysis of selected compounds was evaluated at 20 °C in 0.05 M phosphate buffer, pH 7.4. Kinetics of hydrolysis was monitored by measuring changes in absorbance spectra over incubation time using a SpectraMax ABS Plus spectrophotometer (Molecular Devices, Sunnyvale, CA). Absorbance (A_t) at the characteristic absorption maxima of each compound was measured at the indicated times until no further absorbance decreases occurred (A_∞). Using these measurements, we created semilogarithmic plots of $\log(A_t - A_\infty)$ vs time, and k' values were determined from the slopes of these plots. Half-conversion times were calculated using $t_{1/2} = 0.693/k'$.

• Molecular Modeling

Initial 3D structures of compounds **5a**, **5c**, **5e**, **13d**, **13f**, **19a**, and **22a** were built with ChemOffice Professional (Perkin Elmer, Waltham, MA) and refined by molecular mechanics with MM2 force field [Vanommeslaeghe, K., et al., 2014]. For the docking computations, Molegro Virtual Docker (MVD) software, version 6.0 (CLC Bio, Copenhagen, Denmark), was used as described previously [Crocetti, L. et al., 2013]. The structure of HNE co-crystallized with a peptide chloromethyl ketone inhibitor (1HNE entry of the Protein Data Bank) determined by X-ray diffraction [Navia, M. A. et al., 1989] was used for the docking studies. The co-crystallized peptide ligand and water molecules were removed from the 1HNE structure. A search for docking poses was performed within a spherical area of 10 Å radius centered at the atom in the five-membered ring of the co-crystallized inhibitor. Side chains of 42 residues closest to the center of the sphere [Crocetti, L. et al., 2013] were set flexible, including

the residues surrounding HNE binding site: His57, Cys58, Leu99B, Val190, Cys191, Phe192, Gly193, Asp194, Ser195, Ala213, Ser214, Phe215, Val216. Fifteen docking runs were performed for each compound with full flexibility of a ligand around all rotatable bonds and with flexibility of the above-mentioned side chains of the enzyme amino acid residues. Docking poses of each compound were checked for the ability to form a Michaelis complex between the carbonyl moiety in a ligand and the Ser195 hydroxyl group. For this purpose, the important geometric parameters were determined: d_1 [distance O(Ser195)···C between the Ser195 hydroxyl oxygen atom and the ligand carbonyl carbon atom closest to O(Ser195)] and α [angle O(Ser195)···C=O, where C=O is the carbonyl group of a ligand closest to O(Ser195)] [Ghose, A. K. et al., 1999] (**Figure 37**). The conditions for proton transfer within the key catalytic triad from Ser195 to Asp102 via His57 were also evaluated by the calculation of distances d_2 between the NH hydrogen in His57 and carboxyl oxygen atoms in Asp102, as described in our earlier paper [Crocetti, L. et al., 2013]. The distance between the OH proton in Ser195 and the pyridine-type nitrogen in His57 is also important for proton transfer. However, the OH group of the Ser195 is easily rotatable about the C-O bond. Hence, we measured distance d_3 between the oxygen atom of Ser195 side chain and the basic nitrogen atom in His57 residue. The effective length of the proton transfer channel was determined as $L = \min(d_2) + d_3$.

- **DFT calculations**

Single-molecule DFT calculations were performed with the Gaussian 09w program, Revision-D.01 (Gaussian, Inc., Wallingford CT) for compounds **5a**, **5b**, **5c**, **13b**, **13f**, **17a**, **17b**, **19a**, **19b**, **22a**, **22b**, and **35b** in gas phase. The hybrid B3LYP functional [Becke, A. D. 1993; Stephens, P. J. et al., 1994] and 6-31+G(d,p) basis set [Foresman, J. B. et al., 2015] were used with D3BJ dispersion correction [Grimme, S. et al., 2011] applied. Vibrational frequency analysis was done for all the optimized geometries in order to ensure attaining energy minima for the molecules.

- **GC-MS analysis**

The analysis was performed by Agilent GC-MS system composed with 5973 single quadrupole mass spectrometer, 6890 gas-chromatograph and 7673 autosampler. The sample solution of each analyte was prepared at 10 mg/L in acetone. The samples were analyzed using a DB-17MS (Agilent J&W) column 15 m length, 0.25 mm internal diameter and 0.25 μ m of film thickness. The analytes were separated by using the oven temperatures program, as follows: initial temperature of 50 °C for 1 min, then it was increased to 100 °C at 30 °C/min, finally grow up to 280 °C at 10 °C/min was held for 5.33 min. A 1 μ L aliquot of sample solution was injected in splitless mode (splitless time 1 min) at 280 °C, while the transfer line temperature with the MS detector was 280 °C. The used carrier gas was helium and its flow rate maintained at 1 mL/min for whole run time. The MS acquisition was carried out in ions scan in the range 50-550 m/z.

- **X-ray crystallography**

The structure of the intermediate **59** was determined using single crystal X-ray diffraction.

The diffractometer used was a Bruker APEX II. Diffraction data collection was performed at 100K using the Bruker APEX2 program [Bruker, 2012a] (radiation used is copper K; $\lambda = 1.54178 \text{ \AA}$). The collected data were reduced using the Bruker SAINT program [Bruker, 2012b], no absorption correction was performed. The structure was then resolved using the SIR-2004 program [Burla, M. C. et al., 2005] and refined using the SHELX2018/3 program. [Sheldrick, G. M., 2015].

Non-hydrogen atoms were refined anisotropically, while hydrogen atoms were found experimentally in Fourier differences and refined, leaving their coordinates free, but constraining the thermal factor to the atom to which they are bound. **Table 13** shows the crystallographic and collection data for the intermediate **59**, and **Fig. 54** (see results and discussion section) shows an Ortep-3 figure of the asymmetric unit with the labels of the various atoms.

Table 13: Crystal data and structure refinement for **59**.

Empirical formula	C ₆ H ₆ N ₂ O
Formula weight	122.13
T(K)	100
Wavelength (Å)	1.54178
Crystal system	Monoclinic
Space group	P2 ₁
Unit cell dimensions (Å, °)	a = 4.9347(9) b = 5.1904(9); β = 95,63(1) c = 10.877(2)
Volume (Å³)	277.25(9)
Z	2
D_{calc}	1.463
μ(mm⁻¹)	0.861
Reflections collected / unique	3380 / 1037
Data / Restraints / parameters	1037 / 100
R [I>2σ(I)]; Rw [I>2σ(I)]	0.0494; 0.2437

Table 14: Crystal data and structure refinement for **60c**.

Empirical formula	C ₁₀ H ₁₀ N ₂ O ₂
Formula weight	190.20
T(K)	100
Wavelength (Å)	1.54178
Crystal system	Monoclinic
Space group	P2 ₁ /c
Unit cell dimensions (Å, °)	a = 8.026(2) b = 9.521(2), β = 95.067(7) c = 11.753(3)
Volume (Å³)	984.6(4)
Z	4
D_{calc}	1.412
μ(mm⁻¹)	0.831
Reflections collected / unique	10622/1731 (Rint = 0.0713)
Data / Restraints / parameters	1731/ 157
R [I>2σ(I)]; Rw [I>2σ(I)]	0.0947, 0.2713 0.0967, 0.2846

- **Predicted ADMET values Tables 1S-11S**

Table 1S. SwissADME calculated lipophilicities parameters.

Mol	iLOGP	XLOGP3	WLOGP	MLOGP	Silicos-IT Log P	Consensus Log P
5a	2.41	2.64	2.90	2.10	2.87	2.58
5b	1.87	1.08	1.90	1.02	1.75	1.52
5c	2.32	2.55	2.90	1.84	2.87	2.50
5d	1.81	0.99	1.90	0.75	1.75	1.44
5e	2.31	2.55	2.90	1.84	2.87	2.49
5f	1.77	0.99	1.90	0.75	1.75	1.43
13a	2.51	3.66	4.6	3.79	3.33	3.58
13b	2.06	2.09	3.59	2.73	2.24	2.54
13c	2.55	3.29	2.60	3.00	2.62	2.82
13d	2.24	2.79	2.30	2.24	2.31	2.38
13e	1.67	1.22	1.29	1.13	1.22	1.31
13f	1.25	1.33	1.33	1.59	-0.94	0.91
17a	2.98	3.72	2.99	3.24	2.84	3.15
17b	2.10	1.76	3.59	2.05	2.24	2.35
19a	2.36	2.46	2.30	1.57	2.31	2.20
19b	1.73	0.89	1.29	0.46	1.22	1.12
22a	2.97	2.96	2.60	2.33	2.62	2.70
22b	2.55	1.39	1.60	1.28	1.49	1.66
27	2.59	2.81	2.74	2.47	2.81	2.68
31b	1.5	0.62	1.42	0.94	1.27	1.15
35b	1.41	0.34	1.29	0.32	1.22	0.92

Table 2S. SwissADME calculated water solubility parameters.

Mol	ESOL Log S	ESOL Solubility (mg/ml)	ESOL Solubility (mol/l)	ESOL Class	Ali Log S	Ali Solubility (mg/ml)	Ali Solubility (mol/l)	Ali Class
5a	-3.55	7.43E-02	2.84E-04	Soluble	-3.5	7.84E-02	3.00E-04	Soluble
5b	-2.11	1.62E+00	7.69E-03	Soluble	-1.9	2.63E+00	1.25E-02	Very soluble
5c	-3.49	8.47E-02	3.24E-04	Soluble	-3.4	9.72E-02	3.72E-04	Soluble
5d	-2.06	1.85E+00	8.76E-03	Soluble	-1.8	3.27E+00	1.55E-02	Very soluble
5e	-3.49	8.47E-02	3.24E-04	Soluble	-3.4	9.72E-02	3.72E-04	Soluble
5f	-2.06	1.85E+00	8.76E-03	Soluble	-1.8	3.27E+00	1.55E-02	Very soluble
13a	-4.34	1.38E-02	4.52E-05	Moderately soluble	-4.3	1.36E-02	4.44E-05	Moderately soluble
13b	-2.91	3.13E-01	1.23E-03	Soluble	-2.7	4.83E-01	1.89E-03	Soluble
13c	-3.98	3.22E-02	1.04E-04	Soluble	-4.5	9.32E-03	3.01E-05	Moderately soluble
13d	-3.65	5.92E-02	2.26E-04	Soluble	-3.9	2.95E-02	1.12E-04	Soluble
13e	-2.21	1.31E+00	6.19E-03	Soluble	-2.3	1.02E+00	4.78E-03	Soluble
13f	-2.31	1.13E+00	4.88E-03	Soluble	-2.9	2.94E-01	1.27E-03	Soluble
17a	-4.32	1.54E-02	4.78E-05	Moderately soluble	-4.9	3.49E-03	1.08E-05	Moderately soluble
17b	-2.7	5.06E-01	1.98E-03	Soluble	-2.3	1.06E+00	4.16E-03	Soluble
19a	-3.44	9.55E-02	3.64E-04	Soluble	-3.6	6.48E-02	2.47E-04	Soluble
19b	-2	2.12E+00	9.99E-03	Soluble	-1.9	2.23E+00	1.05E-02	Very soluble
22a	-3.78	5.19E-02	1.68E-04	Soluble	-4.1	2.05E-02	6.63E-05	Moderately soluble
22b	-2.34	1.18E+00	4.53E-03	Soluble	-2.5	7.32E-01	2.82E-03	Soluble
27	-3.62	6.02E-02	2.40E-04	Soluble	-3.4	8.50E-02	3.38E-04	Soluble
31b	-1.73	3.45E+00	1.84E-02	Very soluble	-1.2	1.19E+01	6.34E-02	Very soluble
35b	-1.65	4.71E+00	2.22E-02	Very soluble	-1.4	8.31E+00	3.92E-02	Very soluble

Table 3S. SwissADME calculated pharmacokinetics parameters.

Mol	GI absorp.	BBB perm.	Pgp sub.	CYP1A2 inhibitor	CYP2C19 inhibitor	CYP2C9 inhibitor	CYP2D6 inhibitor	CYP3A4 inhibitor	log Kp (cm/s)
5a	High	Yes	No	Yes	Yes	Yes	No	No	-6.02
5b	High	Yes	No	Yes	No	No	No	No	-6.82
5c	High	Yes	No	Yes	Yes	Yes	No	No	-6.08
5d	High	Yes	No	Yes	No	No	No	No	-6.89
5e	High	Yes	No	Yes	Yes	Yes	No	No	-6.08
5f	High	Yes	No	Yes	No	No	No	No	-6.89
13a	High	Yes	No	Yes	Yes	No	No	No	-5.56
13b	High	Yes	No	Yes	No	No	No	No	-6.37
13c	High	Yes	No	Yes	Yes	Yes	No	No	-5.85
13d	High	Yes	No	Yes	No	Yes	No	No	-5.92
13e	High	No	No	Yes	No	No	No	No	-6.73
13f	High	No	No	Yes	No	No	No	No	-6.77
17a	High	Yes	No	Yes	Yes	Yes	No	No	-5.63
17b	High	Yes	Yes	Yes	Yes	No	No	No	-6.61
19a	High	Yes	No	Yes	No	Yes	No	No	-6.15
19b	High	No	No	Yes	No	No	No	No	-6.96
22a	High	Yes	No	Yes	Yes	Yes	No	No	-6.09
22b	High	No	No	Yes	Yes	No	No	No	-6.89
27	High	Yes	No	Yes	Yes	No	No	No	-5.84
31b	High	Yes	No	Yes	No	No	No	No	-7.00
35b	High	No	No	Yes	No	No	No	No	-7.35

Table 4S. Swiss ADME calculated drug likeness parameters.

Mol	Lipinski #violations	Ghose #violations	Veber #violations	Egan #violations	Muegge #violations
5a	0	0	0	0	0
5b	0	0	0	0	0
5c	0	0	0	0	0
5d	0	0	0	0	0
5e	0	0	0	0	0
5f	0	0	0	0	0
13a	0	0	0	0	0
13b	0	0	0	0	0
13c	0	0	0	0	0
13d	0	0	0	0	0
13e	0	0	0	0	0
13f	0	0	0	0	0
17a	0	0	0	0	0
17b	0	0	0	0	0
19a	0	0	0	0	0
19b	0	0	0	0	0
22a	0	0	0	0	0
22b	0	0	0	0	0
27	0	0	0	0	0
31b	0	0	0	0	1
35b	0	0	0	0	0

Table 5S. pkCSM calculated absorption properties.

Mol	Water solubility	Caco2 permeability	Intestinal absorption (human)	Skin Permeability	P-glycoprotein substrate	P-glycoprotein I inhibitor	P-glycoprotein II inhibitor
5a	-3.56	1.36	100.00	-2.46	No	No	No
5b	-2.62	1.30	98.74	-2.75	No	No	No
5c	-3.59	1.35	100.00	-2.42	Yes	No	No
5d	-2.65	1.29	98.50	-2.68	No	No	No
5e	-3.58	1.34	100.00	-2.45	Yes	No	No
5f	-2.54	1.28	98.50	-2.70	No	No	No
13a	-3.28	1.49	96.53	-2.61	No	No	No
13b	-3.88	1.35	95.50	-2.90	No	No	No
13c	-3.33	1.20	100.00	-2.56	No	No	No
13d	-3.20	0.95	100.00	-2.54	No	No	No
13e	-2.44	0.60	98.93	-2.96	No	No	No
13f	-3.03	0.52	97.35	-2.82	No	No	No
17a	-3.91	1.21	99.84	-2.62	No	Yes	No
17b	-3.97	1.37	95.50	-2.78	No	No	No
19a	-3.18	0.96	100.00	-2.42	No	No	No
19b	-2.58	0.61	98.93	-2.71	No	No	No
22a	-3.23	1.23	100.00	-2.56	No	No	No
22b	-2.83	1.27	98.77	-2.66	No	No	No
27	-2.89	1.35	100.00	-2.27	No	No	No
31b	-1.65	1.31	98.83	-2.84	No	No	No
35b	-2.40	0.69	99.06	-3.10	No	No	No

Table 6S. pkCSM calculated distribution properties.

Mol	VDss (human)	Fraction unbound (human)	BBB permeability	CNS permeability
5a	-0.08	0.26	0.27	-2.66
5b	-0.08	0.40	0.12	-2.80
5c	-0.03	0.24	0.24	-1.81
5d	-0.03	0.37	0.10	-2.79
5e	-0.09	0.24	0.24	-1.79
5f	-0.05	0.37	0.10	-2.78
13a	0.06	0.13	0.89	-1.59
13b	-0.30	0.36	0.37	-2.83
13c	-0.28	0.22	-0.72	-2.88
13d	-0.28	0.28	-0.40	-2.75
13e	-0.31	0.42	-0.34	-2.89
13f	-0.43	0.31	-0.73	-2.96
17a	-0.22	0.19	-0.71	-2.23
17b	-0.28	0.34	0.37	-2.83
19a	-0.17	0.26	-0.40	-2.76
19b	-0.27	0.39	-0.34	-2.91
22a	-0.18	0.21	-0.72	-2.88
22b	-0.42	0.33	-0.66	-3.03
27	0.01	0.26	0.29	-1.68
31b	-0.31	0.48	-0.21	-2.80
35b	-0.32	0.44	-0.34	-2.86

Table 7S. pkCSM calculated metabolism properties.

Mol	CYP2D6 substrate	CYP3A4 substrate	CYP1A2 inhibitor	CYP2C19 inhibitor	CYP2C9 inhibitor	CYP2D6 inhibitor	CYP3A4 inhibitor
5a	No	Yes	Yes	Yes	No	No	No
5b	No	No	Yes	No	No	No	No
5c	No	Yes	Yes	Yes	No	No	No
5d	No	No	Yes	No	No	No	No
5e	No	Yes	Yes	Yes	No	No	No
5f	No	No	Yes	No	No	No	No
13a	No	Yes	Yes	Yes	No	No	No
13b	No	No	Yes	No	No	No	No
13c	No	Yes	Yes	Yes	No	No	No
13d	No	Yes	Yes	Yes	No	No	No
13e	No	No	Yes	No	No	No	No
13f	No	No	Yes	No	No	No	No
17a	No	Yes	Yes	Yes	Yes	No	No
17b	No	No	Yes	No	No	No	No
19a	No	Yes	Yes	Yes	No	No	No
19b	No	No	Yes	No	No	No	No
22a	No	Yes	Yes	Yes	No	No	No
22b	No	No	No	No	No	No	No
27	No	Yes	Yes	Yes	No	No	No
31b	No	No	Yes	No	No	No	No
35b	No	No	Yes	No	No	No	No

Table 8S. pkCSM calculated excretion properties.

Mol	Total Clearance	Renal OCT2 substrate
5a	0.30	No
5b	0.54	No
5c	0.41	No
5d	0.56	No
5e	0.34	No
5f	0.53	No
13a	0.20	No
13b	0.31	No
13c	0.62	No
13d	0.60	No
13e	0.53	No
13f	0.49	No
17a	0.61	No
17b	0.31	No
19a	0.23	No
19b	0.53	No
22a	0.62	No
22b	0.64	No
27	0.27	No
31b	0.50	No
35b	0.63	No

Table 9S. pkCSM calculated toxicity properties.

Mol	AMES tox	Max. dose ^a	hERG I inhibitor	hERG II inhibitor	Oral Rat ^b	Oral Rat ^c	Hepato tox	Skin Sensitisation	T.Pyiformis tox	Minnow tox
5a	Yes	-0.96	No	No	2.23	1.54	No	No	0.74	1.56
5b	Yes	0.14	No	No	2.41	2.39	Yes	No	0.73	1.57
5c	Yes	-0.86	No	No	2.15	1.54	No	No	0.95	1.41
5d	Yes	0.13	No	No	2.35	2.38	Yes	No	0.95	1.48
5e	Yes	-0.88	No	No	2.11	1.50	No	No	0.98	1.44
5f	Yes	0.10	No	No	2.31	2.33	No	No	1.01	1.51
13a	No	0.04	No	No	2.55	1.15	Yes	No	0.33	1.07
13b	No	0.12	No	No	2.71	1.18	Yes	No	0.87	1.59
13c	Yes	-0.47	No	No	2.33	1.17	Yes	No	0.40	1.76
13d	Yes	-0.90	No	No	2.16	1.26	Yes	No	0.60	1.76
13e	Yes	0.22	No	No	2.30	1.27	Yes	No	0.47	1.76
13f	Yes	0.19	No	No	2.38	1.45	Yes	No	0.92	1.44
17a	Yes	-0.29	No	No	2.36	1.69	Yes	No	0.49	1.05
17b	No	0.15	No	No	2.66	1.20	Yes	No	0.74	1.52
19a	Yes	-0.84	No	No	2.17	1.28	Yes	No	0.53	1.69
19b	Yes	0.25	No	No	2.28	1.30	Yes	No	0.42	1.69
22a	Yes	-0.33	No	No	2.31	1.20	Yes	No	0.37	1.69
22b	Yes	0.57	No	No	2.57	1.29	Yes	No	0.32	1.69
27	Yes	-0.37	No	No	2.36	1.74	Yes	No	0.47	0.93
31b	Yes	0.33	No	No	2.37	2.34	Yes	No	0.31	1.64
35b	Yes	0.25	No	No	2.37	0.73	Yes	No	0.56	1.84

^a tolerated dose (human); ^b acute Toxicity (LD50); ^c Chronic Toxicity (LOAEL)

Table 10S. Data warrior calculated toxicity properties.

Mol	Mutagenic	Tumorigenic	Reproductive Effective	Irritant
5a	none	none	none	none
5b	none	none	none	none
5c	none	none	none	none
5d	none	none	none	none
5e	none	none	none	none
5f	none	none	none	none
13a	none	none	none	none
13b	none	none	none	none
13c	none	none	low	none
13d	none	none	none	none
13e	none	none	none	none
13f	none	none	none	none
17a	none	none	low	none
17b	none	none	none	none
19a	none	none	none	none
19b	none	none	none	none
22a	none	none	low	none
22b	none	none	low	none
27	none	none	none	none
31b	none	none	none	none
35b	none	none	none	none

Table 11S. Preadmet calculated toxicity properties.

	Ames_test	Carcino_Mouse	Carcino_Rat	hERG_inhibition	TA100_10RLI _a	TA100_NA _b	TA1535_10RLI _c	TA1535_NA _d
5a	mutagen	negative	negative	medium_risk	positive	positive	negative	positive
5b	mutagen	negative	negative	medium_risk	positive	positive	positive	positive
5c	mutagen	negative	negative	medium_risk	positive	positive	negative	positive
5d	mutagen	negative	negative	medium_risk	positive	positive	positive	positive
5e	mutagen	negative	negative	medium_risk	positive	positive	negative	positive
5f	mutagen	negative	negative	medium_risk	positive	positive	positive	positive
13a	mutagen	positive	negative	medium_risk	negative	negative	positive	negative
13b	mutagen	positive	negative	low_risk	positive	negative	positive	positive
13c	mutagen	negative	negative	medium_risk	positive	positive	negative	negative
13d	mutagen	negative	negative	medium_risk	positive	positive	negative	positive
13e	mutagen	negative	negative	low_risk	positive	positive	positive	positive
13f	mutagen	negative	positive	low_risk	positive	positive	positive	positive
17a	mutagen	negative	negative	medium_risk	positive	positive	negative	negative
17b	mutagen	negative	negative	low_risk	positive	negative	positive	positive
19a	mutagen	negative	negative	medium_risk	positive	positive	negative	positive
19b	mutagen	negative	negative	low_risk	positive	positive	positive	positive
22a	mutagen	negative	negative	medium_risk	positive	positive	negative	negative
22b	mutagen	negative	negative	low_risk	positive	positive	positive	positive
27	mutagen	negative	negative	medium_risk	positive	positive	negative	negative
31b	mutagen	negative	negative	medium_risk	positive	negative	positive	positive
35b	mutagen	negative	negative	low_risk	positive	positive	positive	positive

a. in vitro Ames test result in TA100 strain (Metabolic activation by rat liver homogenate)

b. in vitro Ames test result in TA100 strain (No metabolic activation)**Error! Not a valid link.** in vitro Ames test result in TA1535 strain (Metabolic activation by rat liver homogenate)

c. in vitro Ames test result in TA1535 strain (No metabolic activation)



***B. Study of anti-inflammatory activity of FPR1/2
agonists***

Supervisor: Prof. Mark T. Quinn

Table of Contents

1. FPR receptors	154
1.1. Physiological roles of FPR receptors	155
1.2. Pathophysiologies associated with FPR	156
2. Background and aims of the work	158
3. Result and discussion	160

1. FPR receptors

Formyl peptide receptors (FPRs) belong to the inhibitory G-protein-coupled receptor (GPCR) family and present a seven-transmembrane domain [Simon, M. I. et al., 1991]. They play a key role in leukocyte activation and chemotaxis, and were initially identified for their ability to be activated by N-formylated peptides produced by bacteria, or released from damaged mitochondria [Carp, H., 1982]. In humans, three genes for three different receptor subtypes have been identified so far: FPR1, FPR2 and FPR3 [Perez H. D. et al., 1992].

FPR1 was the first to be identified and cloned from HL-60 differentiated leukemic myeloid cells. The agonist prototype of this receptor is the natural tripeptide derived from *Escherichia Coli* N-formyl-methionine-leucine-phenylalanine (fMLF), which binds FPR1 with high affinity ($K_d < 1$ nM) [Boulay, F. et al., 1990a; Boulay, F. et al., 1990b].

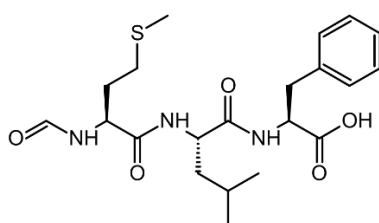


Figure 1. fMLF structure.

Activation of FPR1 results in a directional movement of neutrophils, and, at higher concentrations of the endogenous ligand, bactericidal functions can also be stimulated [Le, Y. et al., 2002]. Phosphorylation of the receptor after ligand binding results in a conformational change leading to interaction with the G_i protein and causing dissociation of the $\beta\gamma$ subunit from the α one. This triggers the activation of various mediators leading to a cascade of signals involved in regulating cellular functions such as chemotaxis, degranulation, superoxide production and the release of inflammatory mediators [Stoyanov, B. et al., 1995]. Activated inflammatory mediators include ERK1/2 and MAPKs [Ma, Y. C. et al., 2000].

FPR2 has a homology of 69% with FPR1, but it shows low affinity for fMLF. Furthermore, it is the target of specific pro-resolving mediators (SPMs) such as protectins, maresins, resolvins and lipoxins, which are crucial for the inflammatory resolution [Crocetti, L. et al., 2020]. Differently from FPR1, FPR2 is an atypical GPCR due to its ability to activate pro-inflammatory, anti-inflammatory and pro-resolution pathways, depending on the type of ligand [Cooray, S. N. et al., 2013]. In terms of anti-inflammatory activity, it induces leukocyte inactivation and detachment, leukocyte apoptosis, increased phagocytosis of apoptotic cells by phagocytes and regulation of COX2 [El Khebir, D. et al., 2007].

Despite the high homology of FPR1 and FPR2, there is a fundamental difference between the two receptors: FPR2 induces a potent cADPR-dependent calcium release from extracellular storages,

while FPR1 uses endoplasmic reticulum deposits to mobilize calcium ion, and, additionally, this mechanism is independent from cADPR [Partida-Sánchez, S. et al., 2004].

Finally, FPR3 has been identified with a homology of 56% to FPR1 and 83% to FPR2. It does not bind N-formylated peptides, but is capable of binding fMMYALF with an EC₅₀ in the micromolar range [Ye, R. D. et al., 2009].

The FPR receptor class is highly susceptible to the phenomenon of desensitization, a process which makes the receptors unresponsive to further stimulations. There are three types of desensitization: homologous, heterologous and cross-desensitization. In 1991, Didsbury and co-workers [Didsbury, J. R. et al., 1991] studied this mechanism on human neutrophils expressing the three isoforms of FPRs, C5a, and α_1 -adrenergic receptors upon stimulation with their respective agonists, and they were able to observe all three types of desensitization. After receptor desensitization, downregulation of the receptor-G-protein complex first and finally internalization of the receptor occurs.

As regard the distribution of FPR receptors, FPR1 is expressed in both monocytes and neutrophils [He, H. Q. et al., 2017], but also in non-phagocytic cells such as astrocytes, microglial cells, hepatocytes, platelets, and immature dendritic cells [Kirpotina, L. N. et al., 2010].

FPR2 has a similar distribution to FPR1, whereas FPR3 is found in monocytes and both immature and mature dendritic cells, but not in neutrophils [Migeotte, I. et al., 2005].

Receptor	Cells/Tissues
FPR1	Monocytes/Macrophages, Neutrophils, Immature Dendritic Cells, Endothelial Cells, Platelets, Hepatocytes, Astrocytes, Microglia Cells, Fibroblasts, Vascular Smooth Muscle Cells, Thyroid, Adrenal Glands, CNS/ANS, Ovaries, Liver, Spleen, Lungs, Heart, Uterus, Placenta, Kidney, Eye, Stomach, Colon, Bone Marrow.
FPR2	Monocytes/Macrophages, Neutrophils, Immature Dendritic Cells, Endothelial Cells, Epithelial Cells, T/B Lymphocytes, Hepatocytes, Astrocytes, Microglia Cells, Fibroblasts, Brain, Spleen, Lungs, Placenta, Bone Marrow.
FPR3	Monocytes/Macrophages, Immature and Mature Dendritic Cells, Spleen, Placenta, Lymph Nodes, Trachea, Liver, Adrenal Glands, Small Intestine.

1.1. Physiological roles of FPR receptors

Chemotaxis: FPR1 was the first receptor identified to have chemotactic properties, and upon binding to fMLF induces a directional movement of neutrophils toward the site of inflammation [Ali, H. et al. 1999].

Degranulation: Through interaction with endogenous agonists, FPR receptors induce the release of neutrophil granule contents. This phenomenon is followed by several effects, including proteolytic

cleavage of adhesion molecules present on the membrane, expression of new adhesion molecules on the cell surface, and also release of pro-inflammatory enzymes and proteins that result in tissue degradation and death of invading microorganisms [Nauseef, W. M. et al., 2007]. FPR-induced degranulation involves diacylglycerol (DAG), PKC, and calcium [Smith, R. J. et al., 1998], even if fMLF agonist has been reported to induce degranulation also in a Ca^{2+} flux-independent manner, suggesting the presence of alternative pathways.

Superoxide production: high concentrations of fMLF (50-100 nM) result in the production of superoxide species; this process is related to the activation of NADPH oxidase, which is present in neutrophils, eosinophils, and mononuclear phagocytes, and catalyzes the formation of O_2^- from O_2 and NADPH [Babior, B. M. et al., 2002].

Neutrophil apoptosis: some studies have shown that stimulation of neutrophils by fMLF promotes apoptosis via superoxide production, while cytokines such as G-CSF and IL-1 prolong their life span [Kettritz, R. et al., 1997]. Programmed death induced by fMLF is linked to the process of resolution of inflammation (RoI), and data to date confirm the central role of FPRs in this mechanism.

Regulation of transcription: another role of fMLF is to induce transcriptional regulation in neutrophils, and modulate the subsequent production of cytokines. An example is IL-8 that is produced after agonist FPR induction accompanied by activation of the NF- κ B pathway [Dorward, D. A. et al., 2015].

1.2. Pathophysiologies associated with FPR

- *Inflammation*

AnxA1 is a glucocorticoid-regulated protein and possesses either pro- or anti-inflammatory activity, partially mediated by FPR1 [Ernst, S. et al., 2004]: it is mainly located in the cytosol, but can also be released through a non-classical secretion, and expressed on the outer cell surface, causing leukocytes to detach and, thus, inhibiting their trans-endothelial migration. Annexin A1 is particularly abundant in neutrophils, where it causes desensitization and inhibition of migration at low concentrations, while at higher concentrations it becomes a potent pro-inflammatory stimulant [Perretti, M., 2003]. It also appears that AnxA1 triggers the expression of FPR2 in T cells, where it is not normally found [Dufton, N. et al., 2010].

Further studies have shown that this peptide is also capable of anti-inflammatory action through activation of FPR2 and FPR3 receptors [Solito, E. et al., 2003].

LXA4 is a lipid molecule synthesized from arachidonic acid, and released during the inflammatory processes, wherein it acts as a potent mediator via activation of FPR2 [Ye, R. D. et al., 2009].

Finally, another important FPRs agonist is serum amyloid A protein (SAA), produced in response to cytokine release by activated monocytes. It is a plasma protein that under normal conditions is present in serum at low concentrations, but increases after trauma, acute infection, and various other physiological stressors, resulting in a response during the acute phase of inflammation. SAA, acting

through the FPR2 receptor, promotes chemotaxis of monocytes, neutrophils, mast cells, and T lymphocytes; furthermore, in neutrophils it also stimulates IL-8 secretion through FPR2 [He, R. et al., 2003].

- *Angiogenesis*

Angiogenesis is a phenomenon that leads to the development of new blood vessels from existing ones, and is fundamental in many physiological and pathological processes. In fact, as a result of tissue damage or infection there is an increase in vascular permeability followed by an increase in the angiogenic activity. Moreover, angiogenesis is involved in chronic inflammatory diseases, such as rheumatoid arthritis or Chron's disease [Schafer, M. et al., 2008].

There are numerous studies highlighting the involvement of FPRs in the angiogenic response related to inflammation and the resolution phase of inflammation [Cerimele, F. et al., 2003]; for example, the peptide fragment LL-37, through the binding with FPR2, promotes neovascularization acting directly on endothelial cells [Koczulla, R. et al., 2003]. The effect of FPR receptors changes from pro- to anti-angiogenic depending on the tissue or mediators involved in the inflammation.

- *Antimicrobial activity*

FPR receptors are important in the host defense against pathogenic microorganisms, and this is supported by the fact that bacteria are the main biological source of formylated peptides [Partida-Sánchez, S. et al., 2001]. As a result of bacterial infection, host-produced antimicrobial peptides, such as LL-37, able to activate human neutrophils, monocytes, and T cells by binding to FPR2, may also be released [Yang, D. et al., 2000].

- *Nociception*

The involvement of FPR receptors in pain transmission has also been demonstrated; it has been observed that both central and peripheral FPRs are involved in the anti-nociceptive effect induced by some FPR ligands such as AnxA1 fragments [Pieretti, S. et al., 2004].

In other studies, it has been shown that some agonists of formylated peptide receptors are able to trigger the neutrophil release of opioid peptides, and confirmed y the observation that in vivo blockade of FPR receptors determines an increase in inflammatory-type pain [Stein, C. et al., 2003].

2. Background and aims of the work

Our research group has been synthesizing for a long time formyl peptide receptors (FPRs) agonist with pyridazinone scaffold, obtaining interesting results for activity and selectivity [Cilibrizzi, A. et al., 2009]. Recently, in vivo tests on animal model of rheumatoid arthritis have highlighted the powerful anti-inflammatory effect of our new compounds, strongly reducing the pain hypersensitivity of the treated animals versus control rats [Crocetti, L. et al., 2020].

On the other hand, many pyridazinone derivatives are known to exhibit an anti-inflammatory effect, as widely documented in the literature, by interacting with different targets. Amhed, E. M. et al. recently published pyridazinones as selective cyclooxygenase 2 (COX2) inhibitors [Ahmed, E. M. et al., 2019]; Elagawany, M, et al. synthesised new inhibitor of DYRK1A and GSK3 with pyridazinone scaffold [Elagawany, M., 2013], while Wakulik, K. et al. showed how pyridazinone derivatives are able to inhibit LPS-induced neuroinflammation [Wakulik, K. et al., 2020]; Merk GMBH used macrocyclic pyridazinone derivatives as interleukin-1 receptor-associated kinase 4 (IRAK4) inhibitors [Jorand-Lebrun, C. et al., 2014a], [Jorand-Lebrun, C. et al., 2014b].

Thus, taking into account our experience on FPR agonists and the valuable information reported in the literature, we planned a 3-phase project:

1. selection of several formylated peptide receptor (FPRs) agonists with a pyridazine-like structure and anti-inflammatory activity previously published by our research group;
2. an extensive research on the anti-inflammatory activity of pyridazinone derivatives reported in the literature to identify one or more likely targets for our compounds;
3. research for another possible anti-inflammatory effect for selected products not related to the formylated peptide receptor signaling pathway (FPRs).

Schematically:

- a) we selected a library of 179 molecules (some compounds have been re-synthesized during this work to perform the below tests), which were firstly screened using a cell-based approach, stimulating the cells with LPS, a major constituent of the Gram-negative outer membrane, and activating the NF- κ B pathway [Mazgaeen, L. et al., 2020], [Barnes, P. J. et al., 1997]. This first step allowed us to identify 48 compounds endowed with a certain activity which were further reduced to 24 terms (the most interesting);
- b) The selected 26 compounds have been evaluated as inhibitor of IL-6 production in macrophage/monocyte cells through ELISA assay, allowing us to further reduce the number of promising products to 2;
- c) finally, the selected 2 compounds were tested on a panel of 97 kinases.

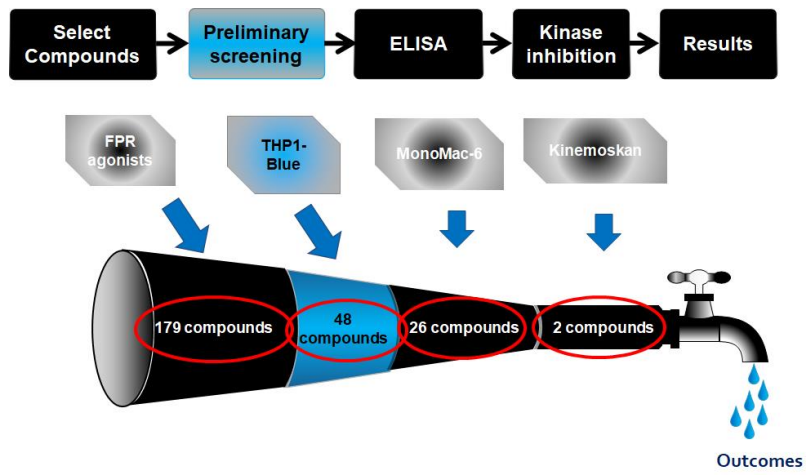


Figure 2. Rational scheme of the process.

3. Result and discussion

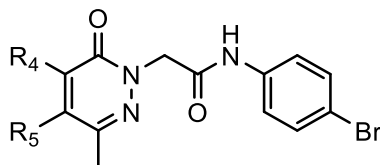
A library of 179 compounds, previously investigated as FPR1/2 agonists, were evaluated on LPS-stimulated NF- κ B/AP-1 pathway on monocytic THP-1Blue cells, using alkaline phosphatase as a marker, in order to highlight their anti-inflammatory activity. These derivatives included compounds with different scaffolds: pyridazinone (**1-120**, series **A1-A4**), 4,5-dihydro-pyridazinone (**121-132**, series **B**), indole (**133, 134**, series **C**), pyridazine (**135-138**, series **D**), 2-pyridinone (**139-148**, series **E**), 2,6-pyridindione (**149-155**, series **F**), pyrazole and pyrazolone (**156-166**, series **G**), thiazol-2-one (**167-175**, series **H**) and 4 bicyclic compounds (**176-179**, series **I**) [Cilibrizzi, A. et al. 2009], [Cilibrizzi, A. et al. 2012], [Crocetti, L. et al. 2013], [Giovannoni, M. P. et al. 2013], [Vergelli, C. et al. 2016], [Vergelli, C. et al. 2017], [Crocetti, L. et al. 2020]. The structures and the FPR1/2 activity are reported in **Table 1**, while anti-inflammatory activity and toxicity on THP-1 Blue cells are reported in **Table 2**.

Table 1. FPR1/2 activity of the selected compounds.

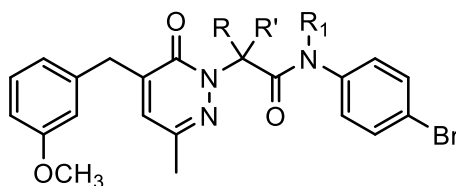
A1. Pyridazinone						
N°	Compound	R	R ₄	R ₆	FPR1-HL60 ^b EC ₅₀ (μM)	FPR2-HL60 ^b EC ₅₀ (μM)
1	AC42	p-Br-Ph	m-(OCH ₃)-Bn	CH ₃	3.4	3.8
2	AC50	m-Br-Ph	m-(OCH ₃)-Bn	CH ₃	N.A. ^a	N.A. ^a
3	AC51	o-Br-Ph	m-(OCH ₃)-Bn	CH ₃	N.A. ^a	N.A. ^a
4	AC52	p-Cl-Ph	m-(OCH ₃)-Bn	CH ₃	2.6	4.0
5	AC53	p-NO ₂ -Ph	m-(OCH ₃)-Bn	CH ₃	10.5	12.3
6	AC55	p,m-(OCH ₃)-Ph	m-(OCH ₃)-Bn	CH ₃	15.5	16.8
7	AC56	p-CF ₃ -Ph	m-(OCH ₃)-Bn	CH ₃	5.7	8.8
8	AC62	p-Br-Ph	m-(OCH ₃)-Bn	Ph	9.0	4.3
9	AC64	p-Br-Ph	CH ₂ -3-thienyl	CH ₃	4.5	14.1
10	AC65	p-Br-Ph	m-(OCH ₃)-Bn	iPr	4.5	7.2
11	AC66	p-Br-Ph	CH ₂ -2-thienyl	CH ₃	8.1	11.4
12	AC67	p-Br-Ph	m-(OCH ₃)-Bn	H	6.1	7.7
13	AC69	p-Br-Ph	CH ₂ -1-naphtyl	CH ₃	13.8	N.A. ^a
14	AC78	p-(tBu)-Ph	m-(OCH ₃)-Bn	CH ₃	N.A. ^a	N.A. ^a
15	AC80	p-F-Ph	m-(OCH ₃)-Bn	CH ₃	7.6	N.A. ^a
16	AC85	Ph	m-(OCH ₃)-Bn	CH ₃	N.A. ^a	N.A. ^a
17	AC86	p-CN-Ph	m-(OCH ₃)-Bn	CH ₃	N.A. ^a	N.A. ^a
18	AC87	p-Br-Ph	m-(OCH ₃)-Bn	C ₆ H ₁₁	10.8	N.A. ^a
19	AC88	p-Br-Ph	p-(OCH ₃)-Ph	CH ₃	11.2	N.A. ^a
20	AC89	p-I-Ph	m-(OCH ₃)-Bn	Et	4.2	5.5
21	AC90	p-I-Ph	p-(SCH ₃)-Bn	CH ₃	2.3	9.4
22	AC91	p-I-Ph	m,m-(OCH ₃)-Bn	CH ₃	7.6	N.A. ^a
23	AC92	p-I-Ph	m-Cl-Bn	CH ₃	9.5	16.9
24	AC95	p-(SCH ₃)-Ph	m-(OCH ₃)-Bn	CH ₃	2.2	8.2
25	AC96	p-I-Ph	H	CH ₃	N.A. ^a	N.A. ^a
26	AC97	p-Br-Ph	NH ₂	CH ₃	8.1	29.4
27	AC98	p-Br-Ph	NHCO-p-Br-Ph	CH ₃	N.A. ^a	N.A. ^a
28	AC101	p-F-Ph	H	C ₆ H ₁₁	N.A. ^a	N.A. ^a
29	AC102	p-F-Ph	Bn	CH ₃	N.A. ^a	N.A. ^a
30	AC103	p-Br-Ph	Bn	CH ₃	5.5	11.6
31	AC104	5-benzod[1,3]dioxole	H	C ₆ H ₁₁	N.A. ^a	N.A. ^a
32	AC105	5-benzod[1,3]dioxole	Bn	CH ₃	6.9	N.A. ^a
33	AC106	5-benzod[1,3]dioxole	m-(OCH ₃)-Bn	Ph	N.A. ^a	N.A. ^a
34	AC107	p-F-Ph	m-(OCH ₃)-Bn	Ph	N.A. ^a	N.A. ^a
35	AC108	5-benzod[1,3]dioxole	m-(OCH ₃)-Bn	2-thienyl	N.A. ^a	N.A. ^a
36	AC109	p-F-Ph	m-(OCH ₃)-Bn	2-thienyl	N.A. ^a	N.A. ^a

37	AC110	p-Br-Ph	p-(OCH ₃)-Bn	2-thienyl	N.A. ^a	N.A. ^a
38	AC111	p-F-Ph	m-(OCH ₃)-Bn	p-(OCH ₃)-Ph	N.A. ^a	N.A. ^a
39	AC112	5-benzod[1,3]dioxole	m-(OCH ₃)-Bn	p-(OCH ₃)-Ph	N.A. ^a	N.A. ^a
40	AC113	p-Br-Ph	p-(OCH ₃)-Bn	p-(OCH ₃)-Ph	N.A. ^a	N.A. ^a
41	AC114	p-Br-Ph	p-(OCH ₃)-Bn	p-Cl-Ph	N.A. ^a	N.A. ^a
42	AC115	p-F-Ph	m-(OCH ₃)-Bn	p-Cl-Ph	N.A. ^a	N.A. ^a
43	AC116	5-benzod[1,3]dioxole	m-(OCH ₃)-Bn	p-Cl-Ph	N.A. ^a	N.A. ^a
44	AC121	p-Br-Ph	p-(OCH ₃)-Bn	p-CH ₃ -Ph	N.A. ^a	N.A. ^a
45	AC122	5-benzod[1,3]dioxole	m-(OCH ₃)-Bn	p-CH ₃ -Ph	N.A. ^a	N.A. ^a
46	AC123	p-F-Ph	m-(OCH ₃)-Bn	p-CH ₃ -Ph	N.A. ^a	N.A. ^a
47	AC124	p-F-Ph	m-(OCH ₃)-Bn	p-F-Ph	N.A. ^a	N.A. ^a
48	AC125	5-benzod[1,3]dioxole	m-(OCH ₃)-Bn	p-F-Ph	N.A. ^a	N.A. ^a
49	AC126	p-Br-Ph	p-(OCH ₃)-Bn	p-F-Ph	N.A. ^a	N.A. ^a
50	AC136	p-Br-Ph	N(p-(OCH ₃)-Ph) ₂	CH ₃	N.A. ^a	N.A. ^a
51	AC141	p-Br-Ph	NH-p-(OCH ₃)-Ph	CH ₃	12.8	7.8
52	AC144	p-Br-Ph	NHCO-m-(OCH ₃)-Ph	CH ₃	9.3	2.8
53	AC147	p-Br-Ph	CO-m-(OCH ₃)-Ph	CH ₃	3.0	1.0
54	AC152	p-Br-Ph	p-(OCH ₃)-Bn	Bn	N.A. ^a	N.A. ^a
55	SZ1	p-Br-Ph	m-Br-Bn	CH ₃	N.A. ^a	N.A. ^a
56	SZ2	p-Br-Ph	m,m-(OCH ₃)-Bn	CH ₃	N.A. ^a	N.A. ^a
57	SZ3	p-F-Ph	CH ₃	Ph	N.A. ^a	N.A. ^a
58	SZ5	p-Br-Ph	p-(SCH ₃)-Bn	CH ₃	N.A. ^a	N.A. ^a
59	SZ6	p-Br-Ph	CH ₂ -3-furyl	CH ₃	5.8	6.3
60	SZ7	p-Br-Ph	CH ₂ -3-Pyridyl	CH ₃	9.3	2.8
61	SZ8	p-Br-Ph	p-Bn-CONH-(p-Br-Ph)	CH ₃	N.A. ^a	N.A. ^a
62	SZ9	p-Br-Ph	p-(CONH ₂)-Bn	CH ₃	29.3	27.2
63	SZ10	p-Br-Ph	p-CN-Bn	CH ₃	N.A. ^a	N.A. ^a
64	SZ11	p-Br-Ph	m-F-Bn	CH ₃	6.6	N.A. ^a
65	SZ12	p-Br-Ph	m-Cl-Bn	CH ₃	10.5	N.A. ^a
66	SZ13	p-Br-Ph	p-CF ₃ -Bn	CH ₃	N.A. ^a	N.A. ^a
67	SZ14	p-Br-Ph	CH ₃	Ph	21.5	10.1

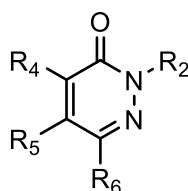
A2. Pyridazinone



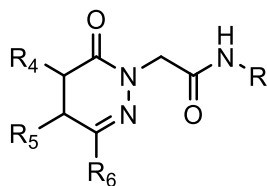
N°	Compound	R ₄	R ₅	FPR1-HL60 ^b EC ₅₀ (μM)	FPR2-HL60 ^b EC ₅₀ (μM)
68	EC2	H	CH ₃	5.7	0.51
69	EC3	m-(OCH ₃)-Bn	CH ₃	0.019	0.043
70	EC7	H	Ph	N.A. ^a	0.15
71	EC8	m-(OCH ₃)-Bn	Ph	2.2	N.A. ^a
72	EC9	NH ₂	CO(CH ₂) ₂ -N(CH ₃) ₂	5.1	5.7
73	EC10	NH-m-(OCH ₃)-Ph	Ac	0.045	0.17
74	EC11	NH ₂	m-Pirazole	8.4	13.5
75	EC12	NH ₂	1-CH ₃ -3-Pyrazole	2.9	1.9
76	EC13	NH-m-(OCH ₃)-Ph	1-CH ₃ -3-Pyrazole	3.6	0.59
77	EC14	NH-p-(OCH ₃)-Ph	1-CH ₃ -3-Pyrazole	4.0	0.035
78	SF1	m-(OCH ₃)-Bn	Et	3.2	1.9
79	SF2	m-(OCH ₃)-Bn	nPr	2.2	4.6
80	SF3	m-(OCH ₃)-Bn	nBu	N.A. ^a	15.7
81	MT1	NH-m-(OCH ₃)-Ph	nBu	3.6	4.5
82	MT5	NH-m-(OCH ₃)-Ph	H	0.24	9.6
83	MT7	NH-m-(OCH ₃)-Ph	nPr	N.A. ^a	N.A. ^a

A3. Pyridazinone


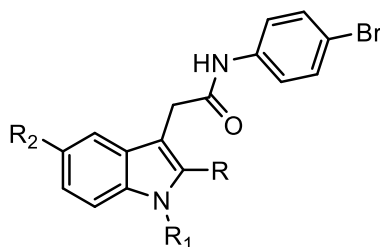
N°	Compound	R	R'	R ₁	FPR1-HL60 ^b EC ₅₀ (μM)	FPR2-HL60 ^b EC ₅₀ (μM)
84	AC75	CH ₃	H	H	3.2 ± 1.5	N.A. ^a
85	AC76	H	H	CH ₃	N.A. ^a	N.A. ^a
86	R(-)-AC99	CH ₃	H	H	8.5	10.2
87	S(+)-AC100	CH ₃	H	H	3.2	16.1
88	AC117	Et	H	H	1.3	2.2
89	AC118	CH ₃	CH ₃	H	6.3	20.4
90	AC128	Et	CH ₃	H	1.5	2.1
91	AC130	nPr	H	H	2.8	3.6
92	AC131	iPr	H	H	2.0	6.5
93	AC132	nBu	H	H	1.1	0.1
94	R(-)-AC134	Et	H	H	2.8	2.3
95	S(+)-AC135	Et	H	H	13.4	22.2
96	R(-)-AC137	iPr	H	H	9.4	5.4
97	S(+)-AC138	iPr	H	H	N.A. ^a	N.A. ^a
98	R(-)-AC139	nPr	H	H	3.0	0.84
99	S(+)-AC140	nPr	H	H	N.A. ^a	N.A. ^a
100	R(-)-AC142	nBu	H	H	0.5	0.089
101	S(+)-AC143	nBu	H	H	20.8	7.0
102	R(-)-AC145	Et	CH ₃	H	4.5	13.7
103	S(+)-AC146	Et	CH ₃	H	7.0	N.A. ^a
104	SZ20	Ph	H	H	3.1	1.8

A4. Pyridazinone


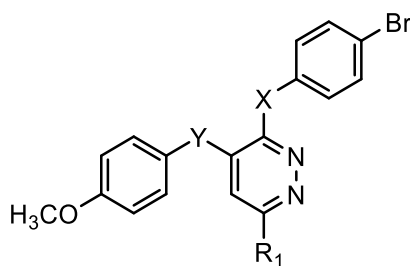
N°	Compound	R ₂	R ₄	R ₅	R ₆	FPR1-HL60 ^b EC ₅₀ (μM)	FPR2-HL60 ^b EC ₅₀ (μM)
105	AC45	p-(OCH ₃)-Bn	Cl	p-(OBu)-Ph	H	N.A. ^a	N.A. ^a
106	AC46	Ph	NH-p-(OBu)-Ph	H	CH ₃	N.A. ^a	N.A. ^a
107	AC47	m-(OCH ₃)-Bn	Cl	p-(OBu)-Ph	H	N.A. ^a	N.A. ^a
108	AC48	m-(OCH ₃)-Bn	p-(OBu)-Ph	OCH ₃	H	N.A. ^a	N.A. ^a
109	AC49	p-(OCH ₃)-Bn	p-(OBu)-Ph	OCH ₃	H	N.A. ^a	N.A. ^a
110	AC54	CH ₂ CO-N-(CH ₃)-Piperazine	m-(OCH ₃)-Bn	H	CH ₃	N.A. ^a	N.A. ^a
111	AC57	(CH ₂) ₂ CONH-p-Br-Ph	m-(OCH ₃)-Bn	H	CH ₃	9.7	5.4
112	AC74	CH ₂ COO-p-Br-Ph	m-(OCH ₃)-Bn	H	CH ₃	N.A. ^a	N.A. ^a
113	AC77	(CH ₂) ₂ NHCONH-p-Br-Ph	m-(OCH ₃)-Bn	H	CH ₃	N.A. ^a	N.A. ^a
114	AC79	(CH ₂) ₂ NHCO-p-Br-Ph	m-(OCH ₃)-Bn	H	CH ₃	N.A. ^a	N.A. ^a
115	AC81	m-(OCH ₃)-Bn	NHCONH-p-Br-Ph	H	CH ₃	N.A. ^a	N.A. ^a
116	AC82	CH ₂ NHCO-p-Br-Ph	m-(OCH ₃)-Bn	H	CH ₃	N.A. ^a	N.A. ^a
117	AC83	m-(OCH ₃)-Bn	NHCO-p-Br-Ph	H	CH ₃	N.A. ^a	N.A. ^a
118	AC84	CH ₂ NHCONH-p-Br-Ph	m-(OCH ₃)-Bn	H	CH ₃	N.A. ^a	N.A. ^a
119	AC127	CH ₂ -CS-NH-p-Br-Ph	m-(OCH ₃)-Bn	H	CH ₃	N.A. ^a	N.A. ^a
120	AC129	CH ₂ CONH-p-Br-Ph	NH-p-(OCH ₃)-Ph	Ac	CH ₃	13.5	1.7

B. 4,5-Dihydro-pyridazinone


N°	Compound	R	R ₄	R ₅	R ₆	FPR1-HL60 ^b EC ₅₀ (μM)	FPR2-HL60 ^b EC ₅₀ (μM)
121	AC93	p-I-Ph	H	H	CH ₃	N.A. ^a	N.A. ^a
122	AC119	p-F-Ph	CH ₃	H	Ph	N.A. ^a	N.A. ^a
123	AC120	5-benzo[d][1,3]dioxole	CH ₃	H	Ph	N.A. ^a	N.A. ^a
124	S(-)-AC156	p-Br-Ph	CH ₃	H	Ph	19.5	10.7
125	R(+)-AC157	p-Br-Ph	CH ₃	H	Ph	24.4	10.0
126	R(+)-AC158	p-F-Ph	CH ₃	H	Ph	N.A. ^a	N.A. ^a
127	S(-)-AC159	p-F-Ph	CH ₃	H	Ph	N.A. ^a	N.A. ^a
128	R(+)-AC160	5-benzo[d][1,3]dioxole	CH ₃	H	Ph	N.A. ^a	N.A. ^a
129	S(-)-AC161	5-benzo[d][1,3]dioxole	CH ₃	H	Ph	N.A. ^a	N.A. ^a
130	SZ15	p-Br-Ph	CH ₃	H	Ph	23.5	7.0
131	EC1	p-Br-Ph	H	CH ₃	CH ₃	13.0	2.6
132	EC6	p-Br-Ph	H	Ph	CH ₃	4.1	0.63

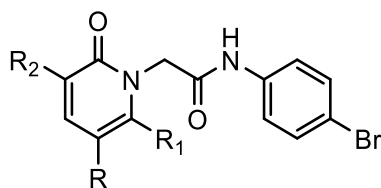
C. Indole


N°	Compound	R	R ₁	R ₂	FPR1-HL60 ^b EC ₅₀ (μM)	FPR2-HL60 ^b EC ₅₀ (μM)
133	SZ18	CH ₃	CO-p-Cl-Ph	OCH ₃	N.A. ^a	N.A. ^a
134	SZ19	H	m-(OCH ₃)-Bn	H	N.A. ^a	N.A. ^a

D. Pyridazine


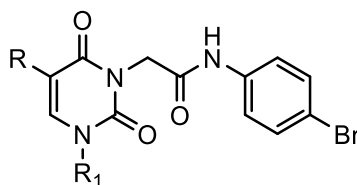
N°	Compound	X	Y	R ₁	FPR1-HL60 ^b EC ₅₀ (μM)	FPR2-HL60 ^b EC ₅₀ (μM)
135	AC153	NHCONH	O	Ph	N.A. ^a	N.A. ^a
136	AC154	NHCO	O	Ph	N.A. ^a	N.A. ^a
137	AC155	NHCH ₂ CONH	O	Ph	N.A. ^a	N.A. ^a
138	AC133	SCH ₂ CONH	CH ₂	CH ₃	N.A. ^a	N.A. ^a

E. 2-Pyridinone



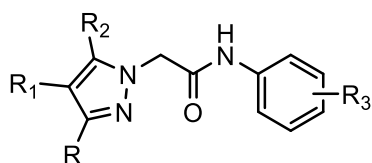
N°	Compound	R	R ₁	R ₂	FPR1-HL60 ^b EC ₅₀ (μM)	FPR2-HL60 ^b EC ₅₀ (μM)
139	AMC1	4-Pyridyl	H	NH ₂	N.A.	N.A.
140	AMC2	m,p-(OCH ₃)-Ph	CH ₃	CN	33.2	0.60
141	AMC3	m-(OCH ₃)-Ph	CH ₃	CN	1.6	0.12
142	AMC4	COOEt	CH ₃	CN	3.0	0.38
143	AMC5	p-(OCH ₃)-Ph	CH ₃	CN	1.6	0.12
144	AMC6	COOEt	CH ₃	CONH-m-(OCH ₃)-Ph	0.4	28.9
145	AMC7	COOEt	CH ₃	CONH-p-(OCH ₃)-Ph	7.9	16.4
146	AMC8	4-Pyridyl	CH ₃	CONH-m-(OCH ₃)-Ph	1.4	1.8
147	AMC9	CONH-m-(OCH ₃)-Ph	CH ₃	CN	3.9	0.31
148	AMC10	CONH-p-(OCH ₃)-Ph	CH ₃	CN	0.96	0.44

F. 2,6-Pyridindione

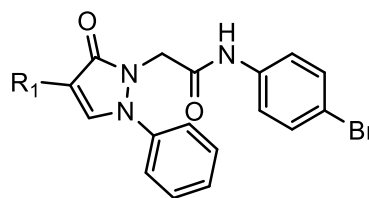


N°	Compound	R	R ₁	FPR1-HL60 ^b EC ₅₀ (μM)	FPR2-HL60 ^b EC ₅₀ (μM)
149	LS1	H	p-CH ₃ -Ph	13.6	14.9
150	LS2	H	m-(OCH ₃)-Ph	4.3	3.6
151	LS3	Ph	p-CH ₃ -Ph	N.A. ^a	N.A. ^a
152	LS4	H	nPr	5.5	4.1
153	LS5	H	Ph	12.5	8.9
154	LS6	m-Ph(OCH ₃)	nPr	3.3	2.4
155	LS7	CN	COO ⁱ Pr	7.7	8.4

G. Pyrazole and Pyrazolone



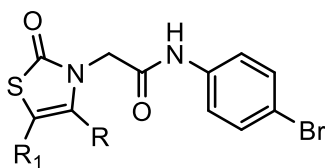
156-164



165-166

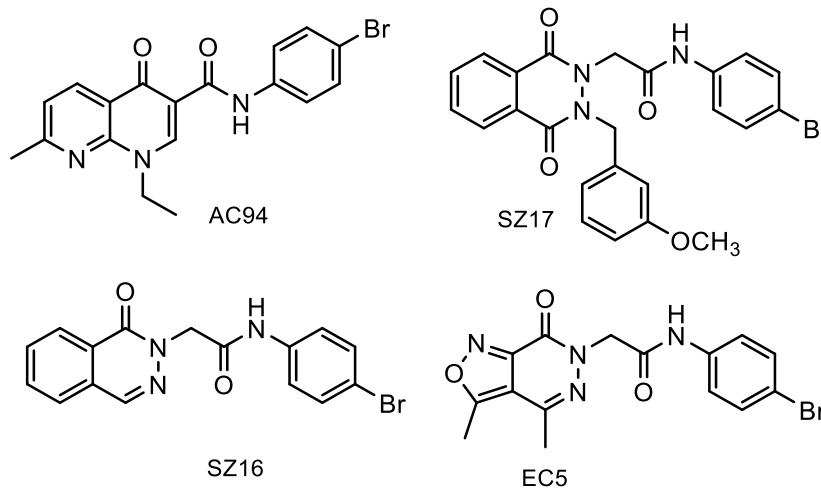
N°	Compound	R	R ₁	R ₂	R ₃	FPR1-HL60 ^b EC ₅₀ (μM)	FPR2-HL60 ^b EC ₅₀ (μM)
156	AN1	H	CN	NH-m-(OCH ₃)-Ph	4-Br	N.A. ^a	N.A. ^a
157	AN2	H	CN	NH-p-(OCH ₃)-Ph	4-Br	N.A. ^a	N.A. ^a
158	AN3	Ph	CH ₃	NH ₂	H	N.A. ^a	N.A. ^a
159	AN4	Ph	CH ₃	NH-m-(OCH ₃)-Ph	4-Br	N.A. ^a	N.A. ^a
160	AN5	Ph	CH ₃	NH-p-(OCH ₃)-Ph	4-Br	N.A. ^a	N.A. ^a
161	AN6	m-(OCH ₃)-Ph	CN	CH ₃	4-Br	8.2	4.8
162	AN7	p-(OCH ₃)-Ph	CN	CH ₃	4-Br	N.A. ^a	N.A. ^a
163	AN8	H	H	NH-m-(OCH ₃)-Ph	4-Br	0.7	28.3
164	AN10	CH ₃	H	OH	4-Br	2.1	39.8
165	AN9	-	H	-	-	42.0	22.8
166	AN11	-	NH-m-(OCH ₃)-Ph	-	-	29	N.A. ^a

H. Thiazol-2-one



N°	Compound	R	R ₁	FPR1-HL60 ^b EC ₅₀ (μM)	FPR2-HL60 ^b EC ₅₀ (μM)
167	ME1	Ph	H	1.8	2.1
168	ME2	m-(OCH ₃)-Ph	H	0.28	0.23
169	ME3	p-(OCH ₃)-Ph	H	2.6	1.8
170	ME4	p-Cl-Ph	H	2.8	2.4
171	ME5	p-NO ₂ -Ph	H	9.1	N.A.
172	ME6	m-Cl-Ph	H	6.0	3.0
173	ME7	p-NH ₂ -Ph	H	34.9	14.7
174	MT2	CH ₃	Ac	8.9	5.8
175	MT3	CH ₃	H	12.4	4.1

I. Bicyclic compounds



N°	Compounds	FPR1-HL60 ^b EC ₅₀ (μM)	FPR2-HL60 ^b EC ₅₀ (μM)
176	AC94	N.A. ^a	N.A. ^a
177	SZ17	N.A. ^a	N.A. ^a
178	SZ16	N.A. ^a	N.A. ^a
179	EC5	18.4	6.4

^aN.A.: No activity was observed at the highest tested concentration (50 μM). ^bEC₅₀ values represent the mean of three independent experiments and were determined by nonlinear regression analysis of the concentration-response curves (5-6 points) generated using GraphPad Prism 5 with 95% confidential interval (p < 0.05).

Among all 179 compounds tested on THP-1 Blue cells, only 48 resulted active with an IC₅₀ < 50 μM and are reported in **Table 2**; compounds **71** and **84** are the most potent showing IC₅₀ = 0.51 and 0.64 μM respectively and three products (**66**, **155** and **159**) showed toxicity.

From results obtained on THP-1 blue cells for active compounds, we can do some preliminary observations:

- For the pyridazinone derivatives (series A1-A4, **1-120**), we can observe that the N-(4-bromophenyl)-acetamide moiety is present in almost all active compounds (with the exception of **109** and **113**), but also some changes in this chain led to active compounds as shown by the activity of **2**, **5** and **15** (m-Br, p-NO₂ and p-F derivatives respectively) in comparison with the N-(4-bromophenyl)-acetamide corresponding derivative (compound **1**);

- the 3-methoxybenzyl group is present in many tested compounds, indicating its potential importance in the interaction with the target; but in some cases, little changes of this chain also led to active compounds as seen for **30**, where the methoxy was removed, or for **64** and **66**, where the same methoxy was replaced with a fluorine or a trifluoromethyl group;
- compounds **42**, **46** and **47** showing the N-(4-fluorophenyl)-acetamide moiety and a substituted phenyl at position 6, which, instead, was found to be negative for FPR activity, show an appreciable potency, in particular compounds **46** and **47**;
- position 5 of the pyridazinone scaffold is mostly unsubstituted in active compounds, but the insertion of an increasingly wider group led to an improved activity, as shown by compounds **69**, **78**, **79**, **80** and in particular **71** bearing a methyl, ethyl, n-propyl, n-butyl, and a phenyl respectively;
- the couples of enantiomers **94/95** and **102/103** showed a similar appreciable activity, thus demonstrating that the different chiral configuration doesn't affect the activity;
- among pyrazole derivatives (series **G**) **156-175** (the most part inactive as FPR agonists), some interesting compounds were found but the most potent compound (**159**, $IC_{50} = 8.77 \mu M$), resulted toxic.

Finally, compounds showing inactivity or $IC_{50} > 50 \mu M$ are the dihydro derivatives **121-132**, the bi-heterocyclics **176**, **177**, **178** and **179**), the indoles **133** and **134** and the pyridazines **135-138**.

Table 2. NF- κ B activation in THP1-blue cells and toxicity.

N°	Compounds	^a IC ₅₀ (μM)		^b EC ₅₀ (μM)	
		NF- κ B ^b	Toxicity	FPR1	FPR2
2	AC50	44.46 ± 2.53	N.T.	N.A. ^a	N.A. ^a
5	AC53	46.13 ± 1.03	N.T.	10.5	12.3
9	AC64	18.02 ± 0.69	N.T. ^b	4.5	14.1
10	AC65	22.03 ± 1.65	N.T. ^b	4.5	7.2
15	AC80	33.56 ± 2.05	N.T. ^b	7.6	N.A. ^a
23	AC92	7.12 ± 2.01	N.T. ^b	9.5	16.9
30	AC103	28.41 ± 5.70	N.T. ^b	5.5	11.6
38	AC111	19.59 ± 4.32	N.T. ^b	N.A. ^a	N.A. ^a
42	AC115	22.54 ± 2.31	N.T. ^b	N.A. ^a	N.A. ^a
46	AC123	8.21 ± 1.23	N.T. ^b	N.A. ^a	N.A. ^a
47	AC124	3.35 ± 0.23	N.T. ^b	N.A. ^a	N.A. ^a
49	AC126	34.52 ± 2.05	N.T. ^b	N.A. ^a	N.A. ^a
50	AC136	32.80 ± 0.71	N.T. ^b	N.A. ^a	N.A. ^a
64	SZ11	27.94 ± 2.1	N.T. ^b	6.6	N.A. ^a
66	SZ13	31.49 ± 2.18	26.41	N.A. ^a	N.A. ^a
67	SZ14	30.85 ± 2.27	N.T. ^b	21.5	10.1
69	EC3	34.50 ± 2.62	N.T. ^b	0.019	0.043
71	EC8	0.51 ± 0.11	N.T. ^b	2.2	N.A. ^a
78	SF1	20.7 ± 0.69	N.T. ^b	3.2	1.9
79	SF2	15.72 ± 1.35	N.T. ^b	2.2	4.6
80	SF3	15.02 ± 1.52	N.T. ^b	N.A. ^a	15.7
83	MT7	14.61 ± 1.44	N.T. ^b	N.A. ^a	N.A. ^a
84	AC75	0.64 ± 0.06	N.T. ^b	3.2	N.A. ^a
88	AC117	39.38 ± 4.15	N.T.	1.3	2.2
89	AC118	29.17 ± 1.03	N.T. ^b	6.3	20.4
90	AC128	39.24 ± 6.69	N.T. ^b	1.5	2.1
94	R(-)-AC134	30.79 ± 6.70	N.T. ^b	2.8	2.3
95	S(+)-AC135	12.085 ± 2.41	N.T. ^b	13.4	22.2
98	R(-)-AC139	10.57 ± 2.33	N.T. ^b	3.0	0.84
102	R(-)-AC145	22.07 ± 1.56	N.T. ^b	4.5	13.7
103	S(+)-AC146	16.62 ± 0.64	N.T. ^b	7.0	N.A. ^a
109	AC49	31.27 ± 1.61	N.T. ^b	N.A. ^a	N.A. ^a
113	AC77	36.99 ± 0.37	N.T. ^b	N.A. ^a	N.A. ^a
122	AC119	46.29 ± 2.41	N.T.	N.A. ^a	N.A. ^a
124	S(-)-AC156	42.73 ± 0.25	N.T.	19.5	10.7
125	R(+)-AC157	22.35 ± 0.69	N.T. ^b	24.4	10.0
141	AMC3	15.30 ± 4.92	N.T. ^b	1.6	0.12
149	LS1	43.01 ± 3.85	N.T.	13.6	14.9
150	LS2	21.35 ± 3.53	N.T. ^b	4.3	3.6
153	LS5	20.81 ± 0.47	N.T. ^b	12.5	8.9
154	LS6	25.61 ± 2.34	N.T. ^b	3.3	2.4
155	LS7	29.28 ± 3.62	47.32	7.7	8.4
157	AN2	25.03 ± 0.39	N.T. ^b	N.A. ^a	N.A. ^a
159	AN4	8.77 ± 1.13	22.36	N.A. ^a	N.A. ^a
161	AN6	28.78 ± 2.0	N.T. ^b	8.2	4.8
166	AN11	35.72 ± 1.94	N.T. ^b	29	N.A. ^a
170	ME4	43.36 ± 4.17	N.T.	2.8	2.4
171	ME5	19.18 ± 0.09	N.T. ^b	9.1	N.A.

^aIC₅₀ values are presented as the mean ± SD of three independent experiments. ^bN.T.: No toxicity was observed at the highest tested concentration (50 μM). ^bEC₅₀ values represent the mean of three independent experiments and were determined by nonlinear regression analysis of the concentration-response curves (5-6 points) generated using GraphPad Prism 5 with 95% confidential interval (p < 0.05).

From all compounds reported in **Table 2**, we then chose 26 more active compounds which were further evaluated as inhibitors of IL-6 production LPS-induced and for the relative toxicity on MonoMac-6 cells and the results are reported on **Table 3**.

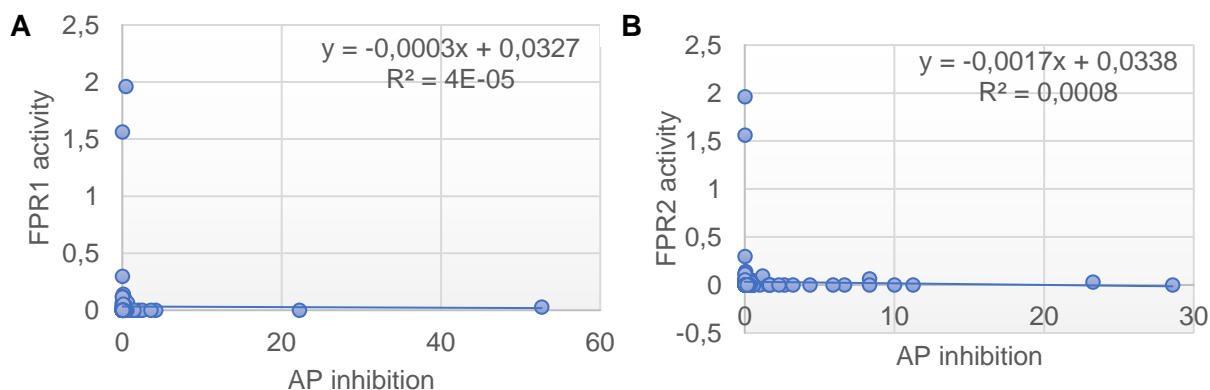
Table 3. IL-6 expression in MonoMac-6 of selected compound and toxicity.

N°	Compounds	^a IC ₅₀ (μM)	
		IL-6	Toxicity
2	AC50	30.7 ± 3.6	N.T. ^c
9	AC64	27.5 ± 1.6	19.04
10	AC65	8.7 ± 1.6	N.T. ^c
23	AC92	13.1 ± 0.3	N.T. ^c
38	AC111	20.3 ± 1.8	N.T. ^c
42	AC115	35.6 ± 3.1	N.T. ^c
46	AC123	N.A. ^b	N.T. ^c
47	AC124	18.8 ± 2.9	N.T. ^c
71	EC8	2.0 ± 0.3	N.T. ^c
78	SF1	17.0 ± 0.4	N.T. ^c
79	SF2	13.7 ± 1.4	N.T. ^c
80	SF3	33.5 ± 2.4	N.T. ^c
83	MT7	15.2 ± 0.2	N.T. ^c
84	AC75	30.7 ± 1.8	N.T. ^c
89	AC118	27.9 ± 2.2	N.T. ^c
94	R(-)-AC134	14.3 ± 2.0	N.T. ^c
95	S(+)-AC135	9.8 ± 1.0	N.T. ^c
98	R(-)-AC139	5.6 ± 0.3	N.T. ^c
102	R(-)-AC145	19.0 ± 3.1	N.T. ^c
103	S(+)-AC146	7.3 ± 1.2	N.T. ^c
125	R(+)-AC157	7.2 ± 0.03	N.T. ^c
141	AMC3	24.5 ± 0.8	N.T. ^c
150	LS2	4.0 ± 1.2	N.T. ^c
153	LS5	10.7 ± 0.1	N.T. ^c
154	LS6	2.6 ± 0.3	N.T. ^c
171	ME5	3.2 ± 0.4	N.T. ^c

^aIC₅₀ values are presented as the mean ± SD of three independent experiments. ^bN.A.: no inhibitory activity was found at the highest concentration of compound tested (50 μM). ^cN.T.: No toxicity was observed at the highest tested concentration (50 μM).

Looking at the obtained results, some considerations can be made. Also in this test, compound **71** showed the highest activity, while for compound **84** a strong decrease of the activity was observed. Pyridine-2,6-dione derivatives (**150**, **153**, **154**) confirmed to be very interesting products, all exhibiting IC_{50s} < 10 μM. Among the best compounds there is also the thiazolone **171** (IC₅₀ = 3.2 μM).

Finally, we correlate the anti-inflammatory activity found for these compounds with their already demonstrated FPR1/2 agonist activity. We then plotted the activity on THP1blue of all 179 molecules with the activity on both FPR1 and 2, and as it can be immediately noted in **Figure 3**, there is no correlation, thus confirming the initial hypothesis of an alternative mechanism, and pushing for further investigation.

**Figure 3.** Correlation between FPR1/NF-κB (A) and FPR2/NF-κB (B).

Finally, we selected compound **84** and **71** for the final step of this study. Both molecules were tested on a panel of 97 kinases (in **Table 4** are reported some examples of the tested kinases), but the results did not provide any positive feedback. In fact, only **84** was shown to be able to weakly inhibit the MKNK2 kinase, while **71** was not able to inhibit any kinase (**Table 4**).

Nevertheless, although these results were not very promising, we tested further 10 different molecules that were of interest in the ELISA assay, but none of them was active on MKNK2 (**Table 5**).

Table 4. Inhibition activity of **84** and **71** on 11 selected kinases.

Target	Compound 84	Compound 71
Gene Symbol	^a %Ctrl @ 10000nM	
KIT(D816V)	89	90
KIT(V559D)	91	100
LKB1	98	95
MAP3K4	59	97
MAPKAPK2	84	100
MARK3	100	96
MEK1	90	91
MEK2	96	91
MET	87	100
MKNK1	78	87
MKNK2	28	82

^aThe calculation of the control value, as percentage, was measured as the difference between the compound signal and the positive control signal, divided by the difference between the negative control signal and the positive control signal. The lower the result of this ratio, the stronger the inhibition toward that kinase.

Table 5. Inhibition activity of 10 selected compounds on MKNK2.

N°	Compound Name	MKNK2
		^a K _d (μM)
9	AC64	>30
10	AC65	>30
23	AC92	>30
47	AC124	>30
79	SF2	>30
83	MT7	>30
89	AC118	>30
95	S-(+)-AC135	>30
98	R-(-)-AC139	>30
103	S-(+)-AC146	>30

^aThe binding constant (K_ds) was calculated with a standard dose-response curve using the Hill equation, setting the Hill slope to -1.

In conclusion, despite the studies till now carried out on the selected compounds seem to indicate a possible different anti-inflammatory mechanism from the FPR system, we cannot postulate any hypothesis. Further investigation will be required to confirm or develop our supposition.

References

- Abboud, R. T.; Vimalanathan, S. Pathogenesis of COPD. Part I. The role of protease-antiprotease imbalance in emphysema. *Int. J. Tuberc. Lung Dis.* **2008**, 12, 361-367.
- Abeles, A. M.; Pillinger, M. H. Statins as antiinflammatory and immunomodulatory agents: a future in rheumatologic therapy? *Arthritis Rheum.* **2006**, 54, 393-407.
- Adkison, A. M.; Raptis, S. Z.; Kelley, D. G.; Pham, C. T. Dipeptidyl peptidase I activates neutrophil-derived serine proteases and regulates the development of acute experimental arthritis. *J. Clin. Invest.* **2002**, 109, 363-371.
- Ahmed, E. M.; Kassab, A. E.; El-Malah, A. A.; Hassan, M. S. A. Synthesis and biological evaluation of pyridazinone derivatives as selective COX-2 inhibitors and potential anti-inflammatory agents. *Eur. J. Med. Chem.* **2019**, 171, 25-37.
- Akira, S.; Uematsu, S.; Takeuchi, O. Pathogen recognition and innate immunity. *Cell.* **2006**, 124, 783-801.
- Alam, S. R.; Newby, D. E.; Henriksen, P. A. Role of the endogenous inhibitor, elafin, in cardiovascular injury from epithelium to endothelium. *Biochem. Pharmacol.* **2012**, 83, 695-704.
- Alcaraz, L.; Heald, R. A.; Sutton, J. M.; Armani, E.; Capaldi, C. Pyrimidone compounds which are HNE inhibitors. *U.S. Pat. Appl. Publ.* US9868740B2, **2018**.
- Ali, H.; Richardson, R. M.; Haribabu, B.; Sneyderman, R. Chemoattractant receptor cross-desensitization. *J. Biol. Chem.* **1999**, 274, 6027-6030.
- Almeida, R. P.; Vanet, A.; Witko-Sarsat, V.; Melchior, M.; McCabe, D.; Gabay, J. E. Azurocidin, a natural antibiotic from human neutrophils: expression, antimicrobial activity, and secretion. *Protein Expr. Purif.* **1996**, 7(4), 355-366.
- Al-Qalaf, F.; Mandani, F.; Abdelkhalik, M. M.; Bassam, A. A. Synthesis of 5-Substituted 3-Amino-1H-Pyrazole-4-Carbonitriles as Precursors for Microwave Assisted Regiospecific Syntheses of Pyrazolo[1,5-a]Pyrimidines. *Molecules.* **2008**, 14(1), 78-88.
- Andersen, G. R.; Koch, T. J.; Dolmer, K.; Sottrup-Jensen, L.; Nyborg, J. Low resolution X-ray structure of human methylamine-treated alpha 2-macroglobulin. *J. Biol. Chem.* **1995**, 270(42) 25133-25141.
- Anderssen, T.; Halvorsen, H.; Bajaj, S. P.; Osterud, B. Human leukocyte elastase and cathepsin G inactivate factor VII by limited proteolysis. *Thromb. Haemost.* **1993**, 70, 414-417.
- António, J. P. M.; Gonçalves, L. M.; Guedes, R. C.; Moreira, R.; Gois, P. M. P. Diazaborines as new inhibitors of human neutrophil elastase. *ACS Omega.* **2018**, 3, 7418-7423.
- Arafat, S. N.; Robert, M. C.; Abud, T.; Spurr-Michaud, S.; Amparo, F.; Dohlman, C. H.; Dana, R.; Gipson, I. K. Elevated neutrophil elastase in tears of ocular graft-versus-host disease patients. *Am. J. Ophthalmol.* **2017**, 176, 46-52.

- Aranov, A.; Lauffer, D. J.; Li, P.; Tomlinson, R. C. Compositions Useful as Inhibitors of Protein Kinases. *PCT Int. Appl.* WO 2005028475 A2, **2005**.
- Armani, E.; Capaldi, C.; Sutton, J. M.; Heald, R. A. Compounds. *U.S. Pat. Appl. Publ.* US9409870B2, **2016**.
- Armstrong, L.; Godinho, S. I.; Uppington, K. M.; Whittington, H. A.; Millar, A. B. Contribution of TNF-alpha converting enzyme and proteinase-3 to TNF-alpha processing in human alveolar macrophages. *Am. J. Respir. Cell Mol. Biol.* **2006**, 34, 219-225.
- Babior, B. M.; Lambeth, J. D.; Nauseef, W. The neutrophil NADPH oxidase. *Arch. Biochem. Biophys.* **2002**, 397, 342-344.
- Bank, U.; Kupper, B.; Ansorge, S. Inactivation of interleukin-6 by neutrophil proteases at sites of inflammation. Protective effects of soluble IL-6 receptor chains. *Adv. Exp. Med. Biol.* **2000**, 477, 431-437.
- Barnes, P. J.; Karin, M. Nuclear factor-kappaB: A Pivotal Transcription Factor in Chronic Inflammatory Diseases. *N. Engl. J. Med.* **1997**, 336(15), 1066-71.
- Barrett, A. B.; Starkey, P. M. The interaction of α 2-macroglobulin with proteinases. Characteristics and specificity of the reaction, and a hypothesis concerning its molecular mechanism. *Biochem. J.* **1973**, 133(4), 709-724.
- Bartroli, J.; Turmo, E.; Alguero, M.; Boncompte, E.; Vericat, M. L.; Conte, L.; Ramis, J.; Merlos, M.; Garcia-Rafanell, J.; Forn, J. New Azole Antifungals. 2. Synthesis and Antifungal Activity of Heterocyclecarboxamide Derivatives of 3-Amino-2-aryl-1-azolyl-2-butanol. *J. Med. Chem.* **1998**, 41, 1855-1868.
- Basak, S.; Kim, H.; Kearns, J. D.; Tergaonkar, V.; O'Dea, E.; Werner, S. L.; Benedict, C. A.; Ware, C. F.; Ghosh, G.; Verma, I. M. A fourth I κ B protein within the NF- κ B signaling module. *Cell.* **2007**, 128, 369-381.
- Becke, A. D. A new mixing of Hartree-Fock and local density-functional theories. *J. Chem. Phys.* **1993**, 98, 5648-5652.
- Belaaouaj, A. A.; Kim, K. S.; Shapiro, S. D. Degradation of Outer Membrane Protein A in Escherichia coli Killing by Neutrophil Elastase. *Science.* **2000**, 289, 1185-1187.
- Belaaouaj, A. A.; McCarthy, R.; Baumann, M.; Gao, Z.; Ley, T. J.; Abraham, S. N.; Shapiro, S. D. Mice lacking neutrophil elastase reveal impaired host defense against gram negative bacterial sepsis. *Nature.* **1998**, 4, 615-618.
- Benarafa, C.; Cooley, J.; Zeng, W.; Bird, P. I.; Remold-O'Donnell, E. Characterization of four murine homologs of the human ov-serpin monocyte neutrophil elastase inhibitor MNEI (SERPINB1). *J. Biol. Chem.* **2002**, 277, 42028-42033.
- Benson, K. F.; Li, F. Q.; Person, R. E.; Albani, D.; Duan, Z.; Wechsler, J.; Meade-White, K.; Williams, K.; Acland, G. M.; Niemeyer, G.; Lothrop, C. D.; Horwitz, M. Mutations associated with

neutropenia in dogs and humans disrupt intracellular transport of neutrophil elastase. *Nat. Genet.* **2003**, 35, 90-96.

- Birrer, P.; McElvaney, N. G.; R deberg, A.; Sommer, C. W.; Liechti-Gallati, S.; Kraemer, R.; Hubbard, R.; Crystal, R. G. Protease-antiprotease imbalance in the lungs of children with cystic fibrosis. *Am. J. Resp. Crit. Care Med.* **1994**, 150(1), 207-213.
- Bobofchak, K. M.; Pineda, A. O.; Mathews, F. S.; Di Cera, E. Energetic and structural consequences of perturbing Gly-193 in the oxyanion hole of serine proteases. *J. Biol. Chem.* **2005**, 280, 25644-25650.
- Bolea, C.; Celanire, S. Substituted 5,6-dihydro-4h-thiazolo[4,5-e]indazoles and their use as positive allosteric modulators of metabotropic glutamate receptors. *U.S. Pat. Appl. Publ.* US8697744B2, **2014**.
- Boulay, F.; Tardif, M.; Bouchon, L.; Vignais, P. Synthesis and use of a novel N-formyl peptide derivative to isolate a human N-formyl peptide receptor cDNA. *Biochem. Biophys. Res. Commun.* **1990a**, 16, 168(3), 1103-1109.
- Boulay, F.; Tardif, M.; Bouchon, L.; Vignais, P. The human N-formylpeptide receptor. Characterization of two cDNA isolates and evidence for a new subfamily of G-protein-coupled receptors. *Biochem.* **1990b**, 29, 11123-11133.
- Bradbury, R. H.; Hales, N. J.; Rabow, A. A. Bicyclic derivatives for use in the treatment of androgen receptor associated conditions and their preparation. *PTC Int Appl.* WO 2009/081197, **2009**.
- Brinkmann, V.; Reichard, U.; Goosmann, C.; Fauler, B.; Uhlemann, Y.; Weiss, D. S. Weinrauch, Y.; Zychlinsky, A. Neutrophil extracellular traps kill bacteria. *Science.* **2004**, 303(5663), 1532-1535.
- Bronze da Rocha, E.; Santos-Silva, A. Neutrophil Elastase Inhibitors and Chronic Kidney Disease. *Int. J. Biol. Sci.* **2018**, 14(10), 1343-1360.
- Bruker (**2012a**). Bruker APEX2. Bruker AXS Inc., Madison, Wisconsin, USA.
- Bruker (**2012b**). Bruker SAINT. Bruker AXS Inc., Madison, Wisconsin, USA.
- Bruni, F.; Chimichi, S.; Cosimelli, B.; Costanzo, A.; Guerrini, G.; Selleri, S. A new entry to pyrazolo[1,5-a]pyrido[3,4-e]pyrimidine derivatives. *Heterocycles.* **1990**, 31, 1141-1149.
- Bruni, F.; Selleri, S.; Costanzo, A.; Guerrini, G.; Casilli, M. L.; Giusti, L. Reactivity of 7-(2-dimethylaminovinyl)pyrazolo[1,5-a]pyrimidines: synthesis of pyrazolo[1,5-a]pyrido[3,4-e]pyrimidine derivatives as potential benzodiazepine receptor ligands. 2. *J. Heterocycl. Chem.* **1995**, 32, 291-298.
- Burgi, H. B.; Dunitz, J. D.; Lehn, J. M.; Wipff, G. Stereochemistry of reaction paths at carbonyl centers. *Tetrahedron.* **1974**, 30, 1563-1572.

- Burla, M. C.; Caliandro, R.; Camalli, M.; Carrozzini, B.; Cascarano, G. L.; Da Caro, L.; Giacobazzo, C.; Polidori, G.; Spagna, R. *J. SIR2004: an improved tool for crystal structure determination and refinement. J. Appl. Cryst.* **2005**, 38, 381-388.
- Butler, M. W.; Robertson, I.; Greene, C. M.; O'Neill, S. J.; Taggart, C. C.; McElvaney, N. G. Elafin prevents lipopolysaccharide-induced AP-1 and NF-kappaB activation via an effect on the ubiquitin-proteasome pathway. *J. Biol. Chem.* **2006**, 281, 34730-34735.
- Cairns, J.; Overbaugh, J.; Miller, S. The origin of mutans. *Nature.* **1988**, 335, 142.
- Cantini, N.; Khlebnikov, A. I.; Crocetti, L.; Schepetkin, I. A.; Floresta, G.; Guerrini, G.; Vergelli, C.; Bartolucci, G.; Quinn, M. T.; Giovannoni, M.P. "Exploration of nitrogen heterocycle scaffolds for the development of potent human neutrophil elastase inhibitors". *Bioorg. Med. Chem.* **2020**, 115836. doi: 10.1016/j.bmc.2020.115836.
- Capaldi, C.; Armani, E.; Jennings A. S. R. Compounds. *PTC Int Appl.* US9862706B2, **2018**.
- Capaldi, C.; Heald, R. A.; Ray, N. C.; Sutton, J. M. Inhibition of enzymes. *PTC Int Appl.* US9199984B2, **2015**.
- Carp, H. Mitochondrial N-formylmethionyl proteins as chemoattractants for neutrophils. *J. Exp. Med.* **1982**, 155, 264-275.
- Cerimele, F.; Brown, L. F.; Bravo, F.; Ihler, G. M.; Koudio, P.; Arbiser, J. L. Infectious angiogenesis: Bartonella bacilliformis infection results in endothelial production of angiopoietin-2 and epidermal production of vascular endothelial growth factor. *Am. J. Pathol.* **2003**, 163, 1321-1327.
- Chatterjee, A. K.; Kumar, M.; Schultz, P. G. Elastase inhibitors. *PTC Int Appl.* US 20170144998A1, **2017**.
- Chen, L.; Deng, H.; Cui, H.; Fang, J.; Zuo, Z.; Deng, J.; Li, Y.; Wang, X.; Zhao, L. Inflammatory Responses and Inflammation-Associated Diseases in Organs. *Oncotarget.* **2017**, 9(6), 7204-7218.
- Chen, P. Y.; Qin, L.; Li, G.; Tellides, G.; Simons, M. Fibroblast growth factor (FGF) signaling regulates transforming growth factor beta (TGFbeta)- dependent smooth muscle cell phenotype modulation. *Sci. Rep.* **2016**, 6, 33407.
- Chillappagari, S.; Müller, C.; Mahavadi, P.; Guenther, A.; Nährlich, L.; Rosenblum, J.; Rubin, B. K.; Henke, M. O. A small molecule neutrophil elastase inhibitor, KRP-109, inhibits cystic fibrosis mucin degradation. *J. Cyst. Fibros.* **2016**, 15, 325-331.
- Chua, F.; Laurent, G. J. Neutrophil elastase: mediator of extracellular matrix destruction and accumulation. *Proc. Am. Thorac. Soc.* **2006**, 3, 424-427.
- Cilibrizzi, A.; Quinn, M. T.; Kirpotina, L. N.; Schepetkin, I. A.; Holderness, J.; Ye, R. D.; Rabiet, M.-J.; Biancalani, C.; Cesari, N.; Graziano, A.; Vergelli, C.; Pieretti, S.; Dal Piaz, V.; Giovannoni, M. P. 6-methyl-2,4-disubstituted pyridazin-3(2H)-ones: A Novel Class of Small-Molecule Agonists for Formyl Peptide Receptors. *J. Med. Chem.* **2009**; 52(16), 5044-5057.

- Cilibrizzi, A.; Schepetkin, I. A.; Bartolucci, G.; Crocetti, L.; Dal Piaz, V.; Giovannoni, M. P.; Graziano, A.; Kirpotina, L. N.; Quinn, M. T.; Vergelli, V. Synthesis, Enantioresolution, and Activity Profile of Chiral 6-methyl-2,4-disubstituted pyridazin-3(2H)-ones as Potent N-formyl Peptide Receptor Agonists. *Bioorg. Med. Chem.* **2012**, 20(12), 3781-3792.
- Claramunt, R. M.; López, C.; Pérez-Medina, C.; Pinilla, E.; Torres, M. R.; Elguero, J. Synthesis and structural study of tetrahydroindazolones. *Tetrahedron.* **2006**, 62, 11704-11713.
- Clark, B. A. J.; Parrick, J.; Dorgan, R. J. J. Formation of certain substituted 5H-pyrrolo[2,3-b]pyrazines by thermal cyclization of pyrazinylhydrazones and a route to 5H-pyrazino[2,3-b]indole; a synthesis of 5H-pyrrolo[2,3-b]pyrazine and some of its properties. *J. Chem. Soc. Perkin Trans 1.* **1976**, 13, 1361-1363.
- Clark, B. A. J.; Parrick, J.; West, P. J.; Kelly, A. K. Diazaindenes (azaindoles). Part III. Reactions of Vilsmeier reagents leading to 3-formyl-1,6-diazaindenes and -1,4-diazabenz[f]indene. *J. Chem. Soc. C.* **1970**, 3, 498-501.
- Clauss, A.; Ng, V.; Liu, J.; Piao, H.; Russo, M.; Vena, N.; Sheng, Q.; Hirsch, M. S.; Bonome, T.; Matulonis, U.; Ligon, A. H.; Birrer, M. J.; Drapkin, R. Overexpression of elafin in ovarian carcinoma is driven by genomic gains and activation of the nuclear factor kappaB pathway and is associated with poor overall survival. *Neoplasia.* **2010**, 12(2), 161-172.
- Clunes, M. T.; Boucher, R. C. Cystic Fibrosis: The Mechanisms of Pathogenesis of an Inherited Lung Disorder. *Drug. Discov. Today Dis. Mech.* **2007**, 4(2), 63-72.
- Cooley, J.; Takayama, T. K.; Shapiro, S. D.; Schechter, N. M.; Remold-O'Donnell, E. The serpin MNEI inhibits elastase-like and chymotrypsin-like serine protease through efficient reactions at two active sites. *Biochemistry.* **2001**, 40, 15762-15770.
- Cowan, K. N.; Heilbut, A.; Humpl, T.; Lam, C.; Ito, S.; Rabinovitch, M. Complete reversal of fatal pulmonary hypertension in rats by a serine elastase inhibitor. *Nat. med.* **2000**, 6, 698-702.
- Crocetti, L.; Bartolucci, G.; Cilibrizzi, A.; Giovannoni, M. P.; Guerrini, G.; Iacovone, A.; Menicatti, M.; Schepetkin, I. A.; Khlebnikov, A. I.; Quinn, M. T.; Vergelli, C. Synthesis and analytical characterization of new thiazol-2-(3H)-ones as human neutrophil elastase (HNE) inhibitors. *Chem. Cent. J.* **2017**, 11(1), 127.
- Crocetti, L.; Giovannoni, M. P.; Schepetkin, I. A.; Quinn, M. T.; Khlebnikov, A. I.; Cantini, N.; Guerrini, G.; Iacovone, A.; Teodori, E.; Vergelli, C. 1H-pyrrolo[2,3-b]pyridine: A new scaffold for human neutrophil elastase (HNE) inhibitors. *Bioorg. Med. Chem.* **2018**, 26(21), 5583-5595. doi: 10.1016/j.bmc.2018.09.034.
- Crocetti, L.; Giovannoni, M. P.; Schepetkin, I. A.; Quinn, M. T.; Khlebnikov, A. I.; Cilibrizzi, A.; Dal Piaz, V.; Graziano, A.; Vergelli, C. Design, synthesis and evaluation of N-benzoylindazole derivatives and analogues as inhibitors of human neutrophil elastase. *Bioorg. Med. Chem.* **2011**, 19(15), 4460-4472.

- Crocetti, L.; Quinn, M. T.; Schepetkin, I. A.; Giovannoni, M. P. A patenting perspective on human neutrophil elastase (HNE) inhibitors (2014-2018) and their therapeutic applications. *Expert Opin. Ther. Pat.* **2019**, 29(7), 555-578.
- Crocetti, L.; Schepetkin, I. A.; Ciciani, G.; Giovannoni, M. P.; Guerrini, G.; Iacovone, A.; Khlebnikov, A. I.; Kirpotina, L. N.; Quinn, M. T.; Vergelli, C. Synthesis and pharmacological evaluation of indole derivatives as deaza analogues of potent human neutrophil elastase inhibitors. *Drug Dev. Res.* **2016**, 77(6), 285-299.
- Crocetti, L.; Schepetkin, I. A.; Cilibrizzi, A.; Graziano, A.; Vergelli, C.; Giomi, D.; Khlebnikov, A. I.; Quinn, M. T.; Giovannoni, M. P. Optimization of N-Benzoylindazole Derivatives as Inhibitors of Human Neutrophil Elastase. *J. Med. Chem.* **2013**, 56, 6259-6272.
- Crocetti, L.; Vergelli, C.; Cilibrizzi, A.; Graziano, A.; Khlebnikov, A. I.; Kirpotina, L. N.; Schepetkin, I. A.; Quinn, M. T.; Giovannoni, M. P. Synthesis and Pharmacological Evaluation of New Pyridazin-Based Thioderivatives as Formyl Peptide Receptor (FPR) Agonists. *Drug. Dev. Res.* **2013**, 74(4), 259-271.
- Crocetti, L.; Vergelli, C.; Guerrini, G.; Cantini, N.; Kirpotina, L. N.; Schepetkin, I. A.; Quinn, M. T.; Parisio, C.; Di Cesare Mannelli, L.; Ghelardini, C.; Giovannoni, M. P. Novel Formyl Peptide Receptor (FPR) Agonists with Pyridinone and Pyrimidindione Scaffolds That Are Potentially Useful for the Treatment of Rheumatoid Arthritis. *Bioorg. Chem.* **2020**, 100, 103880. doi: 10.1016/j.bioorg.2020.103880.
- Czerkies, M.; Kwiatkowska, K. Toll-Like Receptors and their Contribution to Innate Immunity: Focus on TLR4 Activation by Lipopolysaccharide. *Adv. Cell. Biol.* **2014**, 4, 1-23.
- Daina, A.; Michielin, O.; Zoete, V. SwissADME: a free web tool to evaluate pharmacokinetics, drug-likeness and medicinal chemistry friendliness of small molecules. *Scientific Reports.* **2017**, 7, 42717.
- D'Alessio, R.; Bargiotti, A.; Brasca, M. G.; Ermoli, A.; Pevarello, P.; Tibolla, M. Tricyclic pyrazole derivatives as protein kinase inhibitors, process for their preparation and their use as antitumor agents. *PCT Int. Appl* WO2003070236A2, **2003**.
- Decramer, M.; Janssens, W.; Miravittles, M. Chronic obstructive pulmonary disease. *Lancet.* **2012**, 379(9823), 1341-1351.
- Demedts, I. K.; Demoor, T.; Bracke, K. R.; Joos, G. F.; Brusselle, G. G. Role of apoptosis in the pathogenesis of COPD and pulmonary emphysema. *Respir. Res.* **2006**, 7(53), 1-10.
- Demers, M.; Wong, S. L.; Martinod, K.; Gallant, M.; Cabral, J. E.; Wang, Y.; Wagner, D. D. Priming of neutrophils toward NETosis promotes tumor growth. *Oncoimmunology.* **2016**, 5(5), e1134073-e1134081.
- Desai, O.; Winkler, J.; Minasyan, M.; Herzog, E. L. The Role of immune and inflammatory Cells in idiopathic Pulmonary Fibrosis. *Front. Med.* **2018**, 5(43), 1-14.

- Devita, R. J.; Shah, S. K.; Kurukulasuriya, R.; Fung, S.; Colandrea, V. J.; Szewczyk, J. W. Preparation of substituted pyridine derivatives useful as GPR131 agonists. *PCT Int. Appl.* WO2013062887A1, **2013**.
- Di Cera, E. Serine proteases. *IUBMB Life*. **2009**, 61(5), 510–515.
- Didsbury, J. R.; Uhing, R. J.; Tomhave, E.; Gerard, C.; Gerard, N.; Snyderman, R. Receptor class desensitization of leukocyte chemoattractant receptors. *Proc. Natl. Acad. Sci. U.S.A.* **1991**, 88(24), 11564-11568.
- Dinarello, C. A. Anti-inflammatory Agents: Present and Future. *Cell*. **2010**, 140(6), 935-950.
- Dinarello, C. A. Immunological and inflammatory functions of the interleukin-1 family. *Annu. Rev. Immunol.* **2009**, 27, 519-550.
- Doherty, J. B.; Ashe, B. M.; Argenbright, L. W.; Barker, P. L.; Bonney, R. J.; Chandler, G. O.; Dahlgren, M. E.; Dorn, C. P.; Finke, P. E.; Firestone, R. A.; Fletcher, D.; Hagmann, W. K.; Mumford, R.; Ogrady, L.; Maycock, A. L.; Pisano, J. M.; Shah, S. K.; Thompson, K. R.; Zimmerman, M. Cephalosporin antibiotics can be modified to inhibit human-leukocyte elastase. *Nature*. **1986**, 322, 192-194.
- Dorward, D. A.; Lucas, C. D.; Chapman, G. B.; Haslett, C.; Dhaliwal, K.; Rossi, A. G. The Role of Formylated Peptides and Formyl Peptide Receptor 1 in Governing Neutrophil Function during Acute Inflammation. *Am. J. Pathol.* **2015**, 185(5), 1172-1184.
- Dos Santos, M. S.; Bernardino, A. M. R.; Pinheiro, L. C. S.; Canto-Cavalheiro, M. M.; Leon, L. L. An Efficient Synthesis of New 5-(1-Aryl-1H-pyrazole-4-yl)-1H-tetrazoles from 1-Aryl-1H-pyrazole-4-carbonitriles via [3 + 2] Cycloaddition Reaction. *J. Heterocycl. Chem.* **2012**, 49(6), 1425-1428.
- Doumas, S.; Kolokotronis, A.; Stefanopoulos, P. Anti-inflammatory and antimicrobial roles of secretory leukocyte protease inhibitor. *Infect. Immun.* **2005**, 73, 1271-1274.
- Drannik, A. G.; Nag, K.; Yao, X. D.; Henrick, B. M.; Sallenave, J. M.; Rosenthal, K. L. Trappin-2/elafin modulate innate immune responses of human endometrial epithelial cells to PolyI:C. *PLoS One*. **2012**, 7(4), e35866, 1-16.
- Dufton, N.; Perretti, M. Therapeutic anti-inflammatory potential of formylpeptide receptor agonists. *Pharm. Ther.* **2010**, 127, 2, 175-188.
- Egan, W. J.; Merz, K. M.; Baldwin, J. J. Prediction of drug absorption using multivariate statistics. *J. Med. Chem.* **2000**, 43, 3867-3877.
- Ekdahl, C. T.; Claassen, J. H.; Bonde, S.; Kokaia, Z.; Lindvall, O. Inflammation is detrimental for neurogenesis in adult brain. *P. Natl. Acad. of Sci USA*. **2003**, 100, 13632-13637.
- El Kebir, D.; Jozsef, L.; Khreiss, T.; Pan, W.; Peptasis, N. A.; Serhan, C. N.; Janos, G. F. Aspirin-triggered lipoxins override the apoptosis-delaying action of serum amyloid A in human neutrophils: a novel mechanism for the resolution of inflammation. *J. Immunol.* **2007**, 179, 616-622.

- El Rayes, T.; Catena, R.; Lee, S.; Stawowczyk, M.; Joshi, N.; Fischbach, C.; Powell, C. A.; Dannenberg, A. J.; Altorki, N. K.; Gao, D.; Mittal, V. Lung inflammation promotes metastasis through neutrophil protease-mediated degradation of Tsp-1. *Proc. Natl. Acad. Sci. U. S. A.* **2015**, 112(52), 16000-16005.
- Elagawany, M.; Ibrahim, M. A.; Ali Ahmed, H. E.; El-Etrawy, A. Sh.; Ghiaty, A.; Abdel-Samii, Z. K.; El-Feky, S. A.; Bajorath, J. Design, synthesis, and molecular modelling of pyridazinone and phthalazinone derivatives as protein kinases inhibitors. *Bioorg. Med. Chem. Lett.* **2013**, 23(7), 2007-2013.
- Enomoto, T.; Usuki, J.; Azuma, A.; Nakagawa, T.; Kudoh, S. Diabetes mellitus may increase risk for idiopathic pulmonary fibrosis. *Chest.* **2003**, 123(6), 2007-2011.
- Hernandezm T.; Mayadas, T. N. The Changing Landscape of Renal Inflammation. *Trends Mol. Med.* **2016**, 22, 151-163.
- Ernst, S.; Lange, C.; Wilbers, A.; Goebeler, V.; Gerke, V.; Rescher, U. An annexin 1 N-terminal peptide activates leukocytes by triggering different members of the formyl peptide receptor family. *J. Immunol.* **2004**, 172, 7669-7676.
- Esser, N.; Legrand-Poels, S.; Piette, J.; Scheen, A. J.; Paquot, N. Inflammation as a link between besity, metabolic syndrome and type 2 diabetes. *Diabetes Res. Clin. Pr.* **2014**, 105, 141-150.
- Estrada, A. A.; Feng, J. A.; Fox, B.; Leslie, C. P.; Lyssikatos, J. P.; Pozzan, A.; Sweeney, Z. K.; De Vicente Fidalgo, J. Preparation of substituted nitrogen heterocycles as RIPK1 inhibitors useful in treatment of RIPK1-mediated diseases. *PCT Int. Appl.*, WO2017136727A2, **2017**.
- Fernandez, I. E.; Eickelberg, O. New cellular and molecular mechanisms of lung injury and fibrosis in idiopathic pulmonary fibrosis. *Lancet.* **2012** 380(9842), 680-688.
- Ferrero-Miliani, L.; Nielsen, O.; Andersen, P.; Girardin, S. Chronic inflammation: importance of NOD2 and NALP3 in interleukin-1 β generation. *Clin. Exp. Immunol.* **2007**, 147, 227-235.
- Fischer, B. M.; Voynow, J. A. Neutrophil elastase induces MUC5AC gene expression in airway epithelium via a pathway involving reactive oxygen species. *Am. J. Respir. Cell. Mol. Biol.* **2002**, 26, 447-452.
- Fontaine, V.; Touat, Z.; Mtairag, E. M.; Vranckx, R.; Louedec, L.; Houard, X.; Andreassian, B.; Sebbag, U.; Palombi, T.; Jacob, M. P.; Meilhac, O.; Michel, J. B. Role of leukocyte elastase in preventing cellular recolonization of the mural thrombus. *Am. J. Pathol.* **2004**, 164(6), 2077-2087.
- Force, A. D. T.; Ranieri, V. M.; Rubenfeld, G. D.; Thompson, B. T.; Ferguson, N. D.; Caldwell, E.; Fan, E.; Camporota, L.; Slutsky, A. S. Acute respiratory distress syndrome: The Berlin Definition. *JAMA.* **2012**, 307, 2526-2533.
- Foresman, J. B.; Frisch, A.E. Exploring Chemistry with Electronic Structure Methods, 3rd edition, Gaussian, Inc., **2015**.

- Fujinaga, M.; Cherney, M. M.; Oyama, H.; Oda, K.; James, M. N. The molecular structure and catalytic mechanism of a novel carboxyl peptidase from *Scytalidium lignicolum*. *Proc. Natl. Acad. Sci. U.S.A.* **2004**, 101, 3364-3369.
- Gacko, M.; Glowinski, S. Activities of proteases in parietal thrombus of aortic aneurysm. *Clin. Chim. Acta.* **1998**, 271(2), 171-177.
- Gadek, J. E.; Pacht, E. R. The protease-antiprotease balance within the human lung: implications for the pathogenesis of emphysema. *Lung.* **1990**, 168(Suppl), 552-564.
- Garcia-Touchard, A.; Henry, T. D.; Sangiorgi, G.; Spagnoli, L. G.; Mauriello, A., Conover, C.; Schwartz, R. S. Extracellular proteases in atherosclerosis and restenosis. *Arterioscler. Thromb. Vasc. Biol.* **2005**, 25(6), 1119-1127.
- Geraghty, P.; Rogan, M. P.; Greene, C. M.; Boxio, R. M.; Poiriert, T.; O'Mahony, M.; Belaaouaj, A.; O'Neill, S. J.; Taggart, C. C.; McElvaney, N. G. Neutrophil elastase up-regulates cathepsin B and matrix metalloprotease-2 expression. *J. Immunol.* **2007**, 178(9), 5871-5878.
- Ghose, A. K.; Viswanadhan, V. N.; Wendoloski, J. J. A knowledge-based approach in designing combinatorial or medicinal chemistry libraries for drug discovery. 1. A qualitative and quantitative characterization of known drug databases. *J. Comb. Chem.* **1999**, 1, 55-68.
- Ghosh, M.; Shen, Z.; Fahey, J. V.; Cu-Uvin, S.; Mayer, K.; Wira, C. R. Trappin-2/Elafin: a novel innate anti-human immunodeficiency virus-1 molecule of the human female reproductive tract. *Immunology.* **2010**, 129(2), 207-219.
- Giordano, F. J. Oxygen, oxidative stress, hypoxia, and heart failure. *J. Clin. Invest.* **2005**, 115, 500-508.
- Giovannoni, M. P.; Cantini, N.; Crocetti, L.; Guerrini, G.; Iacovone, A.; Schepetkin, I. A.; Vergelli, C.; Khlebnikov, A. I.; Quinn, M. T. Further modifications of 1H-pyrrolo[2,3-b]pyridine derivatives as inhibitors of human neutrophil elastase. *Drug Dev. Res.* **2019**, 80(5), 617-628. doi: 10.1002/ddr.21539.
- Giovannoni, M. P.; Crocetti, L.; Cantini, N.; Guerrini, G.; Vergelli, C.; Iacovone, A.; Teodori, E.; Schepetkin, I. A.; Quinn, M. T.; Ciattini, S.; Rossi, P.; Paoli, P. New 3-unsubstituted isoxazolones as potent human neutrophil elastase inhibitors: Synthesis and molecular dynamic simulation. *Drug Dev. Res.* 2020. 81(3):338-349. *Drug Dev. Res.* **2020**, 81(3), 338-349. doi: 10.1002/ddr.21625.
- Giovannoni, M. P.; Schepetkin, I. A.; Cilibrizzi, A.; Crocetti, L.; Khlebnikov, A. I.; Dahlgren, C.; Graziano, A.; Dal Piaz, V.; Kirpotina, L. N.; Zerbini, S.; Vergelli, C.; Quinn, M. T. Further Studies on 2-arylamide pyridazin-3(2H)-ones: Design, Synthesis and Evaluation of 4,6-disubstituted Analogs as Formyl Peptide Receptors (FPRs) Agonists. *Eur. J. Med. Chem.* **2013**, 64, 512-528.
- Giovannoni, M. P.; Schepetkin, I. A.; Crocetti, L.; Ciciani, G.; Cilibrizzi, A.; Guerrini, G.; Khlebnikov, A. I.; Quinn, M. T.; Vergelli, C. Cinnoline derivatives and analogues as human neutrophil elastase inhibitors. *J. Enz. Inhib. Med. Chem.* **2016**, 31(4), 628-639.

- Giovannoni, M. P.; Schepetkin, I. A.; Quinn, M. T.; Cantini, N.; Crocetti, L.; Guerrini, G.; Iacovone, A.; Paoli, P.; Rossi, P.; Bartolucci, G.; Menicatti, M.; Vergelli, C. Synthesis, biological evaluation, and molecular modelling studies of potent human neutrophil elastase (HNE) inhibitors. *J. Enzyme Inhib. Med. Chem.* **2018**, 33(1), 1108-1124. doi: 10.1080/14756366.2018.1480615.
- Glinski, W.; Jarzabek-Chorzelska, M.; Kuligowski, M.; Pierozynska-Dubowska, M.; Glinska-Ferenz, M.; Jablonska, S. Basement membrane zone as a target for human neutrophil elastase in psoriasis. *Arch. Dermatol. Res.* **1990**, 282, 506-511.
- Gnam, C.; Anderskewitz, R.; Hoesch, H.; Morschhaeuser, G.; Oost, T.; Peters, S.; Ries, U. J. Substituted bicyclic dihydropyrimidones and their use as inhibitors of neutrophil elastase activity. *U.S. Pat. Appl. Publ.* US9657015B2, **2017**.
- Goldfarb, D. S. Method using lifespan-altering compounds for altering the lifespan of eukaryotic organisms, and screening for such compounds. *U.S. Pat. Appl. Publ.* US20090163545A1, **2009**.
- Gong, L.; Cumpian, A. M.; Caetano, M. S.; Ochoa, C. E.; De la Garza, M. M.; Lapid, D. J.; Mirabolfathinejad, S. G.; Dickey, B. F.; Zhou, Q.; Moghaddam, S. J. Promoting effect of neutrophils on lung tumorigenesis is mediated by CXCR2 and neutrophil elastase. *Molecular cancer.* **2013**, 12(1), 154.
- Greene, C. M.; Carroll, T. P.; Smith, S. G.; Taggart, C. C.; Devaney, J.; Griffin, S.; O'Neill, S. J.; McElvaney, N. G. TLR-induced inflammation in cystic fibrosis and non-cystic fibrosis airway epithelial cells. *J. Immunol.* **2005**, 174(3), 1638-1646.
- Gregory, A. D.; Hale, P.; Perlmutter, D. H.; Houghton, A. M. Clathrin pit-mediated endocytosis of neutrophil elastase and cathepsin G by cancer cells. *J. Biol. Chem.* **2012**, 287(42), 35341-35350.
- Gregory, A. D.; Kliment, C. R.; Metz, H. E.; Kim, K. H.; Kargl, J.; Agostini, B. A.; Crum, L. T.; Oczypok, E. A.; Oury, T. A.; Houghton, A. M. Neutrophil elastase promotes myofibroblast differentiation in lung fibrosis. *J. Leukoc. Biol.* **2015**, 98(2), 143-152.
- Grimme, S.; Ehrlich, S.; Goerigk, L. Effect of the damping function in dispersion corrected density functional theory. *J. Comp. Chem.* **2011**, 32, 1456-1465.
- Groom, C. R.; Bruno, I. J.; Lightfoot, M. P.; Ward, S. C. *Acta Crystallogr. Sect. B: Struct. Sci. Cryst. Eng. Mater.* **2016**, B72, 171-179.
- Groutas, W. C.; Dou, D.; Alliston, K. R. Neutrophil elastase inhibitors. *Expert. Opin. Ther. Pat.* **2011**, 21(3), 339-354.
- Groutas, W. C.; Kuang, R. Z.; Venkataraman, R.; Epp, J. B.; Ruan, S. M.; Prakash O. Structure-based design of a general class of mechanism-based inhibitors of the serine proteinases employing a novel amino acid-derived heterocyclic scaffold. *Biochemistry Us.* **1997**, 36, 4739-4750.
- Guo, S.; Song, Y.; Huang, Q.; Yuan, H.; Wan, B.; Wang, Y.; He, R.; Beconi, M. G.; Franzblau, S. G.; Kozikowski, A. P. Identification, Synthesis, and Pharmacological Evaluation of

Tetrahydroindazole Based Ligands as Novel Antituberculosis Agents. *J. Med. Chem.* **2010**, 53, 2, 649-659.

- Gütschow, M.; Kuerschner, L.; Neumann, U.; Pietsch, M.; Loser, R.; Koglin, N., Eger, K. 2-(diethylamino)thieno 1,3 oxazin-4-ones as stable inhibitors of human leukocyte elastase. *J. Med. Chem.* **1999**, 42, 5437-5447.
- Gütschow, M.; Neumann, U. Novel thieno[2,3-d][1,3]oxazin-4-ones as inhibitors of human leukocyte elastase. *J. Med. Chem.* **1998**, 41, 1729-1740.
- Guyot, N.; Bergsson, G.; Butler, M. W.; Greene, C. M.; Weldon, S.; Kessler, E.; Levine, R. L.; O'Neill, S. J.; Taggart, C. C.; McElvaney, N. G. Functional study of elafin cleaved by *Pseudomonas aeruginosa* metalloproteinases. *Biol. Chem.* **2010**, 391(6), 705-716.
- Guyot, N.; Butler, M. W.; McNally, P.; Weldon, S.; Greene, C. M.; Levine, R. L.; O'Neill, S. J.; Taggart, C. C.; McElvaney, N. G. Elafin, an elastase-specific inhibitor, is cleaved by its cognate enzyme neutrophil elastase in sputum from individuals with cystic fibrosis. *J. Biol. Chem.* **2008**, 283(47), 32377-32385.
- Hajjar, E.; Broemstrup, T.; Kantari, C.; Witko-Sarsat, V.; Reuter, N. Structures of human proteinase 3 and neutrophil elastase – so similar yet so different. *Febs. J.* **2010**, 277, 2238-2254.
- Hansen, G.; Gielen-Haertwig, H.; Reinemer, P.; Schomburg, D.; Harrenga, A.; Niefind, K. Flessibilità inaspettata del sito attivo nella struttura dell'elastasi neutrofila umana in un complesso con un nuovo inibitore di diidropirimidone. *J. Mol. Bio.* **2011**, 409 (5), 681-691.
- He, H. Q.; Ye, R. D. The formyl peptide receptors: diversity of ligands and mechanism for recognition. *Molecules.* **2017**, 22, 455-488.
- He, R.; Sang, H.; Ye, R. D. Serum amyloid A induces IL-8 secretion through a G protein-coupled receptor, FPRL1/LXA4R. *Blood* **2003**, 101, 1572-1581.
- Hedstrom, L. Serine protease mechanism and specificity. *Chem. Rev.*, **2002**, 102, 4501-4524.
- Henriksen, P. A.; Hitt, M.; Xing, Z.; Wang, J.; Haslett, C.; Riemersma, R. A.; Webb, D. J.; Kotelevtsev, Y. V.; Sallenave, J. M. Adenoviral gene delivery of elafin and secretory leukocyte protease inhibitor attenuates NF-kappa B-dependent inflammatory responses of human endothelial cells and macrophages to atherogenic stimuli. *J. Immunol.* **2004**, 172(7), 4535-4544.
- Henriksen, P. A.; Sallenave, J. M. Human neutrophil elastase: mediator and therapeutic target in atherosclerosis. *Int. J. Biochem. Cell Biol.* **2008**, 40(6-7), 1095-1100.
- Hert, J.; Hunziker, D.; Kuehne, H.; Luebbers, T.; Martin, R. E.; Mattei, P.; Neidhart, W.; Richter, H.; Rudolph, M.; Pinard, E. Preparation of phenoxymethyl-heterocyclic compounds as autotaxin (ATX) inhibitors. *PCT Int Appl.* WO2017037146A1, **2017**.
- Heutinck, K. M.; Ten Berge, I. J.; Hack, C. E.; Hamanna, J.; Rowshanib, A. T. Serine proteases of the human immune system in health and disease. *Mol. Immunol.* **2010**, 47(11-12), 1943-1955.

- Houard, X.; Leclercq, A.; Fontaine, V. M.; Coutard, M.; Martin-Ventura, J. L.; Ho-Tin-Noe, B.; Touat, Z.; Meilh, O.; Michel, J. B. Retention and activation of blood-borne proteases in the arterial wall. *J. Am. Coll. Cardiol.* **2006**, 9(Suppl. A), A3-A9.
- Houghton, A. M.; Rzymkiewicz, D. M.; Ji, H.; Gregory, A. D.; Egea, E. E.; Metz, H. E.; Stolz, D. B.; Land, S. R.; Marconcini, L. A.; Kliment, C. R.; Jenkins, K. M.; Beaulieu, K. A.; Mouded, M.; Frank, S. J.; Wong, K. K.; Shapiro, S. D. Neutrophil elastase-mediated degradation of IRS-1 accelerates lung tumor growth. *Nat. med.* **2010**, 16(2), 219-223.
- Huang, D. S.; LeBlanc, E. V.; Shekhar-Guturja, T.; Robbins, N.; Krysan, D. J.; Pizarro, J.; Whitesell, L.; Cowen, L. E.; Brown, L. E. Design and Synthesis of Fungal-Selective Resorcyate Aminopyrazole Hsp90 Inhibitors. *J. Med. Chem.* **2020**, 63, 5, 2139-2180.
- Huang, J.; Xiao, Y.; Xu, A.; Zhou, Z. Neutrophils in type 1 diabetes. *J. Diabetes Investig.* **2016**, 7(5), 652-663.
- Humbert, M.; Morrell, N. W.; Archer, S. L.; Stenmark, K. R.; MacLean, M. R.; Lang I. M.; Christman, B. W.; Weir, E. K.; Eickelberg, O.; Voelkel, N. F.; Rabinovitch, M. Cellular and molecular pathobiology of pulmonary arterial hypertension. *J. Am. Coll. Cardiol.* **2004**, 43(12), 13S-24S.
- Hunt, K. K.; Wingate, H.; Yokota, T.; Liu, Y.; Mills, G. B.; Zhang, F.; Fang, B.; Su, C. H.; Zhang, M.; Yi, M.; Keyomarsi, K. Elafin, an inhibitor of elastase, is a prognostic indicator in breast cancer. *Breast. Cancer. Res.* **2013**, 15(1), 1-13.
- Jacobsen, L. C.; Sorensen, O. E.; Cowland, J. B.; Borregaard, N.; Theilgaard-Monch, K. The secretory leukocyte protease inhibitor (SLPI) and the secondary granule protein lactoferrin are synthesized in myelocytes, colocalize in subcellular fractions of neutrophils, and are coreleased by activated neutrophils. *J. Leukoc. Biol.* **2008**, 83, 1155-1164.
- Johnson, T. W.; Richardson, P. F.; Collins, M. R.; Richter, D. T.; Burke, B. J.; Gajiwala, K.; Ninkovic, S.; Linton, M. A.; Le, P. T. Q.; Hoffman, J. E. *Can. Pat. Appl.* CA2915356A1, **2016**.
- Jorand-Lebrun, C.; Kulkarni, S.; Crosignani, S. Merck Patent GmbH. Preparation of pyridazinone-amides derivatives for treating inflammatory disease, autoimmune disorder, cancer or multiple sclerosis. WO2014121931 A1; **2014a**.
- Jorand-Lebrun, C.; Kulkarni, S.; Crosignani, S. Merck Patent GmbH. Macrocyclic pyridazinone derivatives as IRAK inhibitors and their preparation. WO2014121942 A1; **2014b**.
- Kaschwich, M.; Lützen, U.; Zhao, Y.; Tjong, A.; Marx, M.; Haenisch, S.; Wiedow, O.; Preuss, S.; Culman, J.; Zuhayra, M. Biodistribution and pharmacokinetics of the ^{99m}Tc labeled human elastase inhibitor, elafin, in rats. *Drug Metab. Pharmacok.* **2016**, 31, 146-155.
- Kato, N.; Oka, M.; Murase, T.; Yoshida, M.; Sakairi, M.; Yamashita, Y.; Yasuda, Y.; Yoshikawa, A.; Hayashi, Y.; Makino, M.; Takeda, M.; Mirenska, Y.; Kakigami, T. Discovery and pharmacological characterization of N-[2-((2S)-2-cyanopyrrolidin-1-yl)-2-oxoethyl]amino)-2-methylpropyl]-2-methylpyrazolo[1,5-a]pyrimidine-6-carboxamide hydrochloride (anagliptin

hydrochloride salt) as a potent and selective DPP-IV inhibitor. *Bioorg. Med. Chem.* **2011**, *19*, 7221-7227.

- Kawabata, K.; Hagio, T.; Matsuoka, S. The role of neutrophil elastase in acute lung injury. *Eur. J. Pharmacol.* **2002**, *451*, 1-10.
- Kawase, M.; Koyanagi, J.; Saito, S. Site-Selective Trifluoroacetylation of Dimethylamino-Substituted Pyridines and Its Use as a Building Block for Trifluoromethyl-Containing Heterocycles. *Chem. Pharm. Bull.* **1999**, *47*, 718-719.
- Kelly, E.; Greene, C. M.; McElvaney, N. G. Targeting neutrophil elastase in cystic fibrosis. *Expert Opin. Ther. Targets.* **2008**, *12*(2), 145-157.
- Kennedy, L. J. An Expedient Synthesis of Regioisomeric Pyrazole-Fused Cycloalkanones. *Synlett.* **2008**, 2008(4), 600-604.
- Kerros, C.; Tripathi, S. C.; Zha, D.; Mehrens, J. M.; Sergeeva, A.; Philips, A. V.; Qiao, N.; Peters, H. L.; Katayama, H.; Sukhumalchandra, P.; Ruisaard, K. E.; Perakis, A. A.; St John, L. S.; Lu, S.; Mittendorf, E. A.; Clise-Dwyer, K.; Herrmann, A. C.; Alatrash, G.; Toniatti, C.; Hanash, S. M.; Ma, Q.; Mollrem, J. J. Neuropilin-1 mediates neutrophil elastase uptake and cross-presentation in breast cancer cells. *J. Biol. Chem.* **2017**, *292*(24), 10295-10305.
- Keshari, D. R.; Jyoti, A.; Dubey, M.; Kothari, N.; Kohli, M.; Bogra, J.; Barthwal, K. M.; Dikshit, M. Cytokines induced neutrophil extracellular traps formation: implication for the inflammatory disease condition. *PLoS ONE.* **2012**, *7*, 1-10.
- Kessenbrock, K.; Krumbholz, M.; Schönemarck, U.; Back, W.; Gross, W. L.; Werb, Z.; Gröne, H.-J.; Brinkmann, V.; Jenne, D. E. Netting neutrophils in autoimmune small-vessel vasculitis. *Nat. Med.* **2009**, *15*, 623-625.
- Kettritz, R.; Falk, R. J.; Janette, J. C.; Gaido, M. L. Neutrophils superoxide release is required for spontaneous and FMLP-mediated but not for TNF alpha-mediated apoptosis. *J. Am. Soc. Nephrol.* **1997**, *8*, 1091-1100.
- Khlebnikov, A. I.; Schepetkin, I. A.; Quinn, M. T. Structure-activity relationship analysis of N-benzoylpyrazoles for elastase inhibitory activity: A simplified approach using atom pair descriptors. *Bioorg. Med. Chem.* **2008**, *16*, 2791-2802.
- Kim, J. Y.; Wang, Y.; Uddin, Z.; Song, Y. H.; Li, Z. P.; Jenis, J.; Park, K. H. Competitive neutrophil elastase inhibitory isoflavones from the roots of *Flemingia philippinensis*. *Bioorg. Chem.* **2018**, *78*, 249-257.
- Kim, Y. M.; Haghghat, L.; Spiekerkoetter, E.; Sawada, H.; Alvira, C. M.; Wang, L.; Acharya, S.; Rodriguez-Colon, G.; Orton, A.; Zhao, M.; Rabinovitch, M. Neutrophil elastase is produced by pulmonary artery smooth muscle cells and is linked to neointimal lesions. *Am. J. path.* **2011**, *179*, 1560-1572.

- Kirpotina, L. N.; Khlebnikov, A. I.; Schepetkin, I. A.; Ye, R. D.; Rabiet, M. J.; Jutila, M. A.; Quinn, M. T. Identification of novel small-molecule agonists for human formyl peptide receptors and pharmacophore models of their recognition. *Mol. Pharmacol.* **2010**, 77(2), 159-170.
- Klein, M.; Kramer, F.; Golz, S.; Von Nussbaum, F.; Kast, R.; Schäfer, S. *Eur. Heart J.* **2007**, 28, Abstract Suppl.: 55. Abstract of Meeting Papers.
- Koczulla, R.; von Degenfeld, G.; Kupatt, C.; Krötz, F.; Zahler, S.; Gloe, T.; Issbrücker, K.; Unterberger, P.; Zaiou, M.; Lebherz, C.; Karl, A.; Raake, P.; Pfosser, A.; Boekstegers, P.; Welsch, U.; Hiemstra, P. S.; Vogelmeier, C.; Gallo, R. L.; Clauss, M.; Bals, R. An angiogenic role for the human peptide antibiotic LL37/Hcap-18. *J. Clin. Invest.* **2003**, 111, 1665-1672.
- Korkmaz, B.; Moreau, T.; Gauthier, F. Neutrophil elastase, proteinase 3 and cathepsin G: Physicochemical properties, activity and physiopathological functions. *Biochimie.* **2008**, 90, 227-242.
- Krishnamoorthy, S.; Recchiuti, A.; Chiang, N.; Yacoubian, S.; Lee, C. H.; Yang, R.; Petasis, N. A.; Serhan, C. N. Resolvin D1 binds human phagocytes with evidence for proresolving receptors. *Proc. Natl. Acad. Sci. USA.* **2010**, 107, 1660-1665.
- Lain, S.; Drummond, C.; Van Leeuwen, I.; Haraldsson, M. et al. Tetrahydroindazoles for use in the treatment of cancer and viral infections and their preparation. *PCT Int. Appl.* WO2017077280A1, **2017**.
- Langhorst, J.; Elsenbruch, S.; Koelzer, J.; Rueffer, A.; Michalsen, A.; Dobos, G. J. Noninvasive markers in the assessment of intestinal inflammation in inflammatory bowel diseases: performance of fecal lactoferrin, calprotectin, and PMN-elastase, CRP, and clinical indices. *Am. J. Gastroenterol.* **2008**, 103, 162-169.
- Lauffer, D. J.; Bemis, G.; Boyd, M.; Deininger, D.; Deng, H.; Dorsch, W.; Gu, W.; Hoover, R. R.; Johnson, Jr., Mac Arthur; Ledebor, M. W. et al Preparation of pteridinone compds. for the treatment of cellular proliferative disorders. *U.S. Pat. Appl. Publ.* US20190322673A1, **2019**.
- Laurell, C. B.; Eriksson, S: The electrophoretic 1 globulin pattern of serum in 1 antitrypsin deficiency. *Scand. J. Clin. Lab. Invest.* **1963**, 15, 132-140.
- Lawrence, D. A.; Olson, S. T.; Muhammad, S.; Day, D. E.; Kvassman, J. O.; Ginsburg, D.; Shore, J. D. Partitioning of serpin-proteinase reactions between stable inhibition and substrate cleavage is regulated by the rate of serpin reactive center loop insertion into beta-sheet A. *J. Biol. Chem.* **2000**, 275, 5839-5844.
- Lee, K. H.; Lee, C. H.; Jeong, J.; Jang, A.-H.; Yoo, C.-G. Neutrophil elastase differentially regulates IL-8 and VEGF production by cigarette smoke extract. *J. Biol. Chem.* **2015**, 290, 28438-28445.
- Lee, K. M.; Tsai, K. Y.; Wang, N.; Ingber, D. E. Extracellular matrix and pulmonary hypertension: control of vascular smooth muscle cell contractility. *Am. J. Physiol.* **1998**, 274, H76–H82.

- Lee, Y.; Murphy, P. M.; Wang, J. M. Formyl-peptide receptors revisited. *Trends Immunol.* **2002**, 23, 541-548.
- Leitão, H. S.; Doblas, S.; Garteiser, P.; D'Assignies, G.; Paradis, V.; Mouri, F.; Geraldles, C. F.; Ronot, M.; Van Beers, B. E. Hepatic Fibrosis, Inflammation, and Steatosis: Influence on the MR Viscoelastic and Diffusion Parameters in Patients with Chronic Liver Disease. *Radiology.* **2016**, 283, 98–1107.
- Lerman, I.; Garcia-Hernandez, M. L.; Rangel-Moreno, J.; Chiriboga, L.; Pan, C.; Nastiuk, K. L.; Krolewski, J. J.; Sen, A.; Hammes, S. R. Infiltrating Myeloid Cells Exert Protumorigenic Actions via Neutrophil Elastase. *Mol. Cancer. Res.* **2017**, 15(9), 1138-1152.
- Lerman, I.; Hammes, S. R. Neutrophil elastase in the tumor microenvironment. *Steroids.* **2018**, 133, 96-101.
- Liao, D. F.; Yin, N. X.; Huang, J.; Ryan, S. F. Effects of human poly-morphonuclear leukocyte elastase upon surfactant proteins in vitro. *Biochim. Biophys. Acta.* **1996**, 1302, 117-128.
- Liou, T. G.; Campbell, E. J. Nonisotropic enzyme-inhibitor interactions: a novel non-oxidative mechanism for quantum proteolysis by human neutrophils. *Biochemistry.* **1995**, 34(49), 16171-16177.
- Lipinski, C. A.; Lombardo, F.; Dominy, B. W.; Feeney, P. J. Experimental and computational approaches to estimate solubility and permeability in drug discovery and development settings. *Adv. Drug Delivery Rev.* **1997**, 23 3-25.
- Liverton, N. J.; Bolea, C.; Celanire, S.; Luo, Y. Tricyclic compounds as mGluR4 modulators and their preparation and use for treatment and prevention of mGluR4-mediated diseases. *PCT Int. Appl. WO2012006760A1*, **2012b**.
- Liverton, N. J.; Bolea, C.; Celanire, S.; Yunfu, L. Tricyclic fused thiazolopyrazole compounds as allosteric modulators of metabotropic glutamate receptors. *PCT Int. Appl. WO2012008999A1*, **2012a**.
- Loison, F.; Zhu, H.; Karatepe, K.; Kasorn, A.; Liu, P.; Ye, K.; Zhou, I.; Cao, S.; Gong, H.; Jenne, D. E.; Remold-O'Donnell, E.; Xu, Y.; Luo, H. R. Proteinase 3-dependent caspase-3 cleavage modulates neutrophil death and inflammation. *J. Clin. Invest.* **2014**, 124, 4445-4458.
- Lounsbury, N.; Mateo, G.; Jones, B.; Papaiahgari, S.; Thimmulappa, R. K.; Teijaro, C.; Gordon, J.; Korzekwa, K.; Ye, M.; Allaway, G.; Abou-Gharbia, M.; Biswal, S.; Childers, W. Heterocyclic chalcone activators of nuclear factor (erythroid-derived 2)-like 2 (Nrf2) with improved in vivo efficacy. *Bioorg. Med. Chem.* **2015**, 23(17), 5352-5359.
- Lucas, S. D.; Costa, E.; Guedes, R. C.; Moreira, R. Targeting COPD: advances on low-molecular-weight inhibitors of human neutrophil elastase. *Med. Res. Rev.* **2011**, 33, E73-E101.
- Luo, D.; Chen, Q.-Y.; Luesch, H. Total synthesis of the potent marine-derived elastase inhibitor lynbyastatin 7 and in vitro biological evaluation in model systems for pulmonary diseases. *J. Org. Chem.* **2016**, 81, 532-544.

- Lynch, B. M.; Misbahul, A. I.; Teo, H. C.; Pedrotti, F. Pyrazolo[3,4-b]pyridines: Synthesis, reactions, and nuclear magnetic resonance spectral. *Can. J. Chem.* **1988**, 66, 420-428.
- Ma, Y. C.; Huang, J.; Ali, S.; Lowry, W.; Huang, X. Y. Src tyrosine kinase is a novel direct effector of G proteins. *Cell.* **2000**, 102, 635-646.
- Maiorani, O.; Pivetta, E.; Capuano, A.; Modica, T. M.; Wassermann, B.; Bucciotti, F.; Colombatti, A.; Doliana, R.; Spessotto, P. Neutrophil elastase cleavage of the gC1q domain impairs the EMILIN1- alpha4beta1 integrin interaction, cell adhesion and anti-proliferative activity. *Sci. Rep.* **2017**, 7, 39974-39987.
- Majchrzak-Gorecka, M.; Majewski, P.; Grygier, B.; Murzyn, K.; Cichy, J. Secretory leukocyte protease inhibitor (SLPI), a multifunctional protein in the host defense response. *Cytokine Growth Factor Rev.* **2016**, 28, 79-93.
- Majewski, P.; Majchrzak-Gorecka, M.; Grygier, B.; Skrzeczynska-Moncznik, J.; Osiecka, O.; Cichy, J. Inhibitors of serino proteases in regulating the production and function of neutrophil extracellular traps. *Front. Immunol.* **2016**, 7, 1-10.
- Manley, H. R.; Keightley, M. C.; Lieschke, G. J. The Neutrophil Nucleus: An Important Influence on Neutrophil Migration and Function. *Front. Immunol.* **2018**, 9(2867), 1-18.
- Manohar, M.; Verma, A. K.; Venkateshaiah, S.U.; Sanders, N. L.; Mishra, A. Pathogenic mechanisms of pancreatitis. *World J. Gastr. Pharmacol. Therapeut.* **2017**, 8, 10-25.
- Martins, F. T.; Assis, D. M.; Dos Santos, M. H.; Camps, I.; Veloso, M. P.; Juliano, M. A.; Alves, L. C.; Doriguetto, A. C. Natural polyprenylated benzophenones inhibiting cysteine and serine protease. *Eur. J. Med. Chem.* **2009**, 44, 1230-1239.
- Marto, J.; Gouveia, L. F.; Gonçalves, L. M.; Gaspar, D. P.; Pinto, P.; Carvalho, F. A.; Oliveira, E.; Ribeiro, H. M.; Almeida, A. J. A quality by design (QbD) approach on starch-based nanocapsules: a promising platform for topical drug delivery. *Colloids Surf. B: Biointerfaces.* **2016**, 143, 177-185.
- Matsson, H.; Söderhäll, C.; Einarsdottir, E.; Lamontagne, M.; Gudmundsson, S.; Backman, H.; Lindberg, A.; Rönmark, E.; Kere, J.; Sin, D.; Postma, D. S.; Bossé, Y.; Lundbäck, B.; Klar, J.; Targeted high-throughput sequencing of candidate genes for chronic obstructive pulmonary disease. *BMC Pulmonary Medicine*, **2016**, 16, 1-10.
- Matsui, H.; Wagner, V. E.; Hill, D. B.; Schwab, U. E.; Rogers, T. D.; Button, B.; Taylor, R. M.; Superfine, R.; Rubinstein, M.; Iglewski, B. H.; Boucher R. C. A physical linkage between cystic fibrosis airway surface dehydration and *Pseudomonas aeruginosa* biofilms. *Proc. Natl. Acad. Sci. U. S. A.* **2006**, 103(48), 18131-18136.
- Matsuse, H.; Yanagihara, K.; Mukae, H.; Tanaka, K.; Nakazato, M.; Kohno, S. Association of plasma neutrophil elastase levels with other inflammatory mediators and clinical features in adult patients with moderate and severe pneumonia. *Respir. Med.* **2007**, 101(7), 1521-1528.
- Matthay, M. A.; Ware, L. B.; Zimmerman, G. A. The acute respiratory distress syndrome. *J. Clin. Invest.* **2012**, 122, 2731-2740.

- Maynard, G.; Yuan, J.; Rachwal, S. Substituted fused pyrazolecarboxylic acid arylamides and related compounds. *PCT Int. Appl.* WO2003066634A1, **2003**.
- Mazgaeen, L.; Gurung, P. Recent Advances in Lipopolysaccharide Recognition Systems. *Int. J. Mol. Sci.* **2020**, 21(2), 379.
- McGuckin MA, Eri R, Simms LA, Florin TH, Radford-
- Mehta, A. CFTR: More than just a chloride channel. *Pediatr. Pulmonol.* **2005**, 39(4), 292-298.
- Meyer-Hoffert, U.; Wingertzahn, J.; Wiedow, O. Human leukocyte elastase induces keratinocyte proliferation by epidermal growth factor receptor activation. *J. Investig. Dermatol.* **2004**, 123, 338-345.
- Mezyk-Kopec, R.; Bzowska, M.; Bzowska, M.; Mickowska, B.; Mak, P.; Potempa, J.; Bereta, J. Effects of elastase and cathepsin G on the levels of membrane and soluble TNFalpha. *Biol. Chem.* **2005**, 386, 801-811.
- Migeotte, I.; Riboldi, E.; Franssen, J. D.; Grégoire, F.; Loison, C.; Wittamer, V.; Detheux, M.; Robberecht, P.; Costagliola, S.; Vassart, G.; Sozzani, S.; Parmentier, M.; Communi, D. Identification and characterization of an endogenous chemotactic ligand specific for FPRL2. *J. Exp. Med.* **2005**, 201(1), 83-93.
- Miglietta, D.; Carnini, C.; Puviani, V. et al. Pharmacological characterization of CHF6333, a novel potent inhaled inhibitor of neutrophil elastase. *ERS International Congress, London*, **2016**.
- Miller, M. C.; Manning, H. B.; Jain, A.; Troeberg, L.; Dudhia, J.; Essex, D.; Sandison, A.; Seiki, M.; Nanchahal, J.; Nagase, H.; Itoh, Y. Membrane type 1 matrix metalloproteinase is a crucial promoter of synovial invasion in human rheumatoid arthritis. *Arthritis. Rheum.* **2009**, 60, 686-697.
- Milner, J. M.; Patel, A.; Rowan, A. D. Emerging roles of serine proteinases in tissue turnover in arthritis. *Arthritis. Rheum.* **2008**, 58(12), 3644-3656.
- Miravittles, M. Alpha-1-antitrypsin and other proteinase inhibitors. *Curr. Opin. Pharmacol.* **2012**, 12, 309-314.
- Moreau, T.; Baranger, K.; Dade, S.; Dallet-Choisy, S.; Guyot, N.; Zani, M. L. Multifaceted roles of human elafin and secretory leukocyte proteinase inhibitor (SLPI), two serine protease inhibitors of the chelonianin family. *Biochimie.* **2008**, 90, 284-295.
- Moynagh, P. N. The NF-kB pathway. *J. Cell Sci.* **2005**, 118, 4585-4592.
- Mtairag, E. M.; Houard, X.; Rais, S.; Pasquier, C.; Oudghiri, M.; Jacob, M. P.; Meilhac, O.; Michel, J. B. Pharmacological potentiation of natriuretic peptide limits polymorphonuclear neutrophil vascular cell interactions. *Arterioscler. Thromb. Vasc. Biol.* **2002**, 22(11), 1824-1831.
- Muegge, I.; Heald, S. L.; Brittelli, D. Simple selection criteria for drug-like chemical matter. *J. Med. Chem.* **2001**, 4, 1841-1846.
- Murphy, G.; Nagase, H. Reappraising metalloproteinases in rheumatoid arthritis and osteoarthritis: destruction or repair? *Nat. Clin. Pract. Rheumatol.* **2008**, 4, 128-135.

- Nakano, H.; Saito, N.; Parker, L.; Tada, Y.; Abe, M.; Tsuganezawa, K.; Yokoyama, S.; Tanaka, A.; Kojima, H.; Okabe, T.; Nagano, T. Rational Evolution of a Novel Type of Potent and Selective Proviral Integration Site in Moloney Murine Leukemia Virus Kinase 1 (PIM1) Inhibitor from a Screening-Hit Compound. *J. Med. Chem.* **2012**, *55*(11), 5151-5164.
- Nakayama, Y.; Odagaki, Y.; Fujita, S.; Matsuoka, S.; Hamanaka, N.; Nakai, H.; Toda, M. Clarification of mechanism of human sputum elastase inhibition by a new inhibitor, ONO-5046, using electrospray ionization mass spectrometry. *Bioorg. Med. Chem. Lett.* **2002**, *12*, 2349-2353.
- Nathan, C. Points of control in inflammation. *Nature.* **2002**, *420*, 846-852.
- Nauseef, W. M. How human neutrophils kill and degrade microbes: an integrated view. *Immunol. Rev.* **2007**, *219*, 88-102.
- Navia, M. A.; McKeever, B. M.; Springer, J. P.; Lin, T. Y.; Williams, H. R.; Fluder, E. M.; Dorn, C. P.; Hoogsteen, K. Structure of human neutrophil elastase in complex with a peptide chloromethyl ketone inhibitor at 1.84 Å resolution. *Proc. Natl. Acad. Sci. USA.* **1989**, *86*, 7-11.
- Obayashi, Y.; Yamadori, I.; Fujita J.; Yoshinouchi, T.; Ueda, N.; Takahara, J. The role of neutrophils in the pathogenesis of idiopathic pulmonary fibrosis. *Chest.* **1997** *112*(5), 1338-1343.
- Ohbayashi, H. Current synthetic inhibitors of human neutrophil elastase in 2005. *Expert. Opin. Ther. Pat.* **2005**, *15*, 759-771.
- Ohmoto, K.; Yamamoto, T.; Horiuchi, T.; Imanishi, H.; Odagaki, Y.; Kawabata, K.; Sekioka, T.; Hirota, Y.; Matsuoka, S.; Nakai, H.; Toda, M.; Cheronis, J. C.; Spruce, L. W.; Gyorkos, A.; Wieczorek, M. Design and synthesis of new orally active nonpeptidic inhibitors of human neutrophil elastase. *J. Med. Chem.* **2000**, *43*, 4927-4929.
- Oost, T.; Fiegen, D.; Christian, G. Substituted 4-pyridones and their use as inhibitors of neutrophil elastase activity. *PCT Int. Appl.* WO2014029830A1, **2016a**.
- Oost, T.; Fiegen, D.; Gnam, C.; Handschuh, S.; Peters, S.; Roth, G. J. Substituted 4-pyridones and their use as inhibitors of neutrophil elastase activity. *PCT Int. Appl.* WO2014029831A1, **2016b**.
- Owen, C. A.; Campbell, E. J. Neutrophil proteinases and matrix degradation. The cell biology of pericellular proteolysis. *Semin. Cell. Biol.* **1995**, *6*, 67-376.
- Packard, R. R. S.; Peter, L. Inflammation in atherosclerosis: from vascular biology to biomarker discovery and risk prediction. *Clin. Chem.* **2008**, *54*, 24-38.
- Page, M. J.; Di Cera, E. Serine peptidases: classification, structure and function. *Cell Mol. Life Sci.* **2008**, *65*(7-8), 1220-1236.
- Pandey, K. C.; De, S.; Mishra, P. K. Role of proteases in chronic obstructive pulmonary disease. *Front. Pharmacol.* **2017**, *8*, 512.
- Papayannopoulos, V.; Metzler, K. D.; Hakkim, A.; Zychlinsky, A. Neutrophil elastase and myeloperoxidase regulate the formation of neutrophil extracellular traps. *J. Cell. Biol.* **2010**, *191*, 677-691.

- Papayannopoulos, V.; Zychlinsky, A. NETs: a new strategy for using old weapons. *Trends Immunol.* **2009**, 30, 513-521.
- Partida-Sánchez, S.; Cockayne, D. A.; Monard, S.; Jacobson, E. L.; Oppenheimer, N.; Garvy, B.; Kusser, K.; Goodrich, S.; Howard, M.; Harmsen, A.; Randall T. D.; Lund F. E. Cyclic ADP-ribose production by CD38 regulates intracellular calcium release, extracellular calcium influx and chemotaxis in neutrophils and is required for bacterial clearance in vivo. *Nat. Med.* **2001**, 7, 1209-1216.
- Partida-Sánchez, S.; Iribarren, P.; Moreno-García, M. E.; Gao, J. L.; Murphy, P. M.; Oppenheimer, N.; Wang, J. M.; Lund, F. E. Chemotaxis and calcium responses of phagocytes to formyl peptide receptor ligands is differentially regulated by cyclic ADP ribose. *J. Immunol.* **2004**, 172(3), 1896-1906.
- Perez, H. D.; Holmes, R.; Kelly, E.; McClary, J.; Andrews, W. H. Cloning of cDNA encoding a receptor related to the formyl peptide receptor of human neutrophils. *Gene.* **1992**, 118, 303-304.
- Perretti, M. The annexin 1 receptor(s): is the plot unravelling? *Trends Pharmacol Sci.* **2003**, 24, 574–579.
- Peters, M. B.; Merz, K. M. Semiempirical comparative binding energy analysis (SE-COMBINE) of a series of trypsin inhibitors. *J. Chem. Theory Comput.* **2006**, 2, 383-399.
- Peters, S.; Anderskewitz, R.; Gnam, C.; Hoesch, H.; Morschhaeuser, G.; Oost, T.; Ries, U. J. Substituted bicyclic dihydropyrimidones and their use as inhibitors of neutrophil elastase activity. *U.S. Pat. Appl. Publ.* US9458113B2, **2016**.
- Peters, S.; Anderskewitz, R.; Morschhaeuser, G.; Oost, T. Substituted dihydropyrimidones and their use as inhibitors of neutrophil elastase activity. *PCT Int. Appl.* WO2016016366A1, **2018**.
- Pfundt, R.; van Ruissen, F.; van Vlijmen-Willems, I. M.; Alkemade, H. A.; Zeeuwen, P. L.; Jap, P. H.; Dijkman, H.; Fransen, J.; Croes, H.; van Erp, P. E.; Schalkwijk, J. Constitutive and inducible expression of SKALP/elafin provides anti-elastase defense in human epithelia. *J. Clin. Invest.* **1996**, 98(6), 1389-1399.
- Pham, C. T. N. Neutrophil serine proteases fine-tune the inflammatory response. *Int. J. Biochem. Cell Biol.* **2008**, 40, 1317-1333.
- Pham, C. T. N. Neutrophil serine proteases: specific regulators of inflammation. *Nat. Rev. Immunol.* **2006**, 6, 541–550.
- Pieretti, S.; Di Giannuario, A.; De Felice, M.; Perretti, M.; Cirino, G. Stimulus-dependent specificity for annexin 1 inhibition of the inflammatory nociceptive response: the involvement of the receptor for formylated peptides. *Pain.* **2004**, 109, 52-63.
- Pires, D. E. V.; Blundell, T. L.; Ascher, D. B. pkCSM: Predicting Small-Molecule Pharmacokinetic and Toxicity Properties Using Graph-Based Signatures. *J. Med. Chem.* **2015**, 58, 4066-4072.

- Pivetta, E.; Danussi, C.; Wassermann, B.; Modica, T. M.; Del Bel Belluz, L.; Canzonieri, V.; Colombatti, A.; Spessotto, P. Neutrophil elastase-dependent cleavage compromises the tumor suppressor role of EMILIN1. *Matrix. Biol.* **2014**, 34, 22-32.
- Piwowar, A.; Knapik-Kordecka, M.; Warwas, M. Concentration of Leukocyte Elastase in Plasma and Polymorphonuclear Neutrophil Extracts in Type 2 Diabetes. *Clin. Chem. Lab. Med.* **2000**, 38(12), 1257-1261.
- Pott, G. B.; Chan, E. D.; Dinarello, C. A.; Shapiro, L. Alpha-1-antitrypsin is an endogenous inhibitor of proinflammatory cytokine production in whole blood. *J. Leukoc. Biol.* **2009**, 85, 886-895.
- Powers, J. C.; Asgian, J. L.; Ekici, O. D.; James, K. E. Irreversible inhibitors of serine, cysteine, and threonine proteases. *Chem. Rev.* **2002**, 102, 4639-4750.
- Quinton, P. M. Cystic fibrosis: impaired bicarbonate secretion and mucoviscidosis. *Lancet.* **2008**, 372(9636), 415-417.
- Rabinovitch, M.; Guignabert, C.; Humbert, M.; Nicolls, M. R. Inflammation and immunity in the pathogenesis of pulmonary arterial hypertension. *Circ. Res.* **2014**, 115(1), 165-175.
- Ragaller, M.; Richter, T. Acute lung injury and acute respiratory distress syndrome. *J. Emerg. Trauma Shock.* **2010**, 3(1), 43-51.
- Rawlings, N. D.; Barrett, A. D.; Thomas, P. D.; Huang, X.; Bateman, A.; Finn, R. D. The MEROPS database of proteolytic enzymes, their substrates and inhibitors in 2017 and a comparison with peptidases in the PANTHER database. *Nucleic Acids Res.* **2018**, 46, D624-D632.
- Rawlings, N. D.; Barrett, A. J. Evolutionary families of peptidases. *Biochem. J.* **1993**, 290, 205-218.
- Rawlings, N. D.; Barrett, A. J.; Bateman, A. Asparagine peptide lyases: A seventh catalytic type of proteolytic enzymes. *J. Biol. Chem.* **2011**, 286, 38321-38328.
- Rawlings, N. D.; Barrett, A. J.; Bateman, A. Using the MEROPS database for proteolytic enzymes and their inhibitors and substrates. *Curr. Protoc. Bioinformatics.* **2014**, 12(48), 1-33.
- Reeves, E. P.; Lu, H.; Jacobs, H. L.; Messina, C. G. M.; Bolsover, S.; Gabellak, G.; Potma, E. O.; Warley, A.; Roes, J.; Segal, A. W. Killing activity of neutrophil is mediated through activation of proteases by K⁺ flux. *Nature.* **2002**, 416(6878), 291-297.
- Robert, L.; Robert, A. M.; Jacotot, B. Elastin elastase atherosclerosis revisited. *Atherosclerosis.* **1998**, 140(2), 281-295.
- Robertson, S. E.; Young, J. D.; Kitson, S.; Pitt, A.; Evans, J.; Roes, J.; Karaoglu, D.; Santora, L.; Ghayur, T.; Liew, F. Y.; Gracie, J. A.; McInnes, I. B. Expression and alternative processing of IL-18 in human neutrophils. *Eur. J. of Immunol.* **2006**, 36, 722-731.
- Roghanian, A.; Fitch, P. M.; Howie, S. E. M.; Sallenave, J. M. Human neutrophil elastase inhibitors in innate and adaptive immunity. *Biochem. Soc. Trans.* **2006**, 34(2), 279-282.

- Sabeh, F.; Fox, D.; Weiss, S. J. Membrane-type I matrix metalloproteinase-dependent regulation of rheumatoid arthritis synoviocyte function. *J. Immunol.* **2010**, 184, 6396-6406.
- Sabio, G.; Davis, R. J. TNF, MAP kinase signalling pathways. *Semin. in Immunol.* **2014**, 26, 237-245.
- Saito, K.; Nakao, A.; Shinozuka, T.; Shimada, K.; Matsui, S.; Oizumi, K.; Yano, K.; Ohata, K.; Nakai, D.; Nagai, Y.; Naito, S. Discovery and structure-activity relationship of thienopyridine derivatives as bone anabolic agents. *Bioorg. Med. Chem.* **2013**, 21(7), 1628-1642.
- Saleem, M.; Nazir, M.; Hussain, H.; Tousif, M. I.; Elsebai, M. F.; Riaz, N.; Akhtar, N., Natural Phenolics as Inhibitors of the Human Neutrophil Elastase (HNE) Release: An Overview of Natural Anti-inflammatory Discoveries during Recent Years. *Anti-Inflammatory & Anti-Allergy Agents in Med. Chem.* **2018**, 17, 70-94.
- Sallenave, J. M. The role of secretory leukocyte proteinase inhibitor and elafin (elastase-specific inhibitor/skin-derived antileukoproteinase) as alarm antiproteinases in inflammatory lung disease. *Respir. Res.* **2000**, 1, 87-92.
- Sallenave, J. M.; Ryle, A. P. Purification and characterization of elastase-specific inhibitor. Sequence homology with mucus proteinase inhibitor. *Biol. Chem. Hoppe Seyler.* **1991**, 372(1), 13-21.
- Salvador, L. A.; Taori, K.; Biggs, J. S.; Jakoncic, J.; Ostrov, D. A.; Paul, V. J.; Luesch, H. Potent elastase inhibitors from cyanobacteria: structural basis and mechanisms mediating cytoprotective and anti-inflammatory effects in bronchial epithelial cells. *J. Med. Chem.* **2013**, 56, 1276-1290.
- Salvesen, G. S.; Barrett, A. J. Covalent Binding of Proteinases in their Reaction with α_2 -Macroglobulin. *Biochem. J.* **1980**, 187, 695-701.
- Santagati, N. A.; Salerno, L.; Di Giacomo, C.; Vanella, L.; Ronsisvalle, S. Inhibition of human leucocyte elastase by novel thieno-1,3-oxazin-4-ones and thieno-1,3-thioxazin-4-ones. *Lett. Drug. Des. Discov.* **2007**, 4, 386-393.
- Schafer, M.; Werner, S. Cancer as an overhealing wound: an old hypothesis revisited. *Nat. Rev. Mol. Cell. Biol.* **2008**, 9, 628-638.
- Schepetkin, I. A.; Khlebnikov, A. I.; Quinn, M. T. N-benzoylpyrazoles are novel small-molecule inhibitors of human neutrophil elastase. *J. Med. Chem.* **2007**, 50, 4928-4938.
- Schilling, O.; Kittel, H.; Backe, W.; Kremmer, E.; Jenne, D. E. NSP4, an elastase-related protease in human neutrophils with arginine specificity. *Proc. Natl. Acad. Sci. U.S.A.* **2012**, 109(16), 6229-6234.
- Schirok, H.; Griebenow, N.; Füstner, C.; Dilmac, A. M. Use of 3-(trifluoromethyl)-1H-pyrazolo-[3,4-b]pyridine as a versatile building block. *Tetrahedron.* **2005**, 71, 5597-5601.
- Scuderi, P.; Nez, P. A.; Duerr, M. L.; Wong, B. J.; Valdez, CM. Cathepsin-G and leukocyte elastase inactivate human tumor necrosis factor and lymphotoxin. *Cell Immunol.* **1991**, 135, 299-313.

- Seemüller, E.; Lupas, A.; Stock, D.; Löwe, J.; Huber, R.; Baumeister, W. Proteasome from *Thermoplasma acidophilum*: a threonine protease. *Science*. **1995**, 268, 579-582.
- Segal, A. W. How neutrophils kill microbes. *Annu. Rev. Immunol.* **2005**, 23, 197-223.
- Senior, R. M.; Campbell, E. J. Neutral proteinases from human inflammatory cells. A critical review of their role in extracellular matrix degradation. *Clin. Lab. Med.* **1983**, 3, 645-666.
- Serhan, C. N.; Krishnamoorthy, S.; Recchiuti, A.; Chiang, N. Novel anti-inflammatory pro-resolving mediators and their receptors. *Curr. Top. Med. Chem.* **2011**, 11(6), 629-647,
- Serhan, C. N.; Savill, J. Resolution of inflammation: the beginning programs the end. *Nature Immunol.* **2005**, 6, 1191-1197.
- Sharma, R. K.; Younis, Y.; Mugumbate, G.; Njoroge, M.; Gut, J.; Rosenthal, P. J.; Chibale, K. Synthesis and structure–activity-relationship studies of thiazolidinediones as antiplasmodial inhibitors of the *Plasmodium falciparum* cysteine protease falcipain-2. *Eur. J. Med. Chem.* **2015**, 90, 507-518.
- Shaw, L.; Wiedow, O. Therapeutic potential of human elafin. *Biochem. Soc. Trans.* **2011**, 39(5), 1450-1454.
- Sheldrick, G. M. *SHELXT* - Integrated space-group and crystal-structure determination. *Acta Cryst. C.* **2015**, 71, 3-8.
- Siedle, B.; Hrenn, A.; Merfort, I. Natural compounds as inhibitors of human neutrophil elastase. *Planta Med.* **2007**, 73(5), 401-420.
- Simon, M. I.; Strathmann, M. P.; Gautam, N. Diversity of G proteins in signal transduction. *Science*. **1991**, 252, 802-808.
- Smith, G. Intestinal barrier dysfunction in inflammatory bowel diseases. *Inflamm. Bowel Dis.* **2009**, 15, 100-113.
- Smith, R. J.; Sam, L. M.; Justen, J. M. Diacylglycerols modulate human polymorphonuclear neutrophil responsiveness: effects on intracellular calcium mobilization, granule exocytosis, and superoxide anion production. *J. Leukoc. Biol.* **1998**, 43, 411-419.
- Soderberg, T. *Organic Chemistry with a Biological Emphasis Volume II*. University of Minnesota Morris Digital Well: Chemistry Publications; **2019**.
- Sofi, F.; Fabbri, A.; Casini, A. Inflammation and Cardiovascular Disease and Protection by the mediterranean Diet. *Mediterranean Diet: Springer International publishing.* **2016**, 89-96.
- Solito, E.; Kamal, A.; Russo-Marie, F.; Buckingham, J. C.; Marullo, S.; Perretti, M. A novel calcium-dependent proapoptotic effect of annexin 1 on human neutrophils. *Faseb J.* **2003**, 17, 1544–1546.
- Soon, E.; Holmes, A. M.; Treacy, C. M.; Doughty, N. J.; Southgate, L.; Machado, R. D.; Trembath, R. C.; Jennings, S.; Barker, L.; Nicklin, P.; Walker, C.; Budd D. C.; Pepke-Zaba, J.; Morrell, N. W. Elevated levels of inflammatory cytokines predict survival in idiopathic and familial pulmonary arterial hypertension. *Circulation.* **2010**, 122, 920-927.

- Sorroche, P. B.; Acquier, M. F.; Jove, L. O.; Giugno, E.; Pace, S.; Livellara, B.; Legal, S.; Oyhamburu, J.; Saez, M. S. Alpha-1 antitrypsin deficiency in COPD patients: a cross-sectional study. *Arch. Broncopneumol.* **2015**, 51(11), 539-543.
- Sottrup-Jensen, L. Alpha macroglobulins: structure, shape and mechanism of protease complex formation. *J. Biol. Chem.* **1989**, 264, 11539-11542.
- Spanò, V.; Parrino, B.; Carbone, A.; Montalbano, A.; Salvador, A.; Brun, P.; Barraja, P. Pyrazolo[3,4-h]quinolines promising photosensitizing agents in the treatment of cancer. *Eur. J. Med. Chem.* **2015**, 102, 334-351.
- Stacher, E.; Graham, B. B.; Hunt, J. M.; Gandjeva, A.; Groshong, S. D.; McLaughlin, V. V.; Jessup, M.; Grizzle, W. E.; Aldred, M. A.; Cool, C. D.; Tuder, R. M. Modern age pathology of pulmonary arterial hypertension. *Am. J. Respir. Crit. Care Med.* **2012**, 186, 261-272.
- Standish, A. J.; Weiser, J. N. Human neutrophils kill *Streptococcus pneumoniae* via serine proteases. *J. Immunol.* **2009**, 183, 2602-2609.
- Stein, C.; Schäfer, M.; Machelska, H. Attacking pain at its source: new perspectives on opioids. *Nat. Med.* **2003**, 9, 1003-1008.
- Stephens, P. J.; Devlin, F. J.; Chabalowski, C. F.; Frisch, M. J. Ab Initio Calculation of Vibrational Absorption and Circular Dichroism Spectra Using Density Functional Force Fields. *J. Phys. Chem.* **1994**, 98, 11623-11627.
- Stevens, T.; Ekholm, K.; Granse, M.; Lindahl, M.; Kozma, V.; Jungar, C.; Ottosson, T.; Falk-Håkansson, H.; Churg, A.; Wright, J. L.; Lal, H.; Sanfridson, A. AZD9668: Pharmacological Characterization of a Novel Oral Inhibitor of Neutrophil Elastase. *J. Pharmacol. Exp. Ther.* **2011**, 339(1), 313-320.
- Stoyanov, B.; Volinia, S.; Hanck, T.; Rubio, M.; Luobtchenov, M.; Malek, D.; Stoyanova, S.; Vanhaesebroeck, B.; Dhand, R.; Nürnberg, B.; Gierschik, P.; Seedorf, K.; Hsuan, J. J.; Waterfield, M. D.; Wetzker, R. Cloning and characterization of a G protein-activated human phosphoinositide-3 kinase. *Science.* **1993**, 269, 690-693.
- Suter, S. The Imbalance between Granulocyte Neutral Proteases and Antiproteases in Bronchial Secretions from Patients with Cystic Fibrosis. *Antibiot. Chemother.* **1989**, 42, 158-168.
- Takeuchi, O.; Akira, S. Pattern Recognition Receptors and Inflammation. *Cell.* **2010**, 140, 805-820.
- Taylor, C.; Crawford, I. P.; Hugli, T. E. Limited degradation of the third component (C3) of human complement by human leukocyte elastase (HLE): partial characterization of C3 fragments. *Biochemistry.* **1977**, 16, 3390-3396.
- Taylor, T.; Dirir, O.; Zamanian, R. T.; Rabinovitch, M.; Thompson, R. A. A. The Role of Neutrophils and Neutrophil Elastase in Pulmonary Arterial Hypertension. *Front. Med.* **2018**, 5(217), 1-8.
- Teshima, T.; Griffin, J. C.; Powers, J. C. A new class of heterocyclic serine protease inhibitors. Inhibition of human-leukocyte elastase, porcine pancreatic elastase, cathepsin-g, and bovine

chymotrypsin-a-alpha with substituted benzoxazinones, quinazolines, and anthranilates. *J. Biol. Chem.* **1982**, 257, 5085-5091.

- Thille, A. W.; Esteban, A.; Fernandez-Segoviano, P.; Rodriguez, J. M.; Aramburu, J. A.; Peñuelas, O.; Cortés-Puch, I.; Cardinal-Fernández, P.; Lorente, J. A.; Frutos-Vivar, F. Comparison of the Berlin definition for acute respiratory distress syndrome with autopsy. *Am. J. Respir. Crit. Care Med.* **2013**, 187, 761-767.
- Torriglia, A.; Perani, P.; Brossas, J. Y.; Chaudun, E.; Treton, J.; Courtois, Y.; Counis, M. F. L-DNase II, a molecule that links proteases and endonucleases in apoptosis, derives from the ubiquitous serpin leukocyte elastase inhibitor. *Mol. Cell Biol.* **1998**, 18, 3612-3619.
- Tsai, Y. F.; Hwang, T. L. Neutrophil elastase inhibitors: a patent review and potential applications for inflammatory lung disease (2010–2014). *Expert Opin. Ther. Pat.* **2015**, 25(10), 1145-1158.
- Tsuji, N.; Moriwaki, S.; Suzuki, Y.; Takema, Y.; Imokawa, G. The role of elastases secreted by fibroblasts in wrinkle formation: implication through selective inhibition of elastase activity. *Photochem. Photobiol.* **2001**, 74(2), 283-290.
- Tucker, T. J.; Sisko, J. T.; Tynebor, R. M.; Williams, R. M.; Felock, P. J.; Flynn, J. A.; Lai, M.-T.; Liang, Y.; McGaughey, G.; Liu, M.; Miller, M.; Moyer, G.; Munshi, V.; Perlow-Poehnelt, R.; Prasad, S.; Reid, J. C.; Sanchez, R.; Torrent, M.; Vacca, J. P.; Wan, B.-L.; Yan, Y. Discovery of 3-{5-[(6-amino-1H-pyrazolo[3,4-b]pyridine-3-yl)methoxy]-2-chlorophenoxy}-5-chlorobenzonitrile (MK-4965): a potent, orally bioavailable HIV-1 non-nucleoside reverse transcriptase inhibitor with improved potency against key mutant viruses. *J. Med. Chem.* **2008**, 51, 6503-6511.
- Turkington, P. T. Degradation of Human Factor X by Human Polymorphonuclear Leucocyte Cathepsin G and Elastase. *Haemostasis.* **1991**, 21(2), 111-116.
- Uddin, Z.; Li, Z.; Song, Y. H.; Kim, J. Y.; Park, K. H. Visconata: A rare flavonol having long chain fatty acid from *Dodonaea viscosa* which inhibits Human neutrophil elastase (HNE). *Tetrahedron Lett.* **2017**, 58(25), 2507-2511.
- Van der Linden, M.; Meyaard, L. Fine-tuning neutrophil activation: Strategies and consequences. *Immunol. lett.* **2016**, 178, 3-9.
- Vankeerberghen, A.; Cuppens, H.; Cassiman, J. J. The cystic fibrosis transmembrane conductance regulator: an intriguing protein with pleiotropic functions. *J. Cyst. Fibros.* **2002**, 1(1),13-29.
- Vanommeslaeghe, K.; Guvench, O.; MacKerell, A. D. Jr. Molecular Mechanics. *Curr. Pharm. Des.* **2014**, 20, 3281-3292.
- Veber, D. F.; Johnson, S. R.; Cheng, H. Y.; Smith, B. R.; Ward, K. M.; Kopple, K. D. Molecular properties that influence the oral bioavailability of drug candidates. *J. Med. Chem.* **2002**, 45, 2615-2623.

- Veits, G. K.; He, M.; Henderson, J. A.; Nasveschuk, C. G.; Phillips, A. J.; Good, A. C. Preparation of pyrazolylmethylamino isoindoline diones as cereblon binders for the degradation of Ikaros useful in treatment of disease. *PCT Int. Appl.* WO2019191112A1, **2019**.
- Vergelli, C.; Schepetkin, I. A.; Ciciani, G.; Cilibrizzi, A.; Crocetti, L.; Giovannoni, M. P.; Guerrini, G.; Iacovone, A.; Kirpotina, L. N.; Khlebnikov, A. I.; Ye, R. D.; Quinn, M. T. 2-Arylacetamido-4-Phenylamino-5-Substituted Pyridazinones as Formyl Peptide Receptors Agonists. *Bioorg. Med. Chem.* **2016**, 24(11), 2530-2543.
- Vergelli, C.; Schepetkin, I. A.; Ciciani, G.; Cilibrizzi, A.; Crocetti, L.; Giovannoni, M. P.; Guerrini, G.; Iacovone, A.; Kirpotina, L. N.; Ye, R. D.; Quinn, M. T. Synthesis of five and six-membered N-phenylacetamido substituted heterocycles as formyl peptide receptor (FPR) agonists. *Drug. Dev. Res.* **2017**, 78(1), 49-62.
- Vergelli, C.; Schepetkin, I. A.; Crocetti, L.; Iacovone, A.; Giovannoni, M. P.; Guerrini, G.; Khlebnikov, A. I.; Ciattini, S.; Ciciani, G.; Quinn, M. T. Isoxazol-5(2H)-one: a new scaffold for potent human neutrophil elastase (HNE) inhibitors. *J. Enzyme Inhib. Med. Chem.* **2017**, 32(1), 821-831.
- Vergely, I.; Laugaa, P.; Reboud-Ravaux, M. Interaction of human leukocyte elastase with a N-aryl azetidinone suicide substrate: conformational analyses based on the mechanism of action of serine proteinases. *J. Mol. Graphics.* **1996**, 14, 158-167.
- Vergnolle, N. Protease-activated receptors as drug targets in inflammation and pain. *Pharmacol. Ther.* **2009**, 123, 292-309.
- Vogelmeier, C.; Gillissen, A.; Buhl, R. Use of secretory leukoprotease inhibitor to augment lung antineutrophil elastase activity. *Chest.* **1996**, 110, 261S-266S.
- Von Nussbaum, F.; Karthaus, D.; Anlauf, S.; Anlauf, S.; Delbeck, M.; Karthaus, D.; Lustig, K.; Schamberger, J. 4-(4-cyano-2-thioaryl) dihydro pyrimidones and use thereof. *U.S. Pat. Appl. Publ.* US2015045344A1, **2015c**.
- Von Nussbaum, F.; Li, V. M. J. Neutrophil elastase inhibitors for the treatment of (cardio) pulmonary diseases: into clinical testing with pre-adaptive pharmacophores. *Bioorg. Med. Chem.* **2015a**, 25, 4370-4381.
- Von Nussbaum, F.; Li, V. M.; Meibom, D.; Anlauf, S.; Delbeck, M.; Karthaus, D.; Lustig, K.; Schamberger, J. Potent and selective human neutrophil elastase inhibitors with novel equatorial ring topology: in vivo efficacy of the polar pyrimidopyridazine BAY-8040 in a pulmonary arterial hypertension rat model. *Chem. Med. Chem.* **2016**, 11, 199-206.
- Von Nussbaum, F.; Li, V.; Allerheiligen, S.; Anlauf, S.; Bärfacker, L.; Bechem, M.; Delbeck, M.; Fitzgerald, M. F.; Gerisch, M.; Gielen-Haertwig, H.; Haning, H.; Karthaus, D.; Lang, D.; Lustig, K.; Meibom, D.; Mittendorf, J.; Rosentreter, U.; Schäfer, M.; Schäfer, S.; Schamberger, J.; Telan, L. A.; Tersteegen, A. Freezing the bioactive conformation to boost potency: the identification of BAY

85-8501, a selective and potent inhibitor of human neutrophil elastase for pulmonary diseases. *Chem. Med, Chem.* **2015b**, 10, 1163-1173.

- Wakulik, K.; Wiatrak, B.; Szczukowski, Ł.; Bodetko, D.; Szandruk-Bender, M.; Dobosz, A.; Świątek, P.; Gašiorowski, K. Effect of Novel Pyrrolo[3,4- d]pyridazinone Derivatives on Lipopolysaccharide-Induced Neuroinflammation. *Int. J. Mol. Sci.* **2020**, 21(7), 2575.
- Walker, B.; Lynas, J. F. Strategies for the inhibition of serine proteases. *Cell. Mol. Life Sci.* **2001**, 58(4), 596-624.
- Wang, T.; Zhu, Z.; Liu, Z.; Yi, L.; Yang, Z.; Bian, W.; Chen, W.; Wang, S.; Li, G.; Li, A.; Martin, G. S.; Zhu, X. Plasma Neutrophil Elastase and Elafin as Prognostic Biomarker for Acute Respiratory Distress Syndrome: A Multicenter Survival and Longitudinal Prospective Observation Study. *Shock.* **2017**, 48, 168-174.
- Wang, Y.; Xiao, Y.; Zhong, L.; Ye, D.; Zhang, J.; Tu, Y.; Bornstein, S. R.; Zhou, Z.; Lam, K. S.; Xu, A. Increased neutrophil elastase and proteinase 3 and augmented NETosis are closely associated with beta-cell autoimmunity in patients with type 1 diabetes. *Diabetes.* **2014**, 63, 4239-4248.
- Wang, Z.; Beach, D.; Su, L.; Zhai, R.; Christiani, D. C. A genome-wide expression analysis in blood identifies pre-elafin as a biomarker in ARDS. *Am. J. Respir. Cell Mol. Biol.* **2008**, 38, 724-732.
- Weathington, N. M.; van Houwelingen, A. H.; Noerager, B. D.; Jackson, P. L.; Kraneveld, A. D.; Galin, F. S.; Folkerts, G.; Nijkamp, F. P.; and Blalock, J. E. A novel peptide CXCR ligand derived from extracellular matrix degradation during airway inflammation. *Nat. Med.* **2006**, 12, 317-323.
- Wei, L.; Lai, Z.; Gan, X.; Alliston, K. R.; Zhong, J.; Epp, J. B.; Tu, J.; Perera, A. B.; Van Stipdonk, M.; Groutas, W. C. Mechanism-based inactivation of human leukocyte elastase via an enzyme-induced sulfonamide fragmentation process. *Arch. Biochem. Biophys.* **2004**, 429(1), 60-70.
- Wong, J.; Magun, B. E.; Wood, L. J. Lung inflammation caused by inhaled toxicants: a review. *Int. J. of Copd.* **2016**, 11, 1391-1401.
- Wood, A. M.; Stockley, R. A. Alpha one antitrypsin deficiency: from gene to treatment. *Respiration.* **2007**, 74, 481-492.
- Woods, K. W.; Lai, C.; Miyashiro, J. M.; Tong, Y.; Florjancic, A. S.; Han, E. K.; Soni, N.; Shi, Y.; Lasko, L.; Levenson, J. D.; Johnson, E. F.; Shoemaker, A. R.; Penning, T. D. Aminopyrimidinone cdc7 Kinase Inhibitors. *Bioorg. Med. Chem. Lett.* **2012**, 22(5), 1940-1943.
- Wright, J. L.; Farmer, S. G.; Churg, A. Synthetic serine elastase inhibitor reduces cigarette smoke induced emphysema in guinea pigs. *Am. J. Resp. Crit. Care.* **2002**, 166, 954-960.
- Wynn, T. A. Integrating mechanisms of pulmonary fibrosis. *J. Exp. Med.* **2011**, 208(7), 1339-1350.
- Xu, Y.; Zhang, J.; Han, J.; Pan, X.; Cao, Y.; Guo, H.; Pan, Y.; An, Y.; Li, X. Curcumin inhibits tumor proliferation induced by neutrophil elastase through the upregulation of alpha1-antitrypsin in lung cancer. *Mol. Oncol.* **2012**, 6(4), 405-417.

- Yadav, D.; Lowenfels, A. B. The epidemiology of pancreatitis and pancreatic cancer. *Gastroenterology*. **2013**, 144, 1252-1261.
- Yamada, K.; Yanagihara, K.; Araki, N.; Harada, Y.; Morinaga, Y.; Izumikawa, K.; Takeya, H.; Yamamoto, Y.; Hasegawa, H.; Kohno, S.; Kamihira, S. In vivo efficacy of KRP-109, a novel elastase inhibitor, in a murine model of severe pneumococcal pneumonia. *Pulm. Pharmacol. Ther.* **2011**, 24, 660-665.
- Yang, D.; Chen, Q.; Schmidt, A. P.; Anderson, G. M.; Wang, J. M.; Wooters, J.; Oppenheim, J. J.; Chertov, O. LL-37, the neutrophil granule and epithelial cell-derived cathelicidin, utilizes formyl peptide receptor-like 1 (FPRL1) as a receptor to chemoattract human peripheral blood neutrophils, monocytes, and T cells. *J. Exp. Med.* **2000**, 192, 1069-1074.
- Yang, H.; Biermann, M. H.; Brauner, J. M.; Liu, Y.; Zhao, Y.; Herrmann, M. New insights into neutrophil extracellular traps: mechanisms of formation and role in inflammation. *Front Immunol.* **2016**, 7, 1-7.
- Yasumatsu, R.; Altioek, O.; Benarafa, C.; Yasumatsu, C.; Bingol-Karakoc, G.; Remold-O'Donnell, E.; Cataltepe, S. SERPINB1 upregulation is associated with in vivo complex formation with neutrophil elastase and cathepsin G in a baboon model of bronchopulmonary dysplasia. *Am. J. Physiol. Lung Cell Mol. Physiol.* **2006**, 291, L619-L627.
- Ye, R. D.; Boulay, F.; Wang, J. M.; Dahlgren, C.; Gerard, C.; Parmentier, M.; Serhan, C. N.; Murphy, P. M. International union of basic and clinical pharmacology. LXXII. Nomenclature for the formyl peptide receptor (fpr) family. *Pharmacol. Rev.* **2009**, 61, 119-161.
- Yoshinaga, H.; Ikuma, Y.; Ikeda, J.; Adachi, S.; Mitsunuma, H.; Aihara, Y.; Besnard, J.; Bell, A. S. Preparation of fused ring lactam derivatives. *PCT Int. Appl.*, WO2020022237A1, **2020**.
- Zabieglo, K.; Majewski, P.; Majchrzak-Gorecka, M.; Wlodarczyk, A.; Grygier, B.; Zegar, A.; Kapinska-Mrowiecka, M.; Naskalska, A.; Pyrc, K.; Dubin, A.; Wahl, S. M.; Cichy, J. The inhibitory effect of secretory leukocyte protease inhibitor (SLPI) on formation of neutrophil extracellular traps. *J. Leukoc. Biol.* **2015**, 98, 99-106.
- Zani, M. L.; Nobar, S. M.; Lacour, S. A.; Lemoine, S.; Boudier, C.; Bieth, J. G.; Moreau, T. Kinetics of the inhibition of neutrophil proteinases by recombinant elafin and pre-elafin (trappin-2) expressed in *Pichia pastoris*. *Eur. J. Biochem.* **2004**, 271(12), 2370-2378.
- Zimmer, M.; Medcalf, R. L.; Fink, T. M.; Mattmann, C.; Lichter, P.; Jenne, D. E. Three human elastase-like genes coordinately expressed in the myelomonocyte lineage are organized as a single genetic locus on 19pter. *Proc. Natl. Acad. Sci. U.S.A.* **1992**, 89(17), 8215-8219.



RCSI

**An innovative and stereoselective synthesis of the
ADHD drug Atomoxetine**

Supervisor: Prof. Mauro Adamo

Table of Contents

1. Introduction	199
1.1. Attention Deficit/ Hyperactivity Disorder (ADHD)	199
1.2. Clinical picture and pathophysiology	199
1.3. Treatment for ADHD	200
2. Atomoxetine (Strattera®)	200
2.1. Pharmacodynamic Properties	201
2.2. Pharmacokinetic Profile	201
3. Background and aims of the work	202
References	203

1. Introduction

1.1. Attention Deficit/ Hyperactivity Disorder (ADHD)

Attention-Deficit/Hyperactivity Disorder (ADHD) is the most common behavioral disorder in childhood and it affects 3 to 5% of school-age children [Polanczyk, G. V. et al., 2015]. People affected by ADHD present poor attention, hyperactivity and impulsivity, but also difficulty in regulating their emotions. Patients with mainly inattention problems are often slow to formulate ideas due to distractions, but on the other hand, it may happen that ADHD causes “hyperfocus” or over-concentration, which is a phenomenon occurring when patients are involved in very interesting activities for them, such as computer games or online chatting. Hyperactivity is expressed differently in children than adults, in fact, the latter manifest a feeling of restlessness, agitation, and ceaseless mental activity. Occasionally, patients find relief with alcohol or drugs, but also engaging in excessive sport activities. Impulsiveness is associated with interpersonal conflicts and it has impact not only with other people, but it could even affect personal finance when impulsive spending causes debt. Closely related to an impulsive behavior, ADHD may lead to “sensation of seeking” when patients are eager of new stimuli, often involving risk taking behaviors, such as playing with fire, reckless driving, sexual risks, and provocative behavior. Furthermore, ADHD is correlated with emotional instability, characterized by a deficient self-regulation of emotional manifestations such as irritability, frustration and anger. These symptoms are statistically associated with learning difficulties, school dropout, underachievement at work, chronic fatigue, financial problems, gambling, home and traffic accidents, relationship difficulties and intimate partner violence, early onset of addiction, to an increased number of suicide attempts and self-harm in adolescents, and increased criminality [Smoot, L. C. et al., 2007].

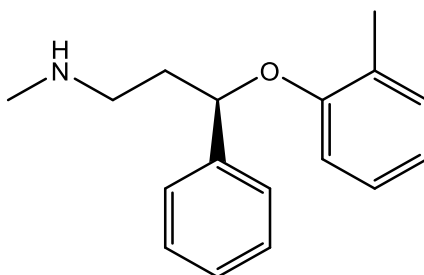
1.2. Clinical picture and pathophysiology

At the moment the experts have difficulty in outlining guidelines for an accurate diagnose of ADHD. In fact, not all children show all symptoms, and with advancing age, some symptoms may disappear or fade, resulting in a decrease of adult patients affected by ADHD, which has recently been estimated about 2.8% across twenty countries. A difference based on sex is also well documented, since girls show less symptoms than boys, making their identification more difficult. Currently the physiopathology of this disease is not yet fully clarified. Extensive neurobiological studies have been conducted revealing small differences in subcortical regions such as amygdala, nucleus accumbens, caudate, hippocampus and putamen between healthy individuals ADHD patients. These diversities support the theory of a dysregulation of the noradrenergic and dopaminergic systems in patients with ADHD. Because of the wide impact of ADHD on the overall performances, this disorder has serious economic repercussions for children, families and society strongly depending on the healthcare system considered [Biederman, J. et al., 2005].

1.3. Treatment for ADHD

ADHD treatment follows a multimodal and multidisciplinary method that includes psychoeducation, pharmacotherapy and cognitive behavior therapy. Before starting the treatment however, it is necessary to determine whether other psychiatric illnesses are involved, as more severe disorders generally have priority. Psychoeducation is generally the first step, mostly for patients with mild symptoms or preschool-aged, but it must be later combined with pharmacological treatment in particular the use of psychostimulants is recommended as first-line drugs, as they have moderate to high clinical efficacy without marked side effects. The drug of choice in children and adolescents is methylphenidate, while in adult amphetamines. Despite conflicting opinions on the use of psychostimulant drugs in children the latest studies seem to highlight that "stimulant therapy in childhood does not increase the risk of drug and alcohol abuse disorders later in life". According to Schoenfelder et al., ADHD medications are not related to an increased risk of cigarette abuse, and actually stimulant treatments such as Ritalin® seemed to reduce this risk. As regards non-stimulant drugs, atomoxetine is considered the drug of choice, followed by guanfacine, clonidine and bupropion [Kooij, J. J. S. et al., 2019].

2. Atomoxetine (Strattera®)



Atomoxetine was the first non-stimulant drug, not previously marketed with other indication, approved by the FDA for the specific treatment of ADHD. It was first synthesized and documented by Eli Lilly in the late '70s showing a significant selectivity towards the norepinephrine reuptake transporter (NET) with respect to both the serotonin reuptake transporter (SERT) and the dopamine reuptake transporter (DAT). Atomoxetine was first approved in 2002, marketed under the name "Strattera®" and indicated for the treatment of ADHD in children over 6 years and adults. Only the R(-) isomer is marketed as it is about 9 fold more potent on NET than the S(+) enantiomer. The atomoxetine increases the level of norepinephrine available in the central nervous system, leading to an enhancement of cognitive functions. It also specifically increases the extracellular levels of dopamine in the prefrontal cortex but not in the nucleus accumbens or striatum.

2.1. Pharmacodynamic Properties

At the present, the precise mechanism of action of Atomoxetine in ADHD is not clear, but it is probably related to the ability to rebalance the dysregulation of the noradrenergic and dopaminergic system found in the disease. As *in vitro* competitive reuptake studies of radio-labeled monoamines in rat synaptosomes, and *ex vivo* uptake and neurotransmitter depletion studies in rats, as well as human pharmacological clinical studies, have shown that atomoxetine is a long-lasting and selective norepinephrine presynaptic transporter. In fact, it is able to increase the concentration of catecholamines in the prefrontal cortex without altering the amount of dopamine in the striatum and accumbens nucleus, unlike the stimulant methylphenidate. Other *in vitro* studies demonstrated a low affinity of atomoxetine on other receptors such as cholinergic, adrenergic, histaminergic and serotonergic ($K_i = 940 - 1090 \text{ nmol/L}$).

2.2. Pharmacokinetic Profile

Atomoxetine is marketed as hydrochloride salt (Strattera®) and the drug shows rapid absorption, reaching maximum plasma concentration in 2 hours. The low half-life, about 3 hours, is consistent with the small amount of atomoxetine measured at the steady state [Yu, G. et al., 2016].

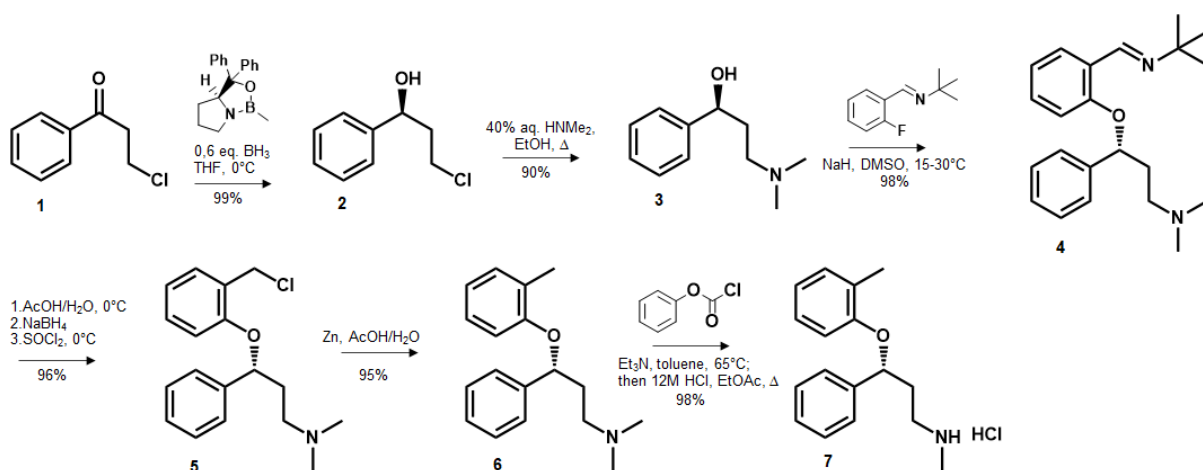
The CNS pharmacokinetics, firstly investigated in rats, show that the transport of atomoxetine through BBB is predominantly passive and that it is not substrate for the P-glycoprotein. In humans there are three principal transformations by phase I metabolism: hydroxylation of the aromatic ring (CYP2D6) which affords the 4-hydroxyatomoxetine with a similar NET inhibition activity, benzylic oxidation, and N-demethylation (CYP2C19). Instead phase II metabolism is principally involved in O-glucuronidation.

3. Background and aims of the work

Among the numerous synthesis of atomoxetine developed since '70s, noteworthy are those of Brown and Sharpless [Gao, Y. et al., 1988; Srebnik, M. et al., 1988], which show several common steps, but differ for the method used to insert stereoselectively the hydroxy group. One of the major problems of the above synthesis is the Mitsunobu reaction, which doesn't allow a manufacturing scale.

Thus, in 2006, Eli Lilly optimized a new synthesis, using the more easily scaled nucleophilic aromatic substitution reaction instead of the Mitsunobu one (**Scheme 1**). Schematically, the first step is the carbonyl reduction of chloroketone **1**, with borane and an oxaborolidine derivative as catalyzer, which provides the hydroxy compound **2**. The reaction is nearly quantitative and affords material with 94% enantiomeric excess. Intermediate **3** obtained by displacement of the chlorine with dimethylamine, is then treated with fluoro-2-(*t*-butylamino)benzene and sodium hydride affording **4**, which, following a three step procedure furnishes compound **5**. Finally, performing a reductive dehalogenation on **5**, intermediate **6** is obtained with a high yield, and further converted into the final **7** by removing the methyl group and by transforming into the corresponding hydrochloride. This method adds a few steps compared to previously developed syntheses above mentioned, but has the advantage of being able to be easily reproduced on a manufacturing scale. In addition, the intermediates obtained are highly pure and in crystalline form, facilitating subsequent reactions, and overall, this approach maintains high chiral purity. [Gray, D. L., 2006].

Scheme 1.



Starting from this background, my work in the Laboratory of Professor Adamo, of the Royal College of Surgeons in Ireland (RCSI), should have concerned the development of a new and stereoselective synthesis of Atomoxetine, which would have reduced the cost and the environmental impact compared to the one developed by Eli Lilly, and would also have been less time-consuming.

Unfortunately, my Dublin experience was interrupted prematurely due to the Covid-19 pandemic; therefore, I was unable to develop my assigned research project as I couldn't attend the laboratory.

References

- Biederman, J.; Faraone, S. V. Attention-deficit hyperactivity disorder. *Lancet*. **2005**, 366(9481), 237-248.
- Gao, Y.; Sharpless, K. B. Asymmetric Synthesis of Both Enantiomers of Tomoxetine and Fluoxetine. Selective Reduction of 2,3-Epoxypropyl Alcohol with Red-Al. *J. Org. Chem.* **1988**, 53, 4081-4084.
- Garnock-Jones, K. P.; Keating, G. M. Atomoxetine: a review of its use in attention-deficit hyperactivity disorder in children and adolescents. *Paediatr. Drugs*. **2009**, 11(3), 203-226.
- Gray, D. L. Approved Treatments for Attention Deficit Hyperactivity Disorder: Amphetamine (Adderall®), Methylphenidate (Ritalin®), and Atomoxetine (Strattera®). *The Art of Drug Synthesis*. **2006**, 241-259.
- Kooij, J. J. S.; Bijlenga, D.; Salerno, L.; Jaeschke, R. et al. Updated European Consensus Statement on diagnosis and treatment of adult ADHD. *Eur. Psychiatry*. **2019**, Feb, 56, 14-34.
- Polanczyk, G. V.; Salum, G. A.; Sugaya, L. S.; Caye, A.; Rohde, L. A. Annual Research Review: A meta-analysis of the worldwide prevalence of mental disorders in children and adolescents. *J. Child. Psychol. Psychiatry*. **2015**, 56(3), 345-365.
- Smoot, L. C.; Boothby, L. A.; Gillett, R. C. Clinical assessment and treatment of ADHD in children. *Int. J. Clin. Pract.* **2007**, 61(10), 1730-1708.
- Srebnik, M.; Ramachandran, P. V.; Brown, H. C. Chiral Synthesis via Organoboranes. 18. Selective Reductions. 43. Diisopinocampheylchloroborane as an Excellent Chiral Reducing Reagent for the Synthesis of Both Optical Isomers of Tomoxetine, Fluoxetine, and Nisoxetine. *J. Org. Chem.* **1988**, 53, 2916-2920.
- Yu, G.; Li, G. F.; Markowitz, J. S. Atomoxetine: A Review of Its Pharmacokinetics and Pharmacogenomics Relative to Drug Disposition. *J. Child. Adolesc. Psychopharmacol.* **2016**, 26(4), 314-326.
- Yu, G.; Li, G. F.; Markowitz, J. S. Atomoxetine: A Review of Its Pharmacokinetics and Pharmacogenomics Relative to Drug Disposition. *J. Child Adolesc. Psychopharmacol.* **2016**, 26(4), 314-326.